Identification of proteins involved in host cell cytosol uptake in the human Malaria parasite *Plasmodium falciparum*

Dissertation with the aim of achieving a doctoral degree at the
Faculty of Mathematics, Informatics and Natural Sciences
Department of Biology
University Hamburg

submitted by

Ernst Georg Wolfgang Jonscher

2018 in Hamburg

Vorsitz der Prüfungskommission: Prof. Julia Kehr

1. **Gutachter der Dissertation: Prof. Tim Gilberger**

2. **Gutachter der Dissertation: Dr. Tobias Spielmann**

Dissertationsdatum: 10.08.2018

Eidesstattliche Versicherung

Hiermit erkläre ich an Eides statt, dass ich die vorliegende Dissertationsschrift selbst verfasst und keine anderen als die angegebenen Quellen und Hilfsmittel benutzt habe.

Hamburg, den 05.07.2018 Ernst Jonscher

Language certificate

I am a native speaker, have read the present PhD thesis and hereby confirm that it complies with the rules of the English language.

Hamburg, July 5th 2018 Mackenzie Rose Jonscher

Summary

The apicomplexan parasite *Plasmodium falciparum* is the cause of the severest form of human malaria. The parasite propagates within human red blood cells (RBCs) where it grows until it fills out most of the host cell. During this growth phase the parasite ingests up to 80 % of the RBC cytosol. This host cell cytosol uptake (HCCU) serves as source for amino acids and provides room for parasite growth. The host cell cytosol consists mostly of hemoglobin that is transported to a lysosome-like organelle, the food vacuole (FV), where it is digested by a series of proteases. The toxic byproduct heme polymerizes to a hemozoin crystal, also termed the malaria pigment. While the digestive processes of hemoglobin in the FV are well understood, less is known how the host cell cytosol actually reaches the FV. Current models based on ultrastructural and inhibitor studies assume that HCCU is related to endocytosis but direct functional data implicating a specific protein in this process is lacking. In previous work a set of potential endocytosis proteins were identified in *P. falciparum* parasites but definite proof of a function of any of these proteins in HCCU is still lacking. Based on these preliminary data, three proteins, the PfClathrin heavy chain (CHC), PfEps15 and PfVPS45, were here chosen for analysis in more detail with the aim to experimentally demonstrate their role in HCCU and to reveal the first molecule in this process.

Clathrin is the most prominent endocytic protein in yeast and mammalian cells. In this work, the *P. falciparum* homologue of the Clathrin Heavy Chain (CHC) was found to be refractory to gene disruption in *P. falciparum* blood stages and inducible inactivation using knock sideways led to reduced parasite growth. GFP tagged CHC expressed from its original genomic locus was found in foci of which the most prominent were proximal to the parasite nucleus, suggesting a Golgi location. To identify possible interactors and compartment neighbors of CHC in *P. falciparum*, dimerization induced quantitative BioID (DiQ-BioID) was carried out, resulting in a series of potential interactors that indicated that CHC serves a function at the Golgi compartment and is not involved in endocytosis. In contrast, PfEps15 did not co-localize with CHC and DiQ-BioID for Eps15 did not identify CHC or its interactors but many unknown proteins that were previously identified in a DiQ-BioID with the Artemisinin resistance marker Kelch13, including for example UBP1 and Kelch13 itself. Co-immunoprecipitation of Eps15 with Kelch13 confirmed a physical interaction of Eps15 with Kelch13. Fast frame rate imaging for Eps15 recapitulated directed movement of Eps15 foci between the parasite plasma membrane and the FV and showed that also Kelch13 followed this movement. Attempts to achieve selectable disruption (SLI-TGD) of the *eps15* gene failed, suggesting it to be essential for blood stage parasites. Knock sideways to conditionally inactivate Eps15 was only partly successful but confirmed that this protein is likely essential for the growth of blood stage parasites. Together with previous data, this indicates a possible role of Eps15 in HCCU and suggests a link of the interacting Kelch13 complex to such a function. Treatment with the Retromer inhibitor Retro-2, inhibiting the Golgi-to-Endosome trafficking in mammalian cells, abolished the localization of CHC to intense patch

like foci but did not show an effect on the localization of Eps15 and Kelch13, indicating that Clathrin and Eps15 and Kelch13 indeed function in different trafficking pathways in *P. falciparum.*

A third protein analyzed in this thesis was the homologue of VPS45 in *P. falciparum*. Knock sideways of VPS45 arrested parasite growth during the trophozoite stage, preventing successful replication, and caused an accumulation of host cell cytosol filled vesicles in the parasite cytosol. These vesicles were found to be positive for phosphatidylinositol 3-phosphate, a marker for early endosomes in eukaryotic cells, indicating that the vesicles are stalled or inflated HCCU intermediates. Inactivation of VPS45 also dramatically reduced the accumulation of hemozoin in the food vacuole and no new hemoglobin arrived in the food vacuole, demonstrating a key function of VPS45 for the delivery of host cell cytosol to the parasite's FV.

Taken together, this work reveals VPS45 as the first (to our knowledge) protein directly involved in HCCU. This molecule therefore represents an entry point to further characterize HCCU in *P. falciparum.* The function of Eps15 remains less clear but this protein may play a role in initial phases of HCCU. Importantly, this work shows that Eps15 interacts with the Artemisinin resistance marker Kelch13 that for instance may constitute a regulatory complex for endocytosis in *P. falciparum*. In contrast, the Clathrin Heavy Chain, an important element of endocytosis in eukaryotic organisms, has no function in endocytosis in *P. falciparum,* but rather plays a role at the Golgi, in agreement with the role of Clathrin in the apicomplexan *Toxoplasma gondii.* These results shed light on HCCU and on the general blue print of the trafficking pathways in malaria parasites.

Zusammenfassung

Die Parasiten der Gattung *Plasmodium* (Apikomplexa) sind die Krankheitserreger der Malaria und die schwerste Verlaufsform von Malaria wird durch *Plasmodium falciparum* versuracht. Der Parasit entwickelt sich innerhalb der menschlichen roten Blutzellen bis er diese fast vollständig einnimmt. Während seines Wachstums nimmt der Parasit bis zu 80 % des Wirtszellzytosols auf. Diese Wirtszellzytosolaufnahme („*host cell cytosol uptake",* HCCU) dient als Quelle für Aminosäuren und stellt Raum für das Wachstum des Parasiten zur Verfügung. Das aufgenommene Wirtszellzytosol besteht hauptsächlich aus Hämoglobin, welches in die Nahrungsvakuole des Parasiten transportiert und dort proteolytisch verdaut wird. Das dabei entstehende toxische Häm polymerisiert zu einem Hämozoin-Kristall (Malaria-Pigment) und wird in der Nahrungsvakuole eingelagert. Obwohl der Verdauungsprozess des Hämoglobins gut charakterisiert ist, ist bis jetzt kaum bekannt, wie das Wirtszellzytosol in die Nahrungsvakuole gelangt. Bestehende Modelle, basierend auf Inhibitor- und elektronenmikroskopische Studien, vermuten, dass die Wirtszellzytosolaufnahme einen endozytotischen Prozess darstellt. Bis dato liegen jedoch keine Daten vor, die ein Protein diesem Prozess direkt zuschreiben. In vorhergehenden Arbeiten wurden potentielle Endozytose-Faktoren in *P. falciparum* identifiziert, aber noch kein Beleg für eine Rolle dieser Proteine in der Wirtszellzytosolaufnahme gezeigt. Drei Proteine wurden basierend auf den vorhergehenden Arbeiten für eine detailliertere Untersuchung mit dem Ziel ausgewählt, experimentelle Evidenzen für eine Funktion dieser Proteine in der Wirtszellzytosolaufnahme zu erlangen und somit das erste Mal ein Protein dieses Prozesses zu identifizieren. Die ausgewählten Proteine sind PfClathrin Heavy Chain (CHC), PfEps15 und PfVPS45.

Clathrin ist einer der am besten bekannten Proteine der Endozytose in Hefe- und Säugetierzellen. In dieser Arbeit wurde gezeigt, dass das Gen des Homologs von Clathrin Heavy Chain in *P. falciparum* zerstört werden kann und die induzierbare Inaktivierung des CHC-proteins zu reduziertem Parasitenwachstum führte. Von dem endogenen Lokus exprimiertes, mit dem Fluorophor GFP fusioniertes CHC lokalisierte in punktuellen Signalen, von denen die offensichtlichsten in der Nähe des Zellkerns zu finden waren. Dies lässt eine potentielle Lokalisation am Golgi vermuten. Um eventuelle Interaktoren und benachbarte Proteine desselben Kompartiments zu identifizieren, wurde induzierbare quantitative BioID (DiQ-BioID) durchgeführt. Dies resultierte in zahlreichen identifizierten Proteinen, die eine Funktion von CHC an dem Golgi-Kompartiment, aber keine Funktion in Endozytose, vermuten lassen. Eps15 co-lokalisierte nicht mit CHC und CHC und dessen Interaktoren wurden nicht mit DiQ-BioID für Eps15 identifiziert. Im Gegensatz dazu, wurden viele potentiell interagierende Proteine des Interaktoms von Kelch13 und Kelch 13 selber, ein Protein, das Artemisinin-Resistenz vermittelt, gefunden. Die Interaktion von Eps15 und Kelch13 wurde mittels Co-Immunoprezipitation bestätigt. Lebendzell-Mikroskopie mit schnellen Bildraten reproduzierte die bereits beschriebene Bewegung von Eps15 zwischen der Zellmembran des Parasiten und der

Nahrungsvakuole und Kelch13 scheint Eps15 in dieser Bewegung zu folgen. Der Versuch das *eps15* Gen mittels selektierbarer Gendisruption (SLI-TGD) zu zerstören, waren nicht erfolgreich. Dies lässt vermuten, dass Eps15 essentiell für das Überleben der Blutstadien von *P. falciparum* ist. Inaktivierung von Eps15 mittels Mislokalisation („*knock sideways*“) war nur teilweise erfolgreich, aber die damit erzielten Ergebnisse unterstreichen, dass Eps15 essentiell für die Blutstadien von *P. falciparum* ist. In Anbetracht der vorhergehenden Daten wird daraus eine mögliche Rolle von Eps15 in der Wirtszellzytosolaufnahme vermutet und ebenfalls das mit Eps15 interagierende Kelch13 einer solchen Funktion zugeführt. Die Behandlung mit dem Inhbitor des Retromers Retro-2, welcher den Transport zwischen Golgi und Endosom verhindert, führte zur Auflösung der intensiv fluoreszierenden, großen Signale von CHC, aber hatte keinen Effekt auf die Lokalisation von Eps15 und Kelch13. Dies führt zur Schlussfolgerung, dass CHC und Eps15 und Kelch13 tatsächlich an unterschiedlichen Transportwegen in *P. falciparum* beteiligt sind.

Ein drittes, in dieser Arbeit untersuchtes Protein, war das Homolog von VPS45 in *P. falciparum*. Die Inaktivierung von VPS45 mittels Mislokaliation stoppte das Parasitenwachstum im Trophozoiten-Stadium und führte zur Ansammlung von mit Wirtszellzytosol gefüllten Vesikeln im Zytosol des Parasiten. Diese Vesikel waren durch Phosphatidylinositol 3-phosphat, ein Marker für frühe Endosomen (*early endosomes*) in eukaryotischen Zellen, markiert. Dies lässt vermuten, dass die akkumulierenden Vesikel aufgehaltene oder aufgeblasene Intermediate der Wirtszellzytosolaufnahme sind. Darüber hinaus wurde gezeigt, dass die Inaktivierung von VPS45 zu einer drastischen Reduktion in der Ansammlung von Hämozoin in der Nahrungsvakuole führt und dass kein Hämoglobin mehr in die Nahrungsvakuole gelangt. Damit wurde eine Schlüsselrolle von VPS45 im Transport von Wirtszellzytosol zur Nahrungsvakuole gezeigt.

Zusammenfassend ist zu sagen, dass in dieser Arbeit mit VPS45 das, nach unserem Wissen, erste Protein mit direkter Beteiligung an der Wirtszellzytosolaufnahme gezeigt wurde. Dieses Protein stellt somit einen Anfang für die weitere Charakterisierung der Wirtszellzytosolaufnahme in *P. falciparum* dar. Die Funktion von Eps15 verbleibt weniger deutlich, aber dieses Protein könnte eine Rolle in frühen Prozessen der Wirtszellzytosolaufnahme übernehmen. Bedeutend ist die hier gezeigte Interaktion von Eps15 und Kelch13, welche möglicherweise einen für die Endozytose regulatorischen Proteinkomplex in *P. falciparum* bilden. Im Gegensatz dazu hat Clathrin Heavy Chain, ein wichtiges Element der Endozytose in Eukaryonten, keine Funktion in der Endozytose in *P. falciparum*, sondern scheint eher eine Rolle am Golgi zu übernehmen, was in Übereinstimmung mit der Rolle von Clathrin in dem *Toxoplasma gondii* (Apicomplexa) ist. Die Ergebnisse dieser Arbeiten geben Aufschluss über die Wirtszellzytosolaufnahme und vermitteln einen Überblick über die Transport-Prozesse in *P. falciparum*.

Table of contents

List of figures

List of tables

Abbreviations

2D	Two-dimensional
3-Box	Protein domain similar to F-Box
3D	Three-dimensional
ACT	Artemisinin-based combination therapy
ADP	Adenosine diphosphate
AMA	Apical Membrane Antigen
ANTH	AP180 N-terminal homology domain
AP	Adaptor protein
ATP	Adenosine triphosphate
BACK	BTB and C-terminal Kelc
BAR	BIN/amphiphysin/Rvs
bp	Base pairs
BSD	Blasticidin S
BTB	Domain from Broad-Complex, Tramtrack and Bric a brac proteins
CAP	Chemically attenuated sporozoites
CCP	Clathrin coated pit
CCV	Clathrin coated vesicle
CHC	Clathrin Heavy Chain
CHMI	controlled human malaria infection
CIE	Clathrin independent endocytosis
CLC	Clathrin Light Chain
CLEM	Correlative light microscopy and electron microscopy
CLIC	clathrin-independent carriers
CLSM	Confocal laser scanning microscope
CME	Clathrin mediated endocytosis
CoIP	Co-immunoprecipitation
CRT	Chloroquine Resistance Transporter
CSP	Circumsporozoite Surface Protein
C-terminal	Carboxy-terminal
DAPI	4'6-Diamino-2-phenylindol
DDT	Dichlordiphenyltrichlorethan
DIC	Differential interference contrast
DiQ-BioID	Dimerization induced quantitative BioID
DNA	Desoxyribonucleicacid
DTT	Dichlorodiphenyltrichloroethane

EE	Early endosome
EH	Eps15 homology
EM	Electron microscopy
ENTH	Epsin N-terminal homology
Eps15	Epidermal growth factor receptor substrate 15
ER	Endoplasmic Reticulum
et al.	et alii
FACS	Fluorescence-activated cell sorting
F-Box	Protein domain first found in cyclin-F
FIB-SEM	Focused ion beam scanning electron microscopy
FKBP	FK 506 binding protein
FYVE	Fab1, YOTB/ZK632.12, Vac1, and EEA1 zinc finger domain
GAP	Genetically attenuated sporozoites
GAP	Guanine nucleotide activating protein
GDP	Guanine diphostphate
GEEC	GPI-enriched endocytic compartment
GEF	Guanine nucleotide exchange factor
GFP	Green fluorescent protein
GTP	Guanine triphosphate
HCCU	Host cell cytosol uptake
hDHFR	Human Dihydrofolat Reductase
HRP	Histidine rich protein
HRP	Horse radish peroxidase
IMC	Inner membrane complex
iRBC	infected red blood cell
ITN	insecticide-treated bednet
KS	Knock sideways
LE	Late endosome
mRNA	Messenger ribonuclei acid
MVB	Multi vesicular body
NA-binding	Nuclei acid binding
N-terminal	Amino-terminal
OD	Optical density
PAA	Polyacrylamide
PAGE	Polyacrylamide gel electrophoresis
PCR	Polymerase chain reaction
PEXEL	Plasmodium export element

$PI(4,5)P_2$	Phosphatidylinositol 4,5-bisphosphate
PI3P	Phosphatidylinositol 3-phosphate
PIP	Phosphatidyl inositol
PLV	Plant like vacuole
PNEP	PEXEL negative exported protein
PPM	Parasite plasma membrane
PV	Parasitophorous vacuole
PVM	Parasitophorous vacuole membrane
PX	Phox homology
Rab	Rho-GTPase associated
RBC	Red blood cell
RING	Really interesting new gene
RPMI	Roswell Park Memorial Institute
SM	Sec1p/Munc18
SNARE	soluble N-ethylmaleimide-sensitive-factor attachment receptor
SNX	Sorting nexin
SOCS-Box	suppressor of cytokine signaling protein domain
TEM	Transmission electron microscopy
UTR	Untranslated region
VAC	Vacuolar compartment of *T. gondii*
VPS	Vacuolar protein sorting
WHO	World Health Organization
yDHODH	Yeast dihydroorotate dehydrogenase

1. Introduction

1.1 Malaria

A story of co-evolution between hominids and the pathogen of 130 Million years (Carter and Mendis, 2002; Escalante and Ayala, 1995) will come to an end if the eradication of the Malaria-disease will truly be achieved in 2040 as planned by the End Malaria Council (endmalariacouncil.org, 2018; WHO, 2017). Malaria has been a threat of humankind for which reports were found dating back to ancient Greece (Sherman, 1998). The disease shaped history like Scotland losing its independence to England due to bankruptcy after its attempt to colonize the region today known as Panama due to tropical diseases of which an important one was Malaria (Little, 2014). Malaria influenced prominent scientists like Camille Golgi (the discoverer of the Golgi-organelle) (Golgi, 1885) or was the subject of Nobel prizes such as for the identification of the transmitting vector in 1902 (Capanna, 2006; Grassi, 1901; Ross, 1889) and for the anti-malaria drug artemisinin in 2015.

First observations linked with Malaria were already made in the antiquity, leading to the conclusion that the febrile, seasonal disease is linked to swamps which resulted in its name Malaria (*mal'aria*), meaning "bad air" in Italian (Sherman, 1998). Later a major breakthrough was the identification and description of the causative agents as single-cell parasites by Alphonse Charles Laveran in 1880 (Laveran, 1880). It was first incorrectly classified as Coccidia, later re-ordered and described in more detail with the help of Camille Golgi and others (Ziemann, 1889). The malaria parasites of the genus *Plasmodium* were found to be transmitted by an invertebrate definitive host, mosquitos of the genus *Anopheles*, to its vertebrate intermediate hosts (Cox, 2010; Ross, 1889). Systematically more than 200 Plasmodium-species have so far been described of which five species are known to infect humans (*P. falciparum*, *P. vivax*, *P. ovale*, *P. knowlesi*, *P. malariae*). In the19th century malaria had a wider distribution than today and for instance was also found in northern Germany as can be recognized in the literature from the early 20th century e.g. in Zielmann's "Ueber Malaria- und andere Blutparasiten" (*About Malaria and other parasites of the blood*) where Malaria-species from tropical regions of Africa were compared with those present in northern parts of Germany (Ziemann, 1889). Malaria was in those times present even farther north in Scandinavia as reported in the 19th century (Hulden, 2011). Its eradication in Europe was achieved just 70 years ago in the 1950s and until then Malaria was still endemic for example in the flatlands of north-western Germany.

Even though that tremendous knowledge accumulated by extensive malaria research and the fact that many former endemic areas were cleared from Malaria, it is still considered as one of the infectious diseases that impacts humans the most.

1.1.1 Distribution and epidemiology of Malaria

Up to 3.2 Billion people live in malaria endemic regions and are therefore considered to be at risk of infection. 216 Million cases of malaria have been estimated in 2016 of which 445 000 resulted in deaths (WHO, 2017). Most affected are children below the age of 5 where malaria is a major cause of mortality. The impact of malaria for children in endemic areas is also reflected in the fact that this disease accounts for 25 % of all deaths in this age group (Figure 1 B, C) (Sachs and Malaney, 2002; White et al., 2014; WHO, 2017). The majority of malaria cases in 2016 were in the African Region (90%), followed by the South-East-Asia Region (7%) and the Eastern Mediterranean Region (2%). The deaths occur mostly in African regions (91 %) and partly in South East Asia (6%) and can be narrowed down to 15 countries of which all are located in the sub-Saharan region and India (Figure 1). In several countries, including for instance Egypt and Morocco, Malaria was successfully eradicated between 2000 and 2015 (Figure 1 A; according to the WHO guidelines). The incidence of *P. falciparum* or *P. vivax*, the two species with the highest incidence rate, is depicted in (Figure 1 A). *P. falciparum* has a higher incidence in Africa (Figure 1 A) which overlaps with the reported numbers of death since *P. falciparum* (Figure 1 B, children under 5 years of age) causes the most severe form of malaria (section 1.1.3). *P. vivax*-Malaria accounts 64 % of cases in the Americas and 30 % and 40 % in South-East-Asia and the Eastern Mediterranean, respectively and is therefore important for the inhabitants of these countries (WHO, 2017). Even though the importance of *P. vivax* is lower than that of *P. falciparum*, its capacity reproduce at lower temperatures allows a wider geographical distribution. In addition its capacity to persist in the human liver as hypnozoites that can later relapse, facilitates overcoming low transmission seasons with low vector populations (Krotoski et al., 1982; Shortt et al., 1948; White, 2011). The other 3 *Plasmodium* species contribute to a lesser extent to the global Malaria burden. *P. ovale*, *P. malariae* are rare and *P. knowlesi* is exclusively zoonotic (Greenwood et al., 2008; Singh and Daneshvar, 2013). *P. ovale* and *P. malariae* often contribute to mixed infections, a fact that is of importance for clinical outcome and diagnostics (Collins and Jeffery, 2005). Based on its heterophasic life cycle (section 1.2.1) the distribution of Malaria is directly linked to the presence of its transmitting vectors, the mosquitos of the genus *Anopheles*. Out of 400 anopheline mosquitos species, 41 are competent to transmit *Plasmodium* parasites. One major transmitting species is *Anopheles gambiae* but there are large variations of the transmitting species dependent on the the ecology-dependent abundance of Anopheles species present (Sinka et al., 2010; Sinka et al., 2012).

Besides its impact due to direct pathological outcomes and loss of lives, Malaria has a great impact on socio-economic success in endemic regions since even mild disease influences productivity and incurs costs for treatment and prevention, worsening the situation of already poor countries (Sachs and Malaney, 2002). Additionally malaria endemicity broadly overlaps with the presence of so called neglected diseases like Chagas disease, Human African trypanosomiasis (sleeping sickness), Onchocerciasis (river blindness), helminthiases, Dengue fever or Snakebites.

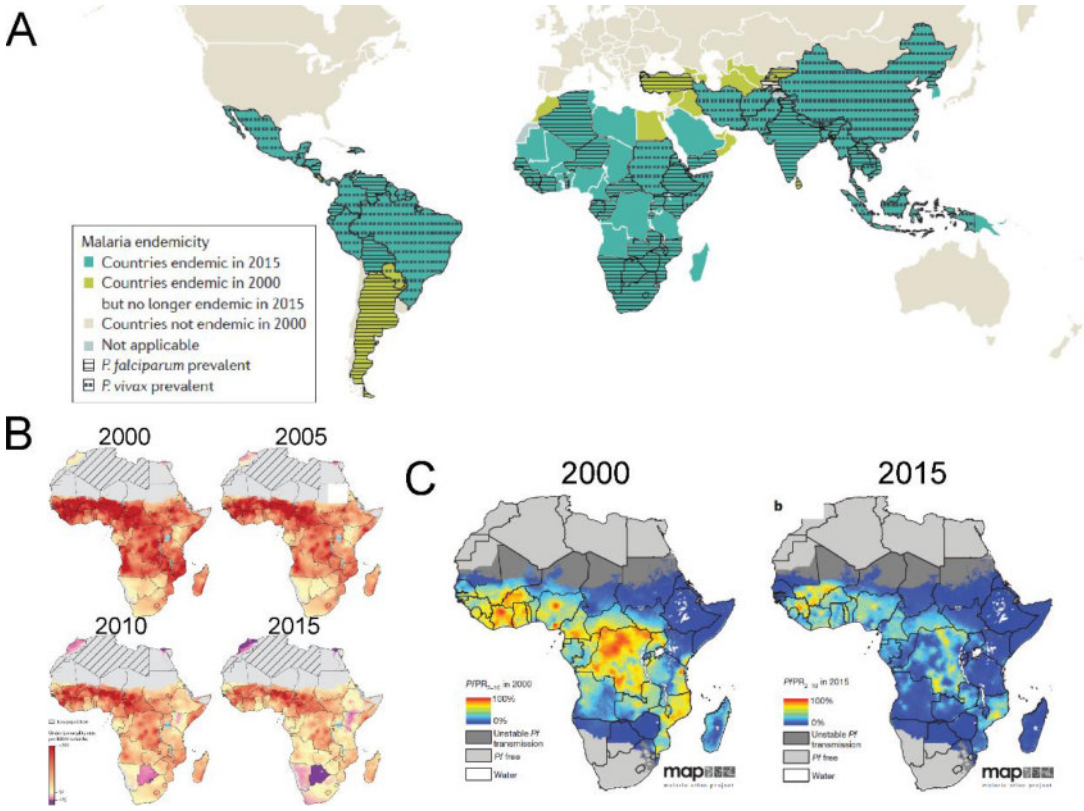

Figure 1: **Malaria endemicity. A)** Map of Malaria endemic regions (also distinguishing between *P. falciparum* and *P. vivax* prevalence) showing countries that eradicated Malaria in between 2000 and 2015 (light green) and countries were Malaria is still endemic in 2015 (turquoise) (Phillips et al., 2017). **B)** Heat map of African countries showing the under-5 overall mortality rate in years 2000, 2005, 2010 and 2015 showing a decline in mortality rates (Golding et al., 2017), **C)** Effect of malaria control shown by decline in infection prevalence in between years 2000 and 2015 indicated by the heat map (Bhatt et al., 2015).

1.1.2 Clinical presentation of Malaria and underlying causes

The clinical symptoms of Malaria depend on the developmental stage of the parasite (Buffet et al., 2011) (section 1.2.1). After the asymptomatic infection of the parasite in the liver (incubation period), the parasites continuously infect, grow and multiply in red blood cells (Ashley and White, 2014; Bartoloni and Zammarchi, 2012). Subsequent rupture of the host cells and the release of the digestion product hemozoin and other molecules such as glycosylphosphatidylinositols trigger the immune system, resulting in inflammatory disease symptoms like malaise, loss of appetite, headache, nausea, muscle ache, sweating and fever (Bartoloni and Zammarchi, 2012; Oakley et al., 2011; Schofield et al., 2002). Due to the massive burden for the spleen and the liver these organs can develop splenomegaly and hepatomegaly (McGregor et al., 2015; Walters and Mc, 1960). The liver can turn dark because of the accumulation of hemozoin in this organ. These symptoms do not allow a clear differentiation from other febrile diseases during diagnosis but periodically re-occurring fever attacks are a typical sign for malaria species other than *P. falciparum*. The periodicity is based on the length and the synchronicity of the blood stages of the respective *Plasmodium* species. *P. vivax* and *P. ovale* induce fever every third day (tertian malaria) whereas *P. malaria* leads to fever every fourth day

(quartan malaria). Since *P. falciparum* stages are not growing synchronously the fever attacks are irregular (Bartoloni and Zammarchi, 2012; Collins and Jeffery, 2005). It is noteworthy that the clearly periodic fevers are often concealed due to mixed infections, resulting in fever-re-occurrence-patterns that are atypical for the infecting species and hence compromise diagnosis on this fact alone.

There are two main reasons for clinical outcomes of *P. falciparum* malaria: anemia and cerebral malaria. Increased Splenic lysis and red blood cell (RBC) lysis by the parasite can result in hemolytic anemia (the decrease of the total amount of red blood cells) (Buffet et al., 2011; Kai and Roberts, 2008). The unique abilities of *P. falciparum* to bind to other infected RBCs (autoagglutination), to uninfected RBC (rosetting) and to the endothelium of capillaries (cytoadherence) is believed to be a main reason for its increased pathology compared to the other malaria species (Doumbo et al., 2009; Miller et al., 2002). Rosetting and cytoadherence are thought to result in the sequestration of the infected red blood cells in small capillaries primarily in the brain and the placenta of pregnant women, but also in the kidneys, heart, lung, and liver (Spitz, 1946). This phenomenon can lead to a disrupted blood flow (Maier et al., 2009), causing organ failure due to hypoxia and lactic acidosis (Miller et al., 2013). A combination of obstruction of blood vessels and the blood-brain-barrier, reduced blood flow and inflammatory effects causing edema and axonal injury seem to play an important role in cerebral malaria (CM) (Hunt et al., 2006; Kampondeni et al., 2013; Medana and Turner, 2006; Wassmer et al., 2015). This was confirmed in analyses of brains post mortem always showed sequestration of RBC in capillaries of the brain (Milner et al., 2014; Wassmer et al., 2015). Imaging of brains of comatose Malaria-patients using magnetic resonance imaging (MRI) suggested that cerebral swelling is finally accountable for CM in African children (Potchen et al., 2012) but this could just partly be reproduced with adult patients in India (Maude et al., 2014; Mohanty et al., 2017). The exact cause and effect in Cerebral Malaria (CM) is not completely clear to date. Interfering with the function of blood vessels also affects pregnant women by causing placental malaria. Reduced supply of the growing embryo impacts birth weight and can reduce the chance of survival for the embryo or the newborn child (Gaccioli and Lager, 2016; Spitz, 1946).

1.1.3 Combating Malaria – chemotherapy, vector control and vaccine development

1.1.3.1 Decrease in Malaria and initiatives

The international political will to combat malaria led to the implementation of several global federal and private organizations and programs like the malaria consortium, Malaria No More UK, WHO Global Malaria Programme, Malaria Eradication Scientific Alliance, Bill and Melinda Gates Foundation (endmalaria2040) and the Roll Back Malaria Partnership.

Considering that Malaria used to be also widespread in Europe, Asia and Oceania, the campaign against Malaria could be seen as at least partially successful. Nevertheless, in other regions of the world the situation improved less and a recent surveillance (1.1.2) showed that still many people suffer

from this disease (Figure 1 A). Different strategies have been applied in the past to eliminate or reduce Malaria. However, many of the applied measures face problems due to their negative ecological impact, reduced compliance of the target population, reduced availability of treatments or resistance of the parasite against drugs.

According to the WHO Malaria Report the disease is in decline and two more countries were certified as malaria free in 2016 and 21 more countries are considered to have the potential to eradicate Malaria by 2020 ("E-2020 countries") (WHO, 2017). Remarkable achievements were reported from Africa, where declining incidence rates are recorded in many regions (Bhatt et al., 2015), and this correlates with a generally reduced number of deaths (Figure 1 B and C).

Despite of these successes, the planned eradication of malaria may hold further challenges. In fact, the mortality rates has remained stable in regions of South-East Asia, the Western Pacific and Africa, between 2015 and 2016 and no further decline was noted (WHO, 2017). In some countries in the Eastern Mediterranean and the Americas previously, considered success stories, incidence rates and mortality have even increased, mostly due to humanitarian crisis such as warfare (WHO, 2017). Lessons learned from the past show that eradication cannot just be achieved with focusing on one aspect or tool but rather by integrating improved diagnostics, development of better chemotherapies, development of vaccines, vector control, block of transmission and improved health care and treatment in endemic countries.

1.1.3.2 Measures against Malaria

1.1.3.2.1 Chemotherapy

Chemotherapy against Malaria dates back to colonial time in the 17th century when the bark of Cinchonoidae (chinchona tree) was used to treat fever (Foley and Tilley, 1998; Miller et al., 2013) and even earlier in South East Asia the plant *Artemisia annua* was used to heal Malaria in traditional Chinese medicine (Klayman et al., 1984; Miller and Su, 2011). The active molecule in the chinchona tree bark is Quinine, of which several derivatives (e.g Chloroquine, Mefloquine, Lumefantrin) have been produced, targeting mostly trophozoite and schizont stage parasites (1.2.1) because these are the stages mostly ingesting and digesting hemoglobin (1.4). These drugs inhibit the polymerization of hemozoin in a special compartment (the food vacuole, 1.2.3 and 1.4), the digestion product of hemoglobin, causing the accumulation of toxic hemozoin. Other drugs are Antifolates (proguanil, trimethoprim, pyrimethamine), targeting purine and pyrimidine synthesis which are important for synthesis of DNA (Gregson and Plowe, 2005; Olliaro et al., 2001). Atovaquone inhibits the electron transport chain in the parasite's mitochondria. Parasites that are resistant to this drug fail to transmit through the mosquito preventing distribution of the resitant conferring allele (Goodman et al., 2016). The predominantly used drug is Artemisinin (in combination with other drugs such as mefloquine,

lumefantrine or piperaquine; termed artemisin-based combination therpy, ACT) and its derivatives artemether, artesunate, and dihydroartemisinin. Their mode of action is just partly understood to date but seems to rely on the formation of radical oxygen species (ROS) and subsequent oxidative stress (Bray et al., 2005; Straimer et al., 2015; Tilley et al., 2016).

Unfortunately, resistance occurred for all so far used anti-malarial drugs. For instance, for the widely used drug Chloroquine that was introduced in 1934, resistance was reported as early as in the 1957 (Payne, 1987). Parasite resistance by expelling the chloroquine out of the food vacuole based on a mutation in the gene for the chloroquine resistance transporter (*crt*) (Fidock et al., 2000; Johnson et al., 2004; Pulcini et al., 2015; Wellems and Plowe, 2001). Resistance to folate inhibitors is conferred by mutations in the targeted enzyme DHFR and DHPS, resulting in reduced affinity for the compound (Gregson and Plowe, 2005; Nzila, 2006). The molecular basis of resistance to artemisinin is unclear. Several molecular markers for resistant strains have been identified of which a C589Y-Mutation in the PfKelch13 gene is the most prominent (mainly a marker for resistance in South-East Asia) (Ariey et al., 2014). Other mutations are also able to confer resistance, particularly in Africa where the quest for markers is still ongoing (Adams et al., 2018).

1.1.3.2.2 Vector and transmission control

Instead of targeting the parasite itself, also its vector, the anopheles mosquito, can be reduced in numbers in order to prevent transmission of the disease. Since many insecticides are available for use in agriculture and pest control, this approach did not demand development of products specifically for malaria control. In fact the eradication of Malaria in Europe and northern Amerika was carried out using DDT in between 1943 and 1972 although this substance is now banned for use in larger amounts due to its negative impact on the ecosystem (Enayati and Hemingway, 2010; Turusov et al., 2002). In some small scale applications DDT is still used for in-house-spraying in Africa because its benefits for human health outweigh its negative effect (Sadasivaiah et al., 2007). However, resistant mosquitoes are also already present (Pluess et al., 2010).

New genetic tools like CRISPR/Cas and the gene drive technology allow novel approaches to create infertile mosquitos that after release can destabilize mosquito-population or to generate mosquito that cannot be infected by *Plasmodium* parasites to break transmission (Eckhoff et al., 2017; Gantz et al., 2015; Hammond et al., 2016). However, the impact of introducing these genetically modified organisms into the ecosystem and the stability of these systems is a matter of discussion in both,the scientific as well as in the public sector (Pennisi, 2015). The currently most effective malaria control measure is the use of insecticide-treated bednets (ITNs) which protects humans from the actual transmitting bite by the mosquito. Even though that resistance against pyrethroids, the only insecticide certified for use in bednets, is reported in 81 % of malaria endemic countries, it is still an effective protection due to its function as a physical barrier (WHO, 2017).

1.1.3.2.3 Vaccination

Vaccination against higher organisms (organisms other than bacteria or viruses) appears to be difficult and also applies for *Plasmodium* parasites. This is likely due to the complex biology of this parasite, its capability to evade the immune system, genetic polymorphisms and antigenic diversity. Since there is naturally acquired, shortly lasting semi-immunity in people living in endemic regions due to multiple exposure and regular infection, it was thought that immunization could also be induced by vaccination. The only immunization strategy that so far showed a significant protection of up to 100 % was the immunization with sporozoites, which resembles the natural infection after the bite of the mosquito (extensively reviewed in António M. Mendes, 2017; Hollingdale and Sedegah, 2017). This approach was already tried by the French scientist Sergent in 1910 (Sergent, 1910) but was brought to a scientific breakthrough with administering attenuated sporozoites, first as proof of concept in mice and later also in humans (Clyde et al., 1973; Nussenzweig et al., 1969; Nussenzweig et al., 1967; Rieckmann et al., 1979). The feasibility of this vaccine is still under discussion, since the production of the sporozoites still needs to be done by infecting mosquitos and a high number of sporozoites is needed for each injection. In the endemic regions infection with different heterologous parasite strains occurs which demands a vaccine that protects against all parasite strains. Different modifications of the approach by using genetically or chemically attenuated sporozoites (GAPs or CAPs) or co-administration of attenuated sporozoites and anti-malaria drugs (controlled human malaria infection, CHMI) have been tried and are still under development to get a better immunization. For instance such efforts have led led to the production of larger scales of highly purified GAP-sporozoites by the company Sanaria® that is used in clinical trials and confers protection against heterologous *Plasmodium* strains (Lyke et al., 2017). Even though that the level of immunity seems promising, the usability of this sporozoite-based-vaccine remains questionable due to challenges in terms of upscaling production, storage, administration and long term immunogenicity (Richie et al., 2015). Recently also chemo-attenuated sporozoites have been used to induce protection in humans and will also go into clinical trials in Africa (Mordmuller et al., 2017).

Further vaccine strategies are the administration of vaccines acting on the liver stage or of antibodies, instead of antigens, targeting different steps in the *Plasmodium* life cycle. The most developed vaccine is a typical sub-unit vaccine called RTS,S in combination with the adjuvants AS01E (Mosquirix®) which is based on the circumsporozoite protein (CSP) bound to a carrier matrix of the hepatitis B surface antigen (HBsAg). The development of this vaccine required more than 35 years and was finally pushed forward by the RTS,S Clinical Trials Partnership 2012 resulting in clinical trials. The fact that a protection in African children of 56 % in acquisition of Malaria and a 47 % reduction for progression to severe malaria was achieved in a phase 3 clinical trial (RTS, 2015) in addition to the lack of other commercially viable vaccines led to the approval of Mosquirix® by the European Medicine Agency (EMA) (RTS, 2015; Vekemans, 2017). Follow up epidemiological studies raised concerns since the long term effects of the vaccination are not fully understood and might even elevate

risk due to lack of the more complex naturally acquired immunity after the protection by the vaccine vanished (Olotu et al., 2013; Olotu et al., 2016).

The emergence and spread of resistances to all commercially available antimalarial drugs and insecticides, the lack of a commercially available highly efficacious vaccine and the fact that the effect of other measures such as insecticide treated bednets is already exhausted and cannot further contribute to lower malaria incidence, highlights the need for new tools and drugs. A key approach to identify vulnerabilities of malaria parasites is to better understand its biology.

1.2 *Plasmodium* biology

During its development (section 1.2.1) the parasite undergoes several drastic morphological changes to adapt to its biochemical and physical needs of each developmental step.

1.2.1 The life cycle of Plasmodium falciparum

P. falciparum is an obligate intracellular parasite that develops in a heteroxenous life cycle switching between the definitive host (female anopheline mosquito) and the intermediate host (vertebrate). The life cycle of is divided into three parts: The sexual mosquito phase, the asexual human liver phase (extraerythrocytic phase) and the asexual human blood phase (intraerythrocytic cycle) (Figure 2), leading to the typical clinical symptoms (1.1.2). Some parasites are committed early in the intraerythrocytic cycle to undergo differentiation into sexual male or female stages (gametocytes). These stages are capable to develop further in the mosquito host after being taken up during the blood meal (Sinden, 2009). Inside the mosquito midgut the female gametocyte develops into the haploid macrogamete which is fertilized by microgametes (deriving from exflagellation of the microgametes), forming the diploid zygote. The zygote further develops into the motile ookinete that leaves the midgut via the epithelium and arrests in the midgut tissue were it forms the immobile oocyst. Within the oocyst hundreds of sporozoites are formed over the course of 10 to 12 days (Aly et al., 2009; Sinden, 2015). Once the oocyst is mature, the sporozoites are released and are transported to the salivary glands from where they can again be injected into a vertebrate host (Aly et al., 2009; Matuschewski, 2006; Sinden, 1974; Sinden, 2009).

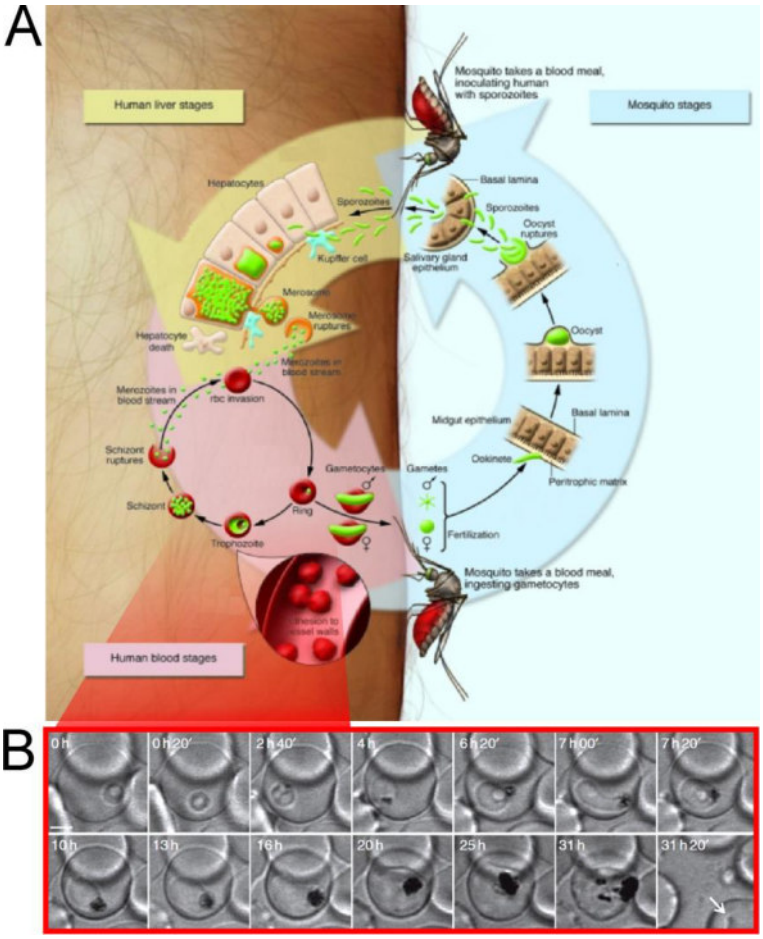

Figure 2: **Life cycle of *P. falciparum*. A)** Illustration of the complete life cycle of *P. falciparum* with mosquito stage (light blue bold arrow), human liver stage (yellow bold arrow) and human blood stages (pink bold arrow). Parasites are in green. Host cells are in red (red blood cells) or bright pink (hepatocytes). Cells of the midgut epithelium are in brown. (Modified from Greenwood et al., 2008). **B)** Live cell images of the *P. falciparum* blood stages developing through ring stages (0-0h20'), trophozoite stages (2h40'-16h) to the schizont stage (20h-31h) and subsequent rupture of the schizont releasing merozoites for re-infection (white arrow) of a red blood cell (31h20h). Accumulation of the hemozoin crystals is apparent as black matter in the food vacuole. Times represent duration of the experiment (not the parasite's age). (Modified from Gruring et al., 2011).

1.2.2 The asexual, intraerythrocytic phase of the life cycle (blood stages)

The asexual development of *P. falciparum* parasites in red blood cells starts with invasion of liver-merozoites, or merozoites from blood stage schizonts after fulfilled replication in a red blood cell. This highly organized process is well understood: First the recognition of and the attachment to the host cell is initiated with the help of merorozoite surface proteins that bind to host cell receptors (Cowman and Crabb, 2006). Then the merozoite re-orientates with its axis orthogonal to the RBC-membrane, bringing its apical tip into contact with the red blood cell. This process also marks the time point where the first elements of the invasion cascade are released from the apical organelles (mainly EBA from the micronemes and PfRH from the Rhoptries; 1.2.3). The release of these ligands facilitates a stronger attachment and induces modifications of the host cell cytoskeleton (Harvey et al., 2012; Weiss et al., 2016). Next a structure called the 'tight junction' is formed by interaction of Rhoptry derived RON-proteins and the Apical Membrane Antigen 1 (AMA1), working as a gasket in between host cell and parasite plasma membrane through which the parasite slides into the host cell (Baum, 2008; Baum et al., 2008). The force to enter into the RBC is generated by an actin-myosin motor complex (Baum et al., 2006; Tardieux and Baum, 2016). During invasion the parasite is surrounding itself by a second membranous vacuole, the parasitophorous vacuole (PV), were he resides in for the

rest of the intraerythrocytic life cycle. After invasion the parasite is termed the ring stage (named after its signet ring-like appearance in Giemsa stained thin blood smears).

Ring stages intensively modify the RBC by exporting parasite derived proteins into the RBC cytosol in order to establish a niche supporting parasite development inside the RBC which is basically a hemoglobin-filled membranous sac and contains no organelles and reduced metabolic capacities which can be used by the parasite (Cooke et al., 2001; Marti et al., 2005). Export into the RBC is mediated via the secretory pathway into the PV and then translocated into the RBC-cytosol by the PTEX-translocon complex (Beck et al., 2014; de Koning-Ward et al., 2009; Elsworth et al., 2014; Mesen-Ramirez et al., 2016). Exported proteins share the PEXEL-sequence motif which undergoes cleavage in the ER and licenses the protein for the export pathway (Boddey et al., 2016; Chang et al., 2008; Russo et al., 2010). There are also PEXEL-negative exported proteins (PNEPs), which are lacking this distinct sequence, but are still exported via an unknown amino acid signal (Gruring et al., 2012; Spielmann and Gilberger, 2010). Host cell modifications include membranous structures that are involved in the trafficking of exported proteins termed 'Maurer's Clefts' and protrusions on the host cell surface termed 'knobs' where the major parasite virulence factor termed PfEMP1, the protein mediating sequestration (1.1.2), is concentrated. Nutrient delivery is maintained by establishing small pores or channels in the RBC membrane termed the New Permeation Pathway that conducts transport of molecules, most importantly for the glycolysis metabolism, the main energy source of the intraerythrocytic parasite (Alkhalil et al., 2004; Desai, 2012; Staines et al., 2007).

Ring stages are mobile in the host cell and cycle between circular and amoeboid, star-fish-like shapes (parasite age 0 to ~18 hours post invasion) and do not grow much. With the transition to the following trophozoite stage (*trophos*: greek for feeding), the parasite arrests inside the RBC (Gruring et al., 2011). The trophozoite stage ranges from ~18 to ~36 hours post invasion and is characterized by a roundish or oval shape and rapid growth until it fills out almost the entire host cell. A key process during this growth phase is the continuous uptake of up to 80 % of the RBC cytosol which mostly contains hemoglobin. This uptake is termed host cell cytosol uptake (HCCU). Less than 20% of the ingested proteins as amino acid source (Krugliak et al., 2002). It therefore is possible that HCCU is needed to gain space for the rapid growth of the parasite rather than for feeding purposes (Krugliak et al., 2002). Independent of its purpose, HCCU and the ensuing hemoglobin degradation is essential for the parasite's survival (Liu et al., 2006). A prominent feature of trophozoites is the malaria pigment, a black crystal structure made of hemozoin, the digestion product of ingested hemoglobin, which is stored in a lysosome-like compartment called the food vacuole (FV).

The trophozoite developes into a schizont, the stage in which the infective merozoites are formed. The parasites undergo multiple mitotic divisions in a manner called schizogony, a form of mitosis were asynchronic nuclear division occurs without condensation of the chromosomes and no parallel cell division (starting at ~30 hours post infection), resulting in a syncytium of 8 to 32 nuclei in *P.*

falciparum. Afterwards the merozoites are assembled in a process that includes the segregation of the mitochondria and apicoplast, formation of the IMC and the PPM and the *de novo* generation of the apical complex (Francia and Striepen, 2014; Kono et al., 2012; van Dooren et al., 2005). The mature schizont ("segmenter") releases the merozoites into the blood stream (egress). This process is induced by parasite factors in a highly organized cascade: disintegration of the PVM, poration of the RBC-membrane and destruction of the RBC-cytoskeleton (Blackman and Carruthers, 2013; Thomas et al., 2018).

Transmission by infection of mosquitos is dependent on the formation of male and female gametocytes. These stages derive from blood stage parasites that commit to gametocytogenesis, a deviation from the normal blood stage development leading to the formation of these stages. Commitment to gametocytogenesis occurs early in the young blood stage parasite (Bruce et al., 1990; Josling and Llinas, 2015) and takes place in the bone marrow (Aguilar et al., 2014; De Niz et al., 2018; Farfour et al., 2012). The developing gametocyte pass through distinct morphological stages (I to V) of which just the stage one (on its way to the bone marrow) and mature stage V-Gametocytes are present in the peripheral blood stream (Butterworth et al., 2013).

1.2.3 Parasite specific organelles of *Plasmodium* blood stage parasites

The defining morphological stages, classifying *Plasmodium* into the Phylum Apicomplexa (Chromalveolata), are the Sporozoite and Merozoite stages. In contrast to other pathogens like bacteria or viruses, Apicomplexan parasites are able to actively penetrate and invade the host cell. The extracellular stages are characterized by an elongated or roundish shape, a flattened membrane system beneath the parasites plasma membrane (termed the 'inner membrane complex' formed by alveols) and specialized organelles located at the apical tip (apical complex). These structures enable the parasite to move (gliding motility of the sporozoites) and to invade the host cells (invasion of sporozoites and merozoites). The apical complex consists of the flask shaped rhoptries, small and elongated micronemes, vesicular dense granule, exonemes and possibly the cytoskeletal conoidal ring (Wall et al., 2016). Further structures crucial for invasion are subpellicular microtubuli and the inner membrane complex. These organelles act together during the invasion process by secreting their content or to serve physical functions. The formation of these organelles (rhoptries, micronemes, dense granules) during merozoite and sporozoite biogenesis is just partly understood but it seems that proteins typically involved in endocytosis in model organisms were repurposed for this secretory pathway in Apicomplexans (Kremer et al., 2013; Pieperhoff et al., 2013; Tomavo et al., 2013).

Once inside the host cell, the parasite loses all of these defining organelles and forms distinct stages that are typical for each phase of the life cycle (1.2.1). As a protozoan cell, malaria parasites contain most of the typical eukaryotic organelles like a nucleus, mitochondrion, endoplasmic reticulum (ER) and a Golgi apparatus. The Mitochondrion as well as the Golgi seem heavily reduced in shape or function in the blood stages (Bannister et al., 2000a; Bannister et al., 2004; Lee et al., 2008; Struck et

al., 2008) but an efficient and substantial secretory pathway trough ER and Golgi is present (Deponte et al., 2012; Lee et al., 2008; Romisch, 2012). The genome of the mitochondrium in *P. falciparum* is reduced encoding just three proteins and many genes for mitochondrial proteins have been transferred to the nucleus (Vaidya and Mather, 2009).

Another Apicomplexa-specific organelle, which is maternally inherited (Okamoto et al., 2009) and present throughout the entire life cycle (Stanway et al., 2009), is the Apicoplast, a plastid with four membranes that likely originates from secondary endosymbiosis of a red algae (Keeling, 2008; McFadden et al., 1996). The apicoplast might have served as a supplier of energy through photosynthesis but lost this ability during the course of evolution. Like for the mitochondrium, most parts of its genome was transferred to the nucleus and the gene products are transported back to the apicoplast (Heiny et al., 2014; Spork et al., 2009). The metabolic function is limited to the synthesis of isoprenoid precursor biosynthesis (Yeh and DeRisi, 2011).

Lysosomes, the cellular vesicular digestive compartments, are common features of eukaryotic cells. Some Apicomplexa do also contain similar organelles but the lysosomal-like compartment of *Plasmodium* attracted special attention due to its very obvious content, the hemozoin crystal. The simple microscopical detection of this also called “Malaria pigment” is used to detect *Plasmodium* infections since the early days of malaria diagnosis. Hemozoin is the product of the degradation of hemoglobin in a well characterized protease pathway (involving for example falcipain, plasmepsin I and II). This degradation releases heme which is partly degraded and a proportion polymerizes to hemozoin (identical to the synthetic β-hematin) (Ginsburg and Krugliak, 1999; Gluzman et al., 1994; Goldberg and Slater, 1992; Pagola et al., 2000). Even though hemozoin is able to polymerize autocatalytically (Egan, 2008), it is suggested that this process is additionally catalyzed by parasite factors which are still under discussion (Pandey et al., 2003; Sullivan et al., 1996). The genesis and storage of hemozoin must take place in a membrane bound compartment because of its toxic effects resulting from enzyme inhibition, peroxidation of membranes and production of reactive oxygen intermediates (Atamna and Ginsburg, 1993; Gluzman et al., 1994). The FV has an acidic lumen to facilitate the lysosomal environment needed for digestive processes and is formed *de novo* in each young trophozoite, possibly by fusion of smaller lysosomal vesicles already present in the ring stages (Abu Bakar et al., 2010; Bannister et al., 2004; Ehlgen et al., 2012; Hanssen et al., 2011).

1.3 Endocytosis in model organisms

Endocytosis describes the uptake of extracellular material into the cell via invaginations or protrusions of the plasma membrane. Endocytosis results in the presence of endocytic vesicles or tubular intermediates (CLICs) inside the cytosol which are then subjected to endocytic trafficking routes like degradation in the lysosomal pathway or transport back to the cellular surface via the recycling pathway. Some endocytosis pathways first direct their cargo to intermediate compartments (for example caveosomes or GEECs) (Wieffer et al., 2009). Endocytic mechanisms are classified based on

the characteristics of the cargo (solutes or particles), size of the cargo (volume of soluble portion, size of particles ranging from macromolecules to whole cells or bacteria), the size and the shape of the resulting vesicle, the proteins mediating uptake (for example Clathrin mediated or not) which defines the mechanism of vesicle formation (reviewed in de Carvalho et al., 2015; Doherty and McMahon, 2009; Mayor and Pagano, 2007; Wieffer et al., 2009). Currently, endocytic events are divided into clathrin mediated endocytosis (CME, "classical endocytosis") and several clathrin independent endocytosis pathways (CIE) (reviewed in Mayor and Pagano, 2007) like phagocytosis, micropinocytosis, caveolin 1-dependent endocytosis (caveolae), endocytic type CLIC/GEEC, ARF6-dependent endocytosis or flotilin dependent endocytosis (Figure 3). Phagocytosis and Macropinocytosis are somewhat exceptional since these processes are responsible for ingestion of big portions or big particles. Pinocytosis is comparable to macropinocytosis with a smaller amount of internalized fluid but in some cases also all endocytosis mechanisms that are not phagocytosis are termed pinocytosis since they all lead to the formation of relatively small endocytic vesicles (Mercer and Greber, 2013). The mechanisms are further distinguished in terms of involvement of dynamin (section 1.3.2.1 for function of dynamin).

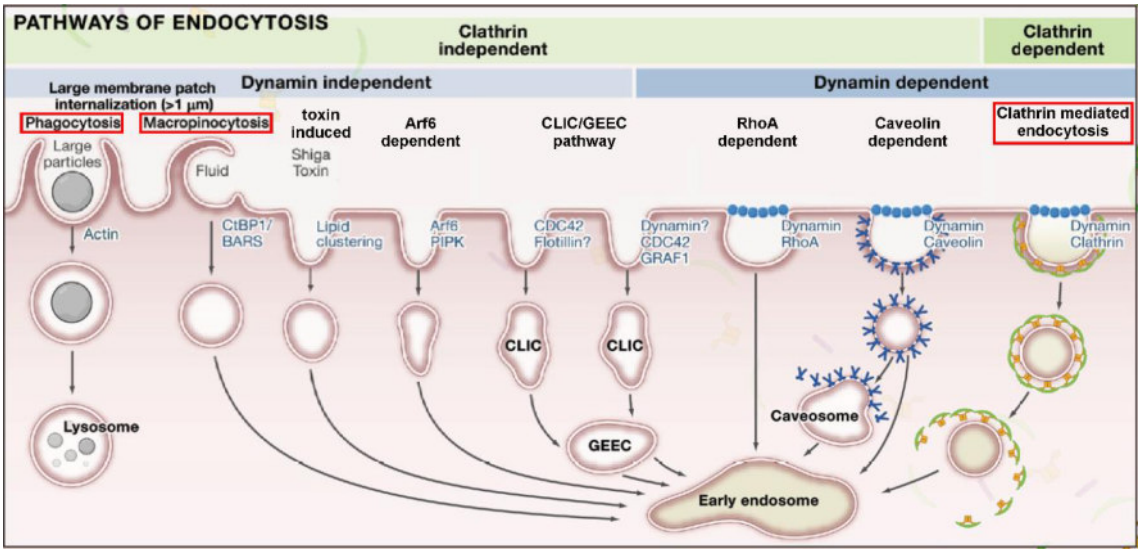

Figure 3: **Endocytosis pathways in model organisms (modified from Wieffer et al., 2009).** Endocytic pathways described in other organisms are shown. Classification upon dependence on clathrin (clathrin mediated endocytosis) or not (clathrin independent endocytosis), involvement of dynamin and types of cargo (phagocytosis and micropinocytosis). Resulting vesicles are depicted with their individual shape, cargo and coat. Structures observed in HCCU of *P. falciparum* are described as Phagocytosis and Macropinocytosis and invaginations of the membrane similar to dynamin dependent endocytic pathways of which clathrin mediated endocytosis is the best investigated pathway in other organisms and therefor choosen here as an example for pit forming uptake mechanisms (encircled by red squares).

1.3.1 Clathrin mediated endocytosis (CME) as an example

Clathrin mediated endocytosis (also Clathrin dependent endocytosis) was first described more than 60 years ago in the oocyte of the mosquito *Aedes egypti* (Roth and Porter, 1964) and became the best investigated endocytosis pathway due to comparably easy visualization and its dominant contribution to the total endocytosis in eukaryotic cells (Bitsikas et al., 2014). CME is a highly orchestrated process were more than 100 proteins dynamically interact with each other and with special lipid species in the membrane. The sequence of events is as follows (Figure 4): 1. Initiation of pit formation (nucleation) and consecutive cargo recruitment, 2. invagination by membrane bending and recruitment of coat proteins, 3. clathrin coated pit (CCP) formation, 4. clathrin coated vesicle (CCV) formation by fission through constriction at its neck. In the following the vesicles are transported along cytoskeletal elements (5.) and concomitantly uncoated (6.) to obtain nascent membranes. The vesicle matures (7.) in order to obtain individual identity for sorting-events to reach its destined destination to finally release its cargo by fusion (8.) with the target organelle. The mechanism of CME was extensively reviewed (Doherty and McMahon, 2009; Kaksonen and Roux, 2018; McMahon and Boucrot, 2011; Wieffer et al., 2009).

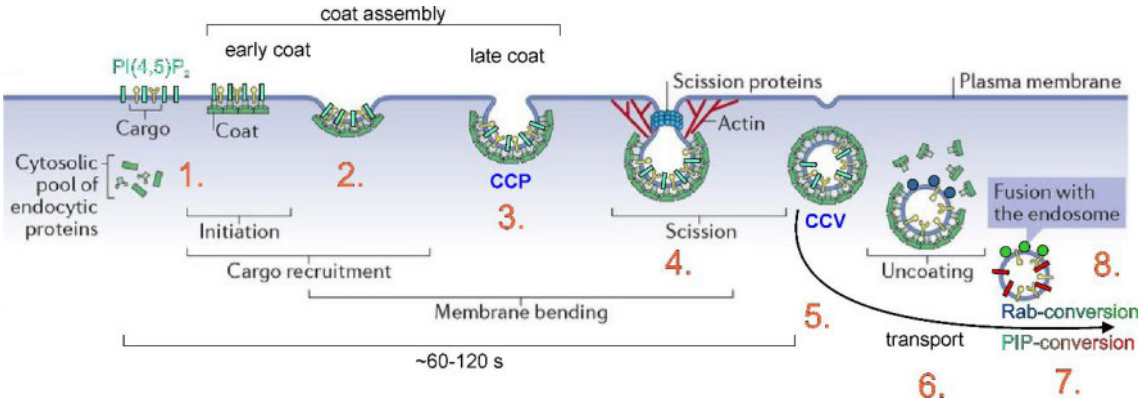

Figure 4: **Critical steps of clathrin mediated endocytosis as an example for endocytosis (modified from Kaksonen and Roux, 2018)**. The following steps are depicted: 1. Initiation of pit formation and consecutive cargo recruitment, 2. invagination by membrane bending and recruitment of coat proteins, 3. clathrin coated pit formation, 4. clathrin coated vesicle formation by fission, 5. transport along cytoskeletal elements, 6. uncoating, 7. maturation and 8. fusion with the target organelle (endosome). Phosphoinositolphosphates (PIP) are represented by light blue and red bars, Rab-proteins are represented by dark blue or green circles. Abbreviations: CCP: clathrin coated pit, CCV: clathrin coated vesicle, $PI(4,5)P_2$: Phosphoinositol (4,5)bisphosphat

1.3.1.1 Vesicle formation

CME is initiated by clustering of adapter proteins, like AP-2 and cargo receptors at domains of the plasma membrane were the phospholipid phosphatidylinositol 4,5-bisphosphat ($PI(4,5)P_2$) is enriched. AP-2 can itself bind $PI(4,5)P_2$ and is recruited via binding to its cargo (Cocucci et al., 2012; Kadlecova et al., 2017; Kelly et al., 2014). This nucleation event defines the site, were the vesicle is going to be formed (also termed pioneer module) and recruits further nucleating proteins like Eps15 (Cocucci et al., 2012; Taylor et al., 2011). Membrane bending needed for pit formation is done by proteins such as Epsin und AP180, which also have $PI(4,5)P_2$-binding-capabilities and are able to interact with the membrane via its ENTH or ANTH domains to induce curvature (Ford et al., 2002; McMahon and Gallop, 2005). The Clathrin binding sites of these proteins and Eps15 can then recruit clathrin and induce clathrin-coat assembly, which might further contribute to membrane curvature and stabilization of the formed membrane-pit (Ford et al., 2002; Lu and Drubin, 2017; Stimpson et al., 2009). During CCP-formation, cargo molecules are clustered and concentrated within the emerging coated pit. At this point the process can still be stopped and the pit aborted (Loerke et al., 2009). In the following, growth of the membrane invagination is facilitated by steady assembly of the coat that becomes more rigid due to incorporation of the clathrin light chain and therefore further stabilizes the pit (discussed in Kaksonen and Roux, 2018). Actin nucleation around the forming pit might additionally contribute to stabilization of the developing structure, at least in yeast (Sun et al., 2006). Once the pit is entirely formed it has to be separated from the plasma membrane. This is done by the GTPase dynamin in cooperation with BAR-domain containing proteins (Daumke et al., 2014; Itoh and Takenawa, 2009; Meinecke et al., 2013). The exact mode of how the constriction of the CCP's neck is achieved is under discussion but relies on GTP hydrolysis by dynamin resulting in a conformational change and compression of the membranes at the neck. BAR-domain proteins contribute by tubulating the membrane, possibly creating the basis for initial assembly of dynamin (discussed in Antonny et al., 2016; Kaksonen and Roux, 2018).

1.3.1.2 Vesicle uncoating, transport and maturation

The endocytic vesicles are transported along the cytoskeleton. In yeast the actin-myosin machinery might be responsible for vesicle-transport (Huckaba et al., 2004) and in mammals the transport happens along microtubules by virtue of kinesins and dynein motor proteins (Kapitein and Hoogenraad, 2011; Lakadamyali et al., 2006). After detachment of the vesicle from the plasma membrane, the vesicles are uncoated by breakage of the clathrin cage by the chaperone HSC70, which is recruited by AP-2, and its interactor auxilin (Barouch et al., 1994; Braell et al., 1984; Ungewickell, 1985). While uncoating of the CCV happens, $PI(4,5)P_2$ is dephosphorylated to Phosphoinositol 4-phsophat (PI4P) (Posor et al., 2015). These alterations of the phosphoinositides (Bissig and Gruenberg, 2013; Di Paolo and De Camilli, 2006) and additional recruitment of small GTPases (Rho-GTPases/ Rab-Proteins) (Rink et al., 2005; Vonderheit and Helenius, 2005) modify the identity of the

vesicle (reviewed in Wandinger-Ness and Zerial, 2014; Zerial and McBride, 2001). They function as molecular switches by changing from the active GTP-bound to the inactive GDP-bound state. The activation or inactivation is catabolized by Guanine nucleotide activating proteins (GAPs) or Guanine nucleotide exchange factors (GEFs), respectively (Guo et al., 2013; Wu et al., 2011; Yoshimura et al., 2010). Rabs together with the AP-2 complex from the initial vesicle formation give rise to characteristics of a formed vesicle that enable precise sorting along the trafficking networks (Schmid and McMahon, 2007). The clathrin-nascent vesicle may acquire Rab5 at this stage, leading it towards the early endosome (Wieffer et al., 2009).

1.3.1.3 Fusion with the target organelle

Fusion of membranes is facilitated by SNARE-Proteins (soluble N-ethylmaleimide-sensitive-factor attachment receptor) (reviewed in Chen and Scheller, 2001; Han et al., 2017; Jahn, 2003; Ungar and Hughson, 2003). These molecules have a stalk-like protein structure and are incorporated either in the donor-membrane of the vesicle (v-SNARE) or in the target membrane (t-SNARE) (Fasshauer et al., 1998) with the stalk extruding from the surface. In the case of endocytic vesicles the v-SNARE would protrude from the vesicle, and the t-SNARE from the early endosome. Both SNAREs interact and go into a docked state. Further alignment of both stalks of v- and t-SNARE pulls both membranes into close proximity (tethering). This ultimately results in mixing of the outer leaflets and fusion of the membranes (Hanson et al., 1997; Rothman and Warren, 1994; Sollner et al., 1993; Sutton et al., 1998). The fusion of membranes must have regulatory mechanisms, since SNAREs should not randomly mediate fusion between membranes (Gerst, 2003; Halachmi and Lev, 1996; Shanks et al., 2012). Several regulating proteins are known, but the exact mode and direction of regulation has so far remained elusive for most of them. Sec1p/Munc18-domain (SM) containing proteins are known to regulate SNARE function (Gerst, 2003; Koumandou et al., 2007; Toonen and Verhage, 2003). This might be done by blocking t- and v-SNARE interaction by binding to the stalks and therefore obscuring/blocking the interaction motifs (Toonen and Verhage, 2003). SM-proteins are known to have positive, as well as negative regulatory functions which differs in between the analyzed cell type and organism (Gerst, 2003; Toonen and Verhage, 2003).

1.3.1.4 The lysosomal pathway

The lysosomal pathway is a well conserved cascade of maturing endosomes in mammalian cells. It starts with the early endosome, which then matures to the late endosome (or multi vesicular body) and finally the lysosome. Each step has its unique identity due to specific phosphatidylinositolphosphates (He et al., 2017; reviewed in Marat and Haucke, 2016) and protein markers, such as Rab-proteins (reviewed in Wandinger-Ness and Zerial, 2014). Since up to 60 Rab proteins are encoded by the human genome, these proteins alone would be capable to establish a complex trafficking network (Stenmark and Olkkonen, 2001).The early endosome (EE) is characterized by Rab5, the presence of PI(3)P in its membrane and the early endosome antigen 1 (EEA1). It is a major hub for sorting of the

initial endocytic vesicles (Eaton and Martin-Belmonte, 2014; Jovic et al., 2010). The decoration with Rab11 (and possibly Rab4) destines a vesicle for recycling back to the plasma membrane (Ullrich et al., 1996), whereas Rab5 to Rab7-conversion leads to transport towards the MVB and the lysosome (Rink et al., 2005). The late endosome and the lysosome are characterized by Phosphoinositide (3,5)bisphosphate ($PI(3,5)P_2$), Phosphoinositol (3,4)bisphosphate ($PI(3,4)P_2$) and Rab7.

The retromer is a protein complex that facilitates the recycling of proteins and cellular components out of the degradative lysosomal pathway (reviewed in Gallon and Cullen, 2015). Retromer trafficking is mediated mostly from early endosome to Golgi but also occurs to other destinations such as the plasma membrane (Seaman et al., 1998). Most prominent elements of the retromer are the sorting nexins (SNX, the mammalian homologues of VPS proteins of the retromer in yeast) that form a complex with BAR-domain containing proteins (Carlton et al., 2004). Another important protein complex for retromer trafficking is the VPS35-29-26-complex (Seaman et al., 1998). Retromer transport is also tightly associated with phosphoinositide-interaction, especially via a phox homology domain (PX) with PI(3)P of the early endosome (Teasdale and Collins, 2012). This pathway is essential for the cellular homeostasis since it retrieves cellular components from degradation and mediates a balanced equilibrium between degradation in the lysosome and recycling by the retromer (Gallon and Cullen, 2015).

1.3.2 Endocytosis factors in model organisms and its homologues in Apicomplexa

Many endocytic proteins and lysosomal trafficking factors known to date were already identified more than 30 years ago in forward-genetics screens in yeast (Bankaitis et al., 1986; Kitamoto et al., 1988; Robinson et al., 2010; Rothman and Stevens, 1986). The so called vacuole is the yeast homologue of the lysosome and therefore the identified factors leading to aberrant vacuoles or vesicular trafficking phenotypes were termed vacuolar sorting proteins (VPS-proteins). Based on their phenotypes they were grouped into five different classes (Banta et al., 1988; Raymond et al., 1992). Subsequent research on individual proteins showed that the VPS-proteins belong to a variety of different protein families that are involved in different trafficking routes ranging from SNARE-proteins, Rab-proteins to Rab-effectors (GAPs and GEFs) or to proteins maintaining the vacuoles or lysosomes acidic environment like vauolar H^+ ATPases (Weisman et al., 1990). These landmark studies represented the starting point for the systematic unraveling of the complex trafficking pathways inside the eukaryotic cell.

The genome of *P. falciparum* encodes many homologues of endocytic factors of which some were already analyzed in more detail and localized in a screen by endogenous GFP-tagging in prior work in our laboratory (Flemming, 2015). Organisation of endocytic pathways can in part be understood from the distribution of PIPs in other organisms (Haucke, 2005; Posor et al., 2015) and the localization of PIPs in *P. falciparum* has been mapped in the different intraerythrocytic stages (Ebrahimzadeh et al., 2018). Except for Phosphoinositol (5)phosphate (PI5P) the distribution of PIPs appears to be stable in

P. falciparum blood stages (Ebrahimzadeh et al., 2018). In *P. falciparum* the lipid PI(4,5)P_2 marks the parasite plasma membrane, comparable to the plasma membrane of eukaryotic cells (Ebrahimzadeh et al., 2018; Kruse, 2014). The phosphoinsotide PI(3)P localizes to the FV-membrane and the apicoplast (Ebrahimzadeh et al., 2018; Tawk et al., 2010), raising the possibility that the FV is an early endosome-like compartment rather than a lysosomal-like compartment. The presence of multiple FYVE-domain and other putative PI(3)P binding domain containing proteins in *Plasmodium* indicates that membrane identity mediated by phosphoinositides is also important in this parasite (Flemming, 2015).

Both, the heavy chain and the light chain of clathrin, the name giving molecule for clathrin mediated endocytosis, are also encoded in the *P. falciparum* genome. Vesicles resembling clathrin coated vesicles, have been observed budding off from the Golgi in *Plasmodium* (Bannister et al., 2000b) which is in agreement with data obtained in *Toxoplasma* where clathrin mediates secretory trafficking from the *trans*-Golgi to the apical organelles (Pieperhoff et al., 2013), but no molecular data on clathrin exists yet for *Plasmodium* parasites. In *T. gondii* trafficking via the Golgi during apical organelle biogenesis was also shown to be dependent on other proteins like Sortilin *(Sloves et al., 2012; Tomavo et al., 2013)* and in *Plasmodium* (Hallee et al., 2018; Krai et al., 2014) and the retromer complex VPS35-29-26 (McGovern and Carruthers, 2016; Sangare et al., 2016) or parts of it (Iqbal et al., 2016; Iqbal et al., 2018). Hence clathrin seems to be repurposed for trafficking to the secretory apical organelles but no function in endocytosis has been shown in Apicomplexans.

Other key players of vesicular trafficking, the adaptor complexes 1 to 4 (AP-1, AP-2, AP-3 and AP-4), but not AP-5 are present in *Plasmodium* parasites (Hirst et al., 2013; Nevin and Dacks, 2009; Robinson, 2004). 11 *rab*-genes, including *rab5* and *rab7* that are homologues of *rabs* involved in endocytosis in other organisms, are found in the genome of *Plasmodium* (Quevillon et al., 2003) which are partly already localized and functionally analyzed. Some showed a conserved localization in comparison to model organisms (PfRab6 at the Golgi) whereas others seem to have been repurposed for a parasite specific function like for example PfRab11 that is involved in membrane formation during merozoites biogenesis and association with the glideosome (Agop-Nersesian et al., 2009) or transport to the micronemes (Kremer et al., 2013). The *rab5*-gene underwent triplication in *P. falciparum*, resulting in three PfRab5-proteins in Plasmodium (PfRab5a, b and c) (Quevillon et al., 2003). Rab5a is just present in red blood cell invading apicomplexans (Rached et al., 2012) and PfRab5a was implicated with host cell cytosol uptake into the FV in *P. falciparum* (Elliott et al., 2008). However, this function was not confirmed in another study, where PfRab5a was found to be important during the merozoite stage (Birnbaum et al., 2017), which might be in agreement with a special role for invasion of RBCs found for TgRab5 proteins in *Toxopolasma gondii* (Kremer et al., 2013). The Rab5b is specific for *Plasmodium* and is potentially modified N-terminally by

myristoylation instead of C-terminal prenylation (Ezougou et al., 2014; Quevillon et al., 2003; Rached et al., 2012). PfRab5b has been localized to the FV and the plasma membrane in *P. falciparum*, which might suggest a role in HCCU although no co-localisation with hemoglobin was detected (Rached et al., 2012). To date, no data is available for PfRab5c.

Eps15 is a well-known component of the early endocytic machinery and its ENTH-domain containing interactor Epsin contributes to membrane bending during pit formation in other organisms (Doherty and McMahon, 2009; Ford et al., 2002). Homlogues of both proteins are also found in *Plasmodium* parasites and based on their spatio-temporal localization thought to be involved in HCCU (Flemming, 2015). Several other ENTH or ANTH-domain containing proteins were identified in the *P. falciparum* (Flemming, 2015) and one of them was shown to be important in formation of the lipid body (a vesicular structure in close proximity to the FV filled with neutral lipids) of late trophozoites (Thakur et al., 2015) but this localization seems to be artefactual (Sabitzki, 2017).

The final step of endocytic vesicle formation is pinching off of the vesicle from its originating membrane. Therefore force needs to be generated to constrict the membranes and induce pinching. This is mediated by the Rho-GTPases Dynamin of which two homologues (the dynamin proteins DYN1 and DYN2) and one dynamin-like protein are found in *Plasmodium*. In *P. falciparum* dynamins are known to be important for fission of the Apicoplast (van Dooren et al., 2005) and might be involved in intracellular trafficking to the secretory organelles in *Toxoplasma* (Breinich et al., 2009). In addition dynamin was linked to HCCU in *Plasmodium* as judged by inhibitor studies (Milani et al., 2015; Zhou et al., 2009).

Another molecule involved in endocytic processes is actin. Actin is encoded twice in *Plasmodium* (*act1* and *act2*) but remains puzzling in *Plasmodium* since it is mainly present as the globular monomeric G-actin (Lazarus et al., 2008; Shaw and Tilney, 1999; Wetzel et al., 2003) and the oligomeric F-actin seems to form just short filaments (Schmitz et al., 2005). As a consequence, intracellular filamentous actin is difficult to visualize in the asexual blood stages of *Plasmodium* (Schuler and Matuschewski, 2006). Actin is important for the invasion process and (Angrisano et al., 2012; Baum et al., 2008; Daher et al., 2010; Das et al., 2017; Opitz and Soldati, 2002) organelle segregation during schizogony in *P. falciparum (Das et al., 2017)* but specific inhibitors indicated also a function in HCCU (Lazarus et al., 2008; Smythe et al., 2008) even though that this is conflicting with data showing that HCCU might be actin-independent (Elliott et al., 2008). Myosins are motor proteins that migrate along actin filaments and are divided into several classes based on their domain structure and function (Foth et al., 2006; Mueller et al., 2017). MyoA was shown to be important during the invasion process (Meissner et al., 2002). Use of a potential Myosin inhibitor suggested that myosins might also be involved in HCCU (Milani et al., 2015).

The *P. falciparum* genome encodes 18 of the SNARE-like proteins (Ayong et al., 2007). Syntaxins, the interactors of the regulating SM-proteins (1.3.1.3), were characterized in other parasitic protozoa (Dacks and Doolittle, 2004) and one of them, pfStx1, the homologue to mammalian syntaxin1, was localized to the plasma membrane in *P. falciparum* (Parish and Rayner, 2009). However, no functional data investigating potential roles of SNARES in HCCU exists to date.

1.4 Host cell cytosol uptake (HCCU) in *Plasmodium*

Already more than 50 years ago first studies on the host cell cytosol uptake, back then termed "feeding", of *Plasmodium* parasites were carried out using electron microscopy (Aikawa et al., 1966a). The parasite is surrounded by two membranes, the parasite plasma membrane and the parasitophorous vacuole membrane, and the electron microscopy studies revealed a tubular or flask-shaped invagination of both membranes, reaching into the parasites cytosol with a narrow neck (the opening towards the host cell) framed by two electron dense areas. This structure is filled with host cell cytosol and was thought to be involved in feeding. Analogous to other protozoa (Aikawa, 1974) this specific feeding structure was named the "cytostome" (*stoma* (greek): mouth or opening; Figure 5 B, C) (Aikawa et al., 1966a; Rudzinska et al., 1965; Slomianny, 1990). Cytosomes can vary in size (160 to 600 nm) and shape (cup shaped, roundish or elongated) and were reported in all parasite stages including rings (Abu Bakar et al., 2010; Elliott et al., 2008; Lazarus et al., 2008; Slomianny et al., 1985; Welch et al., 2011).The cytostomal neck has a rather fixed size of ~ 65 nm (Langreth et al., 1978; Lazarus et al., 2008). Cytostomes are also observed in the merozoites stages, which are not taking up host cell cytosol since they are extraerythrocytic (Beaudoin R. L. , 1972; Garnham et al., 1961) and other Apicomplexan organisms that differ in their biology compared to *Plasmodium* parasites. These structures were also called micropores or ultracytostomes (Levine, 1971; Scholtyseck and Mehlhorn, 1970) and their relation to cytostomes was under discussion (Ferguson et al., 1977). As an example the sporoblast inside the developing oocyst and the final sporozoite of *Eimeria* parasites do also show homologous structures that look very similar in electron microscopy images (Ferguson et al., 1977). Since this stage is present in a completely different niche and represents a different developmental status compared to *Plasmodium* blood stages, this structure might serve different functions in the different Apicomplexans or in different the stages of the *Plasmodium* life cycle.

1.4.1 Models for HCCU in *P. falciparum*

Three different models for mechanisms of HCCU in *Plasmodium* parasites exist (recently summarized in Flemming, 2015) of which two date back to the conclusions made based on the very first ultrastructural studies (reviewed in Sterling, 1972). The main models are shown in Figure 5. It is of note, that these models are based on observations made with different *Plasmodium* species, including species infecting birds, mice, reptiles, apes and humans.

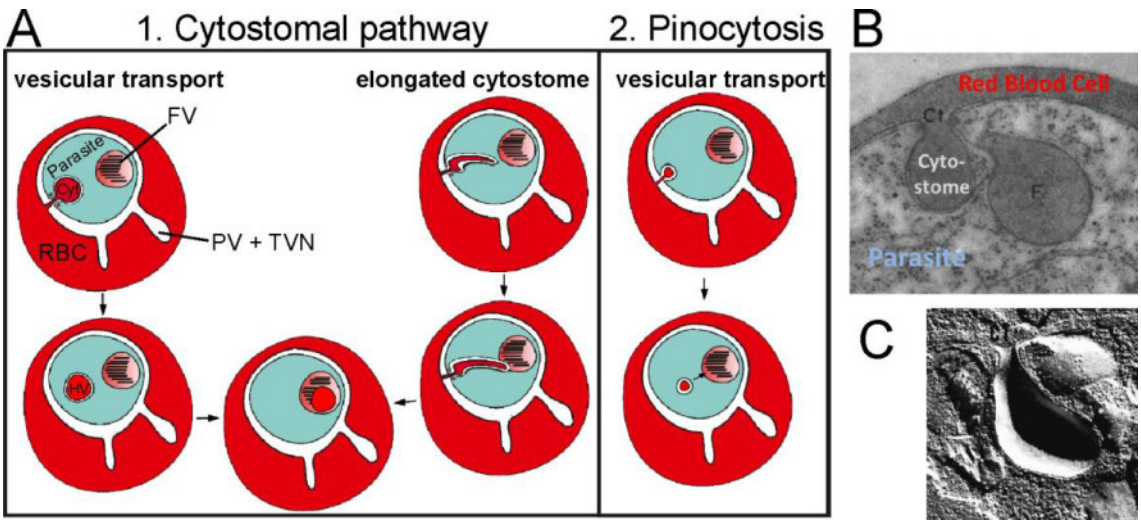

Figure 5: **Models of host cell cytosol uptake (HCCU) pathways in *Plasmodium* blood stages. A)** Summary of the two most prominent models of HCCU (cytostomal pathway or pinocytosis) and their mode of transport (vesicular or elongated cytostome) (modified from Flemming, 2015). Abbreviations: FV: food vacuole, RBC: red blood cell, PV: parasitophorous vacuole, TVN: tubuvesicular network, **B)** Transmission electron microscopy image of a cytostome with its opening to the host cell (longitudinal sectioned) and a cytostome where the connection to the host cell cytosol is not visible (semi-transversal sectioned) (modified from Aikawa et al., 1966a). Invagination of both membranes, the parasitophorous vacuole membrane and the parasite plasma membrane, is visible. **C:** Scanning electron microscopy image of a cytostome after freeze fracturing of the cell showing the lumen of the cytostome and the opening to the host cell (Meszoely, 1972).

The first model was described by Rudzinska and colleagues as phagotrophy (in *P. berghei* infecting rodents) (Rudzinska and Trager, 1958; Rudzinska and Trager, 1959) and the same pathway was later defined as Pinocytosis (in *Plasmodium* infecting humans and monkeys, for example *P. falciparum, P. vivax* and *P. ovale*) (Rudzinska et al., 1965), because the ingested material is a liquid phase with small molecules instead of large particles (Figure 5 A, 1.3) and the observed structures differed in both studies (big flask shaped intrusions of the PPM and PVM versus small microstome-like intrusions). Pinocytosis was also thought to be the uptake mechanisms by other researchers (Blackburn and Vinijchaikul, 1970; Fletcher and Maegraith, 1972) and is still considered in current models based on data generated for the rodent infecting parasite *P. chabaudi* (Slomianny, 1990; Slomianny et al., 1985) or *P. falciparum* (Langreth et al., 1978).

The alternative mechanism is the cytostomal pathway first described by Aikawa in 1966 (Figure 5 A) (Aikawa et al., 1966a; Aikawa et al., 1966b). Since cytostomes share similarity with membrane-invaginations during the formation of endocytic vesicles (1.3.1.1), they may correspond to endocytic uptake structures. It is thought that at the cytostome, a host cell cytosol filled flask shaped invagination characterized by an electron dense collar at its neck (1.2.3), vesicles buds off in a manner similar to endocytosis. These observations were made in several malaria species (Aikawa, 1966; Aikawa, 1971; Aikawa et al., 1969; Aikawa et al., 1966a; Aikawa et al., 1966b; Aikawa et al., 1967; Aikawa and Jordan, 1968; Scorza, 1971). More recent adaptions of these models differ in the mode of how the

distance between the parasites periphery and the FV is overcome. The first model describes a classical transport of cargo filled vesicles that are transported through the host cell cytosol (Yayon et al., 1984). Alternatively it is hypothesized that the cytostom elongates and bridges the parasites cytosol until it reaches the food vacuole and then parts of the cytostom are pinched off concomitantly with the FV contact (Lazarus et al., 2008). Another model combines these two hypotheses, suggesting the bridging of the distance by an elongated cytostom followed by pinching off of small host cell cytosol filled vesicles that are transported across the remaining gap between cytostome and FV (Milani et al., 2015).

As another option there are also models present that suggest both basic uptake processes, phagotrophy and cytostome-mediated uptake (and maybe also phagocytosis), contributing in parallel to the uptake (Cox and Vickerman, 1966; Elliott et al., 2008; Killby and Silverman, 1969; Rudzinska, 1969; Scalzi and Bahr, 1968). Similar to the observations of Rudzinska and colleagues, another study using 3D-EM also came to the conclusion that multiple, stage dependent uptake processes, including a "big gulp"-like event in young blood stage parasites, contribute to HCCU and FV formation in *P. falciparum* (Elliott et al., 2008) and the rodent Malaria pathogen *P. chabaudi* (Wendt et al., 2016). However the "big gulp" could not be observed in live cell imaging of rings (Gruring et al., 2011) or in infected preloaded red blood cells (Abu Bakar et al., 2010; Flemming, 2015).

The plethora of models highlights that it is far from clear how *Plasmodium* parasites actually perform HCCU. All models are based on ultrastructural data obtained and no imaging of HCCU in live cells has been done so far.

1.4.2 Nature of hemoglobin filled vesicles in *Plasmodium*

It is agreed on that the initially formed HCCU vesicles are surrounded by two membranes since they derive from the cytostome or the pinocytic cup which are both invagination of the two surrounding membranes (PPM and PVM) (Aikawa et al., 1966a). The outer membrane, which is derived from the PVM, likely is the membrane that later fuses with the FV-membrane and therefore remains present around the vesicle. The potential desintegration of the inner membrane is controversial: In Chloroquine treated parasites, vesicles surrounded by one membrane were observed inside the FV. This lead to the conclusion, that the vesicles remain surrounded by two membranes and that their fusion with the FV while result in the release of a vesicle being still surrounded by the inner, PPM-derived, membrane. This vesicle could then be quickly digested to release its content into the FV (Yayon et al., 1984). No digestion of hemoglobin was observed in the hemoglobin filled vesicles (Yayon et al., 1984). This observation might have to be revised, since it cannot be excluded that the vesicles were not cytostomes seen in cross section and therefore "false food vacuoles", as already discussed by Aikawa 1971 and Sterling 1972.

Other studies observed that some host cell cytosol filled vesicles were surrounded by just one membrane, indicating that one of the membranes (likely the inner) was digested prior to fusion with

the FV. In this scenario, hemoglobin digestion would begin already inside the vesicles before reaching the FV (Slomianny, 1990) since the destruction of the inner vesicular membrane exposes the vesicular content to the digestion enzyme falcipain II present in the PV space internalised during invagination of the PPM and PVM (Elliott et al., 2008; Klemba et al., 2004).

1.4.3 Proteins involved in HCCU in *P. falciparum*

HCCU in *P. falciparum* was mostly analyzed using inhibitors against proteins involved in endocytosis in other organisms and electron microscopy to visualize the effects on HCCU leading to conflicting data and to date no protein could directly been shown to be involved in HCCU in *Plasmodium*. Actin was studied using actin inhibitors like CythochalasinD and Jasplakinolide, showing that HCCU is actin dependent (Lazarus et al., 2008; Milani et al., 2015; Smythe et al., 2008) whereas another study came to contrary conclusions (Elliott et al., 2008). Inhibitors against Myosins (Inhibitor: BDM) and SNARE-Proteins (Inhibitor: N-Ethanylamide/NEM) showed that these molecules might be involved in HCCU (Milani et al., 2015), however, the inhibitor profile of these compounds in malaria parasites is not clear or might even have strong off target effects (Gruring et al., 2011). DYN1 knock down to a higher amount of cytostomal pit-like structures at the parasite's periphery (Milani et al., 2015) and treatment with the Dynamin-inhibitor Dynasore® led to reduced HCCU (Milani et al., 2015; Zhou et al., 2009). Expression of a constitutively active Rab5a mutant in *P. falciparum* suggested an effect on the uptake structures and size of the FV, implicating a role of Rab5a in HCCU (Elliott et al., 2008) but this function of Rab5a was not confirmed when a conditional knock down that this protein showed had no effect on trophozoite stage parasites (the most active in terms of HCCU,(Abu Bakar et al., 2010)) but showed a phenotype in schizonts (Birnbaum et al., 2017).

1.4.4 Uptake mechanisms in other protozoan parasites

In comparison to other protozoans, the apicomplexans are special due to their obligatory intracellular life style in the vertebrate host. For *Toxoplasma gondii*, the model organism most closely related to *Plasmodium* parasites, has also been shown to endocytose extracellular material via bulk flow, but so far these processes have been investigated to a lesser extend in comparison to other protozoan pathogens (Dou et al., 2014). Based on the data from *Toxoplasma* and recently also in *P. falciparum*, it however is expected that some elements of the endocytic machinery have been repurposed for the biogenesis of the secretory organelles (apical complex) (Breinich et al., 2009; Hallee et al., 2018; Jimenez-Ruiz et al., 2016; Krai et al., 2014; McGovern and Carruthers, 2016; Pieperhoff et al., 2013; Sangare et al., 2016; Tomavo et al., 2013) For intracellular *T. gondii* parasites endocytotic uptake and transport of the endocytosed material to a lysosome like compartment, the vacuolar compartment (VAC), has been shown (ingestion pathway) (Dou et al., 2014). The VAC resembles a plant-like vacuole (VAC/PLV) (Miranda et al., 2010; Pieperhoff et al., 2013) and hence endocytic trafficking might also resemble plants in *T. gondii* (McGovern et al., 2018; Pieperhoff et al., 2013) were endocytosed cargo is transported via the *trans* Golgi to the Rab5 and Rab7-positive early and late

endosomes (Stenmark, 2009). In *P. falciparum* a Rab7-positive endosome-like compartment has been described in addition to the lysosomal food vacuole (Krai et al., 2014). The endosome of *P. falciparum* is in close proximity to the Golgi indicating that trafficking of endocytosed cargo in *Plasmodium* might be similar to the plant-like pathway in *Toxoplasma* (Krai et al., 2014). Even though that the hemoglobin degradation pathway of *Plasmodium* is the parasites Achilles heel for several clinically important drugs (Phillips et al., 2017), the transport processes leading to these steps, i.e. HCCU, is only poorly understood. Since some elements of endocytic pathways seemed to be conserved in other protozoan pathogens, also in *Plasmodium* homologous proteins can be expected to be involved in endocytosis and hence in HCCU. It therefore remains unclear, which proteins need to be targeted to identify the first factors involved in HCCU and to disentangle this pathway from other trafficking pathways inside the Apicomplexan cell.

Many other parasites rely on uptake of extracellular material (also termed heterophagy) for different functions like nutrition, virulence or immune evasion (reviewed in Carruthers, 2015)). Many of these heterophagic mechanisms rely on conserved elements known from eukaryotes (de Souza et al., 2009). Amoebas are known for their extensive uptake of extracellular material via actin-dependent phagocytosis using their pseudopodia. This is also represented by the presence of genes for many endocytic elements in their genome (de Souza et al., 2009) which also holds true for the pathogen *Entamoeba histolytica.* Trypanosomatidae, like *Trypanosoma brucei rhodesiense* and *Trypanosoma brucei gambiense* , the cause of the African sleeping sickness, or *Trypanosoma cruzi*, responsible for the Chagas disease in South America, are also capable of endocytic uptake, which mainly takes place in a specialized membrane compartment termed the flagellar pocket followed by lysosomal digestion in species-specific endosome like compartment named the reservosome (Trypanosoma) or in recycling endosomes (Leishmania) (de Souza et al., 2009; Reyes-Lopez et al., 2015; Ueda-Nakamura et al., 2001). For many of these parasites receptor mediated endocytosis is known, allowing specific uptake of for example hemoglobin or iron (Carruthers, 2015; Reyes-Lopez et al., 2015). The involved proteins can in these organisms. For example, *T. brucei* uses clathrin mediated endocytosis whereas *T. cruzi* relies on a clathrin independent endocytosis pathway (Reyes-Lopez et al., 2015). *Leishmania*, the causative agent of leishmaniosis, also make use of its flagellar pocket for endocytosis but transports the cargo to the so called megasome (Ueda-Nakamura et al., 2001). In *Trypanosomatidae* a typical endosomal pathway is present, consisting of early endosomes, sorting endosomes, multivesicular bodies and lysosomes (Field and Carrington, 2009).

1.5 Aims of this PhD thesis

Albeit host cell cytosol uptake (HCCU) is a key process during the growth of *Plasmodium falciparum* parasites in the red blood cells, it is a comparably poorly understood part of *Plasmodium* biology. Electron microscopy and inhibitor studies indicated that HCCU is an endocytosis related process but no protein has directly been shown to function in HCCU. In previous work typical endocytosis proteins that are present in *P. falciparum* were localized and partly analyzed in the blood stages in an endogenous GFP-tagging screen (Flemming, 2015; Reichard, 2015). Of these one, PfEps15, was found to be a likely candidate to be involved in HCCU but direct functional data was so far missing.

The aim of this thesis was to analyze PfEps15 as well as two further proteins deemed likely to be involved in HCCU, the Clathrin Heavy Chain (one of the best studied endocytosis proteins in model organisms) and VPS45, a protein that upon conditional inactivation in preliminary experiments showed a promising phenotype that may indicate a role in HCCU (Reichard, 2015). Specifically, this thesis was set out to carry out an in depth analysis of these proteins using fast imaging techniques, conditional inactivation using our newly established methodology (Birnbaum et al., 2017), ultrastructural studies and interaction analyses to assess the role of these proteins in HCCU and identify potential interactors that may also be involved in this process. This work is hoped to reveal the first molecules involved in HCCU in malaria blood stages to provide an entry point to unravel the molecular basis for this important process.

2. Materials

2.1 Technichal devices

type	specification	distributor
Agarose gel chamber	Sub Cell GT basic	Bio-Rad, Munich
Analytical Balance	870	Kern
Autoclave	V120	Systec, Wettenberg
Bacterial incubator	Heratherm IGS400	Thermo Scientific, Langenselbold
Centrifuge	J2- HS Ultracentrifuge	Beckman Coulter, Krefeld
Rotor	JA-12	
Centrifuge	Avanti J-26S XP	Beckman Coulter, Krefeld
Rotor	JA-14	
Centrifuge	Megafuge 1.0R	Heraues, Hannover
Centrifuge	Eppendorf table centrifuge	Eppendorf, Hamburg
Confocal microscope	Olympus FV1000	Olympus, Hamburg
Developer	Curix 60	AGFA-Gevaert, Mortsel/Belgium
Developer cassette	Cronex Quanta III	Dupont, Neu Isenburg
Electro blotter	Phase	Bio-Rad, Munich
Electron microscope	FEI Tecnai	FEI, Oregon, USA
Electroporator	X-Cell	Bio-Rad, Munich
Electroporator	Nucleofector II AAD-1001N	Amaxa Biosystems, Germany
Flow cytometer	LSR II	BD Instruments, USA
Fluorescence microscope	Axioscope M1 an M2	Zeiss, Jena
Fluorescence microscope	Olympus IX81 with Cell^R imaging station (MT20 light source)	Olympus, Hamburg
Gel imager	ChemiDoc XRS+	Bio-Rad, Munich
Hamamatsu Digital camera	Orca C4742-95	Hamamatsu Phototonics K.K., Japan
Heated Microscope Stage	Tempcontrol-37 (analog) 1 channel	PeCon GmbH, Erbach
Ice machine	EF 156 easy fit	Scotsmann, Vernon Hills/USA
Laboratory scale	SBA32	Saltec, Göttingen
Laboratory scale	Acculab Atilon-ATL	Sartorius, Göttingen

type	specification	distributor
Light Microscope	Axio Lab A1	Zeiss, Jena
Magnetic stirrer	MR-Hei-Standard	Heidolph, Schwabach
Microtome	Leica EM UC7	Leica, Wetzlar, Germany
Microwave	Micro 750W	Whirlpool, China
Objective Lens Heater	Tempcontrol-mini	PeCon GmbH, Erbach
P. falciparum culture incubator	B6200	Heraeus, Hannover
P. falciparum culture incubator	Heratherm IGS400	Thermo Scientific, Langenselbold
PCR Mastercycler	epgradient	Eppendorf, Hamburg
pH-Meter	SevenEasy	Mettler-Toledo, Gießen
Photometer	BioPhotometer plus	Eppendorf, Hamburg
Photometer	NanoDrop	
Pifoc	PIFOC® Objective Stepper 100 µm economical system	Physik Instrumente (PI), Karlsruhe
Pifoc controller	E-665 PIFOC® controller (PIFOC® 100D System)	Physik Instrumente (PI), Karlsruhe
Pipettes	2 µL, 10 µL, 100 µL, 1000 µL	Gilson, Middleton, USA
Pipettor	Matrix Cellmate II	Thermo Scientific, Schwerte
Pipettor	Pipetboy acu	IBS
Power-supply	Power PAC 300	Bio-Rad, Munich
Roller mixer	SRT6	Bibby Scientific, Stafforshire, USA
SDS-PAGE chamber	MiniProtean TetraCell	Bio-Rad, Munich
Shaking incubator	MaxQ 4000	Thermo Scientific, Schwerte
Sterile bench	SterigardIII, Advance	Baker Company, Standford, USA
Sterile bench	Safe 2020	Thermo Scientific, Schwerte
Thermoblock	Thermomixer 5436	Eppendorf, Hamburg
Ultrapure Water Purification	Milli-Q	Millipore, Bedfort/USA
UV-Transilluminator	Pherolum289	Biotec Fischer, Reiskirchen
Vortexer	Genie 2	Scientific Industries, USA
Vacuum pump	BVC Control	Vacuubrand, Deutschland
Waterbath	1004	GFL, Burgwedel

2.2 Chemicals

reagent	brand/distributor
(4-(2-Hydoxyethyl)-1-piperazineethanesulfonic acid) (HEPES)	Roche, Mannheim
1,4,-dithiothreitol (DTT)	Roche, Mannheim
3-(N-morpholino)propansulfonic acid (MOPS)	Merck, Darmstadt
4',6-diamidino-2-phenylindole (DAPI)	Roche, Mannheim
Acrylamide/Bisacrylamide solution (40 %)	Roth, Karlsruhe
Agarose	Thermo Fisher, Waltham MA (USA)
AlbumaxII	Thermo Fisher, Waltham MA (USA)
Albumin bovine Fraction V (BSA)	Biomol, Hamburg
Ammonium persulfate (APS)	Sigma-Aldrich, Steinheim
Ampicillin	Roche, Mannheim
Bacto™ Pepton	Becton Dickinson, Heidelberg
Bacto™ yeast extract	Becton Dickinson, Heidelberg
Biotin	Sigma Aldrich, Steinheim
Blasticidin S	Thermo Fisher, Waltham MA (USA)
Bromophenol blue	Merck, Darmstadt
Cacodylic Acid- Sodium Salt, TrihydrateSodium Cacodylate	Electron Microscopy Sciences, Hatfield PA (USA)
Calcium chloride ($CaCl_2$)	Sigma Aldrich, Steinheim
Concovalin A	Sigma-Aldrich, Steinheim
Desoxynucleotides (dNTPs)	Thermo Fisher, Waltham MA (USA)
Developer solution G150 (Western blot)	Agfa, Leverkusen
D-Glucose	Merck, Darmstadt
Dihydroethidium (DHE)	Cayman, Ann Arbor, USA
Dimethyl sulfoxide (DMSO)	Sigma-Aldrich, Steinheim
Dipotassium phosphate	Roth, Karlsruhe
Disodium phosphate	Roth, Karlsruhe
DSM1	BEI resources
DSP	Thermo Fisher, Waltham MA (USA)
Dulbecco's Phosphate Buffered Saline (DPBS)	Pan Biotech, Aidenbach
Dulbecco's Phosphate Buffered Saline (DPBS)	Pan Biotech, Aidenbach
Ethanol	Roth, Karlsruhe
Ethidium bromide	Sigma-Aldrich, Steinheim
Ethylene glycol tetraacetic acid (EGTA)	Merck, Darmstadt
Ethylenediaminetetraacetic acid (EDTA)	Biomol, Hamburg

reagent	brand/distributor
Fixation solution G334 (Western blot)	Agfa, Leverkusen
Formaldehyde (10 %)	Polyscience, Warrington PA (USA)
G418 disulfate salt	Sigma Aldrich, Steinheim
Gentamycin	Ratiopharm, Ulm
Giemsa's azure, eosin, methylene blue solution	Sigma-Aldrich, Steinheim
Glutardialdehyd (25 %)	Roth, Karlsruhe
Glycerol	Sigma-Aldrich, Steinheim
Glycine	Sigma-Aldrich, Steinheim
Hoechst33342	Cheomdex, Switzerland
Hydrochloric acid (HCl)	Merck, Darmstadt
Hypoxanthin	Biomol, Hamburg
Isopropanol	Sigma-Aldrich, Steinheim
Magnesium chloride	Merck, Darmstadt
Manganese(II) chloride	Merck, Darmstadt
Methanol	Merck, Darmstadt
Milk powder	Sigma-Aldrich, Steinheim
N, N, N, N-Tetramethylethylenediamin (TEMED)	Sigma-Aldrich, Steinheim
Osmium (VIII) oxide	Electron Microscopy Sciences, Hatfield PA (USA)
Percoll	GE Healthcare, Buckinghamshire (UK)
Phenylmethylsulfonylfluorid (PMSF)	Sigma-Aldrich, Steinheim
Potassium chloride	Sigma-Aldrich, Steinheim
Protease inhibitor cocktail ("Complete Mini")	Roche, Mannheim
Purified water for injection (Ampuwa)	Fresenius Kabi, Bad Homburg
Rapalog (A/C Heterodimerizer AP21967)	Clontech, Mountain View CA (USA)
RPMI (Roswell Park Memorial Institute)-Medium	Applichem, Darmstadt
Rubidium chloride	Sigma-Aldrich, Steinheim
Saponin	Sigma-Aldrich, Steinheim
Sodium acetate	Merck, Darmstadt
Sodium bicarbonate	Sigma Aldrich, Steinheim
Sodium chloride	Sigma-Aldrich, Steinheim
Sodium dihydrogen phosphate	Roth, Karlsruhe
Sodium dodecyl sulfate (SDS)	Sigma Aldrich, Steinheim
Sodium hydroxide	Merck, Darmstadt
Sorbitol	Sigma Aldrich, Steinheim

reagent	brand/distributor
ß-Mercaptoethanol	ß-Mercaptoethanol
Tetanolysin	Sigma, Steinheim
Tetramethylethylenediamine (TEMED)	Sigma Aldrich, Steinheim
Tris base	Roth, Karlsruhe
Tris-EDTA (TE)	Sigma Aldrich, Steinheim
Triton X-100	Biomol, Hamburg
Uranyl acetate dihydrate	Electron Microscopy Sciences, Hatfield PA (USA)
WR99210	Jacobus Pharmaceuticals, Princeton NJ (USA)

2.3 Labware and disposables

item	brand/distributor
CEA RP New Medical X-Ray screen film blue sensitive	AGFA Health Care NV, Mortsel, Belgium
Chromatography paper	Whatman
Conical Falcon tubes (15 and 50 ml)	Sarstedt, Nümbrecht
Nunc Conical Falcon tubes (50 ml) for mass spectrometry	Thermo Fisher, Waltham MA (USA)
Cover slip 24x65 mm Thickness 0.13-0.16mm	R. Langenbrinck, Laboratory and Medicine Technique, Emmendingen
Cryotubes	Sarstedt, Nümbrecht
Culture bottles 50 ml	Sarstedt, Nümbrecht
EM grids (FORMVAR CARBON FILM on 2x1 mm oval slot Copper; FCF2010-Cu)	Electron microscopy sciences, Hadfield PA (USA)
Eppendorf reaction tubes (1.5 and 2 ml)	Eppendorf, Hamburg
Flow cytometry tubes 55.1579	Sarstedt, Nümbrecht
Glass slides	Engelbrecht, Edermünde
Latex Powder-Free Gloves	Kimtech Science EcoShield
Leukosilk tape	BSN medical
Microscopy dishes, uncoated, hydrophobic	Ibidi, Martinsried
Multiply-µStrip Pro 8-Strip PCR-reaction tubes	Sarstedt, Nümbrecht
Nitril Gloves	Kimberly Clark, Koblenz
Nitrocellulose Blotting Membrane Protran (0.45 µm)	Whatman GmbH, Dassel

item	brand/distributor
One way canulass	Braun, Melsungen
One way syringes	Braun, Melsungen
Parafilm	Pechiney, Mühltal
Pasteurpipettes	Brand, Wertheim
Petri dishes (15 x 60 mm and 14 x 90)	Sarstedt, Nümbrecht
Petri dishes (2 ml)	Sarstedt, Nümbrecht
Pipette filter tips 1-10/2-20/20-200/100-1000 µl	Sarstedt, Nümbrecht
Pipette filter tips 1-10/20-200/100-1000 µl	Eppendorf, Hamburg
Pipette tips 1-10/20-200/100-1000 µl	Sarstedt, Nümbrecht
Plastic pipettes (5, 10and 25 ml)	Sarstedt, Nümbrecht
reaction tubes (1.5 and 2 ml)	Sarstedt, Nümbrecht
Sterile filter, 0.22 µm	Sarstedt, Nümbrecht
Transfection cuvettes (0.2 cm)	Bio-Rad, Munich

2.4 Kits

reagent	brand/distributor
NucleoSpin Plasmid	Macherey-Nagel, Düren
NucleoSpin Extract II	Macherey-Nagel, Düren
QIAamp DNA Mini Kit	Qiagen, Hilden
QIAGEN Plasmid Midi Kit	Qiagen, Hilden
Western Blot ECL-Super Signal West Pico Chemiluminescent Substrate Detection Kit	Thermo Fisher, Waltham MA (USA)
Western Blot ECL-Clarity Chemiluminescent Substrate Detection Kit	Bio-Rad, Hercules CA (USA)

2.5 DNA- and Protein ladders

reagent	brand/distributor
GeneRuler™1000 bp ladder	Thermo Fisher, Waltham MA (USA)
PageRuler™ prestained protein ladder	Thermo Fisher, Waltham MA (USA)
PageRuler™ unstained protein ladder	Thermo Fisher, Waltham MA (USA)

2.6 Polymerases and Enzymes

polymerase/enzyme	brand/distributor
FirePol. DNA Polymerase [5 U/µl]	Solis Biodyne, Taipei, Taiwan
Phusion. High-Fidelity DNA Polymerase [2 U/µl]	NEB, Ipswich, USA
Restriction enzymes	NEB, Ipswich, USA
T4 DNA-Ligase [3 U/µl]	NEB, Ipswich, USA
Taq DNA-ligase (40U/ µl)	NEB, Ipswich, USA

2.7 Oligonucleotides

All oligonucleotides were synthesized by Sigma-Aldrich (Steinheim).

Primers for episomal mCherry expression constructs.

Cloned via XhoI and AvrII in pARL2-*hsp86* 5'UTR_Epsin-2xmyc-T2A-1xNLS-FRB-mCherry (BSD^R), (Flemming, unpublished)

Cloned via AflII and NotI in pARL2-*crt* 5'UTR_BirA*-FRB-Cherry (BSD^R), (Kruse and Flemming, unpublished)

primer name	sequence
PfVPS45_XhoI_gib-fwd	CATTTATTATTTTGTTTTTTTTAATTTCTTACATATAACTC GAGCAAAATGGAGAATAATCCTTACGTG
PfVPS45_AvrII_gib-rev	GTTCACCCAAATCCTCTTCTGATATTAACTTCTGCTCCCTA GGTTTCTTGATAAGCTGCAAAACGTCTGCAAG
pArl2-SF3A_5'UTR-p1-gib-fwd	GGTGACACTATAGAATACTCGCGGCCGCTAAAGTCTCCTT TTCTTTATTTTACAGTTGTG
SF3A_5'UTR-BirA-p2-gib-rev	GCTATTAATTTTAATGGTACTGTATTATCTTTCATCTCGAG ATCGGGTGGTACCTTACTTTTAAAATTATATTTTATATATT ATGTATATG
SF3A_5'UTR-BirA-p3-gib-fwd	CATATACATAATATATAAAATATAATTTTAAAAGTAAGG TACCACCCGATCTCGAGATGAAAGATAATACAGTACCAT TAAAATTAATAGC
BirA-frb-p4-gib-rev	CCTGCTCCACTATTTGCACTTCTTGTTGGATCCTTAAGTTT TTCAGCTGATCTTAATGATATTTCACC

Primers for knock in constructs

Cloned via NotI and MluI in pARL1-GFP-2A-Neo^R (hDHFR) (pSLI-TGD) (Birnbaum et al., 2017).

Cloned via NotI and AvrII in pARL1-2xFKBP-GFP-2xFKBP-2A-Neo^R (hDHFR) (pSLIsandwich), (Birnbaum et al., 2017).

primer name	sequence
PF10_0244_Stop_NotI_fwd	GAGCGCGGCCGCTAAGGAACAATGAATAAAGCTTTTAAG
PF10_0244_AvrII_rev	CTGACCTAGGCCATATTTGCATTAACTCACATACCG
PF10_0244_bp675_AvrII_rev	CTGACCTAGGCCATATTTGCATTAACTCACATACCG
PF10_0244_bp640_MluI_rev	CTGAACGCGTAATGGAAATCATTTCTGTACTTATGACGTTACC
Pf3D7_1219100_Stop_NotI_fwd	CAGCGCGGCCGCTAAAGCCAGAATAATCCCTTATCTGTTTG
Pf3D7_1219100_735aa_NheI_rev	CAGCGCTAGCATTATCAAAAACGAATGAGCCAAAGC

Primers for integration check

Gene ID	primer name	sequence
PF3D7_1025000	Eps15_before1000_fwd	CATAAATAAAATAAATATCGAAAACATAAG
PF3D7_1025000	Eps15_3prime-rev	CAAAGGAATATAAAATAATATATAGGG
PF3D7_1025000	Eps15_3'prime_bp675-rev	CAATTCCTTTGTCTTTTAAATCTTC
PF3D7_1025000	PF10_0244_3prime_1402-rev	CTAAATTTAAATATCCATCGTTATCCATATCGG
PF3D7_1219100	ClathrinHC_5'UTR_b4int-fwd	ATATTTATACCTTTATACATATATATC
PF3D7_1219100	Clathrin_aa735_3prime-rev	CGACAAAACAAAATAAGGGTTTCATATC

Primers for sequencing

primer name	sequence
BirA*58-as	CACCTAATTGTTCACCTGAATG
Crt fw	CCGTTAATAATAAATACACGCAGTC
FKBP 253 fw	TCACCAGATTATGCATACGGTG
FKBP 276_fw	CAGGCCATCCTGGCATCATC
FKBP 304_fw	TGCAACTTTAGTATTCGACG

primer name	sequence
FKBP 39 rv	TTGACCTCTTTTTGGAAATGTACG
FKBP 82 rv	CTTTCCATCTTCAAGCATTCCAG
FRB 216 fw	CCAAGAGTGGTGCAGGAAGTAC
FRB 251 fw	GAATGTCAAGGACCTCCTCCAAGC
FRB 42 rv	AAACGAGATGCCTCTTCCAG
FRB 76 rv	TCAAACATGCCTTTCACGTTCC
GFP 272 as	CCTTCGGGCATGGCACTC
GFP 633 fw	GCCCTTTCGAAAGATCCC
GFP 85 rv	ACCTTCACCCTCTCCACTGAC
Hsp sense 40	ACTTTAAAAAGAAATTTTCC
mCherry 620 fw	CTCCCACAACGAGGACTACACC
mCherry 88 rv	GGCCGTTCACGGAGCCCTCC
2xmyc-as	TAAATCTTCTTCGCTTATGAG
2xmyc-sense	GAGCAGAAGTTAATATC
Neo 40 rv	CGAATAGCCTCTCCACCCAAG
Neo 75 rv	CAGAGCAGCCGATTGTCTGTTG
pArl sense 55	GGAATTGTGAGCGGATAACAATTTCACACAGG
pARLminus rv	CAGTTATAAATACAATCAATTGG
SF3A2-5'UTR-955-fw	GTACATATATACATATAC

2.8 Plasmids

plasmid	source
pSLIsandwich (pARL1-2xFKBP-GFP-2xFKBP-T2A-Neo^{R})	(Birnbaum et al., 2017
crt 5'UTR_1xNLS-FRB-mCherry (BSD^{R})	(Birnbaum et al., 2017)
hsp86 5'UTR_3xNLS-FRB-mCherry (BSD^{R})	(Birnbaum et al., 2017)
nmd3 5'UTR_1xNLS-FRB-mCherry (DSM1^{R})	(Birnbaum, 2017)
nmd3 5'UTR_mCherry-Kelch13 (DSM1^{R})	(Birnbaum, 2017)
crt 5'UTR_Epsin-mCherry (BSD^{R})	(Flemming, 2015)
crt 5'UTR_1xNLS-FRB-T2A-P40-mCherry (BSD^{R})	Flemming, unpublished
hsp86 5'UTR_Epsin-2xmyc-T2A-1xNLS-FRB-mCherry (BSD^{R})	Flemming, unpublished
RESP 5'UTR_BirA*-2xGGGGS-FRB-mCherry (DSM1^{R}) (BirA-N^{L})	cloned by Kruse, Flemming, Jonscher, Birnbaum; unpublished (Birnbaum, 2017)
RESP 5'UTR_-mCherry- FRB-2xGGGGS-BirA* (DSM1^{R}) (BirA-C^{L})	cloned by Kruse, Flemming, Jonscher, Birnbaum; unpublished

	(Birnbaum, 2017)

2.9 Bacteria strains and *Plasmodium* strains

organisms	strain/cell line	characteristics/source
Escherichia coli	XL-10 Gold	Tet^{r}Δ(*mcrA*)183Δ(*mcrCB-hsdSMRmrr*) 173 *endA1 supE44 thi-1 recA1 gyrA96 relA1 lac Hte* [F'*proAB lacI^{q}Z ΔM15 Tn10* (Tet^r) Amy Cam^r]
Plasmodium falciparum	3D7	Derived from "limiting dilution cloning" of NF54 isolate (MRA-1000) (Walliker et al., 1987)
Plasmodium falciparum	Clathrin Heavy Chain-2xFKBP-GFP knock in cell line	(Flemming, 2015)
Plasmodium falciparum	Eps15-GFP knock in cell line	(Flemming, 2015)
Plasmodium falciparum	VPS45-2xFKBP-GFP knock in cell line	(Reichard, 2015)

2.10 Antibodies, beads and Streptavidin-Probes

antibody	dilution and application	source
Primary antibodies		
anti-GFP (mouse)	1 : 1,000 for Western Blots	Dianova, Hamburg
anti-mCherry (rat)	1 : 1,000 for Western Blots	Chromotek, Munich
anti-PfAldolase (rabbit)	1 : 2,000 for Western Blots	Secondary antibodies
secondary antibodies		
anti-mouse-HRP (goat)	1:3,000 for Western Blots	Dianova, Hamburg
anti-rat-HRP (goat)	1:3,000 for Western Blots	Dianova, Hamburg
anti-rabbit-HRP (donkey)	1:2,500 for Western Blots	Dianova, Hamburg
Streptavidin probes		
Streptavidin-HRP	1:5,000 for Western Blots	Thermo Fisher, Waltham MA (USA)
Antibody and Streptavidin beads		
anti-RFP (camel) coupled agarose beads	Immunoprecipitation	Chromotek, Munich
anti-RFP (camel) coupled agarose beads	Immunoprecipitation	Chromotek, Munich
Streptavidin-coupled sepharose beads	DiQ-BioID	GE Healthcare life sciences

2.11 Computer software

software	source/brand/distributor
A plasmid Editor (ApE)	Open Source (http://biologylabs.utah.edu/ jorgensen/wayned/ape/)
Axio Vision 40 v4.7.0.0	Zeiss, Jena
Corel Draw X10	Corel Corporation, Ottawa
Corel Photo Paint X10	Corel Corporation, Ottawa
Xcellence rt v5.2.0.3554	Olympus, Hamburg
GraphPad Prism 6.0d	GraphPad Software, La Jolla, USA
ImageJ 64 1.43u	Open Source (http://rsbweb.nih.gov/ij/)
Imaris x64 7.8	Bitplane AG, Zürich, Schweiz
Microsoft Office 2010	Microsoft Corporations, Redmond, USA
Micromanager v1.4.22	Open Source (https://micro-manager.org/)

2.12 Bioinformatic tools and databases

bioinformatics tool/database	source
BLAST	http://blast.ncbi.nlm.nih.gov/Blast.cgi
ClustalOmega	https://www.ebi.ac.uk/Tools/msa/clustalo/
Compute pI/Mw	http://web.expasy.org/compute_pi/
InterPro	https://www.ebi.ac.uk/interpro/
NCBI databases	https://www.ncbi.nlm.nih.gov/
PlasmoDB	http://plasmodb.org/plasmo/
PubMed	http://www.ncbi.nlm.nih.gov/pubmed
UbPred	http://www.ubpred.org/cgi-bin/ubpred/ubpred.cgi

2.13 Solutions, Media and Buffer

2.13.1 Media, buffers and other solutions for microbiologic culture

10x LB stock solution	10 % NaCl 5 % Peptone 10 % yeast extract in dH_2O autoclaved
LB medium	1 % (w/v) NaCl 0,5 % (w/v) pepton 1 % (w/v) yeast extract in dH_2O in dH_2O

LB Agar plate solution	1.5 % Agar-Agar in 1x LB medium
Ampicillin stock solution	100 mg/ml in 70 % ethanol
Kanamycin stock solution	Kanamycin 30 mg/ml in H_2O
Glycerol freezing solution	50 % (v/v) glycerol in 1 x LB medium
TFBI buffer	30 mM acetic acid 50 nM $MnCl_2$ 100 mM RbCl 10 mM $CaCl_2$ 15 % (v/v) glycerol pH 5.8 (with 0.2 N Acetic acid)
TFBII buffer	10 mM MOPS 75 mM $CaCl_2$ 10 mM RbCl 15 % (v/v) glycerol pH 7.0 (with NaOH)

2.13.2 Solutions and buffers for molecular biological experiments

DNA precipitation

Sodium acetate	3 M NaAc, pH 5.2
Tris-EDTA (TE) buffer	10 mM Tris-HCl pH 8,0 1 mM EDTA pH 8,0

DNA seperation

50x TAE	2 M Tris base 1 M Pure acetic acid 0.05 M EDTA pH 8,5
6x Loading buffer	40 % Glycerol (v/v) 2.5 % (w/v) Xylene cyanol 2.5 % (w/v) Bromophenol blue in dH_2O

One-step isothermal DNA assembly buffers

5x isothermal reaction buffer (6ml)	3ml 1M Tris-HCl pH 7.5 150 µl 2M MgCl2 60 µl each of 100mM dGTP/dATP/dTTP/dCTP 300 µl 1M DTT 1.5 g PEG-8000 300 µl 100mM NAD in dH2O
Assemby master mixture (1.2 ml)	320 µl 5x isothermal reaction buffer 0.64 µl 10 U/µl T5 exonuclease 20 µl 2 U/µl Phusion DNA polymerase 160 µl 40 U/ µl Taq DNA ligase add 1.2 ml dH2O

2.13.3 Media and solutions for cell biological experiments

P. falciparum **in vitro culture**

RPMI complete medium	1,587 % (w/v) RMPI 1640 12 mM $NaHCO_3$ 6 mM D-Glucose 0.5 % (v/v) Albumax II 0.2 mM Hypoxanthine 0.4 mM Gentamycin pH 7.2 sterile filtration
Malaria freezing solution (MFS)	4,2 % (w/v) D-Sorbitol 0,9 % (w/v) NaCl 28 % (v/v) Glycerol sterile filtration
Malaria thawing solution (MTS)	3,5 % (w/v) NaCl in dH_2O, sterile filtration
Synchronization solution	5 % (w/v) D-Sorbitol in dH_2O, sterile filtration
Transfection buffer (Cytomix)	120 mM KCl 150 µM $CaCl_2$ 2 mM EGTA 5 mM $MgCl_2$ 10 mM K_2HPO_4 / KH_2PO_4 25 mM Hepes, pH 7.6, sterile filtration

Amaxa transfection buffer	90 mM Na_2HPO_4 5mM KCl 0.15 mM $CaCl_2$ 50 mM HEPES pH 7.3, sterile filtered
Malaria freezing solution (MFS)	4.2 % D-sorbitol 0.9 % NaCl 28 % Glycol sterile filtration
Malaria thawing solution (MTS)	3.5 % NaCl in H_2O sterile filtration
WR99210 stock solution	20 mM WR99210 in 1 ml DMSO sterile filtration
WR99210 working solution	1:1000 dilution of stock solution in RPMI complete medium
Blasticidin S (BSD) working solution	5 mg/ml BSD in RPMI complete medium sterile filtration
G418 working solution	50 mg/ml in RPMI complete medium sterile filtered
DSM1 stock solution (50x)	187,5mM DSM1 in DMSO
DSM1 working solution	100 µl DSM1 stock solution add 5 ml in 95% DMSO / 5% 1xPBS solution
DHE stock solution (10x)	5 mg DHE in 1ml DMSO
DHE working solution (1x)	0.5 mg DHE in 1ml DMSO
Ho33342 stock solution (10x)	4.5 mg Ho33342 in 1ml DMSO
Ho33342 working solution (1x)	0.45 mg Ho33342 in 1ml DMSO
FACS staining stop solution	0.5 µl Glutaraldehyde (25%) in 40ml RPMI complete medium
Rapalog (AP21967) stock solution	500 mM AP21967 in ethanol

Rapalog working solution	1:20 dilution of AP21967 stock solution in RPMI complete medium
Selective lysis buffer	0.03 % (w/v) Saponin in 1x PBS sterile filtration
Parasite lysis buffer	4 % SDS 0.5 % Triton X-100 0.5 x PBS in dH_2O
Percoll stock solution	90 % (v/v) Percoll 10 % (v/v) 10 x PBS
80 % Percoll solution	89 % (v/v) percoll stock solution 11 % (v/v) RPMI compl. medium 4 % (w/v) sorbitole sterile filtration
60 % Percoll solution	67 % (v/v) percoll stock solution 33 % (v/v) RPMI compl. medium 4 % (w/v) sorbitole
40 % Percoll solution	44 % (v/v) percoll stock solution 56 % (v/v) RPMI compl. medium 4 % (w/v) sorbitole
Human red blood cells	Blood bank, Universitätsklinikum Eppendorf (UKE), Hamburg sterile, concentrate; bloodgroup 0_+
Preloading lysis buffer	5 mM K_2HPO_4 20 mM D-Glucose pH 7.4 sterile filtration
5 x Resealing buffer	750 mM NaCl 25 mM Na_2HPO_4 pH 7.4 sterile filtration
Tetanolysin Stock	50 HU /µl in dH2O

2.13.4 Solutions and media for biochemical experiments

SDS-Page and Western blot

10 x Running buffer	250 mM Tris base 1.92 M Glycine 1 % (w/v) SDS in dH_2O
Separating gel (10 %)	2.5 ml 1.5 M Tris-HCl, pH 8.8 4.7 ml H_2O 2.5 ml 40 % Acrylamide/ Bisacrylamide solution 100 µL 10 % (w/v) SDS in dH_2O 100 µL 10 % (w/v) APS in dH_2O 4 µL TEMED
Separating gel (12 %)	2.5 ml 1.5 M Tris-HCl, pH 8.8 4.2 ml H_2O 3.0 ml 40 % Acrylamide/ Bisacrylamide solution 100 µL 10 % (w/v) SDS in dH_2O 100 µL 10 % (w/v) APS in dH_2O 4 µL TEMED
Separating gel (15 %)	2.5 ml 1.5 M Tris-HCl, pH 8.8 3.45 ml H_2O 3.75 ml 40 % Acrylamide/ Bisacrylamide solution 100 µL 10 % (w/v) SDS in dH_2O 100 µL 10 % (w/v) APS in dH_2O 4 µL TEMED
Stacking gel (4%)	1 ml 1 M Tris-HCl, pH 6.8 2.5 ml H_2O 0.5 ml 40 % Acrylamide/ Bisacrylamide 40 µl 10 % (w/v) SDS in dH_2O 20 µl 10 % (w/v) APS in dH_2O 5 µl TEMED
6 x SDS sample buffer	375 mM tris HCl pH 6.8 12 % (w/v) SDS 60 % (v/v) Glycerol 0.6 M DTT 0.06 % (w/v) Bromophenol blue
10 x Western transfer buffer	250 mM Tris base 1,92 M glycerol 0.37 % (w/v) SDS in dH_2O
1 x Western-Transfer buffer	10 % 10 x Western transfer buffer 20 % Methanol

	in dH_2O
Coomassie solution	0.025 % (w/v) Coomassie Brillant Blue R-250 10 % (v/v) pure acedic acid 45 % (v/v) methanol in dH_2O
RIPA Buffer	10 mM Tris/HCl pH 7.5 150 mM NaCl 0.1% SDS 1% Triton X-100 1 mM PMSF 2X Protease inhibitor cocktail
Diluting buffer	10 mM Tris/HCl pH 7.5 150 mM NaCl 1 mM PMSF 2X Protease inhibitor cocktail
DSP (Stock solution)	20 mM in DMSO
Quenching buffer	25 mM Tris-HCl in 1x PBS

3. Methods

3.1 Microbiological methods

3.1.1 Cultivation of *E. coli* strains

E. coli bacteria were cultured in LB medium with 1 mM Ampicillin at 37 °C. For plasmid-preparation in a mini-scale 2 ml bacteria culture in a 2 ml-reaction tube was shaken in a thermoblock and for plasmid-preparation in a mini-scale 100 ml was shaken in an Erlenmeyer-beaker in an incubator. Transgenic bacteria lines were stored in a glycerol freezing solution at -80 °C. For all clonings the strains XL 10gold was used.

3.1.2 Preparation of chemical competent *E. coli* bacteria (Hanahan, 1983)

The bacteria were made chemically competent to take up plasmids by using the rubidium-chloride method which is a variation of the calcium-chloride-method and results bacteria with higher competence for transformation with plasmids. A culture of 20 ml LB medium without selection drug was inoculated with a glycerol stock of XL10gold *E. coli* bacteria and grown over night in a 50 ml falcon (lid not completely closed for air exchange). The next day 200 ml of pre-warmed LB medium without selection drug was inoculated with 8 ml of this overnight culture. The culture was grown with shaking at 750 rpm until it reached an optical density (OD) of 0.5 to 0.6. The bacteria were cooled down immediately on ice and then pelleted at 2,400 g, for 10 to 20 min at 4 °C. The pellets were suspended in 60 ml TFB I buffer and incubated on ice for 10 min, followed by centrifugation. The supernatant was discarded and the pellet was suspended in TFB II buffer, aliquotet in 100 µl aliquots and stored at -80 °C.

3.1.3 Transformation of chemical competent bacteria with plasmids (Dower et al., 1988; Taketo, 1988)

For transformation an aliquot of competent bacteria was thawed on ice and the plasmid (5 µl of a T4 ligation mix, all of a Gibson ligation mix or 1 µl of a diluted plasmid) was added to the competent cells and mixed carefully and incubated in ice for 10 min, followed by a heat shock at 42 °C for 70 seconds and again an incubation on ice for 5 to 10 minutes. Then one milliliter of prewarmed LB-Medium was added and the cells were incubated at 37 °C for one multiplication cycle. The bacteria were plated on LB-agar plates containing the selection marker ampicillin and were incubated at 37 °C for up to 20 hours.

3.2 Molecular biological methods

3.2.1 Polymerase chain reaction (PCR)

Depending on which polymerase was used, different PCR reactions were set up in 50 µl and used as a whole or being split into tubes with 10 µl each for gradient PCR. For amplification of inserts for cloning the high fidelity polymerase Phusion (NEB) was used. In case the amplificate was hard to obtain, like 5´UTRs, the more robust FirePol DNA Polymerase (Solis Biodyne) without proofreading ability has been applied. The same polymerase was also used for screening by colony PCRs after transfection on *E. coli* bacteria with plasmids and integration checks. First a standard PCR, as it was established in the laboratory, was carried out in most of the cases, if no special parameters were already expected (like for GC rich sequences or 5´UTRs), as follows:

Table 1: **PCR mix for Phusion Polymerase (50 µl batch)**

reagent	**volume [µl]**
Highly purified water	30.4
5x Phusion Buffer	10.0
dNTPs (2mM)	5.0
Forward Primer (10 mM)	2.0
Reverse Primer (10 mM)	2.0
Phusion Polymerase (2 U/µl)	0.3
Template	0.3

Table 2: **PCR mix for FirePol DNA Polymerase**

reagent	**Colony PCR for one clone volume [µl]**	**50 µl batch for amplification of inserts volume [µl]**
Highly purified water	6.5	32.2
10x FirePol Buffer	1.0	5.0
$MgCl_2$ (25 mM)	0.6	3.0
dNTPs (2mM)	1	5.0
Forward Primer (10 mM)	0.4	2.0
Reverse Primer (10 mM)	0.4	2.0
FirePol DNA Polymerase	0.1	0.3
Template	-	0.3

The PCR mix for the colony PCR was scaled up according to the number of screened colonies of *E. coli* clones.

Table 3: **PCR Programm for Cloning-PCRs and Colony-PCRs**

step	Temperature [°C] for Standard PCRs	Temperature-Range [°C] for Gradient PCRs	Duration	Cycles
Initial denaturation	95	95	2 minutes	1
Denaturation	95	95	20 seconds	30
Annealing	45	45-65	20 seconds	
Elongation	68	68-72	1.5-2 minutes/1 kbp	
Initial Elongation	68	68	10 minutes	1
Pause	4	4	∞	1

Table 4: **PCR Programm for diagnostic PCRs**

step	Temperature [°C] for Standard PCRs	Duration	Cycles
Initial denaturation	95	2 minutes	1
Denaturation	95	20 seconds	27
Annealing	45	20 seconds	
Elongation	61	1.5-2 minutes/1 kbp	
Pause	4	∞	1

3.2.2 Restriction digestion of DNA by endonycleases

For restriction of PCR-Products 5 µl of buffer (depending on preferences of each enzyme according to manufacturer) to 50 µl of eluted plasmid and 1.5 U Enzyme/ µg DNA (usually 0.5-1 ul) was added. In case a the PCR template was a plasmid, 0.5 µl of DpnI (just cuts methylated DNA of the plasmid) was added to the restriction mix. For restriction digestion of a plasmid, 1 µg of the plasmid was digested in a 50 µl mix.

3.2.3 Purification of PCR products and restriction digestion products

The isolation of Plasmids and DNA fragments (inserts, PCR produkts) was performed with NucleoSpin Extract II Kits based and hypotonic lysis of bacteria. The negatively charged DNA was bound to a silica membrane inside a column. All steps were (clearing of lysate, binding, washing and elution) done by centrifugation at 12 000 rpm, 1 minute. The DNA was eluted in TE-Buffer (50 µl).

3.2.4 Ligation of DNA by T4 DNA Ligase

The fusion of DNA fragments by T4 DNA Ligase was done in a ligation mixture containing 1 µl T4 ligation buffer (aliquotet and one aliquot was frozen and thawed ones and then discarded to ensure intact ATP), 1 µl T4 DNA Ligase, 0,5-1 µl linearized and purified plasmid and 3-5 µl digested and purified insert. The mixture was incubated at room temperature for 20 minutes and then immediately half of the mixture was used for transformation of bacteria or stored at -20 °C.

3.2.5 One-step isothermal DNA assembly (Gibson et al., 2009)

The one-step isothermal DNA assembly allows ligation of up to 6 inserts with a higher specificity due to the use of overlapping, homologous sequences at the ends of the inserts. Similar to the PCR, these homologous sticky ends of the inserts anneal and are then ligated. For this protocol PCR products need to have an overlap of 15-35 bp with the neighboring sequence. A typical reaction was as follows:

Assembly master mixture 7.5 µl

vector DNA 0.5-1 µl

PCR-product 1-1.5 µl

dH_2O ad 10 µl

The Gibson assembly mix was incubated at 50 °C in a PCR thermo cycler for 60 minutes. The cloning with the one-step isothermal DNA assembly is indicated in the names of the primers with the abbreviation “gib”.

3.2.6 Plasmid isolation from *E. coli* bacteria culture

For a Mini-Preparation 2 ml LB Medium with selection marker was inoculated with a colony, which was found being positive by colony PCR, directly from the LB plate and incubated over night at 37 °C vigorously shaking. Further procedures were done with the NucleoSpin Plasmid kit (Machery-Nagel) according to the manufacturer’s protocol.

The Midi Preparation was done with a 100 ml bacteria culture and the QIAfilter Plasmid Midi Kit (Machery-Nagel). The harvested DNA was solved in 200 µl TE Buffer and stored at -20 °C till used for transfection of *Plasmodium* parasites.

3.2.7 Agarose gel-electrophoresis of DNA fragments (Garoff and Ansorge, 1981)

DNA Fragments (originating from PCRs or restriction digestion by endonucleases) were separated in a 1 % agarose gel in 1 x TAE buffer containing 1 µg/ml ethidium bromide. The electric field in which the negatively charged DNA molecules were separated from each other was 10 Volts/cm. As a ladder the 1 kb DNA Ladder (Fermentas) was used. The gel was run for 15 minutes (PCR and restriction digestion) or 30 minutes (integration checks). The samples were prepared with 6x loading dye. The DNA inside the Gel was visualized and photographed on a UV-Light-Tray or in the BioRad Gel Imager.

3.2.8 Sequencing of plasmid DNA

The sequence of each clone was checked for mutations with sanger sequencing. A sequencing mix containing 200 to 800 ng plasmid (ususally 3 µl) was mixed with 3 µl of a sequencing primer and being filled up with highly purified water till 15 µ. The probe was send to Seqlab for the sequencing (Sequence Laboratories Göttingen).

3.2.9 Isolation of genomic DNA from *P. falciparum* infected red blood cells

In order to confirm the correct integration of a plasmid into the targeted genomic locus, genomic DNA was isolated from parasite culture and used for integration check by PCR. The QIAamp DNA Mini Kit was used according to the protocol for tissue and body fluids with 200 µl of blood originating from a culture with circa 5 % parasitemia of mixed stages.

3.3 Cell biological methods and assays

3.3.1 Continuous culture of *P. falciparum* (Trager and Jensen, 1976)

P. falciparum parasites were grown in RPMI1640 containing 0.5% Albumax (Life Technologies) at 37°C according to standard methods (Trager and Jensen, 1976). Cultures were maintained in 0+ erythrocytes (transfusion blood, Universitätsklinikum Hamburg-Eppendorf) at a hematocrit of 5%. Drug concentration for selection of transfected parasites were 4 nM for WR99210 (Jacobus Pharmaceuticals), 2 µg/ml for Blasticidin S (Life Technologies) and 0.9 µM for DSM1.

SLI was done as described (Birnbaum et al., 2017) by adding 400 µg/ml G418 (Sigma) to the culture after the parasites carrying the episomal plasmid appeared after tranfection. After parasitemia recovered under G418 selection, correct integration was checked by PCR across the integration junctions and by a PCR verifying absence of the unmodified locus. Correct expression of the tagged proteins was also confirmed by Western blot using a tankblot device (BioRad) to transfer SDS-PAGE separated protein onto Amersham Protran membranes (GE Healthcare). For knock sideways and DiQ-BioID parasites were grown in the presence of 250 nM rapalog.

3.3.2 Freezing and thawing for storage of *P. falciparum* cultures as cryo-stabilates

P. falciparum parasite cultures can be stored as cryo-stabilates in liquid nitrogen for long term storage or at -80°C for several years. 5 ml of a cell culture containg mostly ring stages (up to 10 % ring parasitemia) is centrifuged (1800 x g, 3 min, room temperature) and the supernatant discarded. The pellet with the infected RBCs is resuspended in 1 ml of malaria freezing solution, transferred in a cryo tube and frozen immediately.

Cryostabilates are thawed in a water bath (37 °C) for 30 to 60 seconds, transferred in a 2 ml Eppendorf reaction tube and centrifuged (1800 x g, 3 min, room temperature). The supernatant is discarded and the RBC-pellet resuspended in malaria thawing solution and centrifuged again. The pellet is washed

with pre-warmed RPMI medium and then transferred in a culture dish with 200 to 400 µl of fresh blood.

3.3.3 Thin blood smears and Giemsa staining

The parasitemia, percentage of the individual stages and the viability of the parasites was analyzed with giemsa stained thin blood smears. A monolayer of cells was prepared with placing 0.3-0.5 µl of cell culture on a microscope slide. A second slide used to distribute the cells. The cells were air dried, then fixed with methanol for 30 seconds and then placed in a 10 % giemsa solution for 15 to 30 minutes. The stained slides were rinsed with water to remove excessive giemsa solution and then air dried. The slides were analyzed with a bright field microscope (Zeiss Axiolab A1).

3.3.4 Synchronization of *P. falciparum* cultures with sorbitol (Lambros and Vanderberg, 1979)

P. falciparum cell cultures were synchronized with sorbitol to obtain ring stages with 0 to 18 hours of age. The synchronization method is based on the new permeation pathways that are established by the parasites after 18 hours of age and leads to a hypotonic lysis of all stages older than 18 hours of parasite age. The culture is centrifuged (1800 x g, 3 min, room temperature) and the supernatant discarded. The RBC-pellet is resuspended in 5x the pellet volume of prrewarmed 5 % D-sorbitol in water. The mixture is incubated for 7 min in a water bath (37 °C) and centrifuged immediately. The parasites are washed with RPMI and transferred to a new culture dish. In order to achieve parasites with an age of 8 to 18 hours of age, the synchronization is repeated after 8 hours of growth as previously described (Gruring et al., 2011).

3.3.5 Percoll (Aley et al., 1986; Heiber et al., 2013)

The parasite blood stages can be separated due to their different density in a Percoll gradient centrifuagation. For isolation of trophozoites a discontinuous percoll gradient made of layered 40 %, 60 % and 80 % Percoll (450 to 500 µl each layer) was prepared in a 2 ml reaction tube. A 5 ml culture containing 3 to 7 % trophozoites was centrifuged (1800 x g, 3 min, room temperature), the supernatant discarded, the pellet of infected RBCs (200 µl) suspended in ~200 µl RPMI medium, carefully layered on the Percoll gradient and centrifuged (16,000 x g, 5 min, room temperature). This resulted in layer containing schizonts and debris on top, on to two layers containing trophozoites of different ages in the middle part of the Percoll cushion and a pellet containing unifected RBCs and ring-infected RBCs at the bottom of the tube. The desired layer was harvested, transferred to a new 2 ml reaction tube and washed three times with RPMI (centrifugation at 1800 x g, 3 min, room temperature).

For schizont- and merozoites transfection a single cushion of 4 ml 60 % Percoll in a 15 ml falcon was used. 10 to 40 ml of culture with 5 % hematocrit was homogenously resuspended in 10 ml RPMI and carefully layered on top of the 60 % Percoll cushion. Centrifugation was done at 2000 x g for 6 minutes at room temperature. The extend RPMI medium was taken off and the Schizonts in the layer

on top of the Percoll cushion were harvested and washed with RPMI (2000 x g, 3 minutes, room temperature).

3.3.6 Transfection of *P. falciparum* by electroporation

Transfections were done with 100 µg of purified plasmid DNA (QIAGEN) using either a Gene Pulser Xcell (BioRad) (Fidock and Wellems, 1997) or an Amaxa system (Nucleofector II AAD-1001N, program U-033) (Moon et al., 2013). First the the plasmid DNA 100 µg of plasmid DNA for the BioRad system or 20 to 50 µg for the Amaxa system was precipitated by adding 1/10 volumes of 3 M sodium acetate solution and 3 volumes of 100 % ethanol solution. After centrifugation at 16,000 x g for 10 min the pellet was washed once with a 70 % ethanol solution, air dried and suspended in 15 or 10 µL of TE buffer for the BioRad system or the Amaxa system, respectively.

The BioRad system was used to transfect cultures with rings of 5 to 10 % parasitemia. Therefore, 385 µL cytomix solution was added to the DNA, mixed with 250-500 µL of a synchronized *P. falciparum* infected RBCs containing 2-10 % ring stage parasites, and transferred to an electroporation cuvette (2 mm, Biorad). The electroporation was performed using a Gene Pulser Xcell (Biorad; conditions: 310 V, 950 µF, ∞ Ω). The transfected parasites were suspended in 10 ml of RPMI complete medium and transferred to a 10 ml petri dish. The parasites were incubated at regular culture conditions. After 5 to 8 hours the medium was changed and the selection drug was added. The medium was changed twice a day for 5 consecutive days and then changed strictly daily for the next 8 days.

The Amaxa system was used to transfect purified late schizont stages and merozoites. The parasites of a synchronous culture of 10 ml with late schizonts of 5 to 7 % parasitemia was separated using a single layer of 60 % percoll. The isolated schizonts were washed once in RPMI and the supernatant discared. The parasite pellet was suspended in 90 µl transfection buffer and mixed with the DNA solution. The mixture was transferred in a electroporation cuvette (2 mm, Biorad) and electroporation was carried out with the program U-033. After electroporation the mixture was immediately transferred into a 1.5 ml reaction tube containing 200 µl medium and 300 µl uninfected RBCs and incubated at 37 °C with agitation of 750 x g for 20 to 30 minutes for invasion of the merozoites into the RBCs. After invasion, the RBCs were transferred in a 5 ml culture dish and fed strictly daily for one week. The selection drug was added one day after transfection.

3.3.7 Selective lysis of the red blood cell membrane by saponin (Burghaus and Lingelbach, 2001; Umlas and Fallon, 1971)

The detergent saponin lyses the membrane of red blood cells and the parasitophorous vacuole membrane but retains the integrity of the parasite plasma membrane at low saponin concentrations. A parasite culture with a parasitemia of 5-10 % was centrifuged (1800 x g, 3 min, room temperature) and washed once in 1.5 x the volume of the initial culture of DPBS. The pellet was suspended in 7 to 20 pellet volumes of ice-cold PBS containing 0.03 % saponin (freshly prepared, saponin powder was

measured with a highly accurate scale). The lysis mixture was incubated on ice for 7 to 10 min and subsequently centrifuged at 11,000 x g for 5 minutes. The supernatant was discarded and the pellet washed with ice-cold DPBS until the supernatant remained clear. The lysis was checked microscopically to confirm complete lysis and rigidity of the parasites. After the last washing step the supernatant was completely taken off and dependent on the size of the pellet 1 to 4 µl of 25x EDTA-free protease inhibitor mix was added directly to the pellet. The parasite pellet was loosened by flipping the closed tube with the finger and then 25 to 100 µl of lysis buffer was added and mixed with the cells by pipetting up and down. The lysate was stored at -20 °C of used immediately for SDS-PAGE.

3.3.8 Selective lysis of the red blood cell membrane by tetanolysin

Tetanolysin is a pore-forming toxin purified from *Clostridium tetani* that selectively permeabilizes the erythrocyte plasma membrane without lysing the PVM and parasite plasma membrane. Infected RBCs from 5 ml culture (5-10% trophozoites) were carefully purified in a Percoll gradient to avoid the presence of uninfected RBCs, which are lysed preferentially by tetanolysin. The enriched RBCs containing trophozoites are washed twice with RPMI medium to remove remaining Percoll and medium. The pellet is transferred into a tube containing 50 to 100 µl of DPBS with 1 HU (hemolytical unit) tetanolysin (Sigma) and incubated at 37°C for 10 min. The lysis mixture was observed at the microscope to verify permeabilization of RBC membrane. The Incubation time or number of HU (dilution of stock solution) was optimized depending on the activity of each tetanolysin batch. Permeabilised parasites were centrifuged at 6000 x g for 3 minutes. Isolated parasites were immediately fixed for electron microscopy.

3.3.9 Flow cytometry growth assay

The growth assay for the knock sideways cell lines was done by daily determination of the parasitemia using flow cytometry as previously described (Malleret et al., 2011). On day zero the parasitemia of a mixed culture was adjusted to 0,1 % (+/- 0,3) and split into 2 ml cultures. One dish was treated with 250 nM rapalog and one was left without rapalog as a control. Every 24 hours the parasites were fed with a premixed medium drug mixture, then resuspended to homogeneity and a sample of 20 or 50 µl was taken. The staining of 20 ul of the sample was done in a FACS tube with 80 µl of RPMI medium containing Hoechst 33342 and dihydroethidium in a final concentration of 4,5 µl/ml and 0.5 µg/ml (final volume 100 ul), respectively. The staining mixture was incubated for 20 min at room temperature and stopped with 400 µl of 0,003 % glutaraldehyde in cold RPMI. The parasitemia was counted with a LSRII flow cytometer by counting 100,000 events and calculating the number of parasites using FACSDiva software. The graph was visualized with GraphPadPrism software.

3.3.10 Growth assay with synchronised parasites

In order to find out when the parasites are dying during the blood cycle, a growth assay with synchronized parasites was performed. Therefore a culture of mixed parasites was synchronized to

ring stages with sorbitol treatment and grown for circa 36 hours till they reached late schizont stage and freshly invaded rings. The rings were cleared from debris and schizonts by a 60 % Percoll gradient centrifugation and again treated with sorbitol to eliminate possible later stages. This procedure resulted in six to eight hours old ring stages. The parasites were split into to 2 ml cultures and were treated with rapalog or left without as control. The parasites were fed and smeared for giemsa staining 6 h, 14 h, 24 h, 30 h, 38 h and 50 hours post induction with rapalog. The giemsa smears were analyzed manually on a microscope and 1500 to 3000 red blood cells were counted to determine total parasitemia and the number of each stage discriminating between pycnotic parasites, ring stages, young trophozoites, mid trophozoites, late trophozoites and schizonts. Statistical analysis and the graph were done with Microsoft Excel software.

3.3.11 **Vesicle accumulation assay**

The rate of the accumulating vesicles was counted in DIC images of synchronized trophozoite stages. Therefore a mixed culture containing up to 5 % rings was synchronized by sorbitol treatment to gain 0 to 18 hours old ring stages which were subsequently grown for 16 hours till the trophozoite stage. The 16 to 34 hours trophozoites were split into eight 2 ml dishes and four of these were treated with rapalog. Pairs of treated and untreated dishes were put into individual boxes and incubated. After 2, 4, 6 and 8 hours one pair was removed from the incubator, dropped on a slide and imaged quickly within the next 30 to 45 minutes. The vesicles in the DIC images were counted blinded for 30 cells.

3.3.10 Bloated food vacuole assay

Successive 5% sorbitol treatment 10 hours apart was used to obtain a culture with ring stage parasites with a stage window of 10-18 hours post invasion. After growth for 8 hours (young trophozoites of 18 to 26 hours post invasion) a sample was removed for imaging to obtain parasite size at time point 0 and the parasites were split into two 1 ml cultures containing 33 µM E64 protease inhibitor (Sigma Aldrich). To one of the cultures rapalog was added to a final concentration of 250 nM, the other culture was kept as control. The cells were cultures for 8 hours, stained with 4.5 µg/ml dihydroethidium for 20 min at room temperature, washed once in RPMI and then immediately imaged. The DIC image was used for scoring bloated food vacuoles and the parasite diameter (at least 32 cells per experiment and condition). Operators conducting the imaging and scoring of the cells in the images were blinded to condition of the sample. Statistics are described in the figure legend. The experiments were done with the help of Marius Schmitt.

3.3.11 Preloading of red blood cells and infection of preloaded cells

Preloaded cells were done according to the protocol of Sven Flemming (Flemming, 2015), which is based on previously used protocols (Abu Bakar et al., 2010; Frankland et al., 2006; Murphy et al., 2007). A volume of 200 µl of fresh red blood cells was washed three times in cold DPBS (2000 x g, 1.5 min). A lysis mixture was set up by pipetting 64 µl of lysis buffer, 1 µl of 30 mM DTT solution, 2 µl of 50 mM MgATP, 1 µl of fluorescently labeled Dextrane and carefull addition of 32 µl of packed

red blood cells. The mixture was put on ice and rotated end over end at 4 °C. The resealing of the lysed red blood cells was done carefully stirring 25 µl of the 5x resealing buffer into the lysis mixture and subsequent incubation at 37 °C Celsius while gently rocking (350 x g) in a thermos mixer for 60 min. The preloaded cells were washed three times with RPMI and stored at 4 to 8 °C. They can be stored for up to three weeks but were best when being used fresh.

The infection of preloaded red blood cells for imaging was as followed: A 5 ml dish of a culture with mixed stages (containing up to 3 % trophozoites) was separated into schizonts, trophozoites and ring stages with Mini-Percoll. The trophozoite layers were harvested, washed three times with RPMI and mixed with the preloaded cells in a 2 ml (half of a preloaded RBC batch) or 5 ml (one full preloaded RBC batch) dish and grown for 43 hours till they reinvaded the preloaded cells and grew till mid trophozoite stages. Note that the parasites grow much slower inside the preloaded cells.

3.3.12 Hemozoin accumulation assay

To measure the hemozoin size, parasites were synchronized by treatment with 5 % Sorbitol and grown till schizont stage for two days. The schizonts were harvested by 60 % percoll centrifugation (2000 x g, 6 min) and washed twice with culture medium (1800 x g, 3 min). The schizonts were mixed in a 5 ml culture dish with 200 ul red blood cells and 5 ml warm culture medium and incubated at 37 °C for 3 or 5 hours for invasion, followed by a sorbitol treatment to eliminate intact schizonts and not invaded merozoites. This results in 3 or 5 hour old ring stages which were subsequently grown till the young trophozoites stage for 21 hours. The 24 or 26 hour old young trophozoites were checked for viability by Giemsa staining, a 100 ul probe was taken for imaging of the parasites (0 h) and the culture was split into to 2.5 ml dishes and treated with 250 nM rapalog or left without rapalog (control) and incubated for 14 hours. The cells were imaged in differential interference contrast focusing on red blood cell and the parasites using the 100 x lens. The channel for mCherry and GFP were acquired to check for successful mislocalisation. The size of the hemozoin was determined by using ImageJ software (version 1.48) for 30 to 50 cells. The hemozoin crystal was surrounded by freehand selection in 400 x zoom and the surrounded area, representing the hemozoin in the focal plane, was measured. The statistical analysis was done with Graph Pad Prism software.

3.3.13 Fluorescent Dextrane uptake assay

The preloaded red blood cells were used to indirectly measure the uptake of host cell cytosol into the food vacuole. Therefore preloaded red blood cells were freshly prepared and infected as already described (3.3.13). At 40 hours post set up of the culture the reinvaded parasites inside the preloaded red blood cells were treated with 33 µM E64 protease inhibitor was added to bloat the food vacuoles, split into two 2 ml-dishes, treated with rapalog or left without rapalog (control) and grown for further 6 hours. Then the parasites were prepared for microscopy. All images were taken with the same exposition time (33 ms). The measurement was done with the help of Melissa Khosh-Naucke using the ImageJ software. The food vacuoles were encircled manually using the oval selection tool and the

integrated density was calculated. The stastitcal analysis and the graphs were done with GraphPad Prism software.

3.3.14 Quantitative western blot assay for hemoglobin uptake

The uptake of hemoglobin by the parasite analyzed using the classical quantitative western blot approach. A culture of 20 to 40 ml containing a total of 800 µl red blood cells (resulting in 2,5 or 5 % hematocrit) with high parasitemia (containing 5 to 10 % ring stages) was synchronized to ring stages using sorbitol and grown for 14 hours till 14 to 32 hours old trophozoites. The cultures were pooled and split into two 10 ml-dishes and one of these was pre-incubated with rapalog for one hour. Then the parasites were split again into two 3 ml cultures in a 6-well-plate (each well containing 120 µl red blood cells). Into one of the wells 33 µM of the E64 protease inhibitor was added to prevent hemoglobin digestion, resulting in the following pattern: Well 1 – plus rapalog, plus E64; Well2 – plus rapalog, minus E64; Well 3 – minus rapalog; plus E64; Well 4 – minus rapalog; minus E64. The plate was incubated for 6 hours, followed by a saponin lysis. The amount of hemoglobin was visualized in Coomassie staining for 30 minutes and destaining in water. Photographs of the coomassie stained PAA-gels were taken with the BioRad Gel imager. The measurement of the signal intensity was done with the ImageLab software (Biorad) and statistical analysis and graphs by Microsoft Excel.

3.4 Biochemical methods

3.4.1 Discontinuous SDS-Page (Laemmli, 1970)

With discontinuous sodium dodecyl sulfate - polyacrylamide electrophoresis (SDS-PAGE) proteins are separated according to their molecular weight. The proteins are negatively charged due to binding of the negatively charged SDS, which is binding to a protein proportional to the protein's mass, and therefore migrate in an electrical field through a gel made of polyacrylamide polymers. The proteins in a probe with isolated and lysed parasites (3.3.7) are de-naturated by heating in 1x Laemmli Buffer and at 85 °C for 5 to 10 minutes.

Polyacrylamide (PAA) -gels were prepared freshly (2.3.4) with 10 % PAA for DiQ-BioID probes, 12 % for standard Western Blot or 15 % for quantitative western blot assays for hemoglobin uptake. The 10 % APS-solution for polymerization was always prepared freshly.

The separation was usually done with 120 V until the border of the dye (glycine with coomassie dye) reached the end of the acrylamide gel (ca. 1.5 to 2 hours). The gels were usually either stained with Coomassie Brilliant Blue to visualize protein bands or used for Western blot (3.4.3). For a Coomassie staining, gels were incubated for 30 min in Coomassie staining solution and then destained by repeated washing with warm water until the background was reduced and the protein bands were clearly visible.

3.4.2 Western blot (Kyhse-Andersen, 1984; Towbin et al., 1979)

A western blot is used to visualize specific proteins that were separated by SDS-PAGE (3.4.2). The negatively charged proteins are transferred from the PAA-Gel on a nitrocellulose membrane in an electrical field. The tank blot method was used for protein transfer. In a Biorad tank blotting chamber, the acrylamide gel from an SDS-PAGE was included in a blot sandwich device containing: one 6 mm sponge, three MM Whatman paper, polyacrylamide gel, nitrocellulose membrane, three MM Whatman paper, and another 6 mm sponge. Transfer was carried out at 100 V for 1 hour at 4 C. For immune-detection of proteins on the nitrocellulose membrane, first unspecific binding was blocked with 5 % milk in 1x PBS for 30 to 60 minutes. Then the membrane was probed with the primary antibody diluted in 5 % milk powder solution or 2.5 % milk powder solution for probing with Streptavidin-HRP and incubated for 1 to 3 hours at room temperature or overnight at 4 °C. After three times washing with DPBS, the secondary, horse radish peroxidase (HRP) coupled antibody was added and incubated for 1 hour at room temperature and subsequently washed off 3 times with 1x PBS. The protein was detected by chemiluminescence with the ECL-kits according to the manufacturer's instructions and the signal detected using X-ray films or the BioRad gel imaging system. Exposition times were adjusted between 3 seconds and 3 hours dependent on the signal intensity.

3.4.3 Dimerization induced *in vitro* proximity biotinylation of interacting proteins (DiQ-BioID)

Small scale experiments were done with 5 ml cultures to test conditions and efficiency of biotinylation and analyzed by Western Blot probed with Streptavidin-HRP. The probes for analysis by mass spectrometry were scaled up to 150 ml of culture per condition (3x 50 ml culture bottles per condition). The mixed stage parasite cultures starting with 2 to 5 % parasitemia were grown for 24 hours in the presence of biotin and rapalog (final concentration of 250 nM) and fed every 8 hours to prevent starvation of the parasites. After 24 hours of growth the parasitemia resulted in circa 10 %. The culture was centrifuged (6000 x g, 20 min, room temperature) and the supernatant discarded. The parasites were lysed with 50 ml of 0.003 % saponin for the pellet of each condition as already described (3.3.7). The isolated parasites were transferred to a 2 ml reaction tube, washed 2 times with DPBS and lysed with 2 ml lysis buffer (lysis buffer for mass spectrometry) and sealed with parafilm. Two freeze-and-thaw cycles at -80 °C and thawing on ice were done for complete lysis of the parasite cells. The cell debris was sedimented by centrifugation at 16,000 x g for 10 min and the supernatant transferred to a 15 ml falcon and diluted in a ratio of 1:2 with 50 nM TrisHCl pH 7.5, 2x protease inhibitor cocktail, 1 mM PMSF. 50 µl of Streptavidin-Sepharose (equilibrated in 50 nM TrisHCL pH 7.5) were added and incubated overnight at 4 °C rotating head over head. The beads were sedimented by centrifugation at 1600 x g for 1 min, transferred in a 1.5 ml reaction tube and washed twice with 500 µl lysis buffer, once in 500 µl cold dH_2O (Ampuwa), two times in 500 µl cold TrisHCl pH 7.5 and three times in 500 µl cold 100 mM TEAB. Centrifugation after each step was carried out with 1600 x g for 2 min at room temperature and incubation done horizontally rolling on a roller mixer for 2 min a for each washing step. After the last washing step the sepharose was re-suspended in 50 µl 100mM

TEAB and shipped on ice for mass spectrometry analyis. The mass spectrometry analysis was performed by Wieteke Hoeijmakers (Radboud Institute, Nijmegen, Netherlands) using dimethyl labeling for quantification (Boersema et al., 2009).

Falcons, reaction tubes and tips were exclusively used from the brands Eppendorf and Nunc for the probes for mass spectrometry to avoid contamination with polymers.

3.4.4 In-cell DSP cross-linking and co-immunoprecipitation (CoIP)

A target protein is isolated out of a cell lysis mixture due to binding to beads coupled to antibodies specific for the target protein or an attached tag on the target protein. Interacting proteins of the target proteins are co-immunoprecipitated together with the target protein. The whole protocol was done on ice. 10 to 20 ml of a parasite culture was centrifuged (1800 x g, 3 min, room temperature) and the supernatant discarded. The lysine-reactive crosslinker Dithiobis[succinimidyl propionate] (DSP) was used to preserve labile protein-protein interactions before co-immunoprecipitation. 20 mM DSP was prepared in DMSO and further diluted in DPBS to 0.3 mM. Cross linking of proximal and interacting proteins was done for 30 min at room temperature while horizontally rolling the falcon. After centrifugation the supernatant was discarded and 10 ml quenching buffer were added to cells and incubated for 10 minutes at RT. Then the parasites were isolated with selective RBC lysis by saponin (3.3.7). The purified parasites were washed twice with DPBS (centrifugation steps at 1800 x g) and re-suspended in 250 µl RIPA buffer (+2x protease inhibitor and 10mM PMSF). Then, the lysates were centrifuged at 16,000 x g at 4 °C and the supernatants diluted with 750 µl dilution buffer (+2x protease inhibitor cocktail) each. The diluted supernatants were pooled in a 2 ml reaction tube and 50 µl transferred to a tube containing 17 µl 4x SDS sample buffer for Western blot analysis (Input). 20 µl GFP-agarose beads were equilibrated in dilution buffer and were then transferred to the diluted supernatants and incubated for 1 to 2 hours at 4 °C with gentle overhead mixing. The agarose beads were pelleted (2500 x g, 3 min, 4°C) and 50 µl of the supernatant was transferred to a tube containing 17 µl 4x SDS sample buffer for Western blot analysis (supernatant). The beads were washed 5 times with dilution buffer (centrifugation steps at 2500 x g) and 50 µl of the supernatant of the last washing step were transferred to a tube containing 17 µl 4x SDS sample buffer for Western blot analysis (final wash fraction). The agarose pellet was incubated with 30 µl of 4x SDS sample buffer at 85 °C for 10 minutes to elute proteins bound to the agarose beads. The beads were pelleted by centrifugation at 2500 x g for 1 minute and the supernatant (eluate). 5 µl of the input, supernatant and final wash step and 10 µl of the eluate were loaded on the PAA-gel for SDS-PAGE (3.4.1) and subsequent Western blot analysis (3.4.2).

3.5 Microscopy

3.5.1 Differential interference contrast and standard fluorescence imaging

Microscopy of parasites was performed as previously described (Gruring and Spielmann, 2012). Images were taken with a Zeiss AxioImager M1 or M2 microscope equipped with a LQ-HXP 120, Zeiss filter sets 49, 44 and 64, a Hamamatsu Orca C4742-95 camera, 100 ×/1.4–numerical aperture lens and a 63 ×/1.4–numerical aperture lenses and using a customized AxioVision (version) software to be able to acquire each channel individually. For the acquisition of some images, due to the low fluorescence levels of the GFP tagged VPS45, the analog gain in the Axiovision software was used (at the maximum of 255). The images were cropped, processed and channels merged in Corel Photo Paint software (version X6 and X7). If necessary, the parasites were stained with 1 µg/ul DAPI for 5 min at room temperature.

3.5.2 Confocal imaging

For confocal imaging an Olympus FluoView 1000 confocal microscope was used. To detect Alexa Fluor 647-conjugated dextran, image stacks were taken (step size of 0.38 µm) with the 635 nm laser line using a 60 x (1.35 numerical aperture) plan apochromate oil immersion lens and a 5 fold zoom using the FluoView software. Images were viewed using Imaris (Bitplane) software and final processing was done in Corel Photo Paint X6.

3.5.3 Fast frame rate microscopy imaging

3.5.3.1. Zeiss AxioImager M2 set up

The Zeiss AxioImager M2 upright microscope is equipped with a Hamamatsu Orca SE camera that in standard modus is controlled by the Axiovision software but no plugin for time lapse imaging was available. To make live cell imaging possible, the MicroManager software was used to control the camera (the AxioVision software needs to be shut off when MicroManager is running). A heated stage (Tempcontrol-37, PeCon GmbH) and a heater for the objective lens (Tempcontrol-mini, PeCon GmbH) were attached to maintain 37 °C of the imaged sample. Acquisition time was reduced through 2x2 binning and maximum gain was applied (gain value of 255). First the minimal acquisition time was identified with one cell. Then the cells chosen for imaging were imaged with the DIC channel followed by fluorescence imaging using the parameters identified for the test cell using MicroManager. During imaging the shutter for brightfield or fluorescence excitation were opened and closed and the filters were switched manually with the touchpad interface attached to the microscope. Due to this requirement no multi-channel acquisition was possible with this set-up. The shutter for the fluorescence excitation was kept open during the entire image series. Since the constant illumination during imaging led to quick bleaching of the fluorescence, in some cases the intensity of the fluorescence excitation light source was turned down (2 to 3 steps of the switch). This set up allowed

2D imaging only and was used to obtain DIC videos and some videos of fluorescence channels that were imaged with very high frame rates (0.2 s per frame).

3.5.3.2 Olympus IX81 Cell^R set up

The Olympus Cell^R imaging system consisted of an Olympus IX81 inverted microscope stand surrounded by a climate chamber and an attached Olympus MT-20-E light source and filter turret and a Hamamatsu Orca SE camera. To improve 3D imaging speed, a Piezo-Electric Objective Drive (PIFOC® Objective Stepper 100 µm economical system, Physical Instruments; 7ms/step in Z-axis) was mounted underneath the objective lens to circumvent the slow Z-movement of the originally mounted motorized Z-stage (300 ms/step in Z-axis). The MT-20 E ("Cell Cube") device was designed for fast imaging applications and therefor contained a high-speed shutter (1 ms shutter time) and the capacity to switch neighboring filters within 58 ms, permitting two-color imaging with fast frame rates (an example is shown in 4.2.3: Figure 25) (Ubl, 2005). No fast switching between DIC and fluorescence imaging was possible, as more than 6 s were needed to change between fluorescence and DIC. Therefore, usually one DIC Z-stack or 2D image was acquired before and after the live cell fluorescence acquisition. This was sufficient to assess the viability of the imaged parasite and provided a reference for the localization of the fluorescence signal. The program Xcellence rt (v5.2.0.3554) was used to create the imaging protocol for automatic opening of the shutters, switching between channels, control of the Pifoc and repeated image acquisition (time lapse). The cells were found and chosen manually by eye with the ocular. Areas with multiple cells per frame were picked in order to image multiple cells at once. Then the automated imaging protocol was able to image at 37 °C within 0.3 s to 1 s per frame depending on the fluorescence intensity (Table 7) in one fluorescence channel. Due to limited signal strength 2x2 binning was applied to enable shorter exposure times, which was necessary to obtain high frame rates. With this setup frame rates of 0.2 to 0.5 frames per second and 1 to 5 stacks per seconds were achieved laser scanning

3.5.4 Transmission electron microscopy (TEM)

Parasites were Percoll-enriched and fixed with 2.5 % glutaraldehyde in 50 mM cacodylate buffer pH 7.4 for 1 h at room temperature. For some experiments the cells were first treated with 1 HU Tetanolysin in Dulbecco PBS (DPBS) for 10 min at 37°C to release the host cell cytosol as described (Mesen-Ramirez et al., 2016) and washed 3 times in PBS prior to fixing. Cells were post fixed with 2 % OsO4 in H2O for 40 minutes at 4 °C in the dark, contrasted with 0.5 % uranylacetate for 30 minutes at room temperature and dehydrated through increasing concentrations of ethanol. Following embedding in epoxy resin (EPON) samples were cut into 60 nm sections and examined with a Tecnai Spirit transmission electron microscope, equipped with a LaB6 filament and operated at an acceleration voltage of 80 kV. The EM image .emi/.ser-files were converted to 8 bit TIFF files using the TIA Reader Plugin for ImageJ (Steffen Schmidt, LMU Munich, unpublished). Batch conversion was performed with simultaneous contrast enhancement using a saturation value of 5.

4. Results

To find proteins that are involved in host cell cytosol uptake (HCCU) in *P. falciparum* three candidates were chosen for detailed analysis. These candidates are Clathrin Heavy Chain (CHC), Eps15 and VPS45 and were previously partially characterized (Flemming, 2015; Reichard, 2015).

4.1 Clathrin is not involved in host cell cytosol uptake in *P. falciparum*

Clathrin mediated endocytosis (CME) is the most prominent endocytic pathway in eukaryotic cells (1.3), where this pathway is the major endocytic route for internalization of extracellular cargo (Bitsikas et al., 2014). The P*lasmodium* genome encodes several components of the CME machinery. PF3D7_1219100 is the homologue of the Clathrin Heavy Chain (CHC). A *P. falciparum* integration cell line with a GFP-tagged CHC had previously been established and initially analysed (Flemming, 2015). Here a more detailed analysis of this cell line was carried out. This included re-examination of the localization dynamics (4.1.2), testing the essentiality of this protein for parasite survival (4.1.3), identification of potential interacting proteins or compartment neighbors and co-localisation with suspected HCCU markers (4.1.4).

4.1.1 Establishing a setup for video-frame-rate live cell imaging of *P. falciparum* blood stages

Endocytosis is a fast and highly dynamic process and therefore demands live cell imaging with fast frame rates (Kirchhausen, 2009; Schmoranzer et al., 2000). High intensity fluorescence signals and photostability are the basis for short exposition times and therefore fast imaging. Since the fluorescent *Plasmodium* cell lines relevant for this work lack both of these attributes, improved fast imaging of low fluorescent signals was needed to be established. For this purpose two existing wide field microscopes were modified (3.5.3 and Table 1) to enable imaging of the cell lines with a sub-second frame rate to track individual foci of fluorescence within the cell and to allow fast 3D live cell observations. In Table 1 the properties of these 2 systems is compared to the confocal microscope Olympus FluoView 1000 which was previously used for time lapse imaging (Flemming, 2015; Gruring et al., 2011) (Table 1 and Table 3). Details about the about the established microscope setups and the imaging procedures are described in the materials and methods section (3.5.3).

Table 5: **Comparison of the available microscopy set ups for high speed live cell microscopy**

Feature/Item	Zeiss AxioImager M2	Olympus IX81 Cell^R imaging station	Olympus FluoView 1000
Microscopy-Type	widefield, upright	widefield, inverted	confocal, inverted
fully motorized	no	yes	yes
climate/environment	heated stage and heated objective	climate chamber	climate chamber
specimen	slides	slides and culture dishes	slides and culture dishes
mounted camera	Hamamatsu Orca ER (CCD)	Hamamatsu Orca ER (CCD)	Photon Multiplier of FluoView 1000
motorized stage	no	yes	yes
auto focus/zero drift correction (ZDC)	no	(yes)	yes
frame rate achieved (with Clathrin as standard)	0.2 – 0.5 s (2D)	0.2 – 0.5 s (2D) 1- 5 s (3D)	0.2 s (2D) 3 – 8 s (3D)
Z-stacks	no	yes	yes
time lapse	yes	yes	yes
imaging of multiple cells per frame	+	++	-
image quality of DIC channel	+++	++	+
quality of fluorescent image (noise level)	++	+	+
imaging of faint fluorescence	++	+	-
bleaching	+	+	+++
imaging of multiple channels	no	yes	yes
shuttering with software	no	yes	yes
software	MicroManager	Olympus Xcellence rt	FluoView
Software enables automated imaging protocol	no	yes	no
handling convenience	-	+	+

4.1.2 PfClathrin Heavy Chain-2xFKBP-GFP localizes to a large patches and small foci

The corresponding cell line for CHC tagged with 2xFKBP-GFP was analyzed microscopically to re-examine its localization. In agreement with previous results (Flemming 2015), GFP tagged endogenous CHC was found to be expressed throughout the intraerythrocytic cycle and showed a diverse localization within the parasites with unregularly shaped patches of intense fluorescence that frequently were in close proximity of a nucleus (Figure 6 A, mid and late Trophozoite: arrow). Some of these patches also appeared to be in close proximity to the parasite plasma membrane or the food vacuole but this may have been a coincidence, as these localizations were only observed in a limited number of cells. The number of foci rose with the age of the parasites from ring to schizonts but was not equal to the number of nuclei (Table 6). *P. falciparum* harbors one single Golgi organelle that is found close to the parasite nucleus. Golgi division takes place prior to multiplication of the nuclei,

resulting in a maximum of 2 Golgi foci per nucleus (Struck et al., 2005). Although the number of intense foci of CHC per nucleus was found to be higher than 2 (Table 6), the close proximity to the nucleus and data from *T. gondii* (Pieperhoff et al., 2013) may nevertheless still indicate a location at this organelle. This would also agree with the almost equal number of CHC intense foci per nucleus in schizonts(1.1/nucleus, Table 6) when the nuclei division has taken place.

Table 6: **Number of intense patch like foci of PfClathrin Heavy Chain-2xFKBP-GFP in 2D images (multiple independent imaging sessions)**

	Rings	young Trophozoites	mid Trophozoites	late Trophozoites	Schizonts
average number of intense ("patch-like") foci	1.1	1.4	2.8	4.5	8.4
detected nuclei	not detectable	1	1.0	2	7.4
ratio foci/nuclei	-	1.4	2.8	2.25	1.1
counted cells	n=15	n=18	n=35	n=16	n=8

Next to these intense patches of CHC a second pool of smaller, less intense, and more regular shaped foci were observed (Figure 6, mid and late Trophozoite: arrowhead). During microscopical analysis it became obvious that these smaller foci were less spatially fixed than the intense foci and therefore difficult to capture due to their appearance and disappearance during the acquisition time. As an example the GFP channel of a late trophozoite was imaged several times within seconds, starting with one small focus (0 seconds: two arrowheads). Seventeen seconds later a second focus of similar low intensity appeared besides the first focus (Figure 6). In contrast, no obvious movement was detected at the intense patches during this time (Figure 6, arrow).

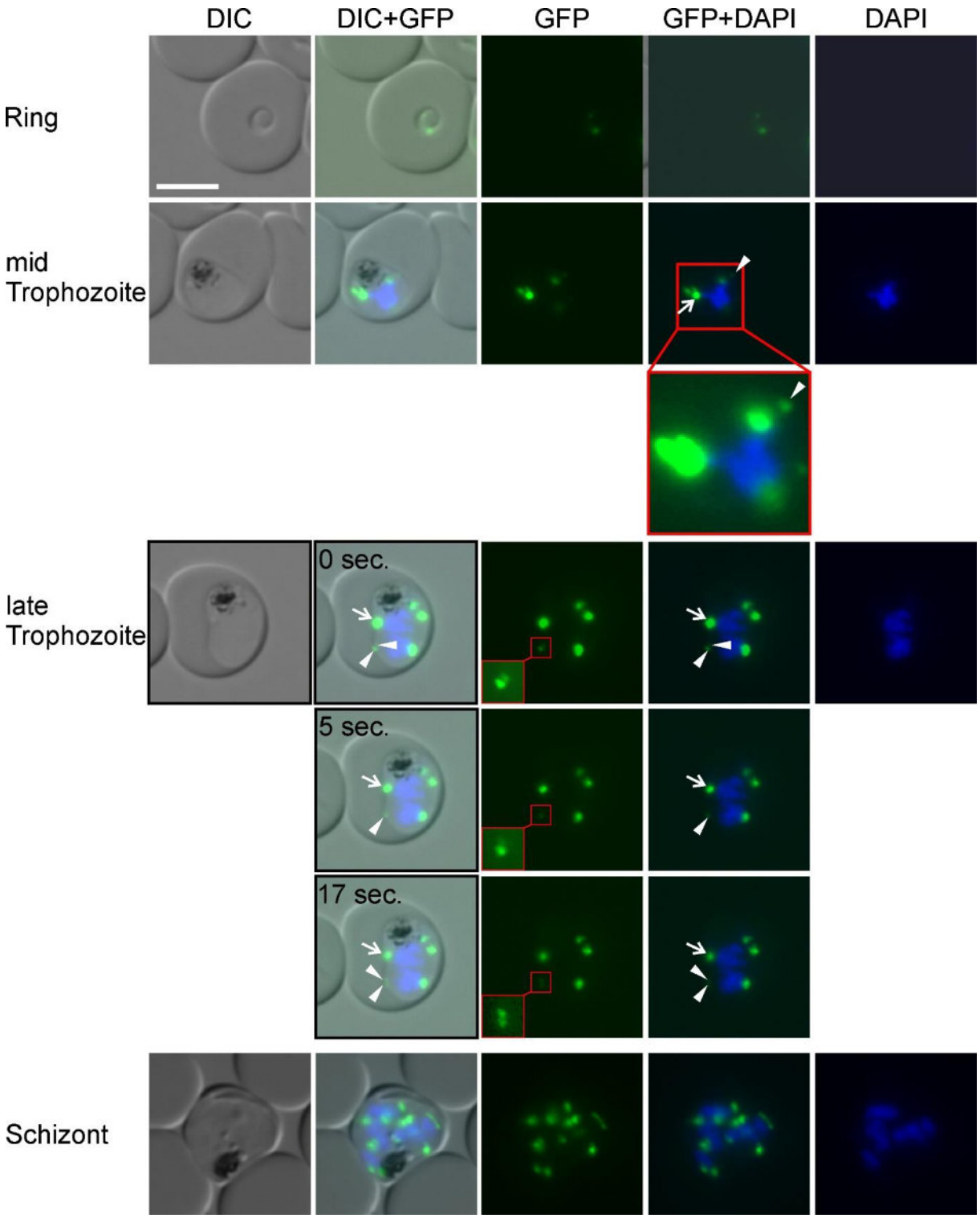

Figure 6: **Localization of PfClathrin Heavy Chain endogenously tagged with 2xFKBP-GFP in live cells during the blood stage showing two types of foci.** Representative live cell images of the cell line with CHC tagged with 2xFKBP-GFP show intensely fluorescent big patch-like foci (arrow) and very faint and small punctate foci (arrowhead). Subsequent Images of a late Trophozoite were taken to show that the small foci may appear and disappear (white arrowheads). Zoom and enhanced intensity to better visualize the faint focus are shown in the red frame.DIC: differential interference contrast; GFP: green fluorescent protein; DAPI: nuclei. Scale bar: 5 µm

The dynamics of a protein might give information about its potential function as has been shown in *P. falciparum* for Eps15 with a directed movement between the parasite periphery and the food vacuole and a potential role in HCCU (Flemming, 2015). To further investigate the nature of the dynamics of the foci of CHC-2xFKBP-GFP and if this represents movement, fast frame rate live cell imaging (4.1.1) was applied. In addition, CHC-2xFKBP-GFP appealed as a good example to test the improved imaging set ups because of the presence of intense and faint foci (Table 7).

Table 7: **Parameters for imaging with the Olympus IX81-Imaging-Setup with Clathrin Heavy Chain-2xFKBP-GFP as example**

Exposition [ms]	binning	Z-Layers	speed [s/stack]	faint foci	intense foci
1000	1x1	5	5.225	+++	+++
1000	2x2	5	5.225	+++	+++
500	2x2	5	2.725	+++	+++
400	2x2	5	2.225	++	+++
355	2x2	5	2.000	+	+++
300	2x2	5	1.725	+-	+++
250	2x2	5	1.475	+-	++
250	2x2	3	0.75	+-	++
200	2x2	5	1.000	+-	++
5	2x2	3	0.150	-	+
30	2x2	3	0.090	-	+

First the Olympus IX81-Imaging-Setup (3.5.2 and 4.1.1) was used since it permits the acquisition of multiple Z-layers per time point in time lapse imaging. The exposure times resulting in the best signal-to-noise ratio and image quality with the CHC-2xFKBP-GFP parasites resulted in a frame rate of 3 to 5 seconds, which is comparable to the Confocal Laser Scanning Microscope (CLSM, Olympus Fluoview 1000) and therefore did not provide any benefit (Table 3). Reducing the exposure time to a minimum of 200 ms made it possible to obtain 1 to 1.25 image stacks per second (3 to 5 frames per stack) while still maintaining an acceptable signal intensity (Table 3 and Figure 7). The imaging in multiple layers did not serve 3D reconstruction but to enhance signal intensity of the faint foci by using the off-focus fluorescence when viewed in maximum intensity projection. It also enabled following imaging of foci through multiple focal planes. With this setup it was also possible to follow multiple cells per focus area (Figure 7 A). 12 consecutive frames of the fast frame rate imaging to analyze the dynamics or possible movement of big intense and small faint foci of CHC tagged with 2xFKBP-GFP are shown in Figure 7 B. No directed movement of the CHC-foci was detected. Instead the observed dynamics represent rearrangement of the foci (Figure 7). In contrast to the standard live

cell imaging (Figure 6), rearrangement of both foci-types, the faint (Figure 7 B; cell 1, 3, 4, 5) as well as the intense foci (Figure 7 B; cell 1, 2, 5), was observed during the fast frame rate live cell imaging. The number of rearranging and stable foci of each type was determined in 21 cells resulting from two independent imaging sessions and (Table 8). The foci in the majority of cells did not show any rearrangement (86 % of the intense big foci and 57 % of the small faint foci) and the small faint foci showed rearrangement in 43 % of the cells in contrast to the intense patch like foci which rearranged in 14 % of the cells (Table 8).

Table 8: **Quantification of rearrangement events in fast frame rate live cell videos (1-1.25 seconds / stack) of Clathrin Heavy Chain-2xFKBP-GFP**

	intense big foci		faint small foci	
	stable	rearranging	stable	rearranging
counted cells: n=21	18	3	12	9
%	86	14	57	43

This might represent dynamics of the CHC or of the cellular structure to that CHC locates to but no regular pattern of movement was detected after inspecting 21 cells. Either the imaging system is not sensitive enough to consistently pick up the small foci to detect directed movement or there is no directed movement across microscopically detectable distances.

Figure 7 (next page): **Fast frame rate live cell microscopy of multiple cells expressing Clathrin Heavy Chain tagged with 2xFKBP-GFP using the OlympusIX81-setup.** Shown is the maximum intensity projection of all 5 layers of 3D fluorescent live cell images expressing endogenously tagged CHC-2xFKBP-GFP. Parameters were 200 ms exposure time, 2x2 binning and 5 z-layers per time point (1 s per interval time between stacks). **A)** Maximum intensity projection of the first image stack of the time lapse experiment with the GFP in false color (green) and the corresponding DIC-channel. DIC, differential interference contrast; overlay, DIC merged with GFP. **B)** Maximum intensity projection of consecutively acquired stacks of the GFP channel displayed in inverted grey scale. The cells are numbered in time point 0. Scale bar: 5 µm

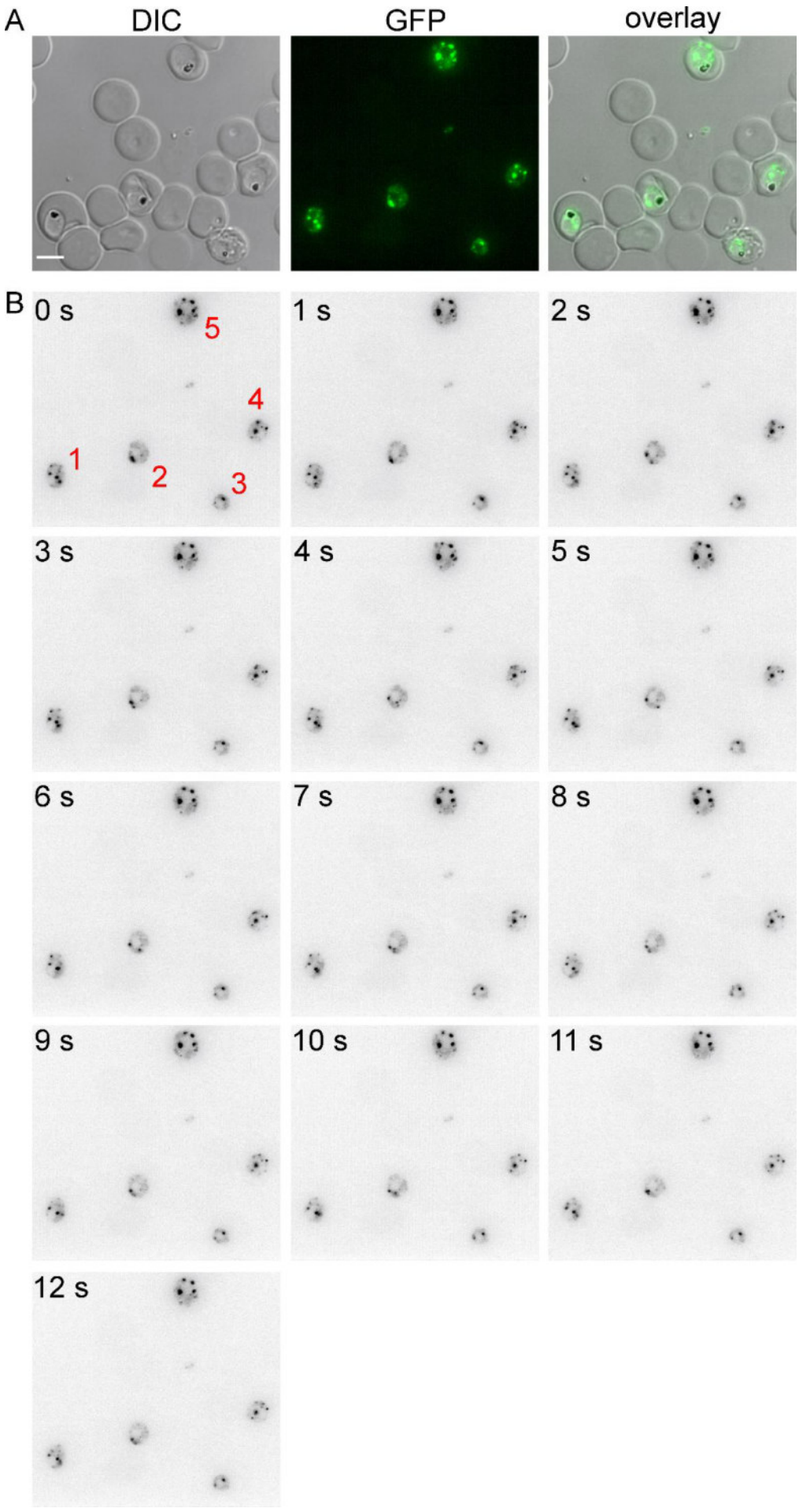
A
DIC
GFP
overlay
B
0 s
5
4
1
2
3
1 s
2 s
3 s
4 s
5 s
6 s
7 s
8 s
9 s
10 s
11 s
12 s

In order to image the observed rearrangement (Figure 7) of the foci of CHC-2xFKBP-GFP in better temporal resolution, the speed of the fast time lapse imaging was further enhanced. Since the OlympusIX81-Imaging-setup yielded a maximum speed of 0.75 seconds per frame in 3D, the speed was enhanced by imaging a single focal plane per frame (2D). For this approach the Zeiss AxioImager2-system was favored because of the high quality for standard imaging of live cells in 2D, assuming that this microscope would allow better quality in 2D fast live cell imaging than the Olympus IX81 system. Frame rates of 200 ms were achieved. The first 55 frames (11 seconds) of subsequent live cell images of CHC-2xFKBP-GFP are shown (Figure 8). One intense focus and two faint foci (white arrowheads) are visible at 0 seconds. During the time course the faint foci go together and might converge (Figure 8; 3.8 seconds) and then move apart again (Figure 8; 6.6 seconds). In two independent imaging sessions 7 cells were analyzed in total of which in 2 cells the small foci of CHC-2xFKBP-GFP converged into each other and then diverged into two foci again. However, no other clearly directed movement of CHC-foci was observed, in agreement with the results with the other Olympus IX81 imaging system.

Figure 8 (next page): **Fast frame rate live cell microscopy of Clathrin Heavy Chain tagged with 2xFKBP-GFP using the Zeiss AxioImager M1 setup**: Fluorescent live cell images of one cell expressing endogenously tagged CHC-2xFKBP-GFP. Parameters were 200 ms exposure time, 2x2 binning and 1 z-layer (focal plane). Consecutive frames of the GFP channel displayed in inverted grey scale of the GFP channel. Arrowheads at 0 s show the small faint foci (white arrowheads).

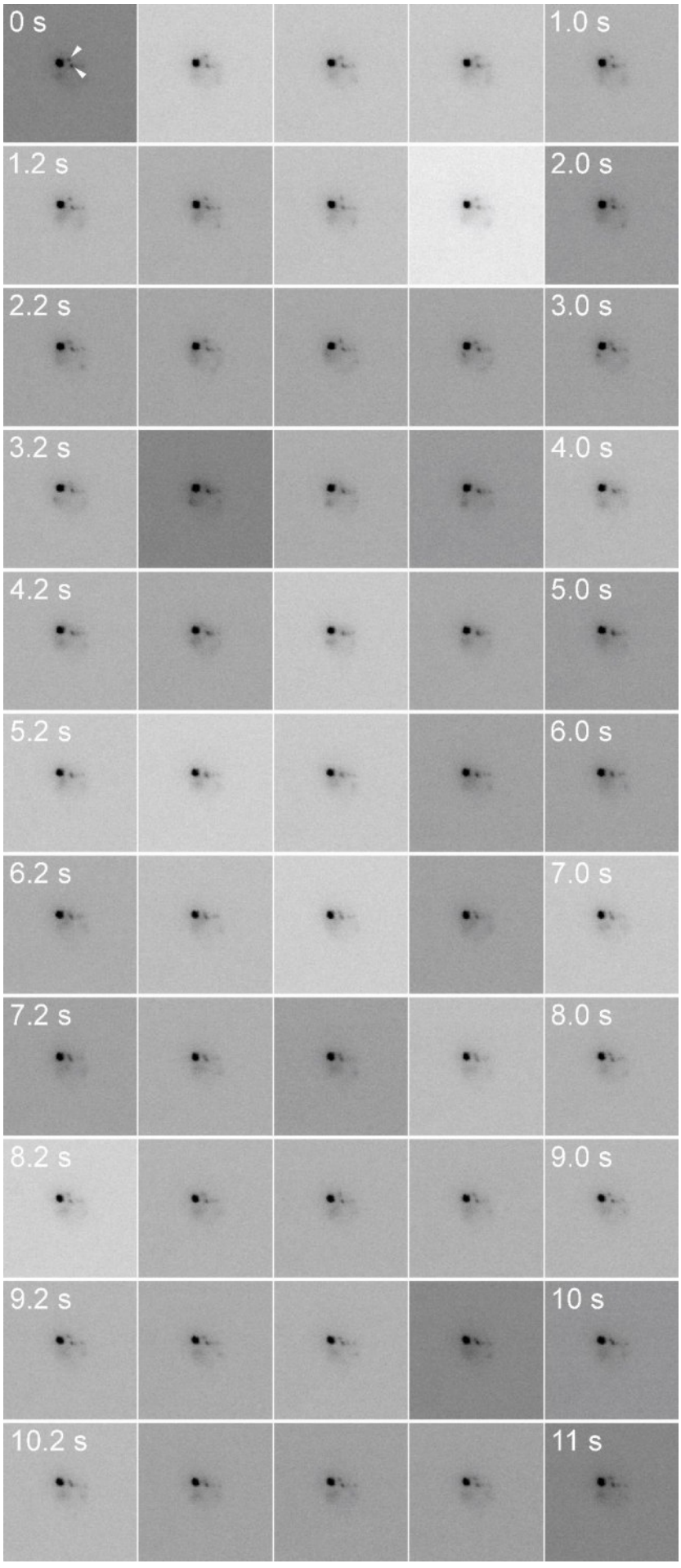
0 s
1.0 s
1.2 s
2.0 s
2.2 s
3.0 s
3.2 s
4.0 s
4.2 s
5.0 s
5.2 s
6.0 s
6.2 s
7.0 s
7.2 s
8.0 s
8.2 s
9.0 s
9.2 s
10 s
10.2 s
11 s

4.1.3 PfClathrin Heavy Chain is important for the survival of blood stage parasites

Since the aim was to study CHC function to test its potential role in HCCU and the live cell imaging of CHC did not reveal any information about such a role, inactivation of CHC was attempted. In order to initially test the importance of CHC for the survival of *P. falciparum* blood stage parasites, a targeted gene disruption (TGD) using selection linked integration (SLI) (Birnbaum et al., 2017) was attempted. First an *in silico* analysis of the CHC homologue was carried out to get information about the protein domains and conserved parts to design the truncated version for the TGD. In other eukaryotes CHC has characteristic domains (N- and C-terminal domains, ankle, distal leg, knee and proximal leg) that form the typical buckled protein structure (1.3.1, Figure 9 A) oligomerizing to the Clathrin triskelion (Musacchio et al., 1999; Smith et al., 1998). PfCHC contains a N-terminal domain (yellow) with a propeller repeat (dark blue), linker (grey), CHC 7-fold repeat (red) and TRP-like domains (tetratrico peptide repeat region; green), typical for the CHC domains as found in a motif scan (InterPro, EMBL-EBI). The presence and the arrangement of these features of CHC in *P. falciparum* are similar to the structure of the homologues in eukaryotes (Figure 9 A).

P. falciparum CHC was aligned using ClustalO (EMBL-EBI) to analyze the conservation of the *P. falciparum* CHC homologue in comparison to that of other protists and eukaryota. The predicted domains are highly homologue (red) to other organisms (using the CHC amino acid sequences of *Plasmodium falciparum*, *Toxoplasma gondii*, *Eimeria maxima*, *Mus musculus*, *Homo* sapiens) and the interspersed regions between the domains are either *P. falciparum* specific (turquoise) or conserved amongst Plasmodium species (green; comparing *P. falciparum*, *P. vivax*, *P. knowlesi*, *P. berghei*, *P. chabaudi* and *P. galinaceum*; similarity of 75 to 73 % depending on species). Taken together these information show a similar composition, structure, and likely function of the CHC in *Plasmodium* species in comparison to well investigated CHC in other model organisms.

For the TGD a targeting region of 2205 bp (out of 5991 bp total) in the region encoding the N-terminal part of CHC was chosen (Figure 9 A). Based on the sequence and motif analysis, this would lead to a truncation that would inactivate PfCHC. By using SLI (Figure 9 B), only parasites that harbor the integrated plasmid will express the neomycin phosphotransferase II protein and will become resistant to G418, hence parasites with the integration event can directly be selected (Birnbaum et al., 2017). If such parasites are not obtained despite G418 selection it can be assumed that the gene is essential for parasite growth (Birnbaum et al., 2017). In two of four attempts to disrupt CHC parasites were recovered after G418 selection.

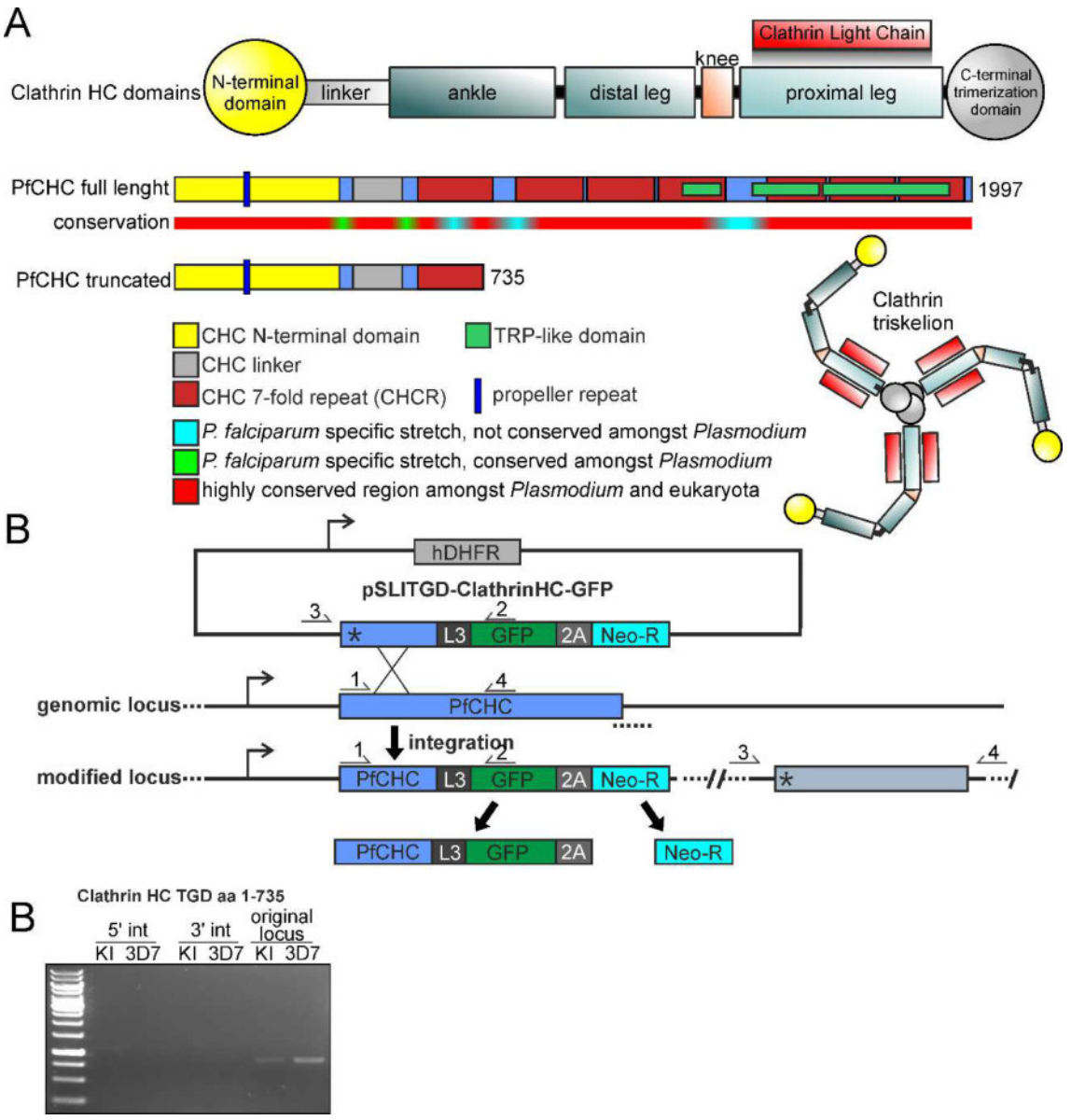

Figure 9: **Domains and structure of *P. falciparum* Clathrin Heavy Chain compared to other eukyryotes and attempted targeted gene disruption of the genomic CHC gene. A)** *In silico* analysis of the CHC protein. Domain features of the *P. falciparum* CHC (PfCHC full length) found with InterPro are aligned to structural elements important for the CHC function (CHC domains) (Musacchio et al., 1999; Smith et al., 1998). Homology of PfCHC in comparison to other protists and eukaryotes (*Toxoplasma gondii*, *Eimeria maxima*, *Mus musculus*, *Homo sapiens*) and amongst the phylum *Plasmodium* (*P. falciparum, P. vivax, P. knowlesi, P. berghei, P. chabaudi* and *P. galinaceum*) were analyzed with ClustalO. Conservation is depicted in colours of the bar. Truncation of the PfCHC used for TGD-SLI (PfCHC truncated). **B)** Schematic visualization of target gene disruption with selection linked integration (TGD-SLI) to test for essentiality of CHC in *P. falciparum* (not to scale). Plasmid used for integration of a truncated version (first 735 amino acids) of *P. falciparum* CHC tagged with GFP into the genome. The hDHFR resistance is for selection of parasites carrying episomal plasmid prior to integration. Integration of the construct via the homology region leads to expression of Neo-R resistance due to the 2A skip peptide. Parasites with integration events expressing Neo-R can thus be selected with G418. Integration of the plasmid was confirmed via PCR using primer pairs 1 and 2 (5'int: integrated plasmid); 3 and 2 (3'int: episomal plasmid, not integrated); 1 and 4 (original locus: intact gene, not integrated). (continued on the next page)

Figure 9 (continuation of previous page): **C)** Diagnostic PCR to check status of genomic locus of PfCHC in the knock in integration cell line (KI) after selection with G418 and the control (3D7). Primers are as described in B. No integration into the genomic locus of CHC was detected. Intact wild type gene in knock in cell line (KI) as in 3D7 genetic background cell line is shown by PCR product with primer pair 1 and 4. Marker: 1kb Gene Ruler (Thermo Fisher).

However, in all cases where parasites were recovered, incorrect integration was demonstrated by PCR, indicating integration into incorrect loci (Figure 9, appendix A-3). These data strongly suggested that CHC is essential for *P. falciparum* blood stage growth.

As based on the SLI-TGD data CHC can be assumed to be essential an inducible inactivation was necessary to assess its function in the parasite. For this an inducible protein inactivation system termed anchor away or knock sideways (Haruki et al., 2008; Robinson et al., 2010) that was recently established in *P. falciparum*, was used (Birnbaum et al., 2017) (Figure 10 A). This system is based on two protein domains, FKBP and FRB that dimerize upon addition of a small molecule (rapalog). One part (FRB) is fused to a nuclear localization signal (NLS) to target the construct to the nucleus. For visualisation the construct is also fused to a fluorophore (mCherry). This construct is termed the mislocalizerN. The second part of the dimerization system (FKBP) is fused to the target protein that also carries a fluorophore (in this case GFP) via genomic integration (to tag, visualize and target the genomically expressd target protein). Upon addition of the small dimerizer rapalog, the FRB and FKBP dimerize and the target protein is re-located to the nucleus due to its attachment to the mislocalizerN and therefore pulled away from its site of action (Figure 5 A). This 'knock sideways' can be visualized by microscopically imaging both fluorophores. When the knock sideways with CHC was attempted by addition of the dimerizer rapalog, no complete re-localization of CHC-2xFKBP-GFP to the nucleus was observed (Figure 10 B). Some of the CHC-2xFKBP-GFP did overlap with the nuclear mislocalizer-signal (Figure 10 B, arrow) but also reverse localization of the mislocalizer towards the Clathrin foci was observed (Figure 10 B, arrowhead). Even though that CHC was not completely re-localized to the nucleus, an average reduction in growth of 96 % (4 % survival) was observed in three independent FACS-based growth assays over 4 days (Figure 10 C, appendix A-1), suggesting that either a reduction of the CHC at its site of action is sufficient to ablate its function or that dimerization of the mislocaliser to the CHC already inactivated it.

Next a more detailed growth analysis using synchronous parasites was carried out to pinpoint the stage the growth defect after CHC inactivation. In a culture synchronized for rings rapalog was added to inactivate CHC and smears were taken after 20, 35 and 46 hours post synchronization. The stages for each of these time points were then quantified and compared to control cells grown without rapalog. This revealed that loss of CHC function had no effect on the development of ring and trophozoite stage parasites but led to an arrest in reinvasion of merozoites (43 % free merozoites with rapalog compared to 8 % in the control at 46 to 64 hours of growth) and a higher number of pycnotic parasites

after reinvasion (14 % with rapalog compared to 2 % in the control at 46 to 64 hours of growth), preventing productive completion of the cycle in red blood cells (Figure 10 E).

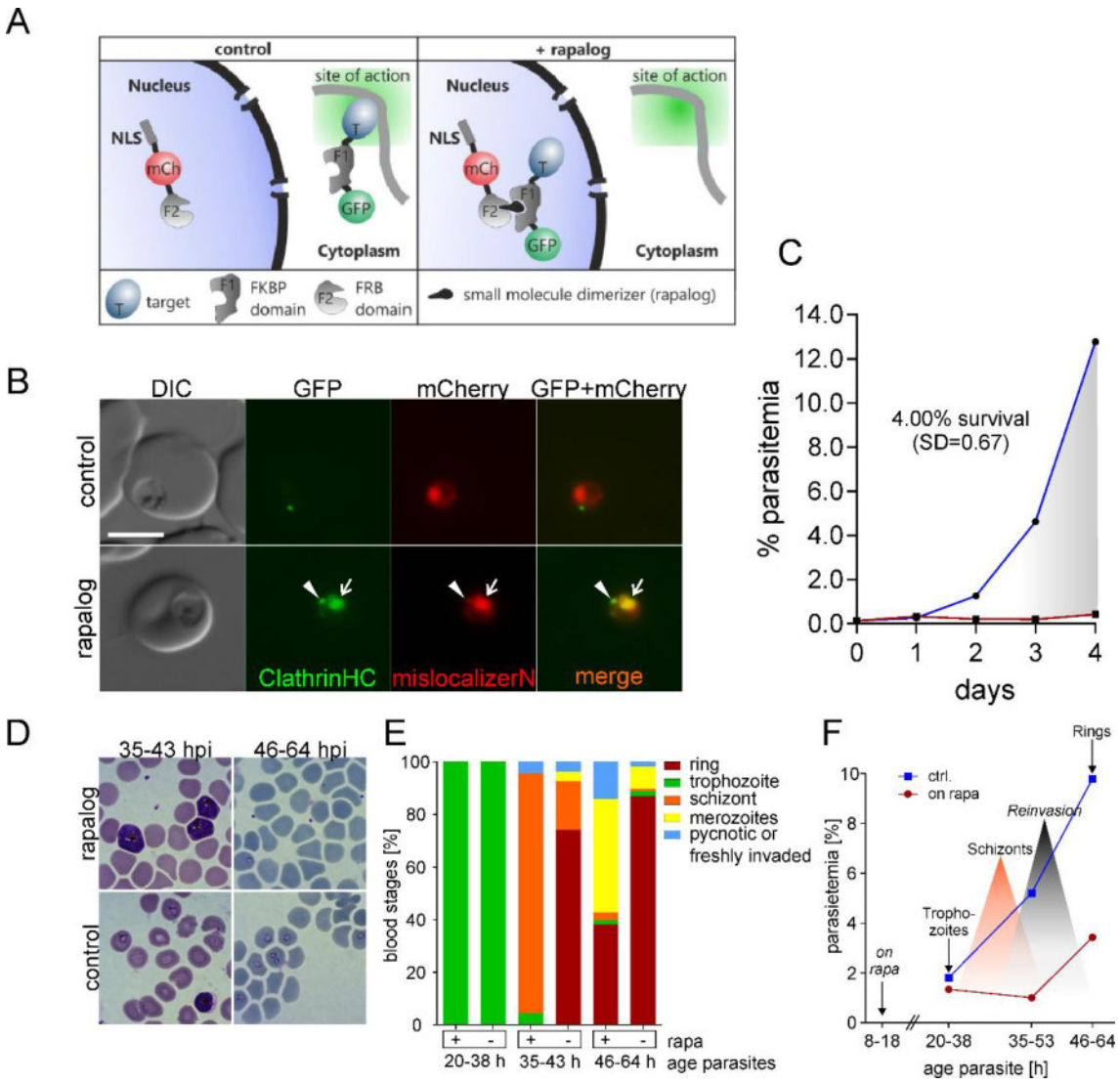

Figure 10: **Inducible inactivation of PfClathrin Heavy Chain using knock sideways**. **A)** Schematic illustration of the principle of the knock sideways (KS) system used to inducibly relocalize CHC into the nucleus (Scheme from Birnbaum et al., 2017). **B**) Representative live cell images of the cell line expressing endogenous CHC-2xFKBP-GFP and episomal mislocalizerN after addition of rapalog and control and incubation for 48 hours. Mislocalization of CHC-2xFKBP-GFP (arrow) and reverse localization of mislocalizerN to CHC-2xFKBP-GFP foci (arrowhead). DIC: differential interference contrast; GFP: green fluorescent protein; DAPI: nuclei. Scale bar: 5 µm. **C)** FACS-based growth assay for 4 days of CHC KS. **D-F)** Stage specific knock sideways experiment with synchronous CHC-2xFKBP-GFP parasites with mislocalizerN grown with or without rapalog (control). Rapalog was added at 8-18 hours of parasite age (second half of ring stage). Giemsa smears were taken at three time points of parasite age: 20-38 (trophozoites to schizonts), 35-53 (schizonts to rings) and 46-64 (rings to trophozoites) post invasion. **D)** Representative images of the giemsa smears of the 35-53 and 46-64 hours post invasion time points. **E**) The number of each stage of the blood phase in the stage specific knock sideways experiment was determined in the Giemsa smears and is plotted as percentage of total parasitemia (proportion of stages). Colours indicate the different stages. **F)** Parasitemia per time point from E is plotted as growth curve. One representative of two independent experiments is shown.

4.1.4 The PfClathrin Heavy Chain shares a compartment with Golgi-related proteins

The CHC of *P. falciparum* is essential for parasite growth but may not be involved in HCCU since its removal from the cell did not show an effect in trophozoites, the stage in which most of the host cell cytosole is taken up (1.4). To gain further insights about the potential role of CHC in malaria blood stages and corroborate the lack of a function in HCCU, next BioID (Roux et al., 2012) was used in a modified approach termed dimerization induced quantitative BioID (DiQ-BioID) to identify interactors and compartment neighbors of this protein. The DiQ-BioID technique was recently developed in our laboratory and combines the FRB-FKBP-dimerization system with proximity Biotin-labeling (BioID) followed by quantitative mass spectrometry (Figure 11 A). The target protein is endogenously tagged with FKBP and GFP as already used for the knock sideways system. The FRB domain is fused to a promiscuous Biotin-ligase (BirA*) and mCherry and expressed episomally. Upon addition of the dimerizer rapalog the BirA* is targeted to the protein of interest due to the dimerization of the FKBP and FRB domain. In the presence of Biotin BirA* labels all proteins in close proximity by unspecifically biotinylating all lysine residues that can be physically reached. Due to the attached Biotin, the labeled proteins can be isolated using Streptavidin beads and subsequently used for quantitative mass spectrometry. In case of the cell culture grown in the presence of rapalog, the protein of interest and its protein environment (including compartment neighbors and interactors) are labeled whereas the control represents all unspecifically labeled proteins (background) which then permits to subtract the background from the proteins in proximity of the CHC. Two different constructs with the BirA* biotin ligase either C- or N-terminally linked via a 7xGGGGS-linker to FRB-mCherry (plasmids cloned with partial work by Florian Kruse, Sven Flemming, Ernst Jonscher and Jakob Birnbaum), were here used to conduct DiQ-BioID with the CHC (Figure 11 B). These two configurations of the biotinylizer construct were used to exclude potentially limited access to the target complex due to the domain organisation of the biotinylizer construct. Upon addition of the dimerizer the cytosolic BirA*-N^L (BirA*-7xGGGGS-FRB-mCherry) was successfully relocated to the CHC-2xFKBP-mCherry as evident from a co-localisation of the two constructs by fluorescence microscopy with the corresponding parasites (Figure 11 C). The typical localization of both, the intense patch-like signal and the fainter foci of CHC was not altered after recruiting the BirA* construct to it. Next, biotin was added to both, the culture containing rapalog and the control and continued to grow for 24 h. A test experiment with 5 ml of culture was done to test for biotinylation in the presence of rapalog and in the control (no rapalog added). A western blot probed with Streptavidin-HRP showed that the cells grown in the presence of rapalog displayed a band migrating above the highest molecular weight represented by the marker (175 kDa) (Figure 11, black arrowhead), that was absent in the control and likely represented biotinylated target CHC-2xFKBP-GFP (calculated MW 314 kDa). This suggested that the procedure was successful and that BirA* biotinylated the target protein and therefore likely also proximate proteins. Several other bands were detected that were not present in the control, including bands of ~65 kDa, ~90 kDa and ~150 kDa (Figure 7, white arrowheads). One very intense

band was visible between 35-40 kDa (Figure 11 , grey arrowhead), potentially corresponding to the Clathrin Light Chain (calculated MW 30.5 kDa).

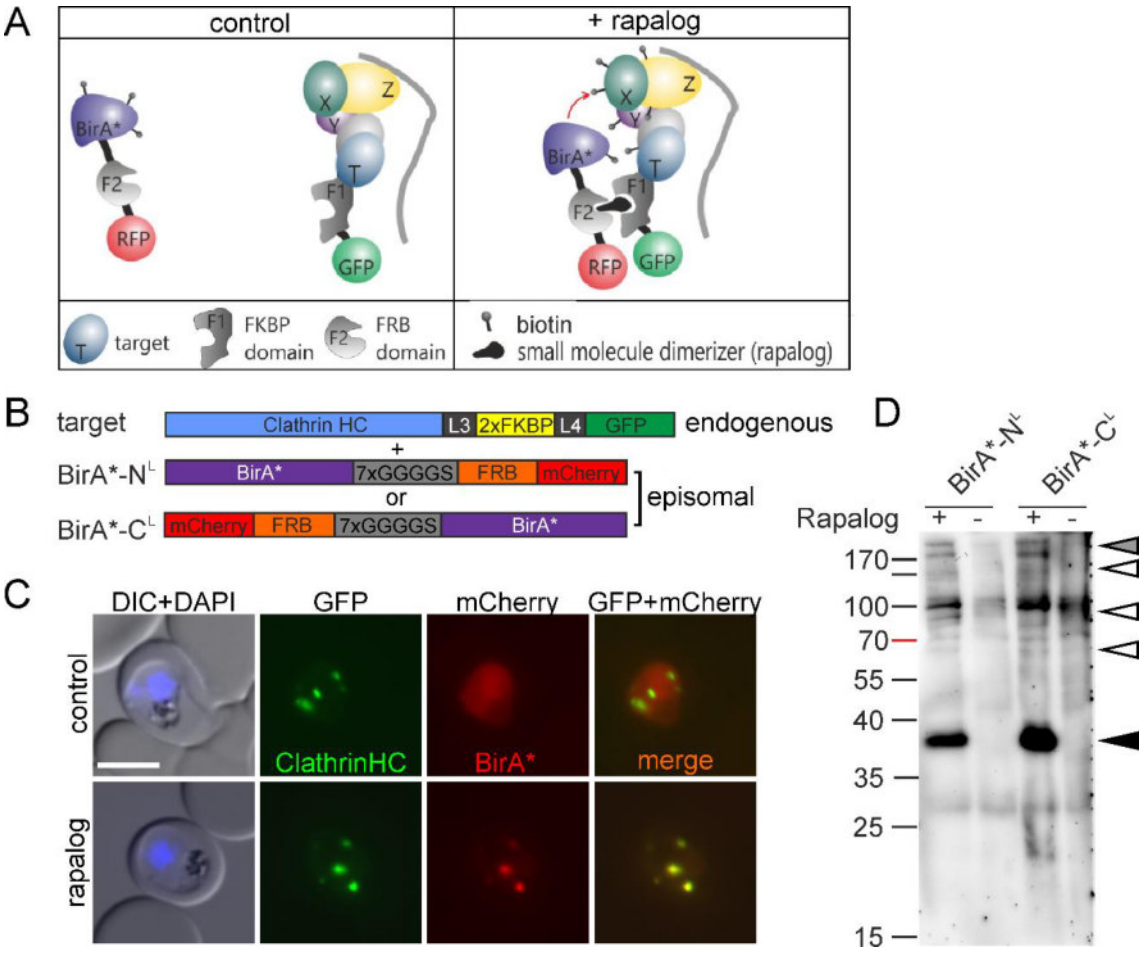

Figure 11: **Dimerization induced quantitative BioID (DiQ-BioID) with Clathrin Heavy Chain**. **A)** Schematic illustration of the principle of the DiQ-BioID system used to biotinylize the target PfCHC, its interactors and compartment neighbors based on inducible localization of the construct with the promiscuous biotin ligase BirA* to the target. Scheme from (Birnbaum, 2017). **B)** Schematic illustration (not to scale) of the target construct and of the used biotinylizer constructs with BirA* being tagged with a linker, FRB and mCherry either C- (BirA*-N^L) or N-terminally (BirA*-C^L). The target construct is expressed from the genomic locus and the mislocalizers are episomally expressed. **C)** Representative live cell images of the CHC-2xFKBP-GFP cell line with the BirA*-C^L mislocalizer grown with rapalog or left without (control) after 24 hours post addition of rapalog and biotin. DIC: differential interference contrast; GFP: green fluorescent protein; mCherry: mCherry red fluorescent protein; DAPI: nuclei; merge: GFP and mCherry channels merged. Scale bar: 5 µm. **D)** Western blot of a small scale experiment with 5 ml culture grown for 24 hours either with rapalog (+) or as the control without rapalog (-) probed with Steptavidin-HRP to see if biotinylization of proteins takes place. The band corresponding to the suspected biotinylated target CHC-2xFKBP-GFP is indicated by a grey arrowhead. The most intense band present in the culture with rapalog only is indicated with a black arrowhead. Several other bands that are not present in the control are indicated by white arrowheads. Molecular weight standard (Page Ruler prestained, Thermo Fisher) is indicated in kDa.

For identification of CHC interactors by DiQ-BioID by mass spectrometry, the experiment was scaled up to 150 ml of culture for each condition (the culture with rapalog and control culture without rapalog both originating from the same parental culture). The parasites for both conditions were grown in the presence of biotin for 24 hours, then lysed and biotinylated proteins purified using Strepatavidin-conjugated beads. The proteins bound to the beads were treated with trypsin to release the peptides of bound proteins followed by quantitative mass spectrometry using dimethyl labelling (carried out by Wieteke Hoeijemaker, Richárd Bártfai Lab, Radboud University). For each of the two cell lines (CHC-2xFKBP-GFP with biotinylizers BirA*-N^L and BirA*-C^L) two independent DiQ-BioID experiments with different culture batches were performed. The results for both experiments per cell line were then plotted by log2 ratio of enrichment in the rapalog culture (post processing performed by Wieteke Hoeijemaker, Richárd Bártfai Lab, Radboud University), resulting in a location in the top right quadrant for all proteins enriched in both experiments (Figure 12).

This analysis revealed a list of proteins specifically enriched in the rapalog containing culture over control. In order to determine the most enriched proteins in all four experiments (intersection of the two replicates and both biotinylizers), the average normalized log2 ratio in all experiments was calculated for proteins that were significantly enriched in at least two of the four experiments. The calculation was done by Wieteke Hoeijemaker (Richárd Bártfai Lab, Radboud University). The threshold for cut off was set at an average normalized log2 ratio of 0.8 which resulted in 43 enriched proteins in total (supplementary list: A-4). The significance of enrichment was determined as the calculated false discovery rate (FDR-value). An FDR value of 1e-2 was used as cut off for a protein to qualify as significantly enriched. Proteins of the 43 hits with annotation as unknown protein or with an unclear annotation were analyzed for homologies using BLAST searches (https://blast.ncbi.nlm.nih.gov/Blast.cgi; search against non-redundant database) to find homologies to known proteins. If no homology was detected, a search for protein domains was done (InterPro protein and sequence analysis & classification tool, https://www.ebi.ac.uk/interpro/) to find out a potential identity or function of the respective protein. Many of the identified proteins are proteins known in other organisms located at the Golgi or are involved in Golgi-trafficking.

The ten most enriched proteins and one of the least enriched proteins (for comparison) according to their average log 2 value of all experiments are listed in Table 9. The rank represents the position in the sorted list according to the value of the corresponding average normalized log2 ratio from highest (best enrichment) to lowest value (less enrichment). This list of the highest enriched proteins (Table 9) contains the CHC itself but also the CLC (even more enriched) and other known Clathrin interactors such as AP-1 components. Interestingly, this included also AP-4 and its only so far known interactor Tepsin (with high enrichment of averaged normalized log2 of 3.76) (Figure 12, Table 9 and Table 10) that are thought to be important for clathrin-independent transport from the *trans* Golgi to the early endosome (reviewed in Park and Guo, 2014; Robinson, 2004). The FDR value indicates the

confidence of the enrichment. The scatter plots (Figure 12) visualize enrichment for all proteins above the threshold (FDR 1e-2) in each independent experiment and revealed confidence of enrichment (FDR value) by overlapping degrees of enrichment of each protein in each experiment.

Comparison of the hits with the two biotinylizers, (BirA*-N^L and BirA*-C^L), showed that a similar set of proteins had been identified with high confidence (low FDR values) (Figure 12, Table 9, Table 10). The cell line with the BirA*-N^L biotinylizer (Figure 12 A) yielded 32 significantly enriched proteins (FDR: 1e2 to 1e-10) with 11 proteins showing very high confidence (FDR: 1e-10) of enrichment and 15 proteins with a high confidence (FDR: 1e-7 to 1e-10) of enrichment. Four proteins were identified that did not reach a significance better than a FDR 1e-7 to 1e-10 in the DiQ-BioID experiment of the CHC-2xFKBP-GFP cell line with the BirA*-C^L biotinylizer. These were PF3D7_0914900 (BSD-domain containing protein), PF3D7_0730200 (AP-4 β subunit), PF3D7_1210100 (SYN2), PF3D7_0804900 (GTPase-activating protein/GAP) and PF3D7_1451800 (sortilin). With the BirA*-C^L biotinylizer (Figure 12 B) 27 significantly enriched proteins (FDR: 1e2 to 1e-10), with 5 proteins showing very high confidence (FDR: 1e-10) of enrichment and 10 proteins with a high confidence (FDR: 1e-7 to 1e-10) of enrichment, were detected. All the very highly enriched proteins (FDR: 1e-10) in the BirA*-N^L probe were also present in the very highly enriched proteins with the BirA*-N^L biotinylizer, including CHC, CLC, PF3D7_0408100 (unknown protein), PF3D7_1459600 (unknown protein/tepsin) and PF3D7_1408700 (unknown protein with armadillo repeats) (Figure 12 and Table 9). Some proteins (for example PF3D7_1432800/HP12 Protein homologue, PF3D7_0904100/ AP-4 ε subunit, PF3D7_1247500 serine/threonine kinase) were detected with very high confidence in BirA*-N^L whereas they had a lower score in BirA*-C^L. All ten proteins in Table 9, that had an FDR of 1e-10 with both biotinylizers are represented among the ten most enriched proteins (Table 9, highlighted in red) and except for PF3D7_1408700 (unknown protein; rank 10) they ranked with the highest enrichment scores (rank 1 to 4). The proteins in ranks 5 to 9 all had low FDRs (from 1e-7 to 1e-10) with both biotinylizers but had a higher average enrichment score than PF3D7_1408700 (unknown protein) which belongs to the above mentioned group of proteins with a very low FDR of 1e-10 with both constructs, showing that the unknown protein PF3D7_1408700 has a comparably lower abundance but indicates that the proximate location or potential interaction had a high confidence. PF3D7_1432800, a HP12 domain protein, had a low FDR of 1e-10 with the BirA*-N^L but a comparably higher FDR score of 1e-6 with the BirA*-C^L (Table 9, highlighted in purple). One example of a protein that is significantly enriched with a comparably high FDR value with the BirA*-N^L biotinylizer only is PF3D7_1451800, a syntaxin (Table 9, highlighted in green). A selection of proteins with high enrichment and good confidence but also proteins with less enrichment and lower confidence, is shown in Table 10. These proteins are hits that supported a possible function and location at the Golgi. These proteins were chosen based on their homology to proteins known to be involved in intracellular trafficking (for example vesicle formation, membrane identity, regulatory functions in multiple trafficking steps, membrane fusion) or based on identified domains typical for

interaction with known trafficking proteins, known localization to a cellular compartment, phosphoinositol-binding, presence of transmembrane domains or suspected capability of protein-protein-interactions. These proteins might include potential clathrin interactors with unknown, possibly *Plasmodium* specific, function.

Table 9: **Sorted list of the most significantly enriched proteins for DiQ-BioID (with both biotinylizers BirA*-N^{L} and BirA*-C^{L}) with Clathrin Heavy Chain determined by the average normalized log2 ratio of all experiments and comparison of the normalized log2 ratios of each replica.**

rank	accession number	common name	log2 Ratio H/L normalized				average log2 Ratio normalized
			CHC +BirA*-N^{L}		CHC +BirA*-C^{L}		
			exp1	exp2	exp1	exp2	
1	PF3D7_1435500	Clathrin Light Chain	4.92	5.04	4.96	5.46	5.10
2	PF3D7_1219100	Clathrin Heavy Chain	4.62	4.70	4.54	4.69	4.71
3	PF3D7_0408100	unknown	4.27	4.29	4.22	4.22	4.25
4	PF3D7_1459600	unknown (Tepsin)	3.54	4.03	3.58	3.97	3.76
5	PF3D7_1455500	AP1 γ subunit	3.97	4.06	3.26	3.51	3.70
6	PF3D7_1118100	AP1 σ subunit	3.56	3.48	3.39	3.61	3.51
7	PF3D7_0202600	unknown (NA-binding)	3.45	3.44	3.10	3.24	3.31
8	PF3D7_1432800	HP12	3.16	2.89	3.39	2.98	3.26
9	PF3D7_0915400	PFK6	3.10	3.02	3.28	3.38	3.19
10	PF3D7_1408700	unknown (armadillo repeats)	3.16	2.89	3.39	2.98	3.11
38	PF3D7_1451800	syntaxin	1.77	1.16	1.06	0.98	1.24

Colors represent FDR values (confidence of enrichment): FDR 1e-10; FDR 1e-6; FDR <1e-

Figure 12 (next page): **Scatter plots of the identified proteins in mass spectrometry DiQ-BioID probes with Clathrin Heavy Chain**. Results of the quantitative mass spectrometry analysis of the DiQ-BioID for CHC with biotinylizer BirA*-N^{L} **(A)** and BirA*-C^{L} **(B)**. Cultures used for DiQ-BioID were split and either grown with rapalog or without rapalog (control). The identified proteins are plotted according to their enrichment represented by the normalized log2-ratios (rapalog over control). Independent experimental replicas are plotted on either axes with Experiment 1 on the X-axis and Experiment 2 on the Y-axis. Significantly enriched proteins are located in the upper right quadrant of the diagram. Significance is shown as the false discovery rate (FDR). Dots of the proteins with the most significant FDR-values (FDR: 1e-2 to 1e-10) are shown as colored diamonds (colors represent different FDR-values). Proteins marked with A or B reached significant negative enrichment. Mass spectrometry, data analysis and graph (modified) were done by Wieteke Hoeijemaker (Richárd Bártfai Lab, Radboud University). NA: nucleic acid.

A

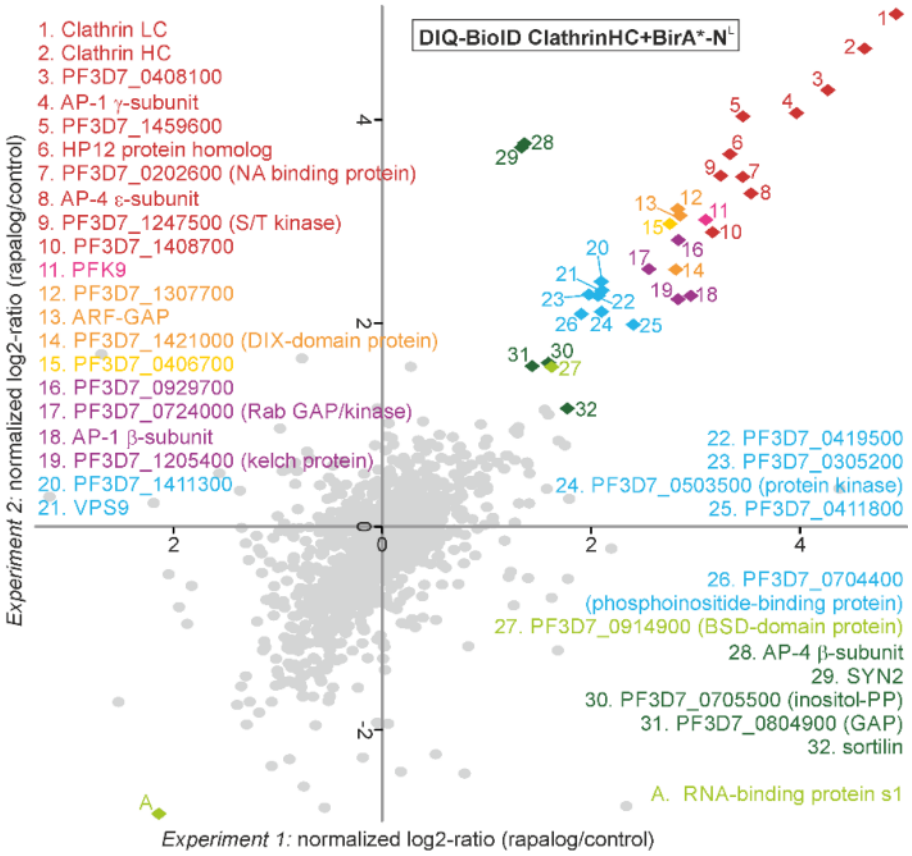

B

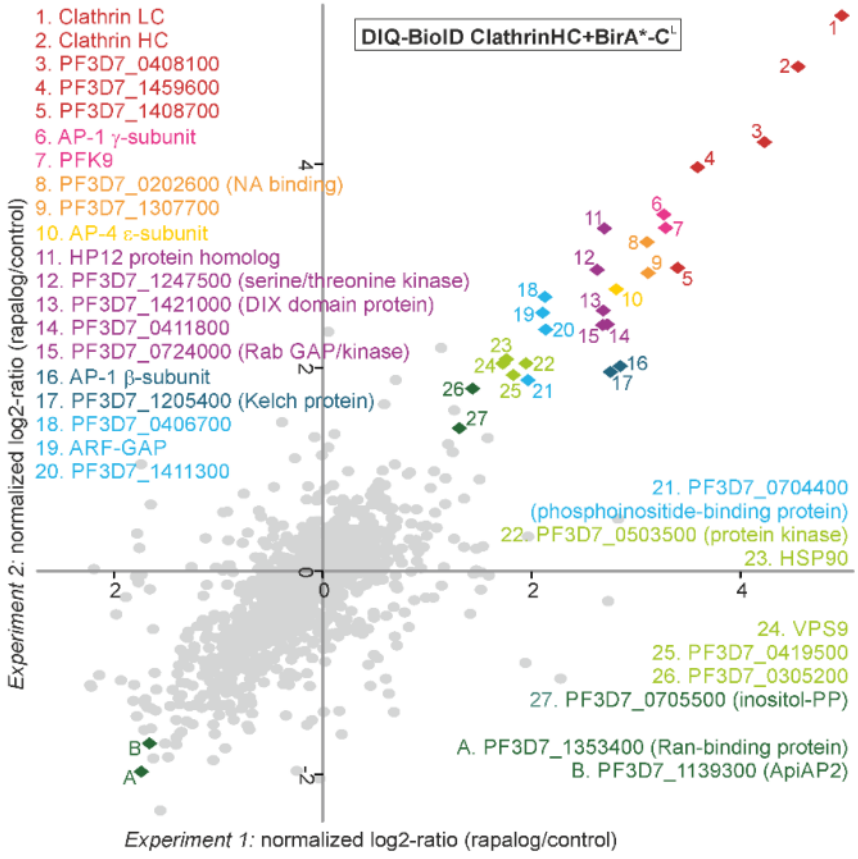

FDR: <1e-2 / 1e-3 / 1e-4 / 1e-5 / 1e-6 / 1e-7 / 1e-8 / 1e-9 / 1e-10

Table 10: **Selected Proteins identified with DiQ-BioID for Clathrin HC**

Accession Number	Annotation/Homologue	Domains	Function	BirA-N_L log2 ratio normalized Exp.1	Exp.2	BirA-C_L log2 ratio normalized Exp. 1	Exp.2	average log2 ratio normalized	Sign. in nr. of exp.
PF3D7_1435500	Clathrin Light Chain		Clathrin Cage Formation, Clathrin Coated Vesicle	4.92	5.04	4.96	5.46	5.10	4
PF3D7_1455500	AP-1 γ-subunit		Adaptor Protein Complex 1; Endosome - Golgi	3.97	4.06	3.26	3.51	3.70	4
PF3D7_1118100	AP-1 σ-subunit		Adaptor Protein Complex 1; Endosome - Golgi	3.56	3.48	3.39	3.61	3.51	4
PF3D7_0528100	AP-1 β-subunit		Adaptor Protein Complex 1; Endosome - Golgi	2.96	2.27	2.84	2.02	2.52	4
PF3D7_0904100	AP-4 ε subunit		Adaptor Protein Complex 4; Golgi	3.53	3.28	2.80	2.77	3.10	4
PF3D7_0730200	AP-4 β subunit		Adaptor Protein Complex 4; Golgi	1.36	3.77	NaN	NaN	2.56	2
PF3D7_1459600	conserved Plasmodium protein, unknown function	Tepsin homology, ENTH/VHS domain	direct interaction with AP-4 β and AP-4 ε; membrane interaction; protein-protein-interaction	3.45	4.03	3.58	3.97	3.76	4
PF3D7_0815800	VPS9		GDP-GTP exchange factor (GEF)	2.11	2.32	1.72	2.04	2.05	4
PF3D7_0526200	ARF-GAP	Protein kinase domain; Rab-GTPase-TBC domain	small GTPase activation	2.85	3.06	2.10	2.54	2.64	4
PF3D7_0724000	Rab GAP/kinase		rab GTPase activation	2.55	2.53	2.67	2.42	2.55	4
PF3D7_0804900	GTPase-activating protein (GAP)		small GTPase activation	1.44	1.58	1.19	1.25	1.36	3
PF3D7_1421000	DIX-domain protein	DIX domain	protein-protein-interaction, signal transduction (vesicles Wnt signalling), association with PDZ-domain	2.81	2.53	2.68	2.56	2.65	4
PF3D7_1205400	Kelch protein	Kelch-type β propeller	protein-protein interaction	2.83	2.23	2.75	1.96	2.44	4
PF3D7_0416900	conserved Plasmodium protein, unknown function	long N-terminal WD40/YVTN repeat-like-containing domain	protein-protein interaction	1.77	0.84	0.69	1.88	1.28	3
PF3D7_1019600	conserved Plasmodium protein, unknown function	Pleckstrin homology (PH) domain	phosphatidylinositol binding, protein recruitment to membranes	1.56	1.15	1.58	NaN	1.43	2
PF3D7_0705500	inositol-phosphate phosphatase (Inositol-PP)	SAC-domain	inositol phosphate metabolism, and phosphatidylinositol signaling system.	1.59	1.61	1.30	1.41	1.48	4
PF3D7_0704400	Phosphoinositide binding protein	phox homologous domain (PX domain); WD40/YVTN repeat-like-containing domain	phosphoinositide-binding, signalling, vesicular trafficking, protein sorting and lipid modification; protein binding	1.91	2.09	1.951.96	1.81	1.96	4
PF3D7_1307700	conserved Plasmodium protein, unknown function	ENTH/VHS-domain	Interaction with PIP-binding clathrin adaptors, membrane binding, protein-protein-interaction	2.83	3.12	3.11	2.93	3.00	4
PF3D7_1451800	Sortilin	2x WD40 domain, VPS10 domain, 2x sialidase domain, sortilin N-terminal & sortilin C-terminal domain	sorting and transport; Sialic acid linkage, sorting receptor	1.77	1.16	1.06	0.98	1.24	2
PF3D7_1210100	syntaxin, Qa-SNARE family, SYN2	tSNARE domain	vesicular fusion	1.33	3.73	0.85	NaN	1.97	2
PF3D7_0305200	conserved Plasmodium protein, unknown function	GRIP domain	typical for Golgins, binding to Golgi-Membranes, localization to Golgi	1.98	2.28	1.43	1.80	1.87	3
PF3D7_1411300	conserved Plasmodium protein, unknown function	Golgin subfamily A member 6-like	located to Golgi, involved trafficking and Golgi strucutre	2.10	2.41	2.13	2.38	2.25	4
PF3D7_0915400	Probable ATP-dependent 6-phosphofructokinase (PFK9)		glycolysis	3.10	3.02	3.28	3.38	3.19	4
PF3D7_0419500	conserved Plasmodium protein, unknown function	5x TM-helix at C-terminus	transmembrane protein	2.07	2.27	1.82	1.93	2.02	4
PF3D7_1227300	conserved Plasmodium protein, unknown function	2x transmembrane domains	transmembrane protein	3.28	NaN	2.84	NaN	3.06	2
PF3D7_0830400	conserved Plasmodium protein, unknown function	2x transmembrane (N- and C-terminal, signalpeptide), Circum- sporozoite-related antigen – domain (CRA)		-0.77	1.65	1.13	2.20	1.05	2
PF3D7_0914900	BSD domain protein	BSD domain	unknown function, found in synapse related proteins	1.62	1.57	1.57	1.31	1.52	3
PF3D7_1408700	conserved Plasmodium protein, unknown function	armadillo like repeat	protein-protein-interaction	3.16	2.89	3.39	2.98	3.11	4

Overall, the hits enriched in the CHC DiQ-BioID show a set of proteins very plausible for a function at the Golgi but no overlap with proteins that were previously identified as potentially being involved in endocytosis and host cell cytosol uptake (HCCU) in *P. falciparum* (Flemming, 2015). Interestingly, the AP-2 complex, which is the Adaptor-Complex responsible for Clathrin mediated endocytosis at the plasma membrane, was absent. These results confirm the results of a lacking colocalisation of the CHC with overexpressed Epsin-mCherry (a supposed endocytosis protein) (Flemming, 2015) (and Figure 8), and overexpressed Kelch13-mCherry (Figure 13), a protein possibly involved in HCCU (section 4.2.3).

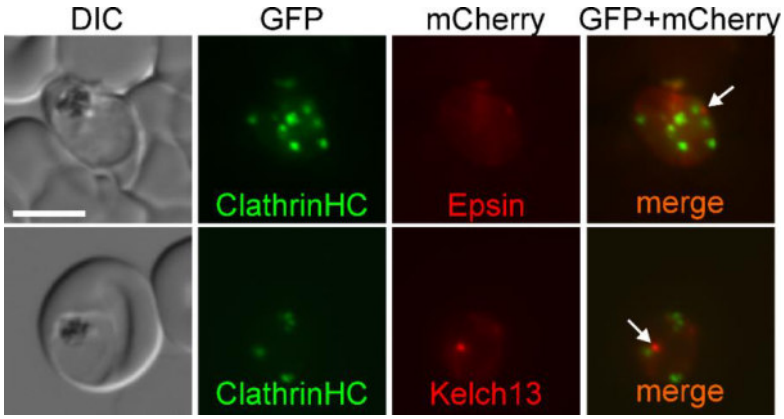

Figure 13: **Lacking colocalisation of Clathrin Heavy Chain-2xFKBP-GFP with putative HCCU markers.** Representative fluorescence microscopy images of live parasites expressing endogenously 2xFKBP-GFP-tagged CHC and the episomally expressed HCCU markers (Epsin and Kelch13) tagged with mCherry. White arrows show foci of Epsin and Kelch13 not colocalizing with CHC foci. DIC: differential interference contrast; GFP: green fluorescent protein; mCherry: mCherry red fluorescent protein; DAPI: nuclei; merge: GFP and mCherry channels merged. Scale bar: 5 µm.

4.1.5 Clathrin Heavy Chain might be involved in Golgi-to-endosome trafficking

The DiQ-BioID results with clathrin (4.1.6), the localization of CHC close to the nucleus similar to the Golgi marker GRASP (Struck et al., 2005) (4.1.2.; Table 6) and a role of CHC in the secretory pathway in *T. gondii* (Pieperhoff et al., 2013) indicates a potential localization of CHC at the Golgi in *P. falciparum.* In agreement with this in *T. gondii* Sortilin, which here was identified in the CHC DiQ-BioID, is involved in secretory trafficking (Hallee et al., 2018; Pieperhoff et al., 2013; Sloves et al., 2012) and this may involve a Golgi proximal endosome-like compartment (McGovern et al., 2018). To test whether CHC may contribute to such a pathway in *P. falciparum* parasites, the effect of the inhibitor Retro-2 (Stechmann et al., 2010) was analyzed. This compound inhibits a syntaxin-5 dependent retromer-trafficking (Endosome to Golgi) pathway (Nonnenmacher et al., 2015). Endogenously expressed CHC-2xFKBP-GFP showed an altered localization upon treatment with 100 µM Retro-2 compared to controls. Instead of the typical patch-like and punctate localization, the GFP signal was dispersed into many very small foci in addition to a cytosolic distribution (Figure 12). Fast frame rate microscopy was performed with the CHC cell line without Retro-2 inhibitor (control) or

after incubation with 100 µM Retro-2 for 4.5 hours, 16 hours and 20 hours (Figure 14 B) and analyzed with the Image J Plugin Time lapse Color Coder to visualize spatiotemporal changes of the fluorescence signals. The control showed the typical CHC pattern with the large patches and the small foci (Figure 12, dynamics represented by gradual change of colors, whereas stationary foci remain white). In contrast 4.5 h of treatment with Retro-2 resulted in a higher number of small foci while the large patches were still present (Figure 12). After 16 and 20 hours of treatment no large patches were found and small vesicles were detected all over the cell next to the prominent cytosolic distribution of fluorescence signal, indicating that the GFP-patches were dispersed (Figure 12).

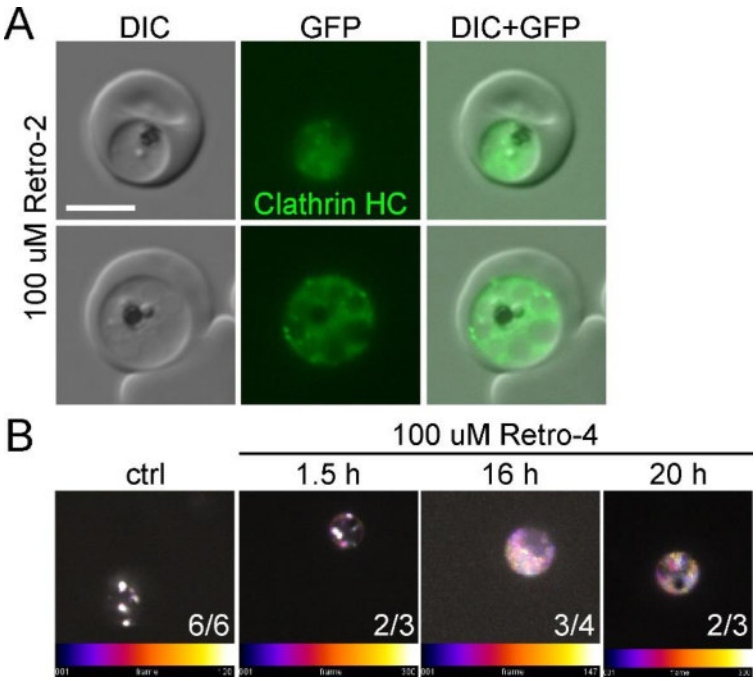

Figure 14: **Clathrin Heavy Chain localization is abolished upon treatment with the retromer inhibitor Retro-2**. Treatment of CHC tagged with 2xFKBP-GFP with the Endosome-to-Golgi Retromer inhibitor Retro-2. **A)** Representative fluorescence live microscopy images of the CHC-2xFKBP-GFP cell line treated for 16 h with Retro-2. DIC: differential interference contrast; GFP: green fluorescent protein. Scale bar: 5 µm. **B)** Fast frame rate live cell videos of untreated CHC-2xFKBP-GFP parasites (ctrl) and after treatment with Retro-2 for 1.5 hours, 16 hours and 20 hours. The grey scale images of the GFP channel were analyzed with the temporal color coder by ImageJ. Dynamics of fluorescent signals are visualized by giving each frame different false colors resulting in differently merged colors in case of dynamic foci or white in case of static foci. The numbers are the counts of the observed Retro-2 phenotypes per total numbers of analyzed cells.

In order to test if the effect of Retro-2 on CHC-2xFKBP-GFP was specific and not just the result of killing the parasites, the Eps15-2xFKBP-GFP cell line (4.2) episomally expressing Kelch13-mCherry (4.2.3) was treated with Retro-2. Eps15 and Kelch13 did not show any obviously altered localization after 24 h of Retro-2 treatment (Figure 15) but still colocalized either in all foci (Figure 15, upper row) or in a subset of foci (Figure 15, lower row). It should be noted that the reason for incomplete overlap of some foci likely was due to movement of the foci while switching the filters to acquire the images of the fluorescence channels (Figure 15 B, second row; movement of Eps15 and Kelch13 analyzed in 4.2.3).

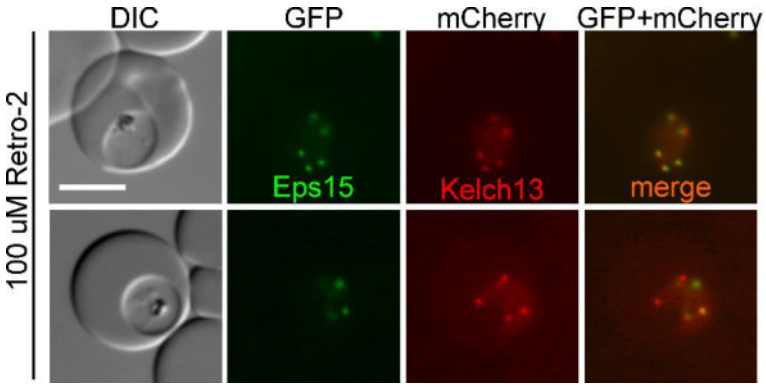

Figure 15: **The retromer inhibitor Retro-2 has no apparent effect on Eps15 and Kelch13 foci.** Representative fluorescence live cell microscopy images of the corresponding cell line of the putative HCCU candidates Eps15 endogenously tagged with 2xFKBP-GFP-2xFKBP and episomally expressed Kelch13 tagged with mCherry after the cells had been incubated with the Endosome-to-Golgi Retromer inhibitor Retro-2 for 20 h. DIC: differential interference contrast; GFP: green fluorescent protein. Scale bar: 5 µm.

Taken together, the DiQ-BioID results and the Retro-2 experiment indicate that CHC has no role in HCCU but may serve in secretory trafficking from post-Golgi to the parasite specific apical organelles similar to the homologue of CHC in *T. gondii* (Pieperhoff et al., 2013).

4.2 PfEps15 as a component of HCCU

CHC mediates the most prominent endocytic pathway in other eukaryotes but the results of this work give no indication for a similar role in *P. falciparum* parasites, suggesting that Clathrin is restriced to secretory functions at the Golgi in Apicomplexans. As the aim of this work was to identify proteins involved in HCCU, further molecules that may be involved in this process were analyzed. The work of Sven Flemming highlighted Eps15 as an interesting protein potentially involved in HCCU based on its protein domains, its localization adjacent to the food vacuole, its shuttling movement between the parasite's plasma membrane and food vacuole and the colocalisation of PfEps15-GFP with hemoglobin filled structures in correlative electron microscopy (Flemming, 2015). However, its role in HCCU has not been functionally demonstrated. As a first step towards this goal, it was necessary to test its essentiality for *Plasmodium* blood stages (4.2.1). In addition the improved microscopy methodology permitting sub-second frame rates of image acquisition (4.1.1) was here used (4.2.3) in an attempt to obtain further information about the spatiotemporal localization of Eps15 that may indicate a role in HCCU. Finally, interaction analysis using DiQ-BioID was used to find Eps15 interactors and compartment neighbors (4.2.3) and conditional inactivation for functional analysis (4.2.1) to obtain a comprehensive view of the potential function of this protein in HCCU.

4.2.1 PfEps15 may be essential for the parasite blood stage

The N-terminus of PfEps15 is homologous to Eps15 proteins from other eukaryotic organisms but the C-terminal part is *Plasmodium* specific (Flemming, 2015). Two EH-Domains, giving the Eps15 identity, are located in the conserved N-terminus followed by 3 DxF-motifs that facilitate putative interaction with the Adaptor Complex 2 (AP-2) during endocytosis processes (Brett et al., 2002). Two clusters of multiple potential ubiqutinylation sites (UIM, ubiquitin interaction motif) were detected (UbPred), one cluster between the second EH-domain and the first DxF-motif and one cluster at the very C-terminus of the protein (Figure 16 A). As a first attempt to test the importance of Eps15 for the parasite, a selectable targeted gene disruption (SLI-TGD) was attempted according to previously published protocols (Birnbaum et al., 2017). Two truncation constructs were generated (Figure 16 A): One that would delete the gene from the region encoding the middle of the second EH-Domain onwards (amino acid 1 to 198) and one that would result in a truncated protein containing the N-terminus ending at the last part of the first EH-Domain (amino acid 1 to 121). Both constructs did either not integrate (five or three attempts, for the 2 constructs, respectively), or when integrants were obtained, they had integrated at incorrect sites, as demonstrated by a diagnostic PCR (Figure 16 D, appendix A-3). Due to the fact that correct integrations can be selected for with this method, and a failure to obtain correct integration so far indeed correlated with the essentiality of a gene (Birnbaum et al., 2017), it is likely that the *eps15* gene is important for the survival of *P. falciparum* blood stages.

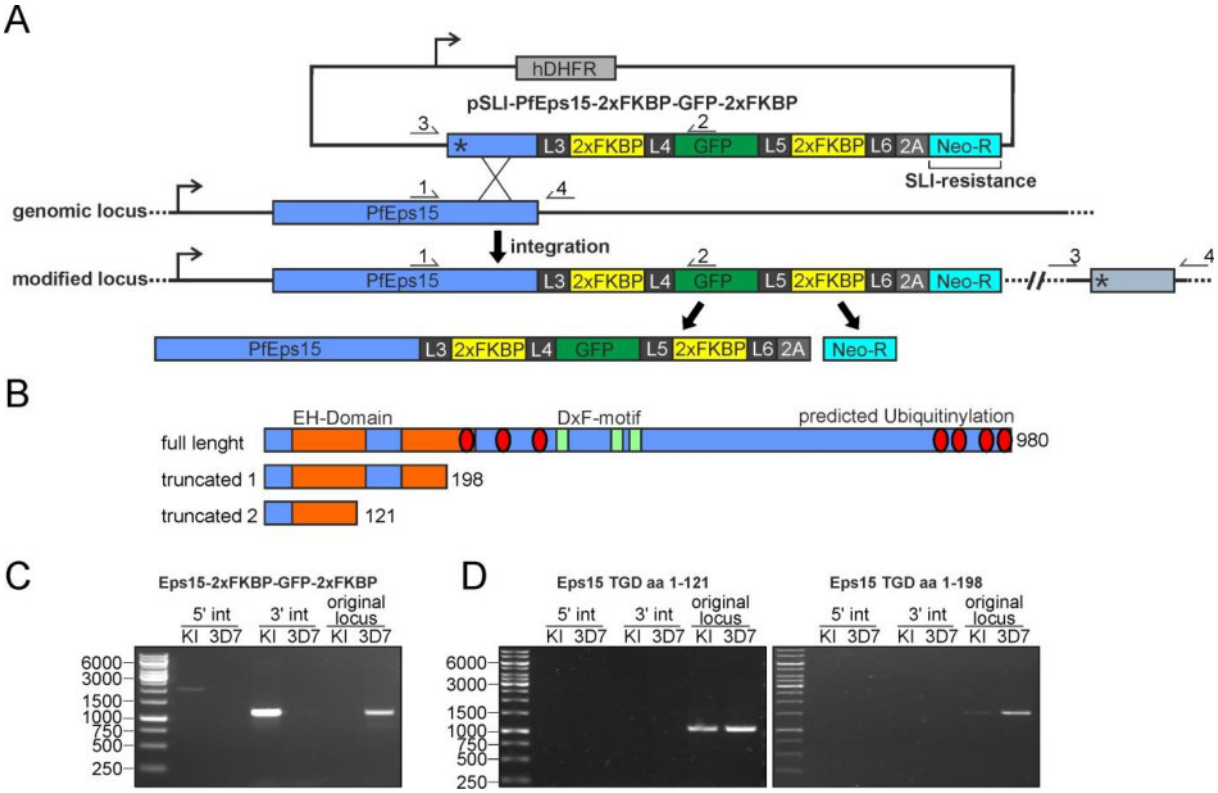

Figure 16: **Generation of Eps15-2xFKBP-GFP-2xFKBP cell line and attempted SLI-TGD of PfEps15**. **A)** Schematic representation (not to scale) of the plasmid used for integration with selection linked integration (SLI) (Birnbaum et al., 2017) to tag Eps15 with 2xFKBP-GFP-2xFKBP endogenously in *P. falciparum*. hDHFR, human dehydrofolate reductase; Neo-R, neomycin phosphotransferase II gene 2A, T2A skip peptide. Parasites with integration events expressing Neo-R can be selected with G418. Arrows with numbers show position of primers used to test for correct integration (see C). **B)** Domain structure of PfEps15 (not to scale). EH Domain (orange bar): Eps15 homology domain. DxF-motif (turquoise bar): Adaptor complex 2 binding motif. UIM (red ovals): predicted ubiquitinylation. Truncated 1 and to show product that would have resulted from successful disruption with selection linked integration (TGD-SLI) of PfEps15. **C)** Diagnostic PCR to check status of genomic locus of Eps15 in the knock in integration cell line (KI) with Eps15-2xFKBP-GFP-2xFKBP after selection with G418 and the control (3D7) using the primers indicated in A. Correct integration into the genomic locus of Eps15 is detected with primer pairs 1 and 2 (5'int: covering the 5' integration junction), 3 and 4 (3' int: covering the 3' integration junction), 3 and 2 (3'int: episomal plasmid, not integrated). Intact wild type gene in 3D7 genetic background cell line is shown by PCR product with primer pair 1 and 4 (original locus: intact gene, not integrated) but is not present in in knock in cell line (KI). **D)** SLI-TGD to test for essentiality of Eps15 in *P. falciparum.* Diagnostic PCR of Eps15 TGD-SLI cell lines retrieved after selection with G418 as described for C) One example out of 3 attempts were there was integration detected for Eps15 TGD aa 1-121 (truncated 2) and for 4 attempts for Eps15 TGD aa 1-198 (truncated 1) are shown. DNA size marker is shown in bp. Marker: 1kb Gene Ruler (Thermo Fisher).

Based on the SLI-TGD results that Eps15 likely is essential for parasite survival, conditional inactivation is necessary to further analyze its function. This was previously attempted using knock sideways in a cell line where Eps15 had been tagged with 2xFKBP-GFP but only a modest inactivation had been achieved (Flemming, 2015). A new cell line was therefore here generated where

Eps15 was endogenously tagged with 2xFKBP-GFP-2xFKBP using the pSandwich-plasmid and SLI (Figure 16 B and C). This sandwiched GFP-tag was found to be the more effective to mislocalize proteins using knock sideways than the 2xFKBP-GFP tag (Birnbaum et al., 2017). The mislocalization system for Eps15 was completed with the nuclear mislocalizer (mislocalizerN) consisting of a single nuclear mislocalization signal (NLS), one FRB-domain and the mCherry fluorophore episomally expressed under the 5' upstream region of the *nmd3* gene (Birnbaum et al., 2017), a further improvement over the previously used *crt* 5'UTR_1xNLS-FRB-mCherry mislocalizer (Flemming, unpublished). Using this configuration, addition of rapalog caused mislocalization of the Eps15 in addition to reverse localization of the mislocalizer towards the foci of Eps15 (Figure 17 A). Next FACS based growth assays over 4 days (2 intraerythrocytic cycles) were carried out to assess the impact of knocking Eps15 aside. This revealed an average reduction in growth of 42 % of the Eps15 knock sideways compared to control (Figure 17 B, appendix A-2).

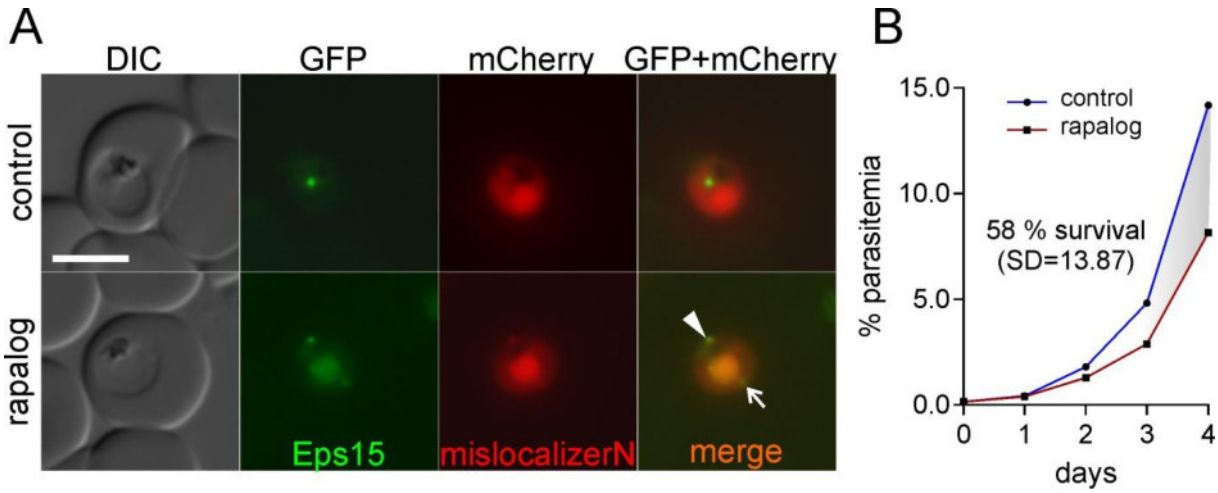

Figure 17: **Knock sideways of PfEps15-2xFKBP-GFP-2xFKBP. A)** Representative live cell images of a parasite of Eps15 tagged with 2xFKBP-GFP-2xFKBp cell line expressing episomal mislocalizerN after addition of rapalog and control. Mislocalization of Eps15-2xFKBP-GFP-2xFKBP (arrow) and reverse localization of mislocalizerN to Eps15-2xFKBP-GFP-2xFKBP foci (arrowheads). DIC: differential interference contrast; GFP: green fluorescent protein; mCherry: mCherry red fluorescent protein; DAPI: nuclei. Scale bar: 5 µm. **B)** FACS based growth assay of Eps15 knock sideways (one representative experiment out of six independent experiments) for 4 days (2 cycles) resulted in a 42 % growth deficit (calculated of all five experiments, SD=13.87).

Taken together these data indicate that PfEps15 is important for *P. falciparum* blood stages. However, no phenotype was obvious after knock sideways with this protein, possibly due to incomplete mislocalization and the activity of the proportion of protein remaining at its site of action.

4.2.2 PfEps15-like shuttles between the parasite's plasma membrane and the food vacuole

Previous work suggested a directed movement of Eps15 foci between the parasite plasma membrane and the FV (Flemming, 2015). Using the confocal laser scanning microscope, two different types of foci were present: First, foci at the parasite plasma membrane (PPM) in close proximity to a focus at

the food vacuole that appear to move towards each other. Second, foci that were more distant to the food vacuole, that appear to gravitate towards the food vacuole and sometimes also move back to their starting point (Flemming, 2015). For simplicity throughout this work, these movements are termed from now on short distance movement and long distance movement, respectively. The previous time lapse experiments had a temporal resolution of 8 seconds for 3D-stacks and 0.2 seconds for 2D stacks. Therefore previous experiments were not able to track foci continuously in 3D. In an attempt to improve this, the established set up for high frame rate microscopy using the Olympus IX81 setup (4.1.1) was applied for Eps15 to replicate the results of Flemming, 2015 in a higher number of cells and with a better resolution in time.

The fast frame rate imaging of Eps15-2xFKBP-GFP-2xFKBP with the Olympus IX81 setup achieved a frame rate of 0.75 to 2 second per stack for tracking Eps15 foci in a Z-stack of 5 to 20 layers. The viability of the cell and the localization of Eps15 GFP foci in relation to the parasite plasma membrane and the FV are shown in merged DIC and GFP green fluorescence channels in Figure 18. The cells shown in Figure 18 were subsequently imaged with fast frame rate life cell microscopy (Figure 19, Figure 20, Figure 21, Figure 22). The number of appearance of each kind of movement was counted in cells imaged in three independent imaging sessions. Cells with more than six foci were not analyzed since these parasites appeared to be schizonts in the corresponding DIC image. Cells were considered as showing no movement of Eps15 foci if any focus of the cell did not move. If a subset of the present foci were moving, the cell was assigned to the equivalent movement.

In agreement with the results of Flemming, 2015 two types of movements were detected. The movement over a short distance of two foci in close proximity at the food vacuole was seen in multiple cells (Figure 19: red arrowhead; Figure 21 cell 1 and cell 2, yellow and orange arrowheads) and appeared to be the most abundant with 52 % of all analyzed cells (Table 11). In some cells the short distance movement appeared to be a stretching of one or multiple foci instead of converging and splitting foci (Figure 21, cell 3, red arrowhead). The movement over longer distance (Figure 20 and Figure 22, cell 2) was observed in 26 % of the analyzed cells (Table 11). The movement over a longer distance was seen in different appearances. A direct movement from the periphery to the FV (Figure 20, red arrowhead) and movement of foci along the periphery before it directly moves to the FV (Figure 22, cell 2, red arrowhead). Also no movement of a subset of the Eps15 foci (Figure 19 and Figure 21, cell 1) or of none of the foci (Figure 22, cell 1) of a cell was present in 22 % the analyzed cells over the observation time frame (Table 11).

Table 11: **Quantification of the appearances of the different types of movements of Eps15 tagged with 2xFKBP-GFP-2xFKBP.** Counts indicate number of foci observed with a given movement. Movement types are explained in the results text.

analyzed cells n=23	long distance movement	short distance movement	no directed movement
Counts	6	20	5
percentage	26 %	52 %	22 %

This data reproduces the results of Flemming 2015 but the movements observed here appeared less clear than described previously (Flemming, 2015). Here, some cells also showed more complex short distance movement of two or more foci in close proximity of the FV (for example Figure 19). This might represent rearrangement of the structure to which the Eps15 foci localize instead of movement of the Eps 15 foci. The movement of Eps15 foci over longer distances was also observed as not always being immediately to the FV as described previously (Flemming, 2015), since preceding movement along the periphery was observed.

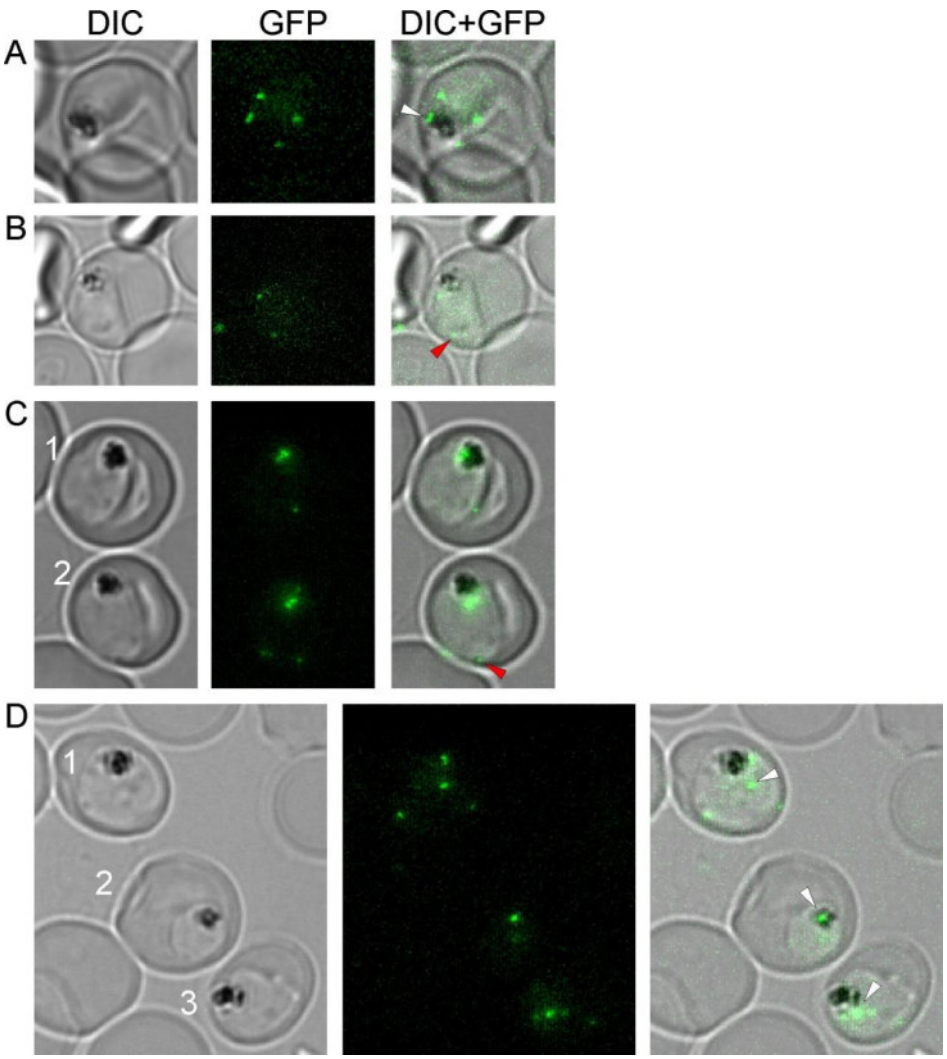

Figure 18: **Localization of Eps15-2xFKBP-GFP-2xFKBP in relation to the FV in cells subsequently imaged with fast frame rate life cell microscopy to analyze movement of Eps15 foci.** Fluorescence life cell microscopy image of cells imaged with fast frame rate microscopy to characterize movement of Eps15 foci inside the *P. falciparum* cell. DIC images visualize the parasite plasma membrane and the FV. Maximum intensity projection of GFP fluorescence microscopy Z-stack at 0 s (first frame of subsequent fast frame rate live cell microscopy), showing localization of Eps15 foci in relation to the FV. Moving foci analyzed with fast frame rate microscopy are highlighted with white arrowheads when close to the FV (undergoing short distance movement) and red arrowheads when distant from the FV (undergoing long distance movement). Cells in **A), B), C)** and **D)** correspond to the fast frame rate live cell microscopy shown in Figure 19, Figure 20, Figure 21, and Figure 22, respectively. Cells are numbered as in the corresponding panels of the fast frame rate live cell microscopy. DIC: differential interference contrast; GFP: green fluorescent protein.

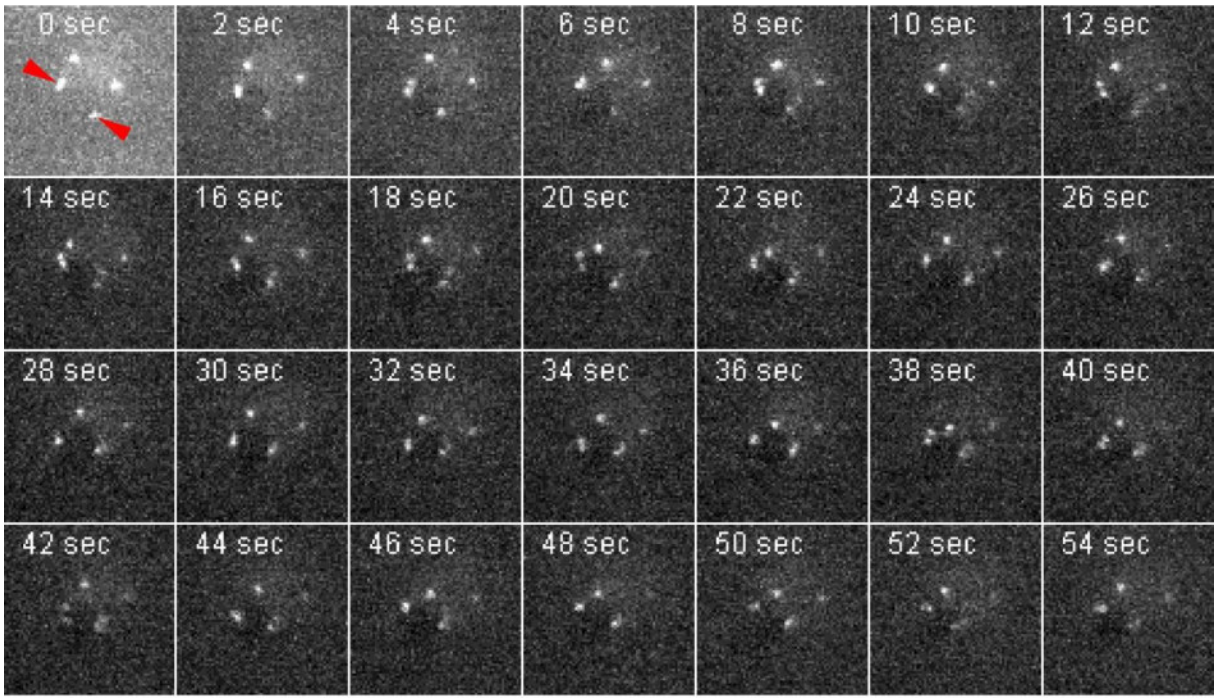

Figure 19: **Fast frame rate live cell microscopy of *P. falciparum* cell expressing Eps15 tagged with 2xFKBP-GFP-2xFKBP shows repeated movement of two foci towards each other and back over a short distance (see Figure 18 A for overlay of this parasite with DIC)**. The OlympusIX81-setup for fast frame rate imaging was used to image movement of Eps15 foci. Shown is the maximum intensity projection of the green fluorescence channel of all layers of 3D fluorescent live cell images of a parasite expressing endogenously tagged Eps15-2xFKBP-GFP-2xFKBP. Parameters were 100 ms exposure time, 2x2 binning and 20 z-layers per time point (2 s per interval time between stacks). Red arrowhead shows foci at the food vacuole that undergo repeated movement.

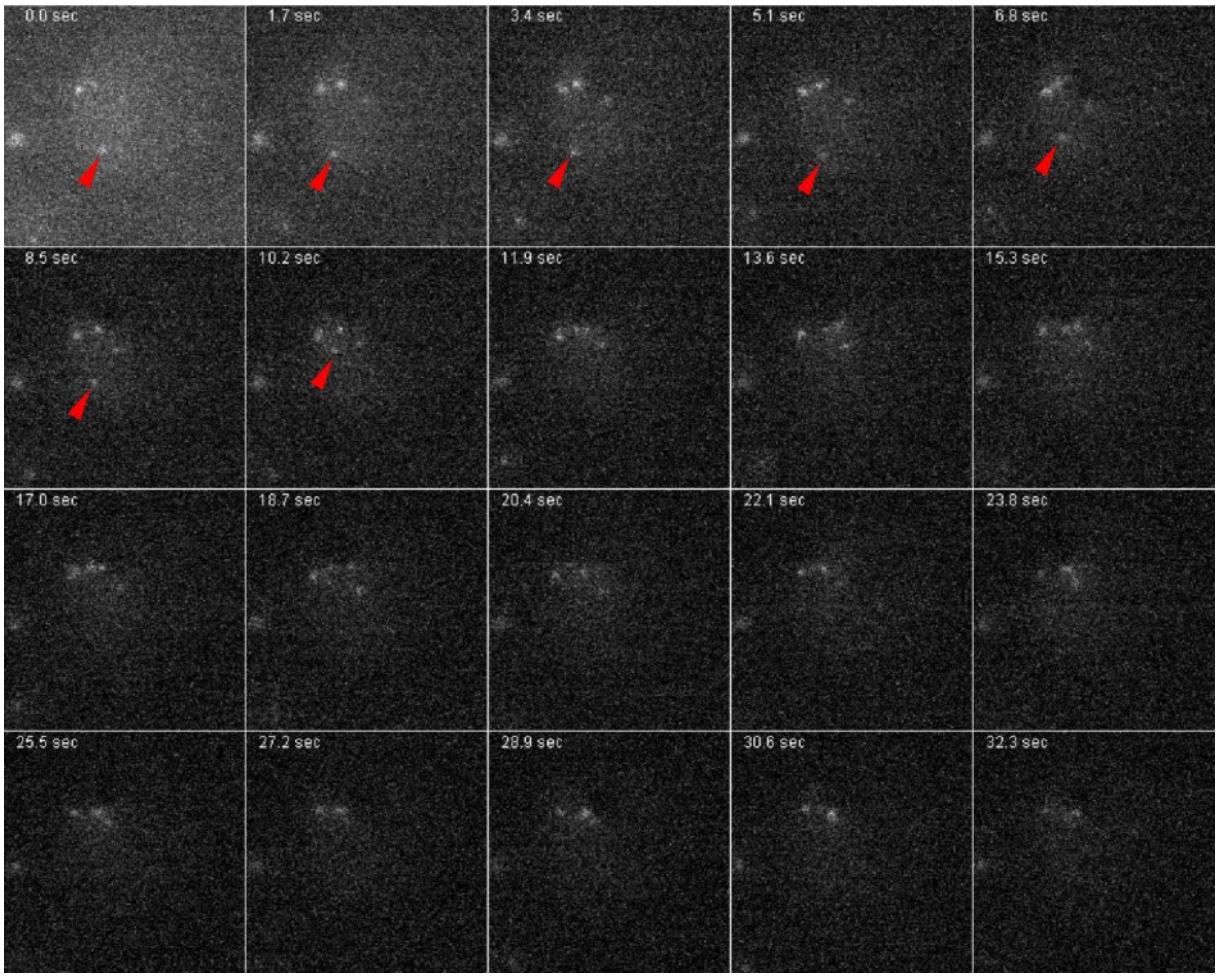

Figure 20: **Fast frame rate live cell microscopy of *P. falciparum* cell expressing Eps15 tagged with 2xFKBP-GFP-2xFKBP shows movement of a focus to the FV over a long distance (see Figure 18 B for overlay of this parasite with DIC).** The OlympusIX81-setup for fast frame rate imaging was used to image movement of Eps15 foci. Shown is the maximum intensity projection of the green fluorescence channel of all layers of 3D fluorescent live cell images of a parasite expressing endogenously tagged Eps15-2xFKBP-GFP-2xFKBP. Parameters were 100 ms exposure time, 2x2 binning and 17 z-layers per time point (1.7 s per stack). Red arrowhead shows focus distant from the FV that moves to the FV.

Figure 21 (next page): **Fast frame rate live cell microscopy of *P. falciparum* cell expressing Eps15 tagged with 2xFKBP-GFP-2xFKBP shows different types of movement of two foci over a short distance (see Figure 18 D for overlay of this parasite with DIC)**. The OlympusIX81-setup for fast frame rate imaging was used to image movement of Eps15 foci. Shown is the maximum intensity projection of the green fluorescence channel of all layers of 3D fluorescent live cell images of parasites expressing endogenously tagged Eps15-2xFKBP-GFP-2xFKBP. Parameters were 155 ms exposure time, 2x2 binning and 5 z-layers per time point (0.775 s per interval time between stacks). Three cells are shown. Cell 1 shows 4 foci of which one undergoes short distance movement (yellow arrowhead). Cell 2 shows two foci which undergo short distance movement (orange arrowhead). Cell 3 shows 3 foci of which two undergo a stretching and merging like short distance movement (red arrowhead).

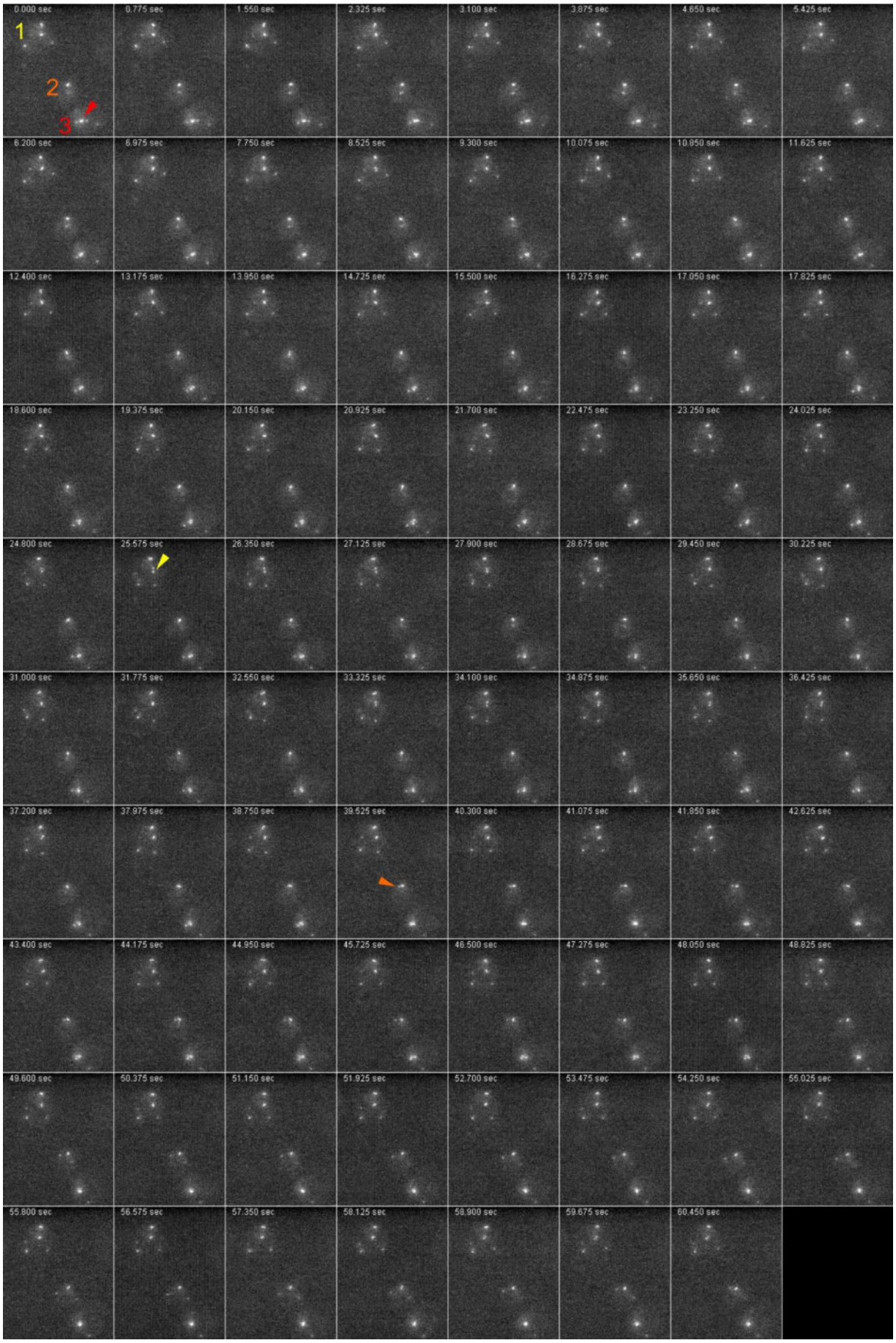
0.000 sec
1
2
3
0.775 sec
1.550 sec
2.325 sec
3.100 sec
3.875 sec
4.650 sec
5.425 sec
6.200 sec
6.975 sec
7.750 sec
8.525 sec
9.300 sec
10.075 sec
10.850 sec
11.625 sec
12.400 sec
13.175 sec
13.950 sec
14.725 sec
15.500 sec
16.275 sec
17.050 sec
17.825 sec
18.600 sec
19.375 sec
20.150 sec
20.925 sec
21.700 sec
22.475 sec
23.250 sec
24.025 sec
24.800 sec
25.575 sec
26.350 sec
27.125 sec
27.900 sec
28.675 sec
29.450 sec
30.225 sec
31.000 sec
31.775 sec
32.550 sec
33.325 sec
34.100 sec
34.875 sec
35.650 sec
36.425 sec
37.200 sec
37.975 sec
38.750 sec
39.525 sec
40.300 sec
41.075 sec
41.850 sec
42.625 sec
43.400 sec
44.175 sec
44.950 sec
45.725 sec
46.500 sec
47.275 sec
48.050 sec
48.825 sec
49.600 sec
50.375 sec
51.150 sec
51.925 sec
52.700 sec
53.475 sec
54.250 sec
55.025 sec
55.800 sec
56.575 sec
57.350 sec
58.125 sec
58.900 sec
59.675 sec
60.450 sec

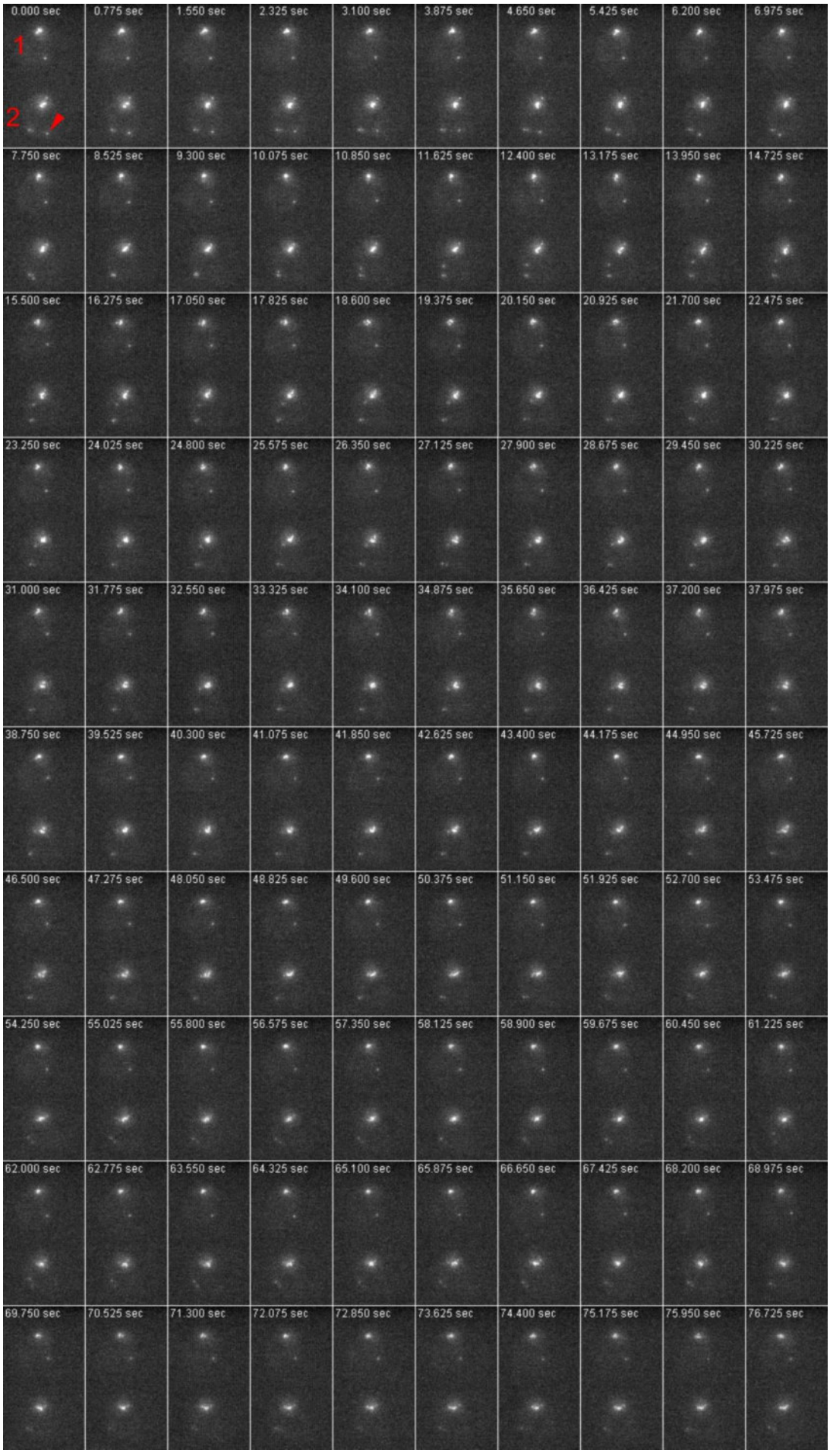
0.000 sec
0.775 sec
1.550 sec
2.325 sec
3.100 sec
3.875 sec
4.650 sec
5.425 sec
6.200 sec
6.975 sec
1
2
7.750 sec
8.525 sec
9.300 sec
10.075 sec
10.850 sec
11.625 sec
12.400 sec
13.175 sec
13.950 sec
14.725 sec
15.500 sec
16.275 sec
17.050 sec
17.825 sec
18.600 sec
19.375 sec
20.150 sec
20.925 sec
21.700 sec
22.475 sec
23.250 sec
24.025 sec
24.800 sec
25.575 sec
26.350 sec
27.125 sec
27.900 sec
28.675 sec
29.450 sec
30.225 sec
31.000 sec
31.775 sec
32.550 sec
33.325 sec
34.100 sec
34.875 sec
35.650 sec
36.425 sec
37.200 sec
37.975 sec
38.750 sec
39.525 sec
40.300 sec
41.075 sec
41.850 sec
42.625 sec
43.400 sec
44.175 sec
44.950 sec
45.725 sec
46.500 sec
47.275 sec
48.050 sec
48.825 sec
49.600 sec
50.375 sec
51.150 sec
51.925 sec
52.700 sec
53.475 sec
54.250 sec
55.025 sec
55.800 sec
56.575 sec
57.350 sec
58.125 sec
58.900 sec
59.675 sec
60.450 sec
61.225 sec
62.000 sec
62.775 sec
63.550 sec
64.325 sec
65.100 sec
65.875 sec
66.650 sec
67.425 sec
68.200 sec
68.975 sec
69.750 sec
70.525 sec
71.300 sec
72.075 sec
72.850 sec
73.625 sec
74.400 sec
75.175 sec
75.950 sec
76.725 sec

Figure 22: **Fast frame rate live cell microscopy of *P. falciparum* cell expressing Eps15 tagged with 2xFKBP-GFP-2xFKBP shows no movement of any foci and a different type of movement over a long distance (see Figure 18 C for overlay of this parasite with DIC)**. The OlympusIX81 Cell^R set up for fast frame rate imaging was used to image movement of Eps15 foci. Shown is the maximum intensity projection of the green fluorescence channel of all layers of 3D fluorescent live cell images of parasites expressing endogenously tagged Eps15-2xFKBP-GFP-2xFKBP. Parameters were 155 ms exposure time, 2x2 binning and 5 z-layers per time point (0.775 s per interval time between stacks). Two cells are shown. Cell 1 shows 2 foci of which none moves. Cell 2 shows three foci which one undergoes long distance movement (red arrowhead) with preceding movement along the parasites periphery.

4.2.3 PfEps15 interactome contains the Artemisinin-resistance marker Kelch13

The movement of Eps15 analyzed with fast frame rate microscopy of Eps15 foci supports the conclusion of Eps15 as potentially involved in HCCU (4.2.2). One of the interaction partners of Eps15 in endocytosis in other eukaryotes is CHC. However, in agreement with lacking support for a role of PfCHC in HCCU in this work, Eps15 was not found among the potential interaction partners of CHC in *P. falciparum* (4.1.4). In order to determine whether Eps15 might be part of a different, potentially endocytosis-relevant complex, DiQ-BioID (4.1.4) was used with the cell line expressing the endogenously 2xFKBP-GFP-2xFKBP tagged Eps15 together with an episomally expressed BirA*-N^L biotinylizer (Figure 23 A). The BirA* overexpression construct was successfully pulled towards the foci of the tagged Eps15 when rapalog was added to the culture (Figure 23 B). In a test experiment with 5 ml culture the cells were incubated with biotin and with or without rapalog for 24 hours. The cells were harvested, and the parasite lysate used for a Western Blot probed with Streptavidin-HRP. A band of > 200 kDa was more prominently labelled in the rapalog sample, suggesting it might correspond to biotinylated Eps15-2xFKBP-GFP-2xFKBP (Figure 23 C, arrowhead). Few other bands were obviously biotinylated and none had clearly increased signal intensity in the rapalog sample compared to the control (Figure 23 C). However, as quantitative mass spectrometry can distinguish enriched proteins also if they are present in comparably small amounts (and based on previous experiments indicating that biotinylation of the target is a good indicator to detect interacting proteins), a large scale sample (150 ml for each condition) was prepared, the parasite isolated, lysed and the biotinylated proteins bound to Streptavidin-coated beads. The proteins bound to the beads were proteolytically cleaved into peptides and used for quantitative mass spectrometry. The large scale culture was repeated on a different occasion to obtain a second replica, resulting in two experiments originating from independent parasite cultures. The quantitative mass spectrometry and the post processing of the dataset were done by Wieteke Hoeijemaker (Richárd Bártfai Lab, Radboud University). .

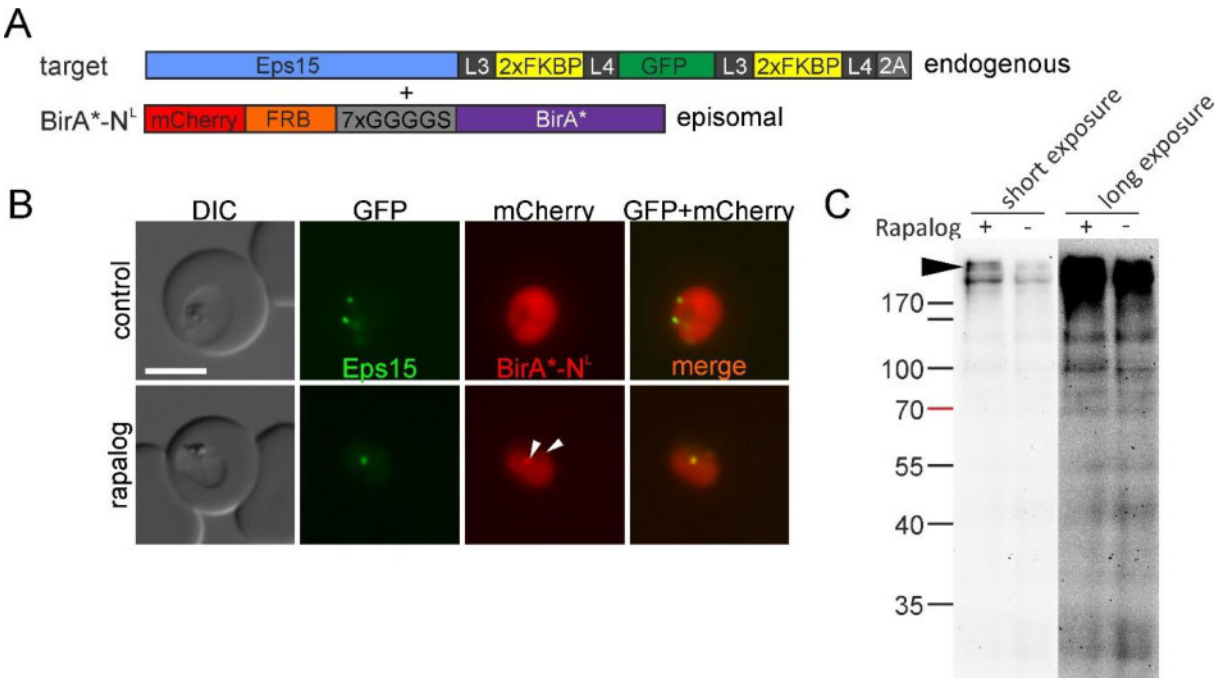

Figure 23: **Dimerization induced quantitative BioID (DiQ-BioID) with Eps15 to find interaction partners**. **A**) Schematic illustration (not to scale) of the target construct Eps15-2xFKBP-GFP-2xFKBP and of the biotinylizer construct with BirA* fused at its C-terminus with a linker, FRB and mCherry (BirA*-N^L). The target construct was integrated into the genome (endogenously expressed) and the mislocalizers was episomally expressed. **B)** Representative live cell images of the Eps15-2xFKBP-GFP-2xFKBP cell line (green) with the BirA*-C^L mislocalizer (red) grown with rapalog or without (control). DIC: differential interference contrast; GFP: green fluorescent protein; mCherry: mCherry red fluorescent protein; merge: GFP and mCherry channels merged. Scale bar: 5 µm. **C)** Western blot of a small scale experiment with 5 ml culture grown either with rapalog (+) or as the control without rapalog (-) probed with Steptavidin-HRP to detect biotinylized proteins. Two different exposure times of the western blot are shown to visualize intense bands (low exposure) and faint bands (high exposure). The band corresponding to the suspected biotinylation of Eps15-2xFKBP-GFP-2xFKBP is indicated by a black arrowhead. Molecular weight standard (Page Ruler prestained, Thermo Fisher) is indicated in kDa.

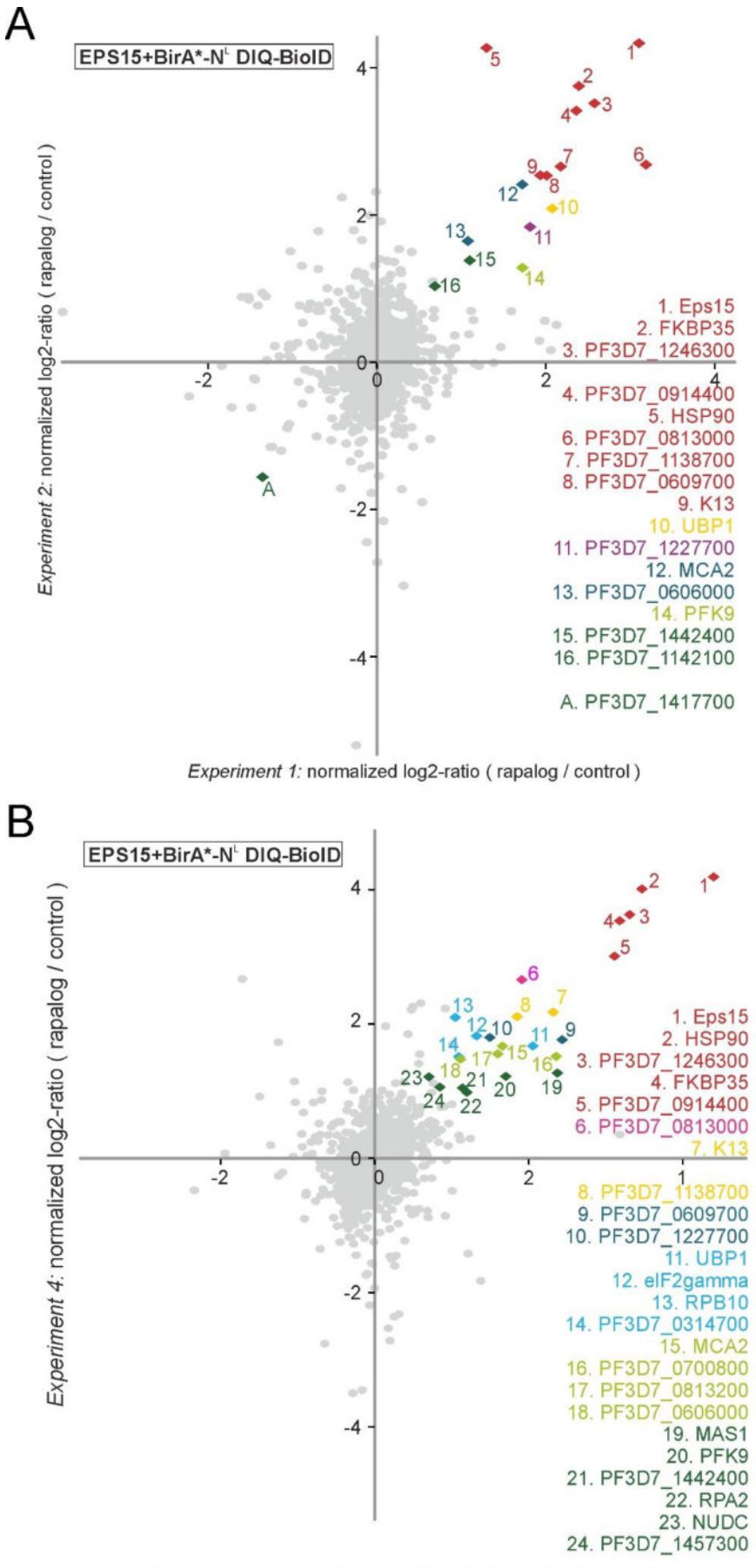
A
EPS15+BirA*-N^L DIQ-BioID
Experiment 2: normalized log2-ratio (rapalog / control)
Experiment 1: normalized log2-ratio (rapalog / control)
1. Eps15
2. FKBP35
3. PF3D7_1246300
4. PF3D7_0914400
5. HSP90
6. PF3D7_0813000
7. PF3D7_1138700
8. PF3D7_0609700
9. K13
10. UBP1
11. PF3D7_1227700
12. MCA2
13. PF3D7_0606000
14. PFK9
15. PF3D7_1442400
16. PF3D7_1142100
A. PF3D7_1417700
B
EPS15+BirA*-N^L DIQ-BioID
Experiment 4: normalized log2-ratio (rapalog / control)
Experiment 3: normalized log2-ratio (rapalog / control)
1. Eps15
2. HSP90
3. PF3D7_1246300
4. FKBP35
5. PF3D7_0914400
6. PF3D7_0813000
7. K13
8. PF3D7_1138700
9. PF3D7_0609700
10. PF3D7_1227700
11. UBP1
12. eIF2gamma
13. RPB10
14. PF3D7_0314700
15. MCA2
16. PF3D7_0700800
17. PF3D7_0813200
18. PF3D7_0606000
19. MAS1
20. PFK9
21. PF3D7_1442400
22. RPA2
23. NUDC
24. PF3D7_1457300
FDR: <1e-2 / 1e-3 / 1e-4 / 1e-5 / 1e-6 / 1e-7 / 1e-8 / 1e-9 / 1e-10

Figure 24 (previous page): **Scatter plots of the identified proteins in mass spectrometry of DiQ-BioID probes with Eps15**. Results of the mass spectrometry analysis of the DiQ-BioID with the 2xFKBP-GFP-2xFKBP-Eps15 cell line expressing biotinylizer BirA*-N^L. Two experimental replicas **(A)** and **(B)** with two technical replicas (Experiment 1 and Experiment2; Experiment 3 and 4) were performed. Cultures used for DiQ-BioID were either grown with rapalog or without rapalog (control). The identified proteins are plotted according to their enrichment represented by the normalized log2-ratios (rapalog over control). Individual experimental replicas are plotted on either axes with Experiment 1 and 3 on the X-axis and Experiment 2 and 4 on the Y-axis. Significantly enriched proteins are located in the upper right quadrant of the diagram. Significance is shown as the false discovery rate (FDR). Dots of the proteins with the most significant FDR-values (FDR: 1e-2 to 1e-10) are shown as colored diamonds (colors represent different FDR-values). The Protein marked with A is negatively enriched. Mass spectrometry, data analysis and graph (modified) were done by Wieteke Hoeijemaker (Richárd Bártfai Lab, Radboud University).

Analysis of the hits obtained from the mass spectrometry analysis of the Eps15 DiQ-BioID experiment revealed a list of significantly enriched proteins in two independent replicas with two independent experiments each (Figure 24, Table 12, supplementary list: A-5). Enrichment of proteins was identified by the normalized log 2 ratio (rapalog over control) in the quantitative mass spectrometry (Figure 24, Table 12, supplementary list: A-5). The identified proteins of each experimental replica (technical replicas: experiment 1 and 2 and experiment 3 and 4) were plotted according to their normalized log 2 ratio (Figure 24). Proteins in the upper right quadrant are the proteins enriched over control in both technical replicas. The significance of enrichment (confidence) was determined as the calculated false discovery rate (FDR-value). An FDR value of 1e-2 was used as cut off for significant enrichment. All proteins with a FDR value above the cut off are highlighted in colors. In the first replica (Figure 24 A) 16 proteins with an FDR value above 1e-2 were identified of which 12 were enriched with very highly confidence (an FDR of 1e-10 or lower). The second replica (Figure 24 B) resulted in 24 proteins more hits with an FDR above 1e-2 but a lower amount (5 proteins with a very high confidence (FDR 1e-10 and lower). Overall, the two experiments showed similar results. All proteins with an FDR 1e-10 in experimental replica 2 (Figure 24 B) had a similar FDR in experimental replica 1 (Figure 24 B).

In order to determine the most highly enriched proteins (rapalog over control) in all four experiments (intersection of the two experimental replicas), the average normalized log2 ratio in all experiments was calculated for proteins that were significantly enriched in at least two of the four experiments (supplementary list: A-5) resulting in 28 significantly enriched proteins. The calculation was done by Wieteke Hoeijemaker (Richárd Bártfai Lab, Radboud University). The most significantly enriched protein was the target protein Eps15 (PF3D7_1025000). As BirA* was not attached to Eps15 but to the biotinyliser, this confirmed that the biotinylation was specific in these experiments. Two other highly enriched proteins were an FKBP protein (PF3D7_1247400), the Plasmodium FKBP35 that likely interacted with the biotinylizer via the FRB domain upon rapalog addition, and a HSP90 protein

(PF3D7_0708400) which likely was a contaminant because it appeared in most of the DiQ-BioID experiments that had been done so far.

All in the mass spectrometry identified potential interactors and compartment neighbors with a significant normalized log2 ratio in at least one replica (including all the most abundant) were analyzed for homologies to known proteins (BLAST search algorithm) unless they had already been clearly annotated (www.plasmodb.org). If no homology was present a search for protein domains was done (InterPro protein and sequence analysis & classification tool provided by EMBL-EBI) to identify domains giving indications for the potential function of the respective protein. A selection of the proteins is collected in Table 12. Proteins were chosen based on their homology to proteins or protein domains with a known function in endocytosis or intracellular trafficking in other organisms. Other proteins were chosen based on their potential roles they had been assigned to in *P. falciparum*.

The proteins with interesting homology or protein domains that could be important for a role in endocytosis or trafficking in other organisms or of known or potential function in Plasmodium are listed in Table 12. One of the most highly enriched proteins was Kelch13 (PF3D7_1343700), a protein linked to Artemisinin resistance (Ariey et al., 2014). Further highly enriched was a ATP-dependent 6-phosphofructokinase (PFK9; PF3D7_0915400), a protein involved in glycolysis, which was also identified in the BioID with CHC and may therefore be an unspecific hit like FKBP35 and HSP90 (see above). Further proteins were a metacaspase-like protein (MCA2; PF3D7_1438400), a proteolytically active enzyme, and ubiquitin carboxyl-terminal hydrolase 1 (UBP1; PF3D7_0104300), an enzyme that deubiquitinates proteins. Many of the other highly enriched proteins did not have any homology to known proteins and therefore likely are P*lasmodium*-specific.

Interestingly one of the lesser enriched proteins is an Epsin-like protein (PF3D7_1245800), which has been already co-localized with Eps15 (Flemming, 2015) and interacts with Eps15 in other organisms (McMahon and Boucrot, 2011). Other interesting proteins Table 12, that were also found amongst the proteins enriched in just one replica, were several VPS and SNARE-proteins (PF3D7_1110500, PF3D7_0103100, PF3D7_0727000, PF3D7_1104100), subunits of the AP-2 complex known to be involved in endocytosis (PF3D7_0217300 and PF3D7_1218300), a phosphoinositol modifying enzyme (PF3D7_1354200), one Golgi-associated protein (PF3D7_1465100) and a protein containing a Neuromodulin gap junction N-terminal domain at its C-terminus (PF3D7_1308700). This domain is also present in the VPS11-homolog (PF3D7_0502000). The VPS11-homolog also harbors a RING finger motif, which is important for ubiquitinylation in other proteins and may therefor represent a link to the identified UBP1 of the highly enriched proteins and a second highly enriched RING finger protein (PF3D7_0314700). The DiQ-BioID revealed that Eps15 might share interacting proteins or compartment neighbors with the Kelch13 protein. However, based on the homology of the other potential interactors, no clear identity of the potential complex that Eps15 and Kelch13 are part of was evident.

Table 12: **Selected Proteins identified with DiQ-BioID for Eps15.**
Proteins that were significantly enriched in the average of all experiments (both replicas) were highlighted in green. Proteins that were significantly enriched in just one replica (not significant in average normalized log 2 values of all experiments) and have been picked for Table 12 are highlighted in red.

Gene number	Annotation/Homologue/Protein domains	log 2 ratio normalized replica 1		log 2 ratio normalized replica 2		average log 2 ratio normalized	enriched in Kelch 13- DIQ-BioID (Birnbaum, 2017)	enriched in Clathrin HC-DIQ-BioID (4.1.4)
		Exp. 1	Exp. 2	Exp. 3	Exp. 4			
PF3D7_0915400	ATP-dependent 6-phosphofructokinase (PFK9)	1.72	1.28	1.70	1.22	1.48	Yes	yes
PF3D7_1343700	kelch protein/ Kelch13	1.94	2.54	2.32	2.18	2.24	Yes	no
PF3D7_1025000	formin 2/ EF-hand calcium-binding domain-containing protein/Eps15	3.10	4.33	4.40	4.19	4.01	Yes	no
PF3D7_1438400	metacaspase-like protein (MCA2)	1.72	1.28	1.70	1.22	1.48	Yes	no
PF3D7_0104300	ubiquitin carboxyl-terminal hydrolase 1/UBP1	2.08	2.09	2.05	1.67	1.97	Yes	no
PF3D7_0314700	zinc finger protein/RING finger protein RNF1	0.26	1.53	1.09	1.51	1.10	no	no
PF3D7_1345800	conserved, unknown function /WD40 YVTN armadillo repeats	0.28	1.25	0.76	1.12	0.85	no	no
PF3D7_1447300	conserved, unknown function /armadillo type fold	0.08	1.10	0.85	1.06	0.77	no	no
PF3D7_0314700	Zinc finger protein/RING finger protein RNF1/RING FYVE PHD-type	0.26	1.53	1.09	1.51	1.10	no	no
PF3D7_1245800	clathrin coat assembly protein AP180/epsin-like protein	3.50	0.69	3.45	0.84	-	no	no
PF3D7_0217300	clathrin coat assembly protein/AP-2 complex subunit sigma	1.72	0.58	-1.15	NaN	-	no	no
PF3D7_1110500	vacuolar sorting protein 35	2.92	0.36	3.59	0.90	-	no	no
PF3D7_0103100	conserved, unknown function/vacuolar protein sorting-associated protein 51	1.16	-0.02	2.83	0.66	-	no	no
PF3D7_0727000	conserved, unknown function/ vacuolar protein -associated protein 53	-1.11	0.26	-0.16	0.46	-	no	no
PF3D7_1104100	syntaxin, Qa-SNARE family (SYN13)	1.10	-0-17	-0.03	-0.52	-	no	no
PF3D7_0709000	chloroquine resistance transporter (CRT)	1.70	-1.43	-1.44	1.70	-	no	no
PF3D7_1308700	conserved, unknown function/Gap junction protein N-terminal region PHD finger, RING finger	2.22	0.55	3.61	0.38	-	no	no
PF3D7_1465100	conserved oligomeric Golgi complex subunit 6	1.12	0.70	0.45	-0.16	-	no	no
PF3D7_1354200	inositol-polyphosphate 5-phosphatase, putative	0.86	0.10	1.09	-1.64	-	no	no
PF3D7_1218300	AP-2 µ subunit	0.59	0.65	0.73	0.66	-	no	no

The DiQ-BioID system tags proteins in close proximity of the target protein, indicating that they are either interactors or compartment neighbors. In order to confirm that the Kelch13 identified in the Eps15 DiQ-BioID is indeed in close proximity to Eps15, mCherry-Kelch13 was episomally expressed in the Eps15-2xFKBP-GFP-2xFKBP cell line to determine if these proteins co-localised. An overlap of the foci of both proteins was consistently visible (Figure 25 A). Occasional slight shifts in the colocalisation of the foci were observed (Arrow Fig 20A) that likely were due to the movement of foci during acquisition of the image. To ensure this interpretation was correct and confirm that the proteins truly co-localized, their localization was tracked by fast frame rate, 2D-two color time lapse microscopy. Of five imaged cells, all showed short distance movement of Eps15 foci (Figure 25, Figure 26 and Figure 27, white arrowheads) and in one cell long distance movement was present but the foci of Eps15 did not reach the FV, likely because the imaging stopped prior to arrival of the Eps15 foci at the FV (Figure 27, black arrowhead). The observed movement of Eps15 is in agreement with the observations already made for Eps15 (Flemming, 2015); and this thesis (4.2.2., Figure 19 to Figure 22). Three of the cells showed co-localization of Eps15 and Kelch13 of the short and long distance movement (one example of short distance movement shown in Figure 25; long distance movement shown in Figure 27, cell 2) and in one cell the Eps15-GFP foci did not clearly co-localize with Kelch13-mCherry foci (Figure 27, cell 1). One cell showed interesting characteristics of the relation of Eps15 and Kelch13 movement with co-localization of Eps15 and Kelch13 during initial short distance movement followed by independent movement of Eps15 (Figure 25 B, black arrowhead) and Kelch13 foci (Figure 26, black arrowhead). Foci of co-localizing Eps15 and Kelch13 also remained static during the imaging period in the two cells (one example shown in Figure 25).

Fast frame rate 2D-two color microscopy of movement of the foci in a cell line containing Eps15 tagged with GFP and mCherry tagged Kelch13 showed that both proteins co-localize during their movement in an Eps15-like manner, but occasionally movement events of Eps15 or Kelch13 foci without co-localization of both proteins was present. These observations explain why some foci completely overlapped (static foci), some partially overlapped (moving foci) and some did not overlap (individually moving foci) when imaged with longer exposition times during regular imaging (Figure 20 A).

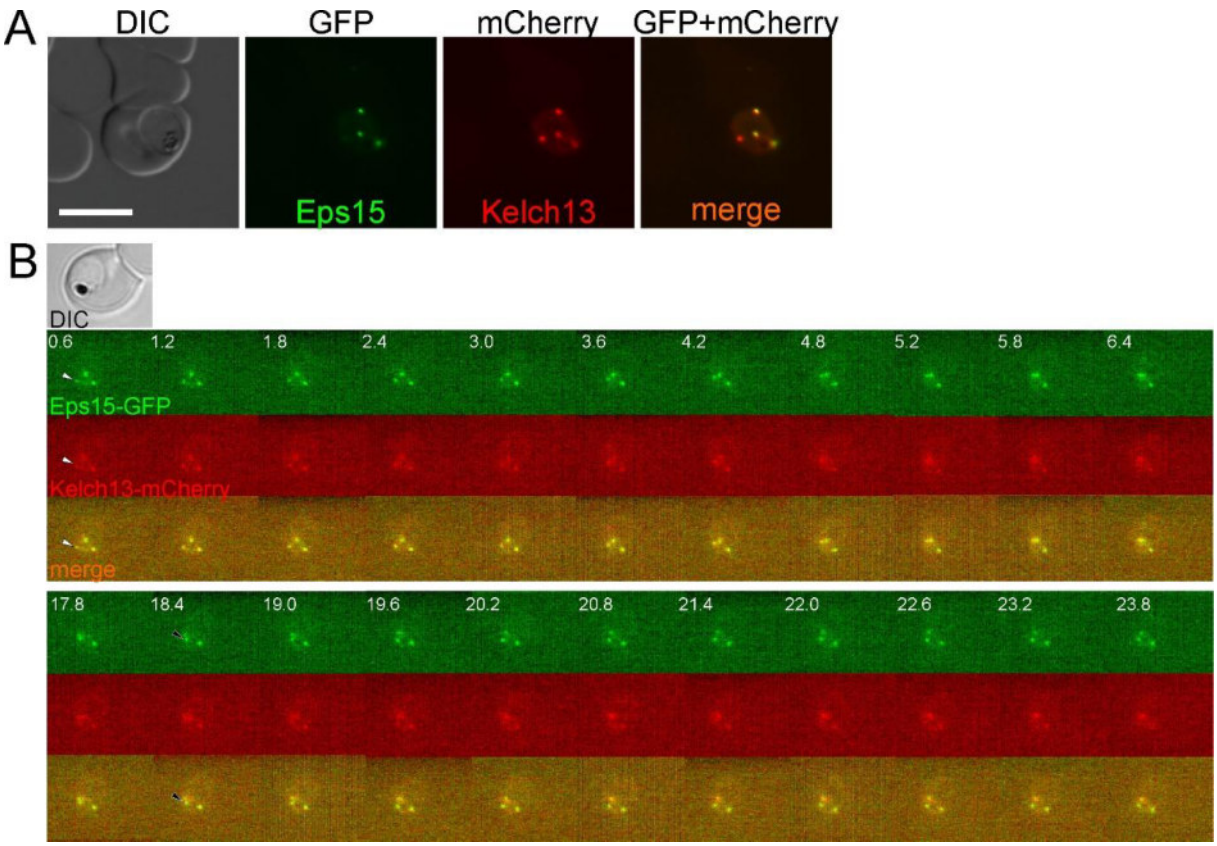

Figure 25: **Eps15-2xFKBP-GFP-2xFKBP and Kelch13-mCherry co-localized in static live cell images and in fast frame rate 2D-two color microscopy showing short distance movement.** Fluorescence life cell images using the Olympus IX81 Cell^R system of endogenously 2xFKBP-GFP-2xFKBP-tagged Eps15 expressing parasites also expressing and episomally encoded Kelch13 tagged with mCherry for co-localization. **A)** Representative static live cell images showed partially co-localization of Eps15-2xFKBP-GFP-2xFKBP and Kelch13-mCherry. **B)** Fast frame rate live cell microscopy (0.6 seconds per frame) in 2D of two channels (GFP and mCherry) showed co-localization of Eps15-2xFKBP-GFP-2xFKBP and Kelch13-mCherry during short distance movement (white arrowhead) and individual movement of Eps15 (black arrowhead). DIC: differential interference contrast, GFP: green fluorescent protein; mCherry: mCherry red fluorescent protein; merge: merged green and red channel. Numbers are seconds. Scale bar: 5 µm.

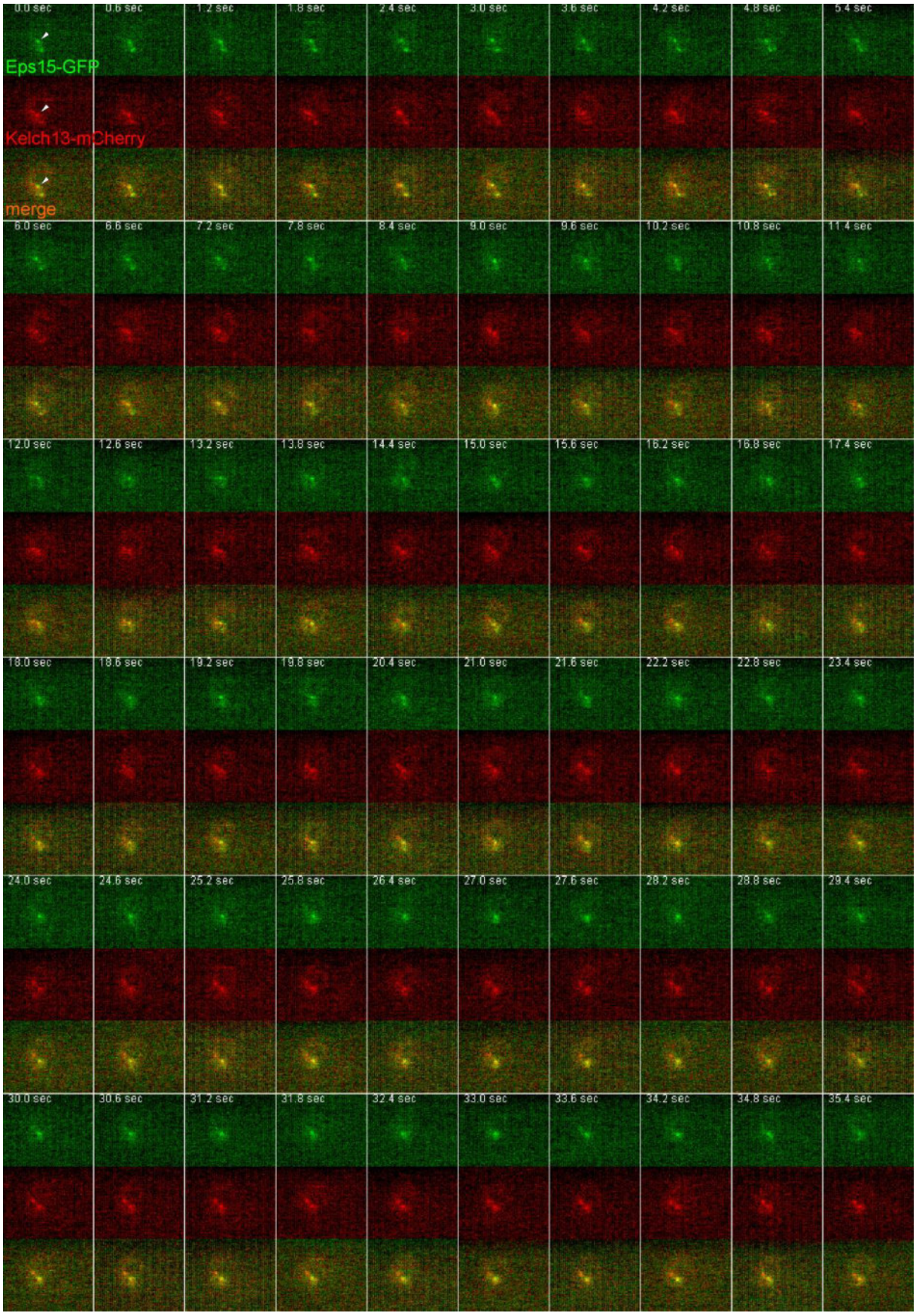

Figure 26: Panel continued and description on the next page.

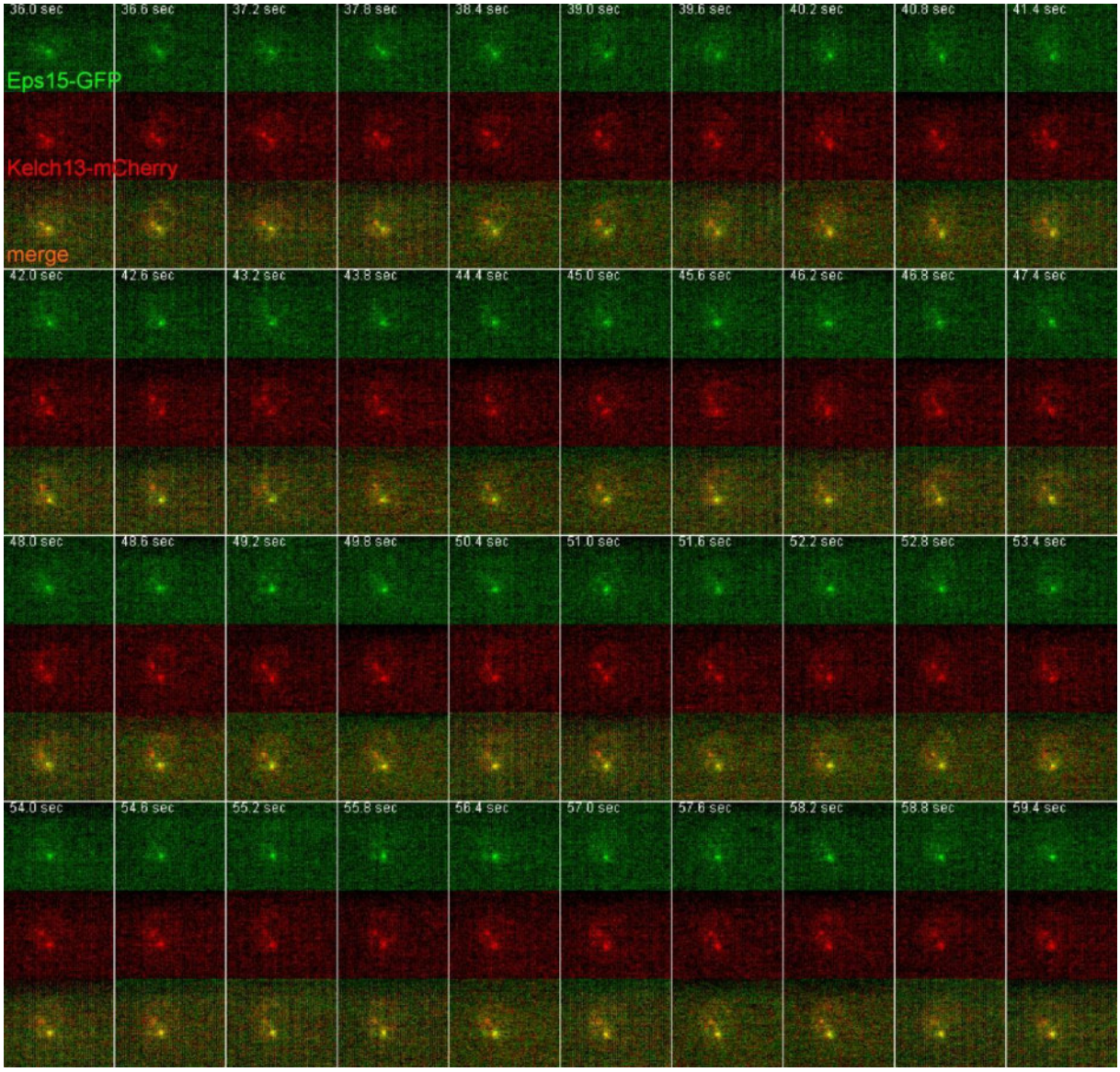

Figure 26 (including the previous page): **Fast frame rate 2D-two color microscopy of Eps15-GFP and Kelch13-mCherry shows co-localization during short distance movement and individual movement of Kelch13.** Fluorescence life cell images using the Olympus IX81 Cell^R system of endogenously 2xFKBP-GFP-2xFKBP-tagged Eps15 expressing parasites also expressing and episomally encoded Kelch13 tagged with mCherry for co-localization. Fast frame rate live cell microscopy (0.6 seconds per frame) in 2D of two channels (GFP and mCherry) showed co-localization of Eps15-2xFKBP-GFP-2xFKBP and Kelch13-mCherry during short distance movement (white arrowhead) and individual movement of Kelch13 (black arrowhead). GFP: green fluorescent protein; mCherry: mCherry red fluorescent protein; merge: merged green and red channel.

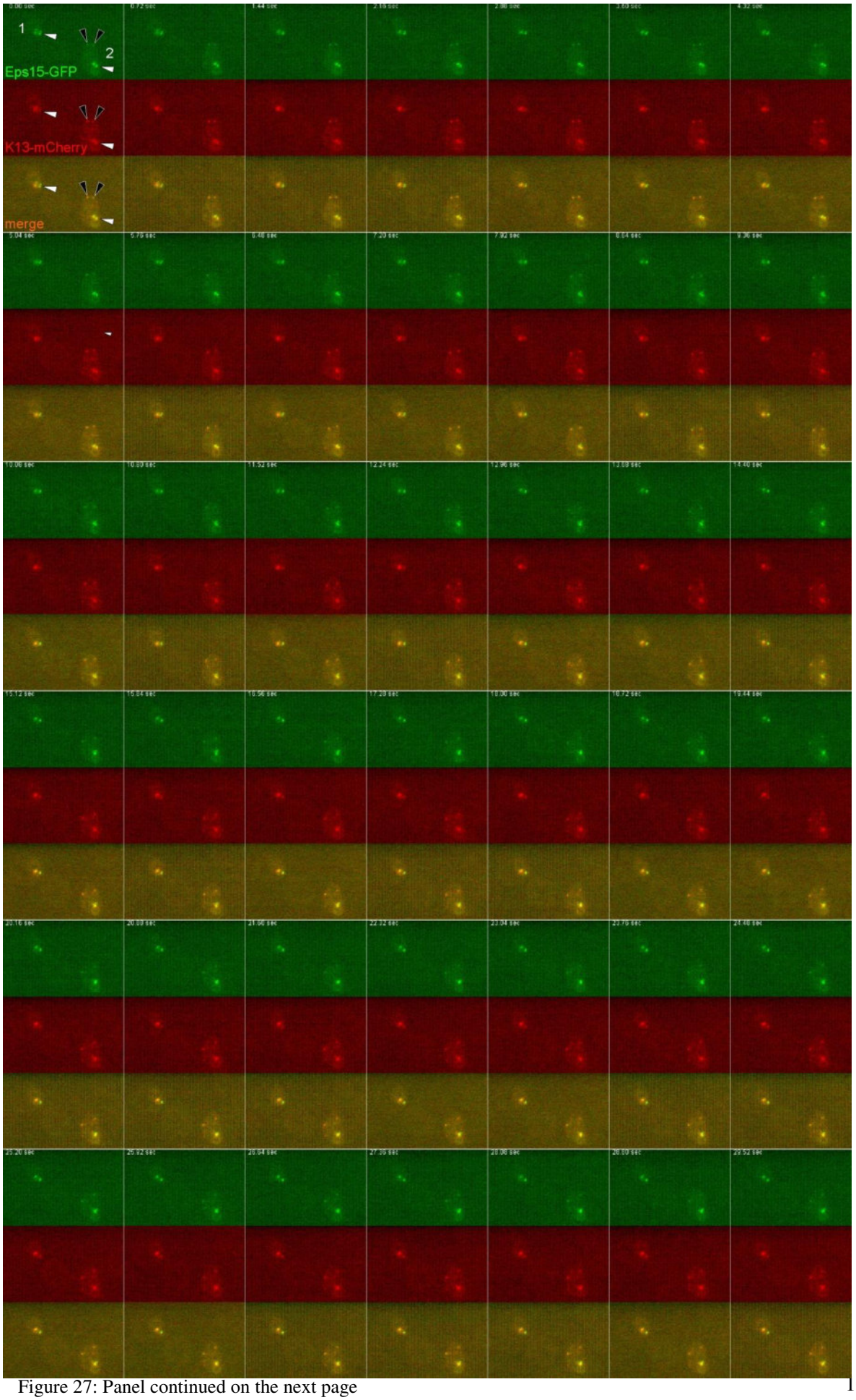

Figure 27: Panel continued on the next page

Figure 27: Panel continued and description on the next page

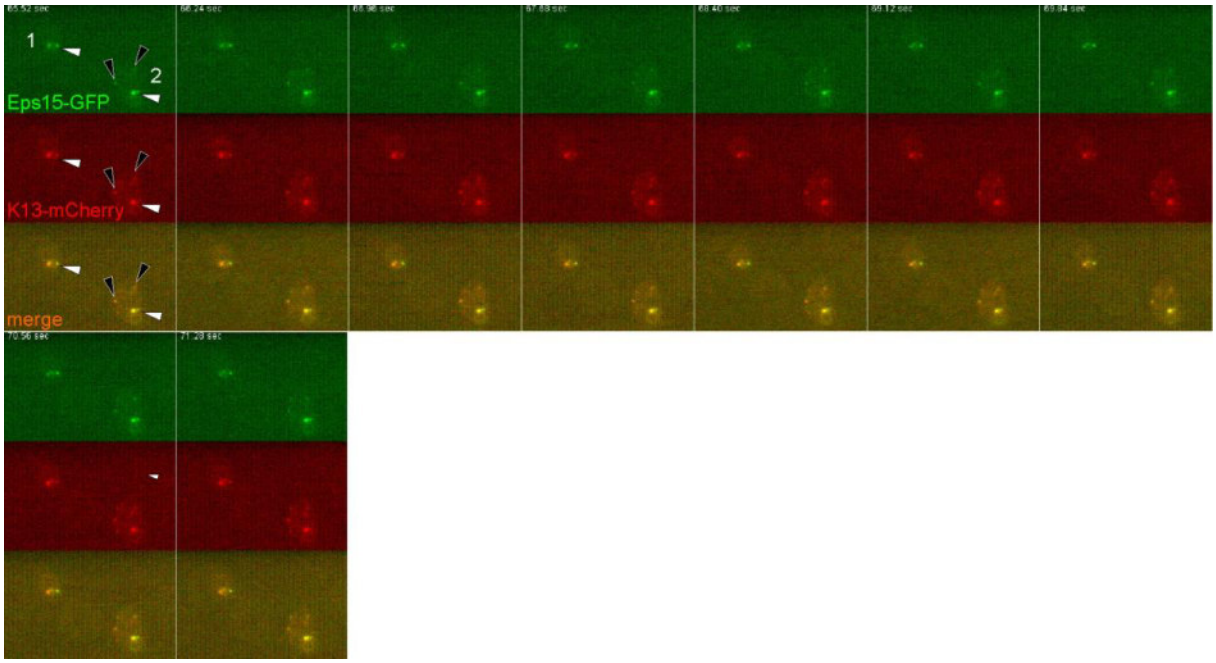

Figure 27 (including the previous two pages): **Fast frame rate microscopy of Eps15-GFP and Kelch13-mCherry shows long distance movement of co-localizing Eps15 and Kelch13.** Fluorescence life cell images using the Olympus IX81 system of two cells (1 and 2) with endogenously 2xFKBP-GFP-2xFKBP-tagged Eps15 expressing parasites also expressing and episomally encoded Kelch13 tagged with mCherry for co-localization. Fast frame rate live cell microscopy (0.72 seconds per frame) in 2D of two channels (GFP and mCherry) showed no co-localization (cell 1, white arrowhead) or co-localization of Eps15-2xFKBP-GFP-2xFKBP and Kelch13-mCherry during short distance movement and long distance movement (cell 2, black arrowheads). GFP: green fluorescent protein; mCherry: mCherry red fluorescent protein; merge: merged green and red channel. Numbers are two different cells.

Based on the identification of Kelch13 in the DiQ-BioID with Eps15 and the co-localisation, an interaction of Eps15 and Kelch13 is possible. To experimentally determine this, Co-Immunoprecipitation (CoIP) was carried out. Because of weak or no binding of the anti-GFP beads (used for Immuno-precipitation) and the anti-GFP primary antibody (used for detection in the western blots) to the sandwich tag (2xFKBP-GFP-2xFKBP) used for the Eps15 cell line, a integration cell line of Eps15 tagged with GFP alone without FKBP (Flemming, 2015) was used together with episomally expressed mCherry-Kelch13 (Figure 28). Using anti-mCherry beads, Kelch13 was immunoprecipitated and it was determined whether Eps15-GFP was co-precipitated using anti-GFP antibodies (Figure 28, CoIP and Western Blot were carried out by Ulrike Fröhlke). A band corresponding to Eps15-GFP was found in the mCherry bead eluate, whereas a control protein (Aldolase) was not enriched. These data supports that Eps15 and Kelch13 physiologically interact in *P. falciparum* parasites and are therefore true interaction partners. It can therefore also be assumed that other high confidence hits of the Eps15 DiQ-BioID may also be true Eps15 interaction partners.

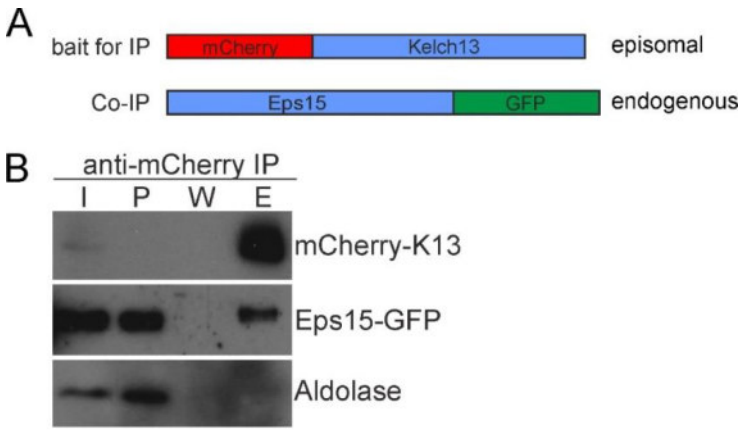

Figure 28: **CoIP with Kelch13-mCherry as bait and co-immunoprecipitation of Eps15-GFP to confirm results if DiQ-BioID.** Co-immunoprecipitation with a cell line expressing endogenously Eps15-GFP and episomally overexpressed Kelch13-mCherry to determine whether Kelch13 protein interacts with Eps15 or not. **A)** Schematic representation of the constructs used for CoIP (not to scale). Kelch13 N-terminally tagged with mCherry was used as bait for immunoprecipitation with anti-mCherry beads. Co-immunoprecipitation of Eps15 tagged with mCherry was analyzed. **B)** Western blot probed with the input for the CoIP (I), the pellet (P), the first wash step of the beads (W) and the eluate (E) detected with anti-mCherry (detecting Kelch13), anti-GFP (detecting Eps15) and anti-Aldolase as loading and purification control. CoIP and Western Blot was done by Ulrike Fröhlke.

4.3 PfVPS45 is important for HCCU

4.3.1 The Sec1-domain containing protein PfVPS45

To gain further insights into endocytosis in P. falciparum blood stages, VPS45, a protein suspected to be involved in this process from preliminary data (Reichard, 2015), was here analysed in depth. The protein sequence of the VPS45 homologue in *P. falciparum* harbors three Sec1 domains (Figure 29 A). In order to localize and functionally analyze *P. falciparum* VPS45 (PF3D7_0216400), the endogenous *vps45* gene was tagged with the sequence encoding 2xFKBP-GFP using SLI (Birnbaum et al., 2017). The corresponding cell line was established by Nick Reichard (Reichard, 2015) and here further analysed. PfVPS45-2xFKBP-GFP was present in foci and accumulations in the parasite cytoplasm in addition to a pool of VPS45 that was evenly distributed in the parasite cell (Figure 29 A). Some of the accumulations were in close proximity or directly at the parasite's food vacuole, and this was particularly prominent in trophozoites (Figure 29 A, arrowheads). Other foci were further away from the food vacuole, often close to the parasite nuclei (Figure 29 A). In ring stages, not all cells showed a focus but this may have been a detection problem, as the VPS45 signal was very low at this stage (Figure 1A).

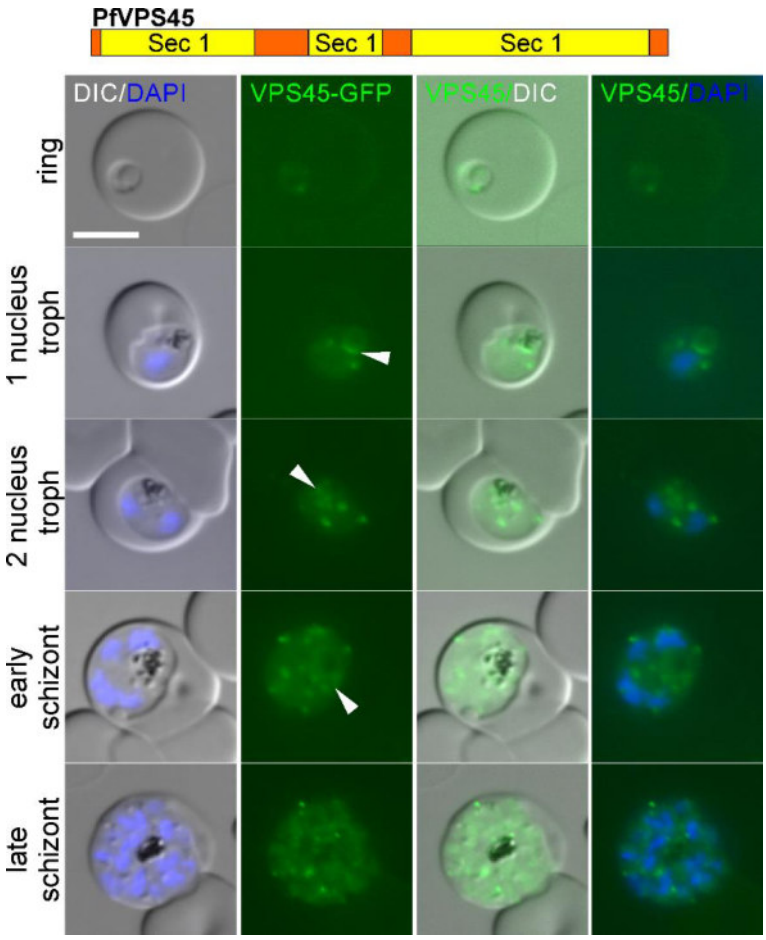

Figure 29: **Characterization of endogenously 2xFKBP-GFP tagged PfVPS45**. Domains structure and location of 2xFKBP-GFP tagged PfVPS45 expressed from the endogenous locus. Representative fluorescence microscopy images of live parasites at different stages of asexual development are shown. Arrowheads show signals at the food vacuole. DIC: differential interference contrast; merge: merged green and red channel; DAPI: nuclei. Size bars are 5 µm

4.3.2 PfVPS45 is essential for blood stage development

To assess the function of PfVPS45, it was conditionally inactivated using knock sideways. Although a mislocaliser cell line was already available for VPS45 (Reichard, 2015), the original integration cell line was first transfected with the newest generation of NLS mislocaliser (mislocalizerN; 1xNLS-FRB-mCherry with yDHODH-marker under expression of the 5'UTR of *nmd3*-gene; Birnbaum et al., 2017) to ascertain the best possible knock sideways effect (for simplicity throughout this section this cell line will be referred to as the 'VPS45 knock sideways cell line'). Upon induction of the knock sideways with rapalog for 1 h in this cell line, VPS45 was efficiently (no foci of fluorescence remaining in the cytoplasm as detected by microscopy) mislocalised to the nucleus (Figure 30 A).

In order to test the importance of VPS45 for parasite development, parasite growth was monitored over 4 days (2 growth cycles). This revealed a loss of growth in the parasites where VPS45 was inactivated by knock sideways while controls (the same culture grown without rapalog) proliferated at typical rates (Figure 30 B, appendix A-7). To ascertain the growth defect after the VPS45 knock

sideways was not caused by the presence of VPS45 in the nucleus rather than loss of VPS45 function, complementation the knock sideways with an episomally expressed functional copy of VPS45 was done. When the endogenous copy of VPS45 was mislocalised in this cell line (Figure 30 C), the complementation construct rescued the growth phenotype (Figure 30 D, appendix A-7). These results indicate that the observed growth defect is due to loss of VPS45 function and not an indirect effect of mislocalisation. This also showed that rapalog alone had no negative effect on the parasite, as demonstrated previously (Birnbaum et al., 2017). It is to note that in the complemented cell line the endogenous 2xFKBP-GFP-tagged VPS45 showed fewer foci and much less food vacuole-associated protein than in the non-complemented line (Figure 30 C).

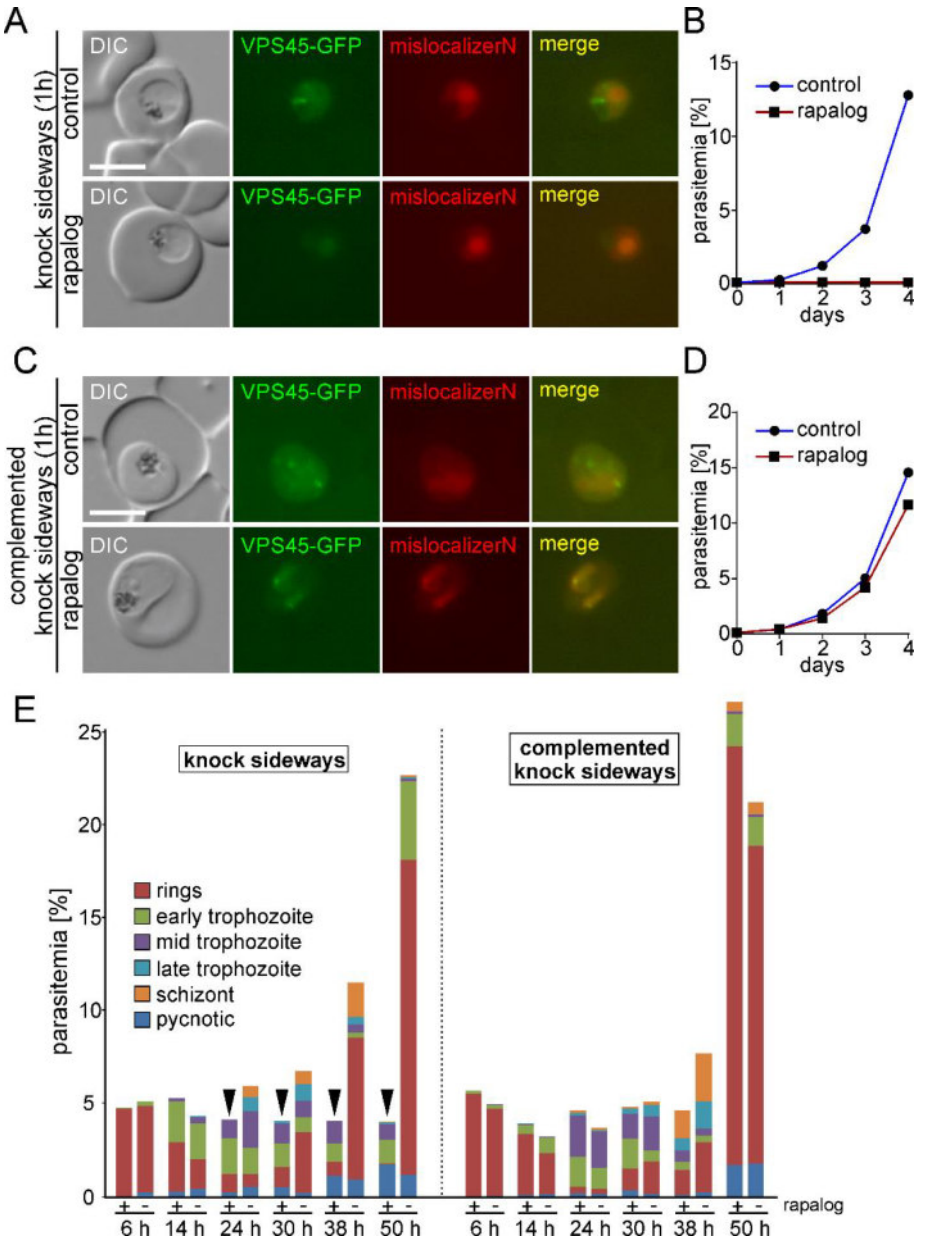

Figure 30: **PfVPS45 is important for the survival of *P. falciparum* parasites. A)** Knock sideways of PfVPS45-2xFKBP-GFP (VPS45-GFP) using a nuclear mislocaliser (MislocaliserN) (Birnbaum et al., 2017). Images were taken 1 h after induction of knock sideways of the cells grown with and without

rapalog. **B)** Flow cytometry growth curve over 2 growth cycles (one representative of 3 independent experiments, all replicas shown in Figure S1) of the PfVPS45-2xFKBP-GFP knock sideways parasites grown with rapalog (inactivated PfVPS45) and without rapalog (control). **C)** Knock sideways as shown in (B) but using the PfVPS45-2xFKBP-GFP parasites where an episomally expressed untagged copy of PfVPS45 complements the mislocalised PfVPS45. **D**) FACS growth curve with the complemented PfVPS45-2xFKBP-GFP knock sideways parasites (one representative of 3 independent experiments. **E)** Synchronised PfVPS45-2xFKBP-GFP parasites with the nuclear mislocaliser (left) were grown with (inactivated VPS45) or without (control) rapalog and parasitemia and parasite stages counted using Giemsa smears at the indicated time points. Right shows the corresponding experiment carried out with the complemented parasite line (one representative of two independent experiments is shown). Size bars are 5 μm; DIC, differential interference contrast; merge, merged green and red channel; DAPI (nuclei).

Next a more detailed growth analysis using synchronous parasites was carried out to pinpoint the stage the growth defect after VPS45 inactivation took effect. This revealed that loss of VPS45 function had no effect on the development of ring and young trophozoite stage parasites but led to an arrest in trophozoites and schizonts, preventing productive completion of the cycle in red blood cells (Figure 30 E). In contrast, the complemented parasites did not show a growth arrest in trophozoites and schizonts after addition of rapalog but completed the cycle and produced nearly the same amount of new (second generation) ring stages than the culture grown without rapalog (Figure 30 E). Inspection of differential interference contrast (DIC) images of the parasites 6 hours after inactivation of VPS45 revealed the presence of what appeared to be multiple vesicles in the parasite cytoplasm (Figure 31 A, arrowhead). Control or complemented parasites only occasionally showed more than 2 vesicle per parasite and never large clusters as apparent after VPS45 inactivation (Figure 31 A -C). Quantification over time revealed that after induction of the VPS45 knock sideways, the number of vesicles per parasite increased steadily while the number of vesicles remained low in control parasites (Figure 31 C, datasets of individual experiments shown in appendix A-8). After 8 hours the knock sideways parasites contained an average of 12.0 vesicles per parasite (S.D +/- 7.7) compared to 1.7 vesicles (S.D. +/- 1.7) in the control at this time point and 1.0 (S.D +/- 1.4) vesicles per parasite before addition of rapalog (Figure 31 C).

The accumulation of vesicles was also imaged over time taking advantage of the fast frame rate microscopy with the Zeiss AxioImager M2 setup (4.1.1). The parasites were incubated with rapalog under cell culture conditions for 30 min to induce complete knock sideways of VPS45 and then imaged with 5 frames per second for 162 minutes (192 min after addition of rapalog) at room temperature. In Figure 32 every 100^{th} time point of the acquired image sequence is displayed, showing accumulation of vesicles in the same cell (in contrast to quantification of vesicles in Figure 31 B were different cells were analyzed per time point). Although the number of vesicles clearly increased over time, the actual vesicle generation event was not observed, likely due to the complex dynamics of the vesicles and because only a single layer could be imaged.

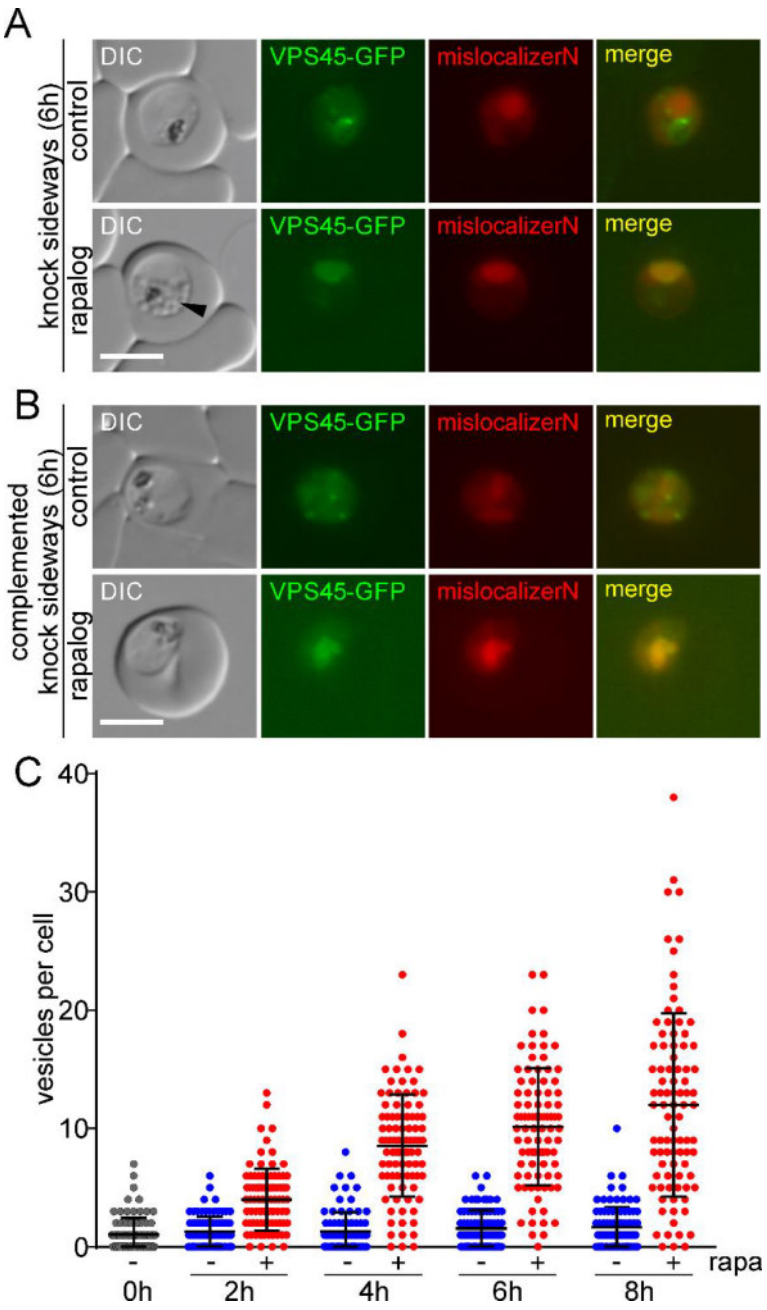

Figure 31: **Inactivation of PfVPS45 leads to accumulation of vesicular structures in the parasite. A, B)** Representative fluorescence microscopy and differential interference contrast (DIC) images of live parasites 6 h after induction of knock sideways in PfVPS45-2xFKBP-GFP parasites shows accumulation of vesicular structures (A, arrowhead) in the knock sideways parasites (rapalog) compared to the control and the complemented knock sideways parasites (B). Size bars are 5 µm; merge, merged green and red channel; DAPI, nuclei. **C)** Trophozoites of the PfVPS45-2xFKBP-GFP parasites were grown with rapalog (+) or without (-) and the number of vesicles per cell counted at different time points after induction of the knock sideways as indicated (data pooled from 3 independent experiments with a total of 90 cells per time point and condition; error bars show S.D.).

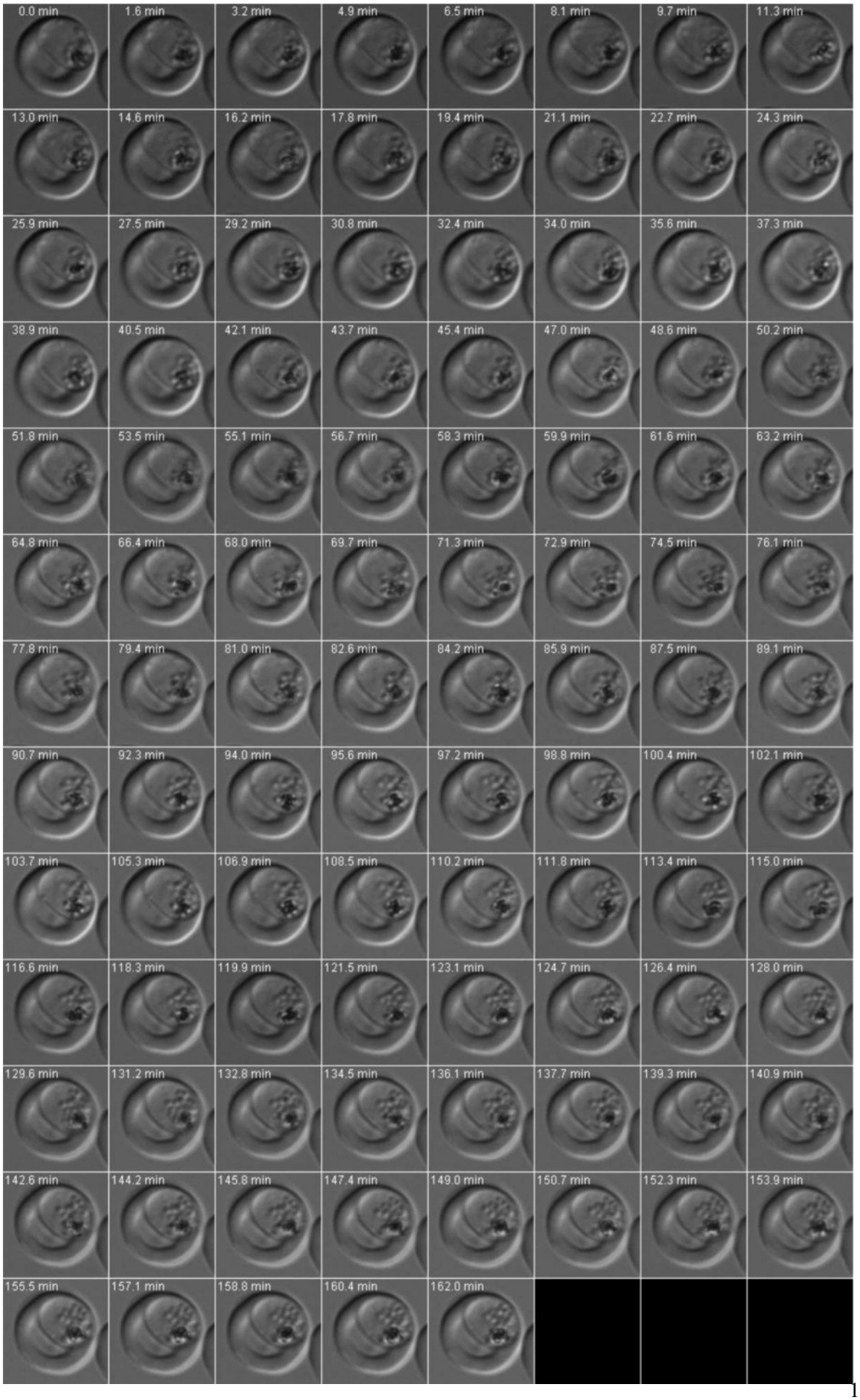
0.0 min
1.6 min
3.2 min
4.9 min
6.5 min
8.1 min
9.7 min
11.3 min
13.0 min
14.6 min
16.2 min
17.8 min
19.4 min
21.1 min
22.7 min
24.3 min
25.9 min
27.5 min
29.2 min
30.8 min
32.4 min
34.0 min
35.6 min
37.3 min
38.9 min
40.5 min
42.1 min
43.7 min
45.4 min
47.0 min
48.6 min
50.2 min
51.8 min
53.5 min
55.1 min
56.7 min
58.3 min
59.9 min
61.6 min
63.2 min
64.8 min
66.4 min
68.0 min
69.7 min
71.3 min
72.9 min
74.5 min
76.1 min
77.8 min
79.4 min
81.0 min
82.6 min
84.2 min
85.9 min
87.5 min
89.1 min
90.7 min
92.3 min
94.0 min
95.6 min
97.2 min
98.8 min
100.4 min
102.1 min
103.7 min
105.3 min
106.9 min
108.5 min
110.2 min
111.8 min
113.4 min
115.0 min
116.6 min
118.3 min
119.9 min
121.5 min
123.1 min
124.7 min
126.4 min
128.0 min
129.6 min
131.2 min
132.8 min
134.5 min
136.1 min
137.7 min
139.3 min
140.9 min
142.6 min
144.2 min
145.8 min
147.4 min
149.0 min
150.7 min
152.3 min
153.9 min
155.5 min
157.1 min
158.8 min
160.4 min
162.0 min

Figure 32 (previous page): **Fast frame rate microscopy of accumulating vesicles upon VPS45 knock sideways.** Acquisition of the differential interference contrast -channel (DIC) with fast frame rates (5 frames / second) using the Zeiss AxioImager M2 system showing accumulation of vesicles after knock sideways of VPS45. Every 100th frame of the image sequence is arranged in the panel. Minutes indicate time after start of the video. Cells were incubated with rapalog at 37°C for 30 min prior to start of imaging. Imaging was done at room temperature.

4.3.2.1 Accumulation of host cell cytosol filled vesicles is induced upon PfVPS45 knock sideways

If VPS45 has a role in HCCU, it would be expected that the structures accumulating in the parasite after conditional inactivation of VPS45 consist of host cell cytosol-filled vesicles. To test this, transmission electron microscopy (EM) of parasites 8 h after inactivation of VPS45 by knock sideways was carried out. This revealed an abundance of vesicular structures in the parasite that contained material with a density similar to that of the host cell cytosol (Figure 33 A). The number of these vesicles per parasite section was significantly higher than in the control culture grown without rapalog (9.6 +/-5.8 compared to 1.6 +/-2.1; Figure 33 B). To confirm that the material found in the vesicles in the parasite indeed consisted of host cell cytosol, red blood cells were pre-loaded with Alexa 647 nm conjugated dextran and infected them with the VPS45-2xFKBP-GFP parasites. Parasites growing in the preloaded cells showed that the vesicular structures observed after inactivating VPS45 contained fluorescent material, confirming that they held internalized host cell cytosol (Figure 33 C).

From single EM sections alone it can not be concluded that the structures observed after inactivation of VPS45 are indeed autonomous vesicles, as they may still be connected to the host cell in a different plane of the cell. To further characterize these structures, we therefore treated infected red blood cells with tetanolysin to release the host cell cytosol (leaving the parasite intact) and then analyzed the cells using EM. After this treatment, the accumulated hemoglobin-filled structures in the parasites retained their content (Figure 33 D), demonstrating that they were not in contact with the host cell cytosol but represented autonomous, host cell cytosol-filled vesicles in the parasite cytoplasm. Closer inspection of the vesicles accumulation after VPS45 inactivation revealed that some of them appeared to contain smaller vesicles (Figure 33 E). The significance of this is at present unclear. We also noted that some of the vesicles appeared to be double membraned (Figure 33 F), a feature previously observed with HCCU and consistent with structures originating from cytostomes which are double-membrane invaginations (including both, the parasite plasma membrane and the parasitophorous vacuolar membrane surrounding the parasite in the host cell) (Aikawa et al., 1966a).

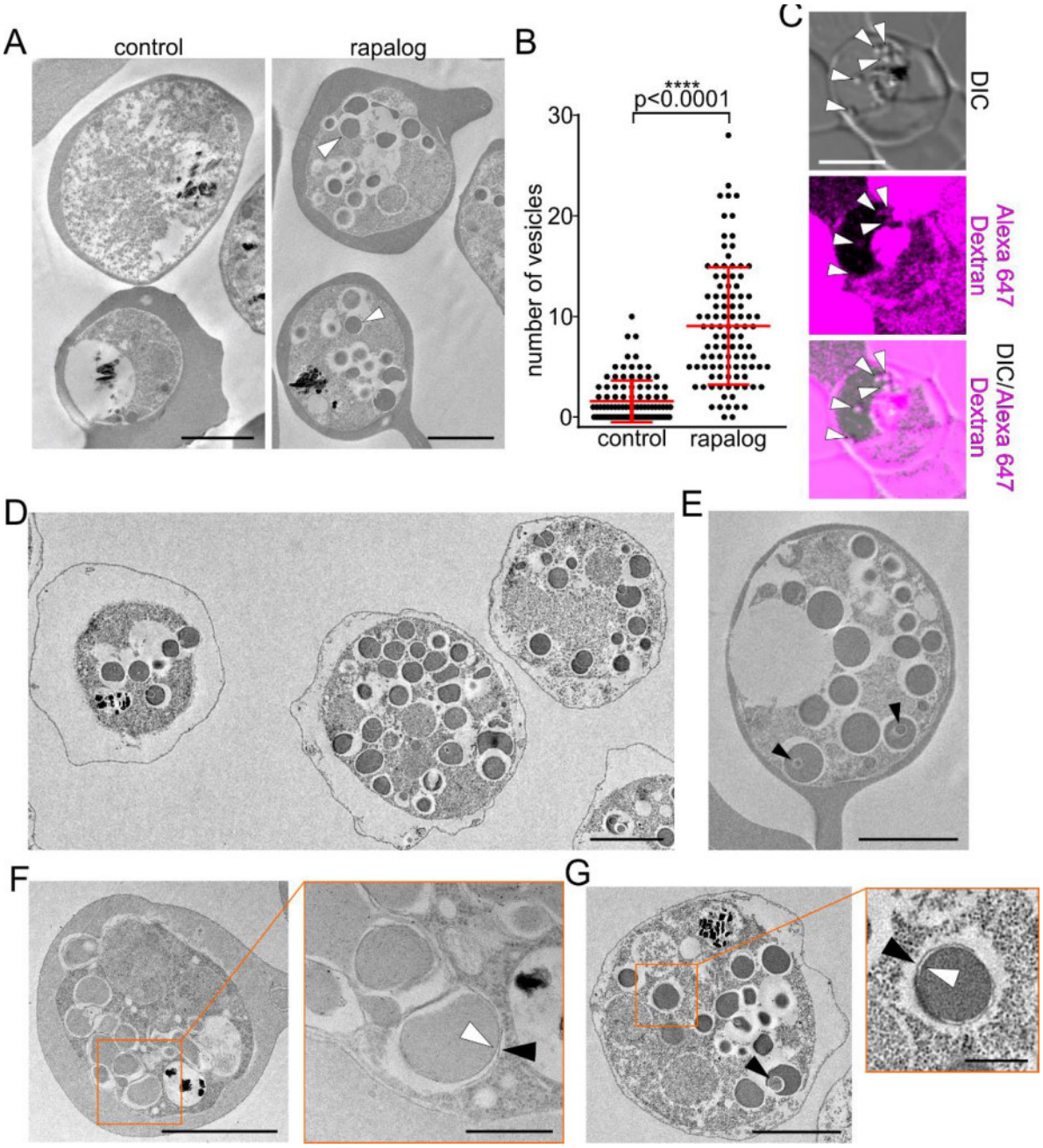

Figure 33: **Vesicles accumulating through inactivation of VPS45 are filled with host cell material.** **A)** Representative areas of transmission electron microscopy (EM) images of percoll-enriched PfVPS45-2xFKBP-GFP parasites 8 h after induction of the knock sideways with rapalog compared to control. White arrowheads show examples of vesicular structures in the parasite that were filled with material with a density similar to the host cell cytosol. **B)** Quantification of the number of vesicles per cell section of the EM images generated for A (n=101 cells for each, the control and the knock sideways parasites; bars show S.D.). **C)** Confocal microscopy images (single z-plane of an image stack) of PfVPS45-2xFKBP-GFP parasites grown in RBCs preloaded with Alex 647-conjugated 10 kDa Dextrane. Arrowheads show induced vesicles and their Dextrane content. DIC, differential interference contrast. **D)** EM images of PfVPS45-2xFKBP-GFP parasites 8 hours after inducing the knock sideways and treatment with tetanolysin to release the host cell cytosol before embedding, demonstrating that the vesicular structures did not maintain a connection to the host cell. (continued on next page)

Figure 33 (continuation of previous page): **E)** EM images of PfVPS45-2xFKBP-GFP parasites after knock sideways, showing vesicles within the induced vesicles (black arrowheads). **F, G)** EM images show evidence of double-membraned vesicles induced after inactivation of PfVPS45-2xFKBP-GFP in parasites in intact red blood cells (F) and after release of host cell cytosol with tetanolysin (G). The boxes (orange frames) show enlargements; white and black arrowheads in the enlargements indicate the inner and outer membrane of the vesicles, respectively; black arrowhead in the main image in G) shows vesicle within a vesicle. Size bars: A, B, D, E: 2µm; C: 5 µm; F, G: 2 µm and enlargements 0.5 µm.

4.3.2.2 PfVPS45 knock sideways leads to reduced hemoglobin uptake

While the results so far are in agreement with a role of VPS45 in hemoglobin uptake, the experiments did not exclude that the observed vesicles derived from a fragmentation of the food vacuole. To show that VPS45 is indeed needed for HCCU and that the observed vesicles were HCCU intermediates derived from endocytosis, it was assessed whether new hemoglobin reached the parasite food vacuole after inactivation of VPS45. Firstly it was investigated whether new hemozoin (the degradation product of hemoglobin) accumulated in the food vacuole after inactivating VPS45. In the control (without rapalog), the size of the hemozoin crystal per food vacuole increased significantly over 14 h of assay time (Figure 34). In contrast, in the parasites where VPS45 was knocked aside, the levels of hemozoin increased only little over the same time span and were much lower than the amount that had accumulated in the control or the corresponding sample of the complemented parasite line (Figure 34). This suggested that inactivation of VPS45 almost entirely abolished transport of hemoglobin to the food vacuole and that the accumulating vesicles are HCCU intermediates.

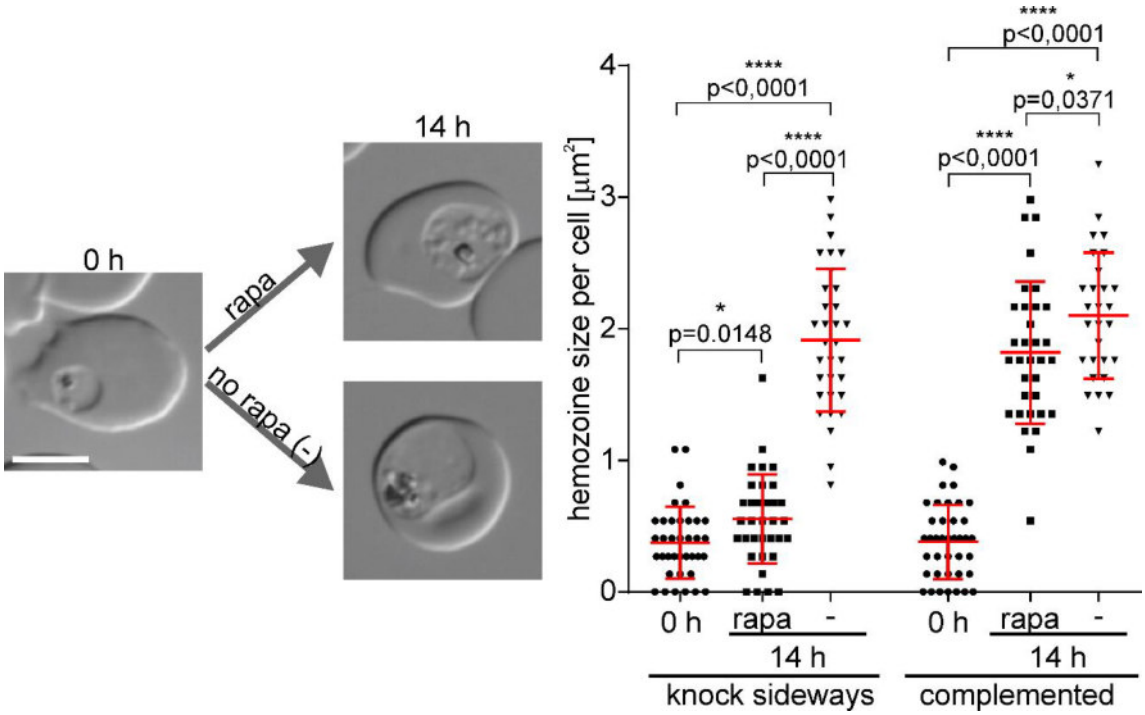

Figure 34 (previous page): **VPS45 inactivation results in smaller crystal-sizes of the hemoglobin digestion product hemozoin.** Quantification of hemozoin accumulation per cell after inactivation of VPS45 by knock sideways (rapalog) compared to control in the PfVPS45-2xFKBP-GFP parasites. Left shows representative example DIC images and the outline of the assay. Right shows the quantification of hemozoin (as area of black pigment), including the complemented knock sideways line (one representative of 3 independent experiments with each n > 27 cells per time point and condition; error bars, S.D.; p values are indicated, two-tailed, unpaired t-test; all three experiments shown in appendix A-10). Size bars: 5 µm.

To further corroborate this finding, the degradation of hemoglobin in the food vacuole using the protease inhibitor E64 (Bailly et al., 1992; Sijwali and Rosenthal, 2004) was blocked. While control cells developed bloated food vacuoles, as evident by DIC microscopy (Figure 35 A) and by EM (Figure 35 B), more than 90 % of the cells with inactivated VPS45 had no bloated food vacuoles (Figure 35 A-C). This demonstrated that inactivation of VPS45 prevented the delivery of host cell cytosol to the food vacuole. At the same time, cell size still increased, albeit to a lesser extent than in the control cells (Figure 35 D). This indicated that the lack of material in the food vacuole was not a secondary effect due to a loss of parasite viability and also shows that a lack of hemoglobin uptake and digestion for 8 h does not immediately arrests parasite development in agreement with the stage profile in synchronised VPS45 knock sideways parasites (Figure 30 E).

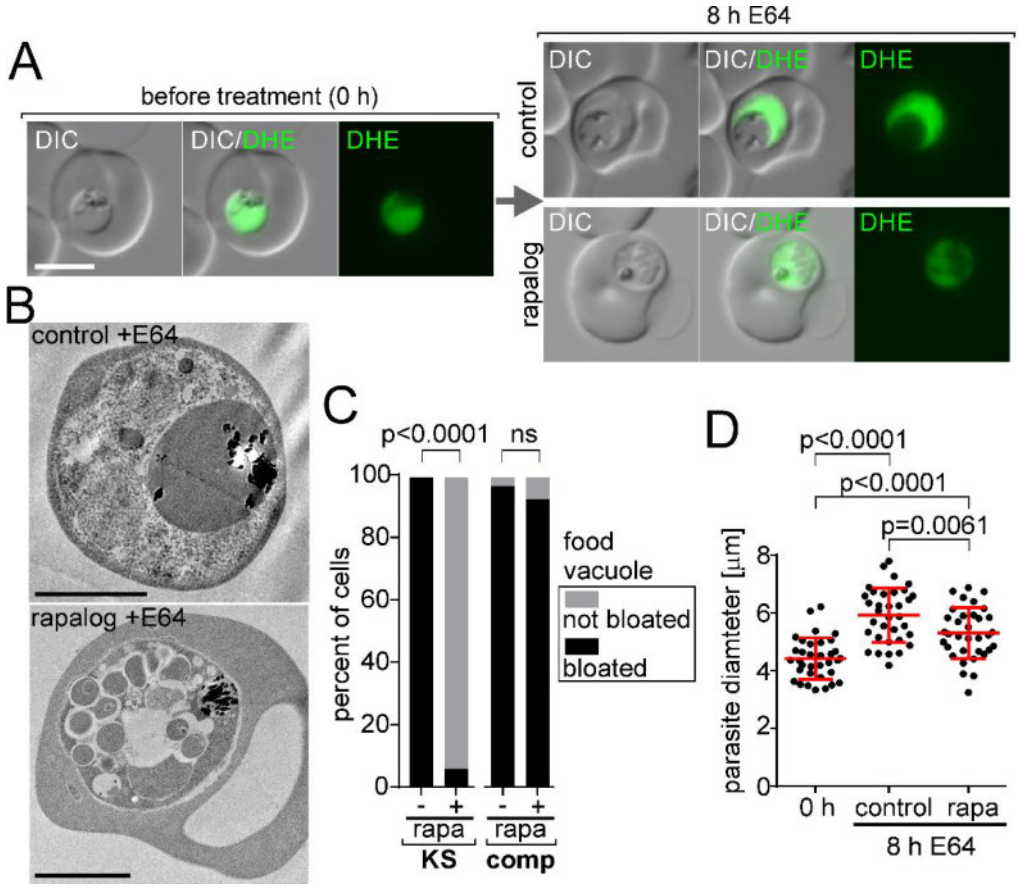

Figure 35 (previous page): **VPS45 inactivation prevents arrival of hemoglobin in the food vacuole.** E64 hemoglobin uptake assay with PfVPS45-2xFKBP-GFP parasites 8 h after induction of knock sideways (rapalog) compared to control. **A)** DIC and fluorescence microscopy images show representative parasites before addition of E64 and rapalog (left) and 8 h after (right). For imaging the parasite cytoplasm was stained with dihydroethidium (DHE). **B)** EM images of the parasites 8 h on E64 show lack of bloated food vacuole if VPS45 is inactivated but a bloated food vacuole in the control. **C)** Quantification of number of cells with bloated food vacuoles (indicative of delivery of host cell cytosol into the food vacuole) in the experiment shown in A), including the complemented parasite line. For all conditions n=34 cells were assessed; significance was determined using Fisher's exact test; one representative of 3 independent experiments is shown; rapa, rapalog. **D)** Diameter of the cells of the PfVPS45-2xFKBP-GFP knock sideways parasites of the assay shown in A) and scored for bloated food vacuoles in C) (error bars, S.D.; p values are indicated, two-tailed, unpaired t-test; one of 3 independent experiments is shown; all three experiments shown in appendix A-9). Size bars: 5 µm

If grown in red blood cells pre-loaded with fluorescent dextrans, the parasites unspecifically takes up the dextranes together with the RBC cytosol and transport them into the food vacuole. To further measure the amount of host cell cytosol uptake, the VPS45 knock sideways parasites were grown in red blood cells preloaded with dextrane conjugated to Alexa647 and the uptake of fluorescence into the parasites was assessed after inactivation of VPS45 as an indirect measurement for HCCU (Figure 36 A). If HCCU is reduced, also a reduced dextrane uptake is expected. To circumvent the very high intensity of fluorescence in the food vacuole that led to a permanent overexposure during image acquisition, again E64 was used to expand the volume of the FV and evenly spread the dextrane over a larger volume, resulting in similar intensities in the rapalog treated culture and the control. This allowed imaging with the same parameters in the two samples. As shown in Figure 36 B, the FV is bloated in the untreated control and dextrane is located inside the FV whereas the FV of the rapalog treated cells is much smaller. This corroborated the results of the bloated food vacuole assay. Measurement of the integrated density of the dextrane inside the FVs was significantly lower in the cells were rapalog was added (Figure 36 C), supporting the conclusion that less host cell cytosol is transported to the FV upon VPS45 knock sideways.

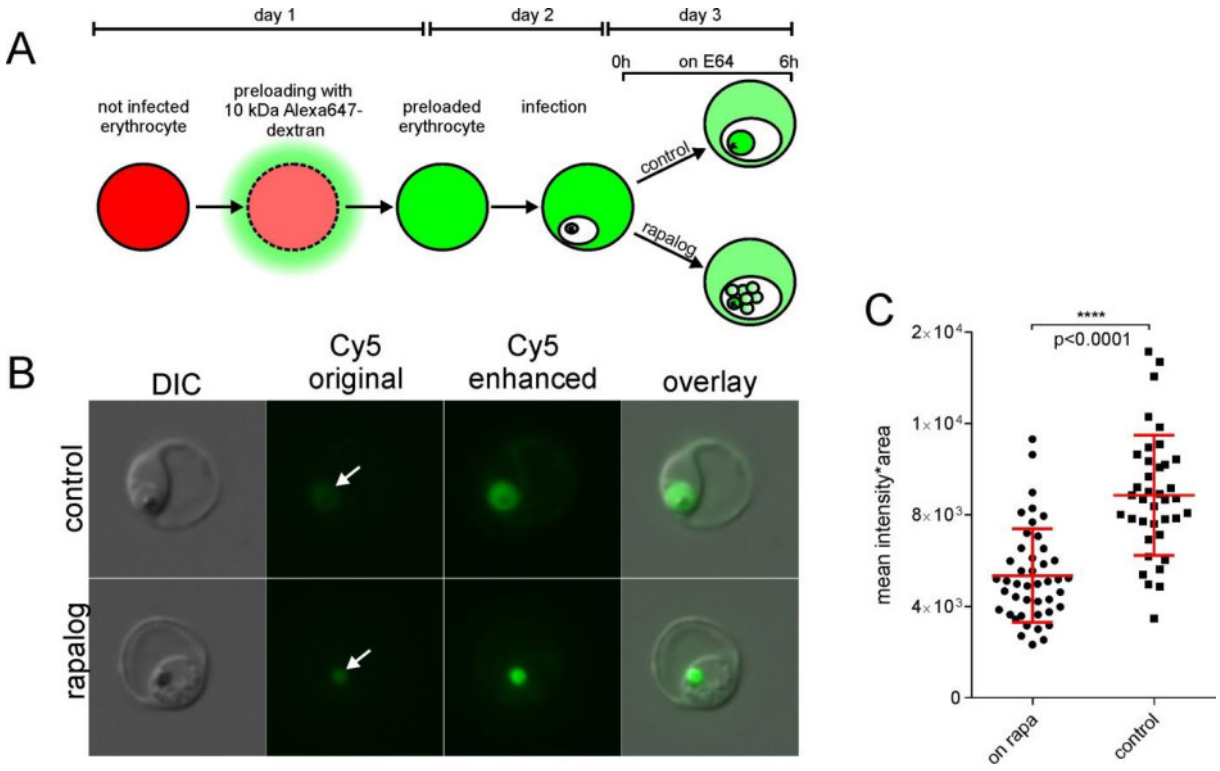

Figure 36: **Fluorescent dextrane uptake assay shows reduced dextrane uptake upon knock sideways of PfVPS45. A**) Workflow of the fluorescence uptake assay with preloading of uninfected red blood cells (red) with Alexa-647 labelled 10 kDa dextrane (green), subsequent infection with parasites (white), growth up to the trophozoite stage with hemozoin crystal (black) in the food vacuole (FV) and induction of PfVPS45 knock sideways and accumulation of dextrane filled vesicles (bright green small circles). **B**) Representative image of infected preloaded red blood cells infected with VPS45-2xFKBP-GFP parasites showing the VPS45 knock sideways phenotype 6 h after inactivation of VPS45 (rapalog compared to the control without rapalog). Alexa-647 labelled dextran was imaged using the Cy5-filter. The experiment was carried out in the presence of E64 for proper imaging (Cy5 original, white arrows). Post-processed image of the Cy5-channel (Cy5 enhanced) for better visualization of the accumulated dextran in the FV are also shown. **C**) Measurement of integrated density (mean intensity of dextrane multiplied by measured area) of the food vacuole area. (one single experiment with n > 30 cells per condition; error bars, S.D.; p values are indicated, two-tailed, unpaired t-test). DIC: differential interference contrast; Cy5: Alexa 647 fluorescently labelled dextrane images in Cy5 channel, overlay: merged DIC and Cy5 channels. Size bars: 5 µm.

In order to directly show the effect of VPS45 knock sideways on hemoglobin uptake, parasites were isolated using selective lysis of the red blood cells to remove all of the hemoglobin in the host cell cytosol. The resulting parasites containing only the hemoglobin they had taken up into their food vacuole and hemoglobin filled vesicles, were lysed and their proteins separated in SDS-PAA-electrophoresis, visualized with Coomassie-staining and the band corresponding to hemoglobin was quantified. The VPS45 knock sideways cell line, the VPS45 knock sideways cell line with the complementing VPS45 copy and the 3D7 lab strain were used, of which the first one accumulates vesicles upon addition of rapalog and the latter do not show accumulation of vesicles in presence of

rapalog. For these assays, 4 different conditions were chosen (Figure 37 A): (i) Addition of rapalog and E64 protease inhibitor, expected to result in the accumulation of hemoglobin filled vesicles due to the VPS45 knock sideways and prevention of hemoglobin digestion inside the FV; (ii) addition of just rapalog to induce host cell cytosol filled vesicle accumulation; (iii) addition of just E64 allowing the transport of the host cell cytosol to the FV but not digestion of the hemoglobin and (iv) no E64 inhibitor nor rapalog, resulting in transport to the FV and digestion of hemoglobin.

Coomassie Gel analysis (Figure 37 B) revealed comparably intense bands of the hemoglobin monomer in all E64 treated cells (with and without rapalog). The control (no rapalog and no E64) did show faint bands of the hemoglobin monomer in all cell lines. The cultures were just rapalog was added (Figure 32 lanes marked with +-) showed also a faint band in the complemented cell line and 3D7. In contrast, the VPS45 knock sideways cell line showed an intense band in the presence of rapalog similar to E64 treatment. This indicated that this more intense hemoglobin band after VPS45 knock sideways corresponded to the hemoglobin found in the vesicles. To obtain a more quantitative impression of this, the amounts of hemoglobin was quantified from 3 independent experiments (Figure 37 C, Coomassie stained PAA gels of individual experiments in A-9). The sample with E64 alone (Figure 32 lanes marked with -+) was set to one hundred percent because this represents the total amount of hemoglobin that is transported to the food vacuole during the experiment (Figure 37 C, red dotted line). The controls with neither E64 nor rapalog (Figure 32 lanes marked with --) contained three- to fourfold less (25 to 30 percent of total) hemoglobin (Figure 37 C, blue dotted line) in comparison to the just E64 treated cell culture. This baseline represents the amount of hemoglobin that is not digested in the FV under normal conditions. The presence of rapalog alone (Figure 32 lanes marked with +-) or rapalog additional to E64 (Figure 32 lanes marked with ++) in the complemented cell line and 3D7 did not show any elevated levels of hemoglobin in comparison to the baseline of the control (Figure 32 lanes marked with --) or just E64 alone (Figure 32 lanes marked with -+) since no secondary elevation of intracellular hemoglobin due to accumulating host cell cytosol containing vesicles happened. In contrast, in the VPS45 knock sideways cell line much more hemoglobin was detected in the cells grown in presence of rapalog alone (Figure 32 lanes marked with +-). The amount was on average the same as the cells treated with E64 alone (Figure 32 lanes marked with -+), indicating that all the hemoglobin ingested during the experiment was trapped inside the accumulating vesicles (Figure 37 C). Interestingly in the VPS45 knock sideways cell line where both, rapalog and E64, were added, an elevated level of hemoglobin to 135 percent in comparison to the just E64 treated cells (Figure 32 lanes marked with -+) and just rapalog added culture (Figure 32 lanes marked with +-) was detected.

This data indicates that the host cell cytosol inside the vesicles accumulating after VPS45 inactivation indeed contains similar amounts of hemoglobin than typically internalized into the FV in a similar timeframe and and this was not observed in the complementation but contained comparable proportions of hemoglobin in the parasites to that found in the 3D7 lab strain.

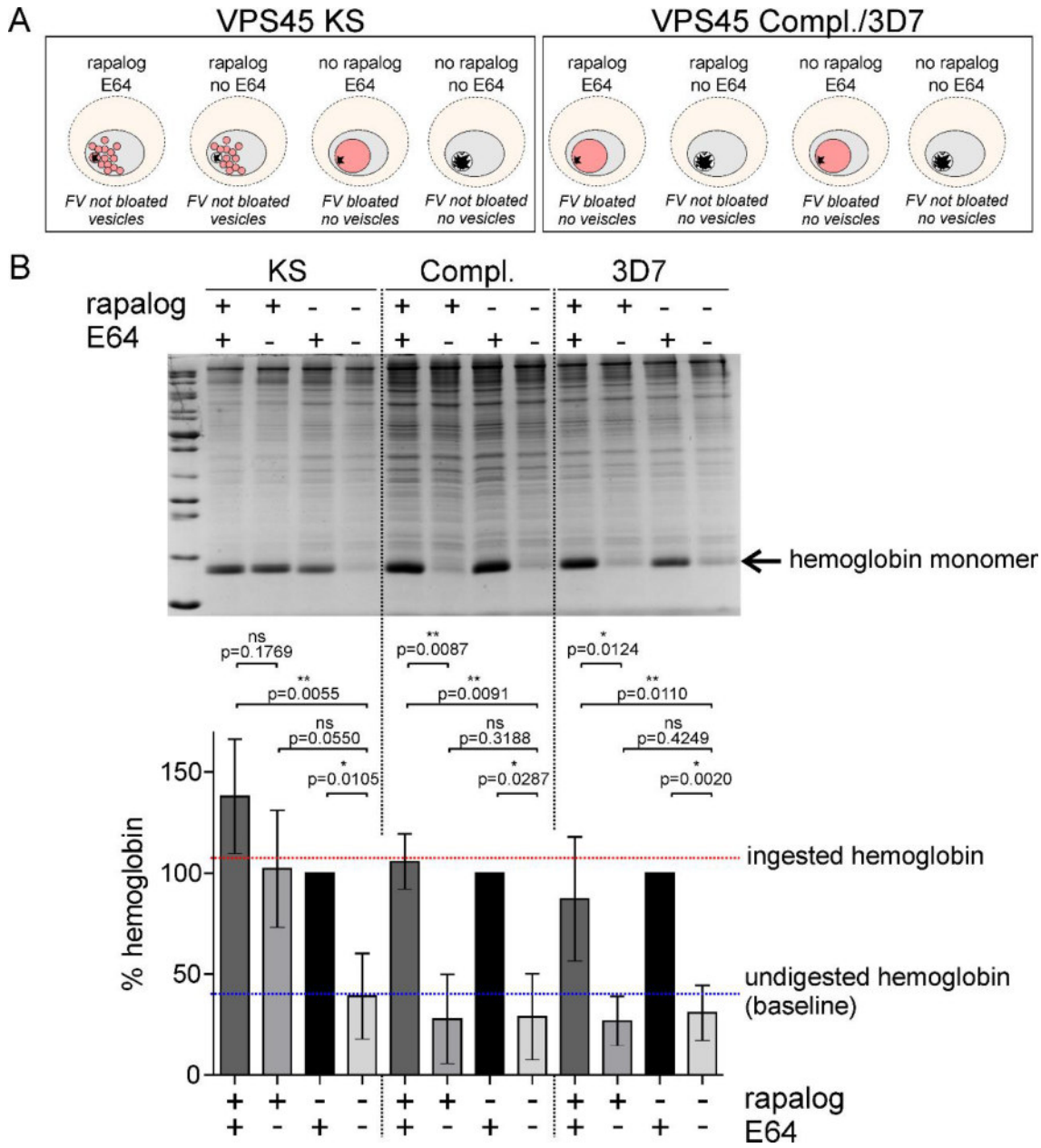

Figure 37: **Hemoglobin accumulation assay quantified in Coomassie-stained SDS-PAA-Gels.** Quantification of the intracellular amount of hemoglobin monomer in an assay with the protease inhibitor E64 preventing the digestion of hemoglobin in the FV. **A**) Scheme showing red blood cells (bright pink) selectively lysed with saponin to release hemoglobin from the host cells containing parasites (grey). The FV vacuole is marked by the hemozoin (black crystal). The effects of adding rapalog and E64 to the VPS45 knock sideways cell line, the VPS45 knock sideways complemented cell line or 3D7 (no integrated VPS45 construct into the genome, no mislocalizer plasmid) is shown. Addition of E64 leads to accumulation of hemoglobin (red) in the FV in all cell lines. Rapalog induces the accumulation of vesicles in just the VPS45 knock sideways cell line. The control (no rapalog, no E64) shows no intracellular hemoglobin in all cell lines. **B)** Coomassie stained 12 % SDS-PAA gel of probes as indicated in A (1 experiment out of three experiments shown). Samples were lysates of saponin treated infected red blood cells. Arrow shows hemoglobin monomers (expected as ~16 kDa band, detected slightly below the 15 kDa marker-band). KS: VPS45 knock sideways cell line; Compl.: VPS45 knock sideways cell line complemented with a VPS45 copy; 3D7: laboratory strain. Marker: Thermo Fisher Page Ruler Unstained Protein Ladder. (continued on next page).

Figure 37 (continuation of previous page): **C)** Quantification of the hemoglobin monomer in the Commassie stained SDS-PAA-gels. Data of three independent experiments was pooled (error bars, S.D.; p values are indicated, two-tailed, paired t-test). X-Axis shows percentage of hemoglobin amount in relation to the just E64 treated culture (-+). Blue dotted line represents amount of undigested hemoglobin present in the control (--). Red dotted line represents amount of hemoglobin that is taken up during the time of the experiment. Coomassie stained PAA-Gels of all three experiments shown in Appendix A-11.

4.3.2.3 VPS45 knock sideways HCCU vesicles have early endosomal properties

Phosphatidylinositol-3-phosphate (PI3P) is a hallmark of membranes of early endosomes (Balla, 2013). To determine whether the host cell cytosol-filled vesicles induced by VPS45 inactivation had an endosomal membrane signature and HCCU had endosomal characteristics, it was investigated whether the intermediates were positive for PI3P. To this end we tagged a PI3P sensor previously used in *P. falciparum* (Boddey et al., 2016; Kanai et al., 2001; Tawk et al., 2010) with mCherry and expressed it in the VPS45 knock sideways cell line for which we used a non-fluorescently tagged version of the mislocalizer. In the control cells (where VPS45 was not inactivated), the PI3P-sensor was found at the food vacuole membrane and in accumulations that frequently were close to the food vacuole, as observed previously (Boddey et al., 2016; Tawk et al., 2010) (Figure 38 A). In the cells grown in the presence of rapalog to inactivate VPS45 for 6 h, a proportion (65.8%, +/- 20.4%, n=28 cells from 2 independent experiments) of the induced HCCU intermediates were positive for PI3P (Figure 38 A-B). This suggests that the intermediates are related to early endosomal structures, arguing that a pathway resembling classical endocytic vesicle maturation may form the basis of HCCU.

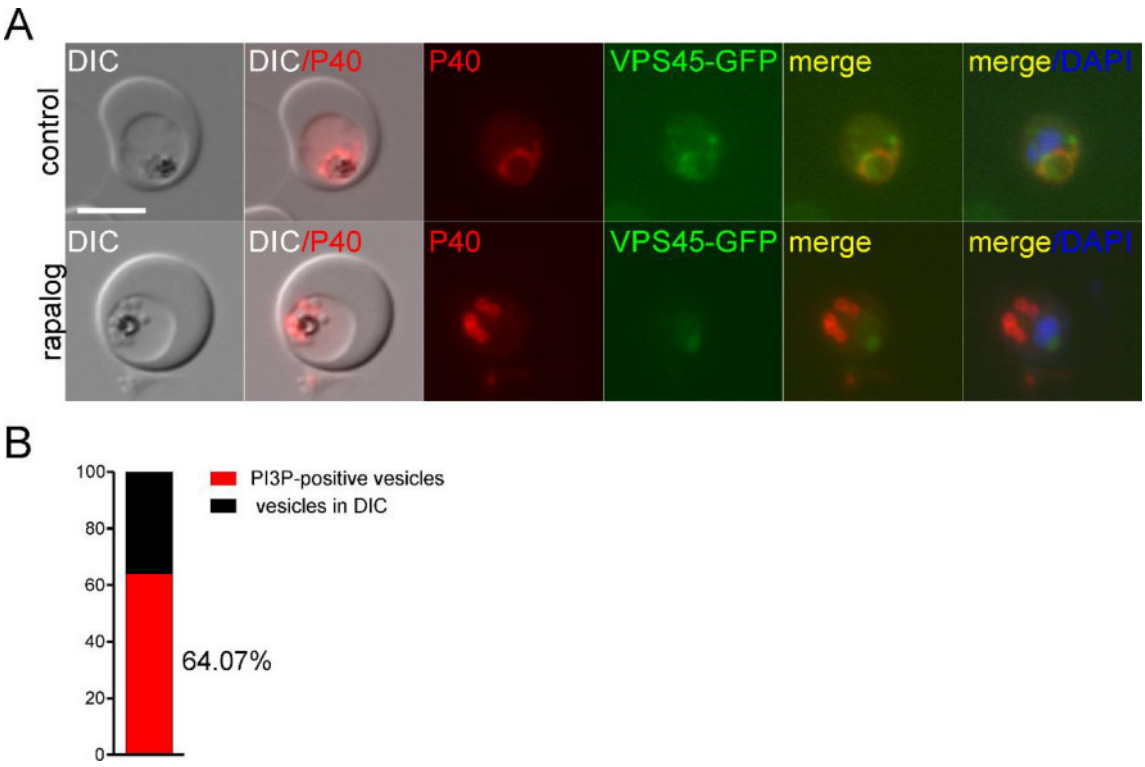

Figure 38: **Vesicles accumulating through inactivation of VPS45 positive fort he early endosome marker PI3P. A)** Representative fluorescence images of live VPS45-2xFKBP-GFP knock sideways parasites expressing P40PX-mCherry (P40) to detect phosphatidylinositol-3-phosphate (PI3P). Images were taken 6 h after inactivation of VPS45 using knock sideways (rapalog) and compared to control without rapalog. DIC: differential interference contrast; merge: green channel merged with red channel; DAPI: nuclei. Size bars: 5 µm. **B)** Quantification of percentage of PI3P-positive vesicles in VPS45 knock sideways induced vesicles.

4.3.2.4 The actin inhibitor CytochalasinD resembles the VPS45 knock sideways phenotype

Previous work has shown that the actin inhibitor CytochalasinD caused an accumulation of hemoglobin filled structures in the parasites similar to what here was observed with the Vps45 knock sideways (Lazarus et al., 2008; Milani et al., 2015; Smythe et al., 2008). To reconciliate this and compare to the VPS45 knock sideways results, CytochalasinD treatment was used and vesicle accumulation analysed in DIC (Figure 39). Interestingly, the CytochalasinE-induced vesicles accumulated mostly at the opposite side of the parasite in relation to the FV (Figure 34), whereas the VPS45 knock sideways vesicles accumulated usually proximal to the food vacuole (for example Figure 38). A subset of these vesicles was also PI3P-positive as visualized with the marker protein P40PX (Figure 39, white arrow). These results indicate that Actin inhibition by CytochalasinD at least partially resembles the VPS45 knock sideways phenotype.

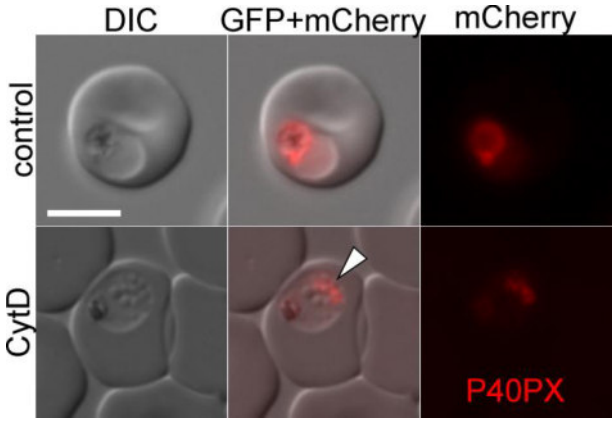

Figure 39: **CytochalasinD treatment of throphozoites leads to accumulation of vesicular structures similar to VPS45 knock sideways phenotype.** Representative fluorescence images of live VPS45-2xFKBP-GFP knock sideways parasites expressing P40PX-mCherry (P40) to detect phosphatidylinositol-3-phosphate (PI3P) treated with 10 mM CytochalasinD (CytD). DIC: differential interference contrast; mCherry: red fluorescent protein; DAPI: nuclei. Size bars: 5 µm

5. Discussion

5.1 Fast frame rate live cell imaging is a valuable tool to investigate intracellular trafficking in *P. falciparum* blood stages

Great efforts have been invested to visualize endocytosis and other vesicle trafficking processes in model systems like eukaryotic cell lines and yeast, resulting in advanced techniques allowing imaging with very fast frame rates (subsecond per frame) in 3D and in multiple colors (Jones et al., 2012; Jones et al., 2011; Kirchhausen, 2009; Schmoranzer et al., 2000). Even though that imaging techniques for *Plasmodium* cells made progress (De Niz et al., 2017; Gruring et al., 2011), the visualization of fast moving foci remains difficult to do in *P. falciparum* blood stages. Challenges that need to be overcome are low signal intensities of many cell lines if marker proteins are expressed from their endogenous promotor and the small size of the parasite between 2 to 7 µm (roughly equivalent to the size of a mammalian nucleus or a yeast cell). Due to the presence of the photoreactive hemoglobin and hemozoin, the specimens are prone to phototoxicity and changes in cellular pH due to illumination have been observed (Wissing et al., 2002). The existing set up for live cell imaging with a confocal laser scanning microscope (CLSM) (Gruring et al., 2011) was feasible for imaging of cell lines above a certain threshold of signal intensity. These cell lines were imaged with a maximum rate of ~5 seconds per 3D stack. Special manual handling and adjustment while imaging allowed imaging at a sub-second frame (Flemming, 2015), but this approach is too complicated to extensively study endocytic processes in *Plasmodium* cells. During the work for this thesis, two different microscopes were modified to overcome these obstacles and to track individual and multiple foci of fluorescence in the parasites without gaps in their movement in between frames. Nevertheless these systems were in some cases still not able to detect very faint foci or to completely track foci without gaps which shows that there is still room for improvement. In comparison to the existing CLSM the new imaging systems allow imaging of cell lines with considerably lower fluorescent signal intensity but does not outcompete the CLSM in terms of resolution along the Z-axis (3D) and optical resolution. Long term imaging, as it has been shown for the CLSM, was not tested with the new set ups since this work focused on fast endocytic processes. The possibility to image multiple cells with one experiment due to the widefield illumination, whereas the CLSM demands cropping to one cell to reduce the scanned area of the laser and therefor gaining speed, is beneficial to detect events that occur more rarely and enables easier quantification due to the higher number of analyzed cells in one experiment. Further benefits are the fast imaging of multiple channels and the acquisition of high quality DIC time lapse images at a video frame rate temporal resolution. Therefore these two new microscope-set-ups close the gap of imaging techniques for fast frame rate imaging. As they use already existing equipment, they provide a cost effective and convenient solution on site. These fast imaging set ups will also enable to analyze the dynamics of other potential trafficking processes and to study the spatio-

temporal dynamics of the involved structures and proteins. In general, these imaging systems may also facilitate screening of further inhibitors or compounds that may affect the endocytosis and trafficking processes in *P. falciparum*.

5.2 The role of the Clathrin Heavy Chain in *P. falciparum* blood stages

Clathrin Mediated Endocytosis (CME) is the best investigated endocytic process in model organisms. Many other uptake pathways, grouped as Clathrin Independent Pathways (CIE), are known but are often not as well understood as CME. To distinguish if host cell cytosol uptake is CME or rather CIE the homologue of CHC in *P. falciparum* was further characterized in this work. Clathrin was found to be refractory to disruption and growth is reduced even after just partial mislocalization and therefore seems to be important for survival of *P. falciparum* blood stages.

5.2.1 PfCHC may have a function at the Golgi compartment

Lacking directed movement analyzed with fast frame rate imaging and missing interaction partners identified in DiQ-BioID indicate that Clathrin is not involved in HCCU. Rather the data overall suggests a role of PfCHC at the Golgi. The identification of typical Golgi-associated proteins AP-1 complex, AP-4 complex and a Golgin-like protein in the DiQ-BioID support a location of CHC at the Golgi compartment. Co-localization with the Golgi marker PfGRASP (Struck et al., 2005; Struck et al., 2008) using overexpressed mCherry tagged PfGRASP protein or the anti-PfGRASP antibody (Struck et al., 2005) could give certainty to this assumption and show that CHC localizes at the Golgi in *P. falciparum*. At least partial co-localization of PfGRASP and CHC can be expected because the localization-pattern of the intense patch-like foci and their number is at least partly similar to the localization described for PfGRASP (Struck et al., 2005).

Interestingly not only the large patch-like foci, but also smaller foci were observed with CHC-2xFKBP-GFP. The observed faint foci, were more regular in shaped and might represent clathrin coated vesicles (CCVs). The lack of directed movement can be explained with a short life-time of CCVs due to rapid disassembly of the clathrin coat during vesicle transport. Formation of CCVs is further supported by high conservation of the domain structure of CHC in comparison to other CHC homologues in other model organisms, indicating that *P. falciparum* CHC serves a similar function. In addition PfCHC does not contain larger *Plasmodium*-specific parts that may indicate a deviating or additional function. This also indicates that it is not a good target for chemotherapeutic intervention although the interactome contains *Plasmodium*-specific proteins without homology to known proteins. These proteins could be involved in parasite-specific pathways and therefore harbor potential for specifically inhibiting parasite development. CHC could help as a marker to describe these proteins and to examine their function in the biology of *Plasmodium* blood stages.

5.2.2 PfCHC may be involved in retromer trafficking

A Golgi localisation of CHC in *P. falciparum* would be in agreement with the *Toxoplasma*-homologue of Clathrin which is reported to function in post Golgi trafficking (Pieperhoff et al., 2013). One pathway of post Golgi trafficking is the retromer pathway from the Golgi to the endosomes. The identification of elements of the retromer like sortilin (Pan et al., 2017) in the DiQ-BioID experiments with the PfCHC, gives further indication of Clathrin performing Golgi derived trafficking and in case of the retromer possibly to endosomal or lysosomal compartments. A functional retromer trafficking from the Golgi to the early endosome has been described in *T. gondii* (Sangare et al., 2016) but was found to be required for the biogenesis of special excocytotic organelles of the apical complex and this was also shown for other endolysosomal factors like VPS9, sortilin, Rab5 and Rab7 (Breinich et al., 2009; Hallee et al., 2018; Kremer et al., 2013; Pieperhoff et al., 2013; Sangare et al., 2016; Sloves et al., 2012; Tomavo et al., 2013). A function of CHC in retromer trafficking in *P. falciparum* agrees with the finding that CHC localization is completely altered after treatment with the retromer-inhibitor Retro-2. The observed fast moving foci after applying Retro-2 may represent blocked retrograde intermediates. This effect appears to be specific, since the foci marked by Eps15 and Kelch13 were not affected by Retro-2 treatment.

If Clathrin is indeed involved in retrograde trafficking to the FV, a bloated food vacuole assay would tell if Clathrin dependent cargo is trafficked to the food vacuole via the retromer or another Clathrin mediated pathway and if there is similarity to the transport to the VAC compartment of *T. gondii*, which is thought to be an intersection of secretory and endocytic trafficking routes in this organisms (McGovern et al., 2018).

5.2.3 PfCHC interacting proteins suggest an unusual configuration of a Golgi associated trafficking complex

Along with more detailed analysis of the Retromer-Complex, it would also be of great interest to have a closer look on the other Clathrin-interacting proteins and if they define particular trafficking pathways in *P. falciparum*. Especially the Adaptor Complexes 1 and 4 (AP-1 and AP-4) and the known AP-4 interactor Tepsin are of great interest since they are ascribed to different Golgi-trafficking routes in other organisms (Park and Guo, 2014). In support of a Golgi location and interaction with CHC, AP-1 was shown to be important for apical organelle biogenesis in *T. gondii* (Venugopal et al., 2017). More surprising is the finding that AP-4 was associated with PfCHC, rather than AP-3. AP-4 is generally regarded as a Clathrin independent adaptor (Hirst et al., 1999; Hirst et al., 2013; Robinson, 2004), although a single study provided evidence to the contrary (Barois and Bakke, 2005). It therefore may be that the DiQ-BioID experiments uncovered an interaction that so had been missed in other organisms or alternatively, that PfCHC interacts with different adaptors. This would be supported by the fact that the DiQ-BioID experiment provided little evidence for an interaction of PfCHC with AP-3, which is a well-accepted clathrin adaptor at the Golgi (Dell'Angelica

et al., 1998; Kural et al., 2012). Together with the lacking association of clathrin with AP-2, this indicates an unusual configuration of the vesicle trafficking machinery in malaria parasites.

The proteins identified with DiQ-BioID for CHC harboring Phosphoinositide (PIP)-binding-domains like Pleckstrin-homology domain or PX-domain are also of interest because PIPs are known to specify membrane identity in trafficking processes (Haucke, 2005; Posor et al., 2015). The distribution of PIPs has already been surveyed in *P. falciparum* (Ebrahimzadeh et al., 2018; Tawk et al., 2010) and the endocytosis relevant PI3P was found to be located at the FV and possibly at the apicoplast (Tawk et al., 2010). In contrast PI3P is also considered being important for export of proteins into the host cell (Bhattacharjee et al., 2012; Vaid et al., 2010) and changes in the PI3P-homeostasis is thought to confer artemisinin resistance (Bhattacharjee et al., 2018; Mbengue et al., 2015). Further investigation of the here identified phosphatidylinositol phosphate-interacting proteins of a potential protein complex at the Golgi could identify other functions of phosphatidylinositol phosphate.

5.2.4 PfCHC mediated trafficking might be important for the secretory pathway

VPS9, which was found in the interactome, was already tagged in a localization based screen and found to localize to foci that may represent the Golgi (Flemming, 2015). VPS9 is a GDP-GTP exchange factor (GEF) and a regulators of Rab-proteins (Carney et al., 2006). Interestingly, VPS9 was shown to be important for apical organelle biogenesis in *T. gondii* (Sakura et al., 2016). Repurposing of CHC mediated pathway for secretory organelle biogenesis might also have happened in *P. falciparum* because the ablation of CHC by knock sideways here led to a phenotype in the schizont and merozoites stages resulting in less newly invaded red blood cells, suggesting an invasion defect. Sortilin, a protein which was also found with the DiQ-BioID for CHC in *P. falciparum*, was also shown to be essential for apical organelle biogenesis in *P. falciparum* (Hallee et al., 2018) and for the Sortilin-like receptor TgSORTLR in *T. gondii* (Sloves et al., 2012). The CHC knock sideways can now be used to test the role of this protein for secretory organelle biosynthesis and secretory trafficking. However, due to the limited efficiency of the knock sideways with CHC that may permit certain functions to continue, it will be absolutely necessary to tag CHC with the more efficient sandwich FKBP tag to enhance mislocalization efficiency (Birnbaum et al., 2017). Another option would be to inactivate CHC on the RNA-level using the ribozyme-system as it has been done with its interacting protein Sortilin (Hallee et al., 2018) or using diCre based gene elimination (Andenmatten et al., 2013; Birnbaum et al., 2017; Collins et al., 2013; Jullien et al., 2007; Knuepfer et al., 2017) or combinations thereof.

Taken together the localization of CHC foci, the lack of directed movement and the potential interactors and compartment neighbors of CHC do not favor a function in HCCU. Identification of potential interacting proteins typical for the Golgi compartment and the sensitivity of CHC localization to the retromer inhibitor Retro-2 suggest a function in retromer and secretory trafficking. Inactivation of CHC with knock sideways partially arrested the parasite's life cycle during invasion of

merozoites into new RBCs or shortly after invasion, giving first indications for a potential role of CHC in secretory trafficking from the Golgi to the parasite specific apical organelles important for invasion consistent with the role in the apicomplexan *T. gondii* (Pieperhoff et al., 2013). However, further experiments permitting improved conditional inactivation of CHC and detailed studies using potential cargo are needed to fully understand the function of Clathrin in *Plasmodium* parasites.

5.3 Eps15 interacts with Kelch13 and is possibly involved in endocytosis

5.3.1 Eps15 positive structures cycle between food vacuole and parasite plasma membrane and Eps15 likely is essential for parasite survival

Eps15 was found as the most promising candidate in a screen searching for factors involved in endocytosis in *P. falcaiparum* (Flemming, 2015). Such a function is supported by its localization at the FV, the co-localization with host cell cytosol filled structures adjacent to the FV and the shuttling movement between the parasite plasma membrane (PPM) and the food vacuole (FV) (Flemming, 2015). This thesis succeeded in inactivating Eps15 and reproduced the known shuttling movement ('cycling') of the foci positive for this potential endocytosis-factor. However, it also found that the movement of Eps15 foci appeared to be more complex when imaged with the newly established set ups. There is evidence that different types of movement are present: Movement over very short distances close to the FV which could be the place where the co-localization of Eps15 with hemoglobin filled structures was described in correlative fluorescence and electron microscopy (CLEM) (Flemming, 2015). Therefore the short-distance movement at the food vacuole is likely to be associated with a dynamic host cell cytosol filled structure which is possibly the HCCU-machinery. Then there is movement over longer distances also towards the FV of foci originating from a distant localization in relation to the FV. Whether these different movements represent different pathways or recycling of Eps15 remains unclear but also in these instances a CLEM experiment supported a co-location with hemoglobin filled structures (Flemming, 2015).

One reason why previous work focused on PfEps15 was also because the majority of the molecule shares no homology with Eps15 from other organisms but is conserved amongst P*lasmodium* species and lacks homologues in other apicomplexans (Flemming, 2015). This sequence specificity in the genus *Plasmodium* combined with the possible essentiality of the protein, as shown here, holds promise for a potential target for intervention against the Malaria parasite and combat of this disease. To investigate whether Eps15 is important for blood sage survival, its essentiality for the parasite was in this thesis analyzed with attempted gene disruption of *eps15* and inducible knock sideways of the Eps15 protein. Since the knock sideways was only partly successful, different approaches for knock down or knock out of the protein are necessary to further characterize the phenotype of Eps15 ablation in *P. falciparum.*

5.3.2 Less significant hits identified with DiQ-BioID with Eps15 indicate a function in endocytosis

Typical Proteins known to interact with Eps15 during endocytosis in model organisms were identified in the DiQ-BioID with Eps15 but none of the identified proteins showed significant enrichment (average normalized log 2 ratio below 1.10). It can also not be excluded that these proteins were tagged by unspecific, transient proximity for example in the secretory pathway during protein synthesis, post-translational modification and protein transport as it very likely happened with the identified exported protein EXP1 or the ER-resident trans-membranous Protein YOP1.

One of the less enriched proteins was Epsin (significant normalized log 2 ratio of ~3.50 in two experiments, the other two experiments showed low enrichment of a normalized average log 2 ratio of 0.69 and 0.84), a well-known Eps15 interacting protein (Chen et al., 1998) that was previously co-localized with Eps15 as a putative marker for endocytosis in *P. falciparum* (Flemming, 2015). This hit raises the confidence for the DiQ-BioID data with Eps15. In addition, this shows that the parameters used for the initial screen by Sven Flemming to find proteins involved in endocytosis may have been appropriate.

Phosphatidylinositol phosphate-interacting and –modifying proteins can also be involved in endocytosis since these lipids also regulate vesicle formation, trafficking and maturation by giving membranes and compartments identity as shown for the inositol-polyphosphate 5-phosphatase (low enrichment with normalized log 2 ratios of -1.64 to 1.09) for example in plants (Golani et al., 2013). Inositol-polyphosphate 5-phosphatase has been shown to interact with the Adaptor Protein 2 (AP-2) (Ungewickell et al., 2004) which was also identified in the DiQ-BioID for Eps15 with low enrichment (normalized log 2 ratio of 0.59 to 0.73 in the individual experiments). The AP-2 µ subunit of the AP-2 complex has already been tagged during work following up of the screen searching for endocytosis factors by Sven Flemming. The identification of AP-2 (normalized log 2 ratio of 0.59 to 0.73 in DiQ-BioID with Eps15), but no identification of AP-1 or AP-4, implies that the Eps15 protein complex may indeed be involved in endocytosis, in contrast to CHC. Further analysis of this cell line will be of importance to corroborate this hypothesis.

Eps15 and Epsin together with the Adaptor Complex 2 (AP-2) are important for Clathrin coated pit formation, the first step of CME, at the plasma membrane but this does not seem to be the case in *Plasmodium*. The presumably high adaption of endocytic processes to the needs of the parasite's unique niche might have been led to the evolution of a parasite-specific endocytosis machinery independent from Clathrin. It has been shown that Eps15 alone is able to form stable structures for endocytic pit formation (van Bergen En Henegouwen, 2009; van Delft et al., 1997b). The exact role of Eps15 in this process remains unclear. No evidence for stalled pits or accumulation of invaginations resembling small cytostomes at the plasma membrane, as seen with a Dynamin knock down (Milani et al., 2015), could be observed neither microscopically, nor in ultrastructural observations using electron

microscopy (EM) (not shown preliminary data). This could be because of either that there are no pits formed at all or the formed pits are aborted quickly as also observed for CME (Ehrlich et al., 2004; Loerke et al., 2009). If there are only a small number of pits present per cell at one time point, it would also be almost impossible to detect these in individual sections in EM. An elegant assay to test for early steps of HCCU would be a method to stall HCCU intermediates (5.4 for characterization of HCCU intermediates) prior to delivery of its content to the FV and then check if HCCU-intermediates still accumulate upon knock sideways of potential early HCCU-factors. If no vesicles can be formed after addition of rapalog, there should be no accumulation or a reduced number of HCCU-intermediates present. This could be achieved with a potent specific inhibitor, which is not available to date, or by using a simultaneous knock sideways of VPS45.

There were also elements of other trafficking complexes identified with low enrichment: VPS51 (normalized log 2 ratios -0.02 to 2.83) and VPS53 (normalized log 2 ratios -1.11 to 0.46) are parts of the GARP complex (Golgi-associated retrograde protein) that is retrieving proteins from the endosomes to the TGN and does retrograde transport in other model organisms (Perez-Victoria et al., 2010). These are also described as part of the EARP complex (endosome-associated recycling protein) which is important for receptor recycling to the plasma membrane (Schindler et al., 2015). Surprisingly also VPS35 (normalized log 2 ratios 0.36 to 3.59), which is the core element of the retromer complex (Arighi et al., 2004; Verges et al., 2004), were identified with DiQ-BioID for Eps15. The nature of this interaction is unclear since Eps15, in contrast to Clathrin Heavy Chain, is not affected by the Retromer inhibitor Retro-2. In *Toxoplasma* endocytic uptake pathway were shown to intersect with secretory trafficking pathways (McGovern et al., 2018) which might be similar in *Plasmodium* resulting in the identification of proteins of other trafficking routes like VPS35 with low enrichment due to transient proximity at for example Golgi or early endosome.

5.3.3 The Eps15-Kelch13 protein complex – a potential regulator of endocytosis and a possible role in artemisinin resistance in *P. falciparum*

The protein-complex, of which Eps15 is part of, is well described for CME in model organisms but seems to be different in *P. falciparum* according to the results of the DiQ-BioID with this protein. Identification of potential interaction partners using the BioID technique, which allows *in vivo* tagging of proximal proteins, revealed a protein complex that is likely specific for *Plasmodium*. The proteins identified in the Eps15 DiQ-BioID do not suggest an obvious endocytosis-complex, but with a closer look based on amino acid homologies roles in endocytosis can be hypothesized for some of the identified proteins and this is discussed in the following paragraphs.

The results of the DiQ-BioID were confirmed with CoIP for Eps15 and Kelch13. This newly identified interactor Kelch13 is not just temporarily interacting with Eps15 but rather accompanying during the cycling of Eps15 movement between the PPM and the FV. Kelch-domain containing proteins are usually present in high numbers in eukaryotic genomes and have versatile functions (Adams et al.,

2000; Stogios et al., 2005). Specific roles are often defined by molecular architecture of the Kelch domains, additional functional domains or different binding partners of each Kelch-domain containing protein (Adams et al., 2000). The function of Kelch13 of *P. falciparum* was extensively discussed but remains unclear (Dogovski et al., 2015; Mbengue et al., 2015). It was already linked to the here also identified de-ubiquitinating enzyme (DUB) called UBP1 which is the critical hint toward a potential function in ubiquitination-pathways (Leznicki and Kulathu, 2017). This is in agreement with the identification of several RING-domain (Really Interesting New Gene-domain) containing proteins in the DiQ-BioID for Eps15. Proteins with such domains play a key role in ubiquitin-protein ligase interaction, often due to binding to UIM-containing proteins (Genschik et al., 2013; van Bergen En Henegouwen, 2009). Along with other multiple functions, ubiquitination has been shown to regulate endocytic and trafficking processes by controlling protein-protein interaction of E3 ubiquitin ligase, scaffolding proteins and Eps15 in Cullin3-based E3 ligase complexes (MacGurn et al., 2012; Yuan et al., 2014). This complex assembly relies on the RING-domain, the UIM of Eps15 and the BTB domain of a Kelch-protein (also termed BTB-Kelch) (Stogios et al., 2005). This BTB-Kelch domain is also present in the Eps15-interacting Kelch13 but a function in endocytosis has been excluded due to the lack of a BACK domain which is usually located between the BTB-Domain and the Kelch-Repeats (Tilley et al., 2016). Even though that many BTB-Kelch proteins do contain the BACK-domain, its importance and precise function has not been shown yet (Stogios et al., 2005). Crucial protein interaction with proteins of the Cullin3-based E3 ligase complexes is rather dependent on a short amino acid sequence at the C-terminus of the BTB-domain termed the 3-Box (structural similarity to F-Box or SOCS-Box) which is the binding site for Cullin3 in the BTB-Cul3 Ubiquitin Ligases (Canning et al., 2013; Stogios et al., 2005; Zhuang et al., 2009). Kelch13 indeed contains such a 3-Box sequence in its BTB domain (Figure 40). It is therefore possible that Kelch13 has a function in an endocytosis regulating Ubiquitin-Ligase dependent complex via ubiquitination of PfEps15 itself or interaction of ubiquitinated enzymes with the UIM of PfEps1.

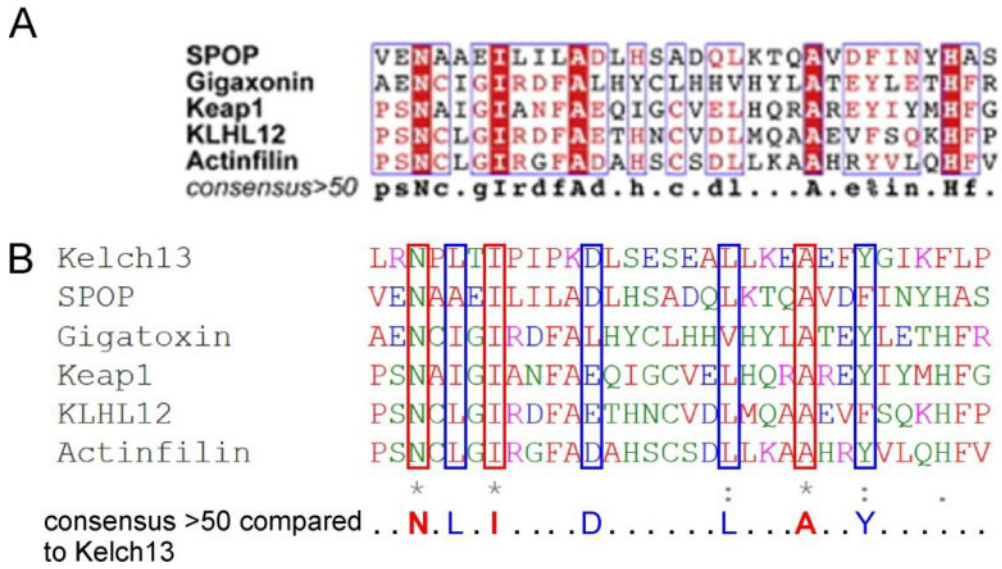

Figure 40: **The Kelch13 protein of *P. falciparum* contains a 3-Box domain for potential binding of ubiquitin ligases. A)** The consensus sequence of the conserved 3-box of the BTB-domain in five eukaryotic proteins is shown. Structure based sequence alignment of 32 amino acids corresponding to 3-boxes from five Cul3-interacting BTB domain containing proteins. Consensus sequence of amino acids conserved in more than 50 % of the aligned proteins. Amino acids with red background are present in all aligned proteins. Blue boxes show conserved amino acid residues (highlighted with red font) (modified from Zhuang et al., 2009). **B)** Alignment (ClustalO) of the Eps15 interacting protein Kelch13 of *P. falciparum* with the 5 proteins from A. The 32 amino acids corresponding to the putative 3-box of PfKelch13 were found by alignment of the whole Kelch13 amino acid sequence to the consensus sequence from A. Amino acids present in Kelch13 that are conserved in more than 50 % of the aligned eukaryotic proteins are shown as consensus sequence. Amino acids conserved in all aligned proteins are shown in red bold letters and are highlighted by red frames in the alignment. Proteins conserved in 50 % to 80 % are highlights in blue letters and blue frames.

Due to the fact that ubiquitinylating enzymes were concurrently linked with Artemisinin resistance, it was hypothesized that it is based on oxidative stress response and the proteasomal degradation pathways reacting to Artemisinin (Adams et al., 2018; Dogovski et al., 2015). Based on the indication from this thesis that Kelch13 and UBP1 interact with the possible endocytic protein Eps15 in *P. falciparum,* different explanation of which role these de- and ubiquityniting enzymes play in this context is offered. The formation of endocytic vesicles is a highly orchestrated process which requires multiple regulation-sites. Besides membrane identity by different species of phosphatidyl inositides and protein-phosphorylation, ubiquitynliation is a modification that does not just destine proteins for degradation but also is used for regulation of protein-protein-interactions (Andersen et al., 2005). This has been shown especially for Eps15 (van Bergen En Henegouwen, 2009; Weinberg and Drubin, 2014). Since PfEps15 contains several putative ubiquitinylation-sites and a possible ubiquitin interaction motif (UIM) at its C-terminus, which has been shown to be of importance for regulation of endocytosis in neurons (Fallon et al., 2006; van Delft et al., 1997a), UBP1, which is one of the most significantly enriched proteins in the DiQ-BioID experiment for Eps15, could be the enzyme being

responsible for modification of Eps15 at its UIM. Overexpression of Eps15 was not possible before but since a codon-adjusted, intron-free *eps15* gene of *P. falciparum* is available (unpublished), overexpression of Eps15 proteins with mutated or deleted ubiqitynilation-sites could be used to check for an altered localization or movement of these mutants. In case an efficient knock down or knock out of PfEps15 is available in the future, complementation with functional mutants after ablation of the endogenous protein to analyze the phenotype of the induced mutations would be highly informative in this respect.

Seen in a bigger context the hypothesized interactions of Eps15, Kelch13 and UBPs or DUBs are a matter of particular interest since mutations in Kelch13 are associated with resistance to the first-line anti-malaria drug Artemisinin (Ariey et al., 2014). It has already been shown, that Artemisinin function is dependent on Hemoglobin uptake (hence HCCU), hemoglobin digestion (Dogovski et al., 2015; Klonis et al., 2011; Mbengue et al., 2015; Tilley et al., 2016) and radical activation of Artemisinin by heme (Klonis et al., 2013; Meshnick et al., 1993) but no convincing mode of function of Artemisinin resistance could be drawn from these results (O'Neill et al., 2010). Data from this and previous work (Flemming, 2015) indicate a role for Eps15 in HCCU. Hence, the interacting artemisinin-resistance marker Kelch13 might also function in endocytosis. If HCCU is reduced because of Kelch13 variants, less hemoglobin is present and can be digested in the FV. This directly leads to less activated Artemisinin, possibly lowering it below the effective threshold inside the cell and therefore may allow survival of the parasites. A role of endocytosis in Artemisinin-resistance is supported by the identification of AP-2 in the DiQ-BioID with Eps15, which was recently shown to confer Artemisinin resistance (Adams et al., 2018; Henriques et al., 2014; Henriques et al., 2013; Henriques et al., 2015; Sutherland et al., 2017). Taken together this offers an alternative hypothesis for Artemisinin resistance based on reduced HCCU.

Several also high confidence hits in the Eps15 DiQ-BioID are not obvious candidates of a potential enodcytosis complex. This includes a metacaspase, functioning as a possible cysteine-protease, or the 6-phsphofructokinase, which is important for glycolysis. The proteins identified with DiQ-BioID with Eps15 were confirmed with the *vice-versa* experiment using Kelch13 as target for DiQ-BioID (Birnbaum et al., 2017), supporting the identified interacting proteins and compartment neighbors for Eps15.

5.3.4 Conclusion for Eps15

The data for Eps15 is supporting the conclusions of Flemming which has suggested Eps15 and Epsin being involved in HCCU. The BioID interactome shows that Eps15 might be at least transiently be in close proximity of Epsin supporting the already shown co-localization of these, in other model organisms interacting, proteins.

Eps15 is described as being important for initiation and pit formation of the early steps of endocytosis at the plasma membrane (McMahon and Boucrot, 2011). The observed shuttling movement of Eps15 positive foci in *P. falciparum* remains puzzling. Possibly the different types of movement serve different function, as one possibly may consist of the actual HCCU and the other movement could be recycling of Eps15 for restoration of Eps15-pools were they are needed. The additionally observed characteristics might appear due to simultaneous imaging of all foci of a cell during fast frame rate live cell imaging in 3D increasing the likelihood of observing different characteristics of the Eps15 movement in contrast to focusing on two foci in a single 2D layer. Especially the short distance movement was consistently observed in half of the analyzed parasites. The localization of this movement close to the FV and in between the parasites periphery and the FV coincides with the colocalisation of Eps15 foci with hemoglobin filled structures in correlative light and electron microscopy (Flemming, 2015) assuming that HCCU might take place at this short distance between PPM and FV in the *Plasmodium* parasite.

It can not be ruled out that Eps15 also serves other processes besides HCCU. Interaction with parts of the Adaptor Complex 2 (AP-2) indicates that at least one function of Eps15 is indeed endocytosis at the PPM since this protein is a marker for this pathway in other model organisms (van Delft et al., 1997b). Potential essentiality of Eps15 for the *P. falciparum* blood stages, which is also the case for Kelch13, UBP1 and one further interacting protein (Birnbaum et al., 2017), and the parasite specificity of parts of Eps15 (Flemming, 2015) may therefore be a reflection of the importance of endocytosis and hence HCCU for the parasite. The interaction with Kelch13 raises particular interest since Artemisinin resistance is linked to this protein. These results provide insights into the putative function of this endocytosis complex and allow an alternative mode of function of Artemisinin-resistance in *Plasmodium* parasites.

5.4 VPS45 is required for host cell cytosol uptake (HCCU) in *P. falciparum* blood stages

5.4.1 Nature of HCCU intermediates induced by VPS45 knock sideways

Given that inactivation of Eps15 and its interacting protein possibly blocks HCCU-vesicle-formation, it is difficult to gain insights into the actual pathway of HCCU after pinching off of hemoglobin cargo vesicles from the PPM. In contrast VPS45 likely acts downstream after vesicle formation and the establishment of assays for HCCU allows in-detail analysis of this process for the first time. Conditional inactivation of VPS45 led to the accumulation of hemoglobin filled, PI3P-positive vesicles inside the parasite representing HCCU intermediates. The accumulation of vesicles in proximity to a digestive vacuole is a hallmark of endocytic trafficking phenotypes as it was initially used to identify the first proteins in vesicular trafficking termed vacuolar sorting proteins (VPS) (Robinson et al., 1988). In the course of further research these proteins were found to fulfill versatile

functions ranging from the actual biophysical mediation of membrane fusion (SNARE-Proteins) to enzymatic regulation of for example small GTPases, just to mention two of them (Coonrod and Stevens, 2010). VPS45 was grouped into the class E mutants of VPS-proteins which are characterized by an exaggerated endosome-like compartment (Raymond et al., 1992). Specificity for SNARE-mediated membrane fusion is conferred by effector proteins, such as Rab-proteins or SM-Proteins like VPS45 (Carr et al., 1999; Carr and Rizo, 2010). In yeast and plants VPS45 is involved in Golgi to endosome trafficking (Bryant et al., 1998; Cowles et al., 1994; Piper et al., 1994; Zouhar et al., 2009) and in animal cells roles in endocytosis and maturation of early endosomes were reported (Gengyo-Ando et al., 2007; Morrison et al., 2008; Nielsen et al., 2000; Scheidel et al., 2018; Schottenfeld-Roames et al., 2014). Knock down of VPS45 in yeast and *Drosophila* lead to a similar phenotype with accumulating, endosomal vesicles (Morrison et al., 2008; Robinson et al., 1988). Whether this phenotype is a result of an inhibited fusion of the vesicles with the FV or a jammed maturation of these endocytic vesicles cannot be answered. Interestingly similar vesicles were here observed upon treatment with the actin-inhibitor Cytochalasin D, which was already observed (Lazarus et al., 2008) but further proof about the nature of these vesicles are needed to see if they are similar HCCU-intermediates. Since the VPS45 knock sideways induced vesicles mostly accumulate around the FV whereas the Cytochalasin D vesicles are located at a distant, opposite site of the FV, these two locations could represent the destination and the point of origin of the vesicles, respectively. However, no movement of the vesicles nor fusion events could be observed in video-frame rate imaging of the accumulation of the vesicles. The VPS45 knock sideways vesicles rather seemed to directly appear at the FV and not being transported through the cell. It can also not being ruled out, that the treatment with Cytochalasin D induces multiple effects and is blocking also other processes like cavity formation. The cavity, an invagination of the PPM (Grüring et al., 2011), is often located opposite of the FV (Kruse, 2014), the place where also the Cytochalasin D vesicles appear. Since the vesicles appearing upon Cytochalasin D treatment are marked with the early endosome marker PI3P, they might represent endosomal intermediates rather than a fragmented cavity which is positive for $PI(4,5)P_2$. Treatment of the VPS45-2xFKBP-GFP cell line expressing fluorescently labelled Plc delta, a protein domain binding $PI(4,5)P_2$ (Garcia et al., 1995), could be used to clearly show if the VPS45 knock sideways induced vesicles are derived from the cavity and undergo conversion of $PI(4,5)P_2$ to PI3P similar to other eukaryotes (Posor et al., 2015). Characterization of these vesicles provide a valuable tool for further investigation of HCCU and to differentiate endolysosomal factors involved in Apicomplexan-specific secretory trafficking from those involved in endocytosis to arrive at a general concept of vesicular trafficking in these parasites.

5.4.2 Improved hemoglobin uptake assays show reduced HCCU when VPS45 is knocked aside

Here a conditional inactivation system combined with hemoglobin uptake assay revealed the first protein (to our knowledge) directly shown to be involved in HCCU. To demonstrate that VPS45 indeed is a protein in HCCU, several assays were developed to show uptake of host cell cytosol and its

directed delivery to the FV. In the hemozoin size assay the data that VPS45 inactivation almost entirely inhibits the formation of new hemozoin, suggests that either there is only a single pathway of delivering host cell cytosol to the food vacuole or multiple pathways rely on the function of VPS45. The lack of material in the food vacuole was not a secondary effect due to a loss of parasite viability and also shows that a lack of hemoglobin uptake and digestion for 8 h does not immediately arrests parasite development, in agreement with the stage profile in synchronized VPS45 knock sideways parasites. This is crucial, as only if parasites still grow it can be concluded that loss of HCCU is not a secondary effect of parasite death. The reduced uptake of host cell cytosol was corroborated with the fluorescent dextrane uptake assay using preloaded host cells, a method established earlier and already proven useful for screening for potential endocytosis factors in *Plasmodium* (Flemming, 2015). This kind of assay is used in mammalian cells to show endosomal trafficking and acidification defects (Clayton and Cousin, 2009; Commisso et al., 2013; Masedunskas and Weigert, 2008) but in case of *P. falciparum* would need further development of the preliminary protocol focusing on 3D-imaging of the FV and measurement of the fluorescent intensity of the enire FV-volume and a proper background subtraction as previously done for *P. falciparum* (Flemming, 2015). Even though that this would be an elegant method to demonstrate reduced HCCU into the FV, the availability of quicker and easier reproducible assays did not make further development of this assay necessary. It should also be noted that this assay is also confounded by potential concentration-dependent quenching effects of the fluophore in the FV and that the lower pH in this compartment might also introduce further uncertainties. The direct visualization of hemoglobin taken up into the parasite instead of indirect measurement in Coomassie stained gels allows semi-quantitative measurement of the undigested hemoglobin inside the FV in presence of the protease inhibitor E64 in comparison to the amount of hemoglobin inside the accumulating vesicles. This assay showed that the amount of hemoglobin correlates with the number of vesicles in the rapalog treated cell line and with the number of bloated food vacuoles in the E64 treated cell lines, respectively. The big standard deviation in the rapalog treated cell line might be due to the varying number of vesicles, as shown in the dynamics of vesicle accumulation over time between the different samples. Nevertheless, on average, the amount of hemoglobin inside the vesicles was similar to the amount of hemoglobin accumulating in the food vacuoles (E64-treated) during the time frame of the experiment. Even more hemoglobin seemed to be present inside the cells when rapalog and E64 were added. The uptake is increased of ca. 40 % in comparison to the amount of hemoglobin taken up under natural conditions (just E64 treatment). Arguing that the VPS45 phenotype has some leakiness allowing still some HCCU intermediates to fuse with the food vacuole (which then must be a leakiness of ~ 40 % of the vesicles), the hemoglobin leaked into the FV during VPS45 knock sideways is digested since no E64 is present whereas in the culture were E64 added to the knock sideways, the leaked hemoglobin remains undigested in the FV and is detected. Other possible explanations are for instance the high amount of hemoglobin in the VPS45 knock sideways induced vesicles could cause a positive feedback effect due to the presence of

both drugs causing reduced protease levels in the FV, lower amounts of hemoglobin delivered to the FV or the reduced VPS45-regulation-pathway. It could also be that in parallel to the hemoglobin also digestion factors are transported in the hemoglobin filled vesicles to the FV as shown for Plasmepsin II (Klemba et al., 2004). But this does not explain the observed phenotype, because in this case in the sample treated with rapalog alone the hemoglobin should already have been partly digested in the vesicles. But no hemozoin was detected in these vesicles, suggesting that either they possessed limited digestive capacity or that polymerization to hemozoin did not occur at appreciable levels. The presence of digestive factors inside the vesicles could be tested with overexpressing these in a mislocalizer construct using the skip peptide as done in this thesis for the PI3P-marker P40PX or the complementation plasmid and see if these factors are present inside the VPS45 knock sideways induced vesicles.

5.4.3 The origin of the VPS45 knock sideways induced vesicles is not clear

Closer inspection of the vesicles accumulating after VPS45 inactivation revealed that some of them appeared to contain smaller vesicles. The significance of this is at present unclear. We also noted that some of the vesicles appeared to be double membraned, a feature previously observed with HCCU and consistent with structures originating from cytostomes which are double-membrane invaginations (including both, the parasite plasma membrane and the parasitophorous vacuolar membrane surrounding the parasite in the host cell) (Aikawa et al., 1966a). However, the double membrane vesicles observed here were not cytostomes, as they were also present after release of the host cell cytosol with tetanolysin, indicating that they were not in contact with host cell cytosol. Notably, the smaller internal vesicles were also observed after tetanolysin treatment. Adjacent to the FV several structures of unknown functions have been described like a PI3P- and Rab5b-positive extension of the food vacuole or a Rab7 positive ring like structure (Abu Bakar et al., 2010; Flemming, 2015; Krai et al., 2014; Tawk et al., 2010). The endolysosomal pathway in eukaryotes follows a maturation of early endosomes via multi-vesicular-bodies to late endosomes and finally lysosomes. Those distinct maturation steps were not observed in *Plasmodium* yet, but it is likely that a similar digestion pathway is present. The VPS45 knock sideways phenotype holds potential to further unravel the presence of these compartments, hypothesizing that the large hemoglobin filled vesicles induced by the VPS45 knock sideways are early endosome like structures which are constantly supplied with host cell cytosol but cannot further mature or pass on its content the lysosom-like compartment, the FV. This would explain why no actual transport of the vesicles is observed, since they are fed by smaller vesicles containing portions of endocytosed cargo. The presence of PI3P at the food vacuole is confusing, since this marker is typical for early endosomes and the luminal vesicles of multi vesicular bodies (Marat and Haucke, 2016), giving the impression that *Plasmodium* parasites may possess an unusual endocytic pathway. The significance of the smaller vesicles inside the VPS45 knock sideways-induced vesicles remains unclear but could for instance be reminiscent of multi-vesicular-body-like structures . Further information about the structure of these inner vesicles could be gained using 3D-electron

microscopy techniques like FIB-SEM (focused ion beam scanning electron microscopy) or tomography. It could also not be ruled out that these vesicles are artefacts induced by the massive accumulation of membranous structures.

5.4.4 Intersected trafficking of endocytic and secretory pathways

Evidence from *T. gondii* indicates that uptake of material from the host cell indeed also takes place in other Apicomplexan parasites (Dou et al., 2014; Jimenez-Ruiz et al., 2016; McGovern et al., 2018). Endocytosed material is then transported via the Golgi to the vacuolar compartment (VAC). In *Toxoplasma* it was recently shown that endocytosis intersects with a Golgi-proximal compartment where also the secretory pathway takes place (McGovern et al., 2018). This would also explain the foci of VPS45 localizing close to the nucleus, the place were also the Golgi-compartment is present (Struck et al., 2005). It could also be that the accumulating HCCU-intermediates are derived from the Golgi or represent blown-up Golgi sub-compartments. Therefor it would be worth testing the integrity of the Golgi and the distribution of Golgi markers upon induction of the VPS45 knock sideways phenotype. It would be of further interest to co-localize VPS45 with Eps15 and Kelch13 maybe also in presence with Golgi-markers to see in detail if there is an overlap during the possible maturation of vesicles at a hypothetic intersection at the Golgi. Other proteins involved in maturation of endocytic vesicles like Rab5 and Rab7 and Phophatidylinositolphosphates would also be of interest in order to analyze trafficking and maturation of these HCCU-vesicles.

It will also be interesting to inactivate VPS45 to reveal uptake processes in other parasite stages and in other Apicomplexans that propagate in host cells where endocytosis is less conspicuous than in red blood cells. It is thought that *Plasmodium* unspecifically engulfs host cell cytosol (Abu Bakar et al., 2010; Elliott et al., 2008). Even though that this is likely the case (based on the fact that dextranes and exported proteins are unspecifically taken up) and that there is not much to select since the host cell cytosol mostly contains hemoglobin, it would be of interest if there is any kind of receptor or regulating molecule at the outer leaflet of the parasitophorous vacuole membrane controlling and timing HCCU initiation. As a first step for identifying these putative regulatory elements or receptors, the isolation of HCCU intermediates and proteomic analysis of its content and its membrane bound molecules could be done. Furthermore the VPS45 knock sideways phenotype could be exploited to analyze upstream endocytic processes through endogenous tagging of VPS45 and potential endocytotic proteins such as Eps15 and using the number of accumulating VPS45 knock sideways vesicle as read out for reduced HCCU.

5.5 Working model for role of Eps15, VPS45 and CHC in *P. falciparum* blood stages

Summing up this thesis, the following working model is proposed (Figure 41): HCCU is not a Clathrin mediated endocytosis (CME) process because CHC has been found to interact with Golgi-related proteins and therefore is likely involved in Golgi trafficking, as already shown for *Toxoplasma* (Pieperhoff et al., 2013). VPS45 knock sideways leads to the accumulation of HCCU-intermediates that cannot deliver their content, the host cell cytosol, to the FV. The molecular basis for this block remains unclear but could be due to altered regulation of the maturation or fusion of HCCU-vesicles due to absence of the SM-protein VPS45. Eps15 also possibly plays a role in HCCU. The Eps15 interactome does not share much similarity with already well investigated Eps15 protein complexes but allows the hypothesis that it represents a complex with regulatory function in early steps of HCCU, namely the formation of HCCU-vesicles at the parasite-host cell-interface. It has also been shown for Eps15 that it has the capacity to interact with membranes in order to induce membrane curvature necessary for pit formation (McMahon and Gallop, 2005; van Bergen En Henegouwen, 2009; Wang et al., 2016). The HCCU pathway possibly relies on transport mediated by a classical Myosin-driven force generating machinery along Actin. Since the role of Actin is highly elusive and studies using inhibitors such as Cytochalasin D often induce unspecific off-target effects or multiple effects that are difficult to interpret, this idea has to be handled with caution and requires more data. Recent advances in visualization of actin in *Toxoplasma* using ectopically expressed nanobodies (Periz et al., 2017) might provide a tool to also shed light on actin dynamics in *Plasmodium* and its role in HCCU. It cannot be ruled out that HCCU and Golgi-trafficking (especially *trans*-Golgi trafficking) intersects as recently shown in *Toxoplasma* for endocytic uptake via the Golgi and transport to the digestive vacuole (VAC-compartment in *T. gondii*). The results from the DiQ-BioID indicates that even if there is a crossing of the pathways at the Golgi, Clathrin-mediated trafficking is separated from HCCU. However, HCCU itself might be dependent on Clathrin-trafficking since Retromer-transport (Golgi-to-Endosome) might contribute to transport of digestion factors to the FV. This was indicated by the fact that the Retromer-Inhibitor affects Clathrin localization and dynamics, but not Eps15. Clathrin mediated trafficking via the Golgi was reported to be essential for secretion to the apical organelles. This could just partly be shown in this work, possibly due to insufficient inactivation of CHC by the knock sideways. Many questions remain open concerning HCCU and Golgi-trafficking. Even though already proposed for other endocytic homologues, here for the first time a protein, VPS45, was directly shown to be important for HCCU. This offers a door opener to the so far obscure endocytic pathway in *Plasmodium* and gives the chance to uncover this complex trafficking network also in other Apicomplexans such as *Toxoplasma*.

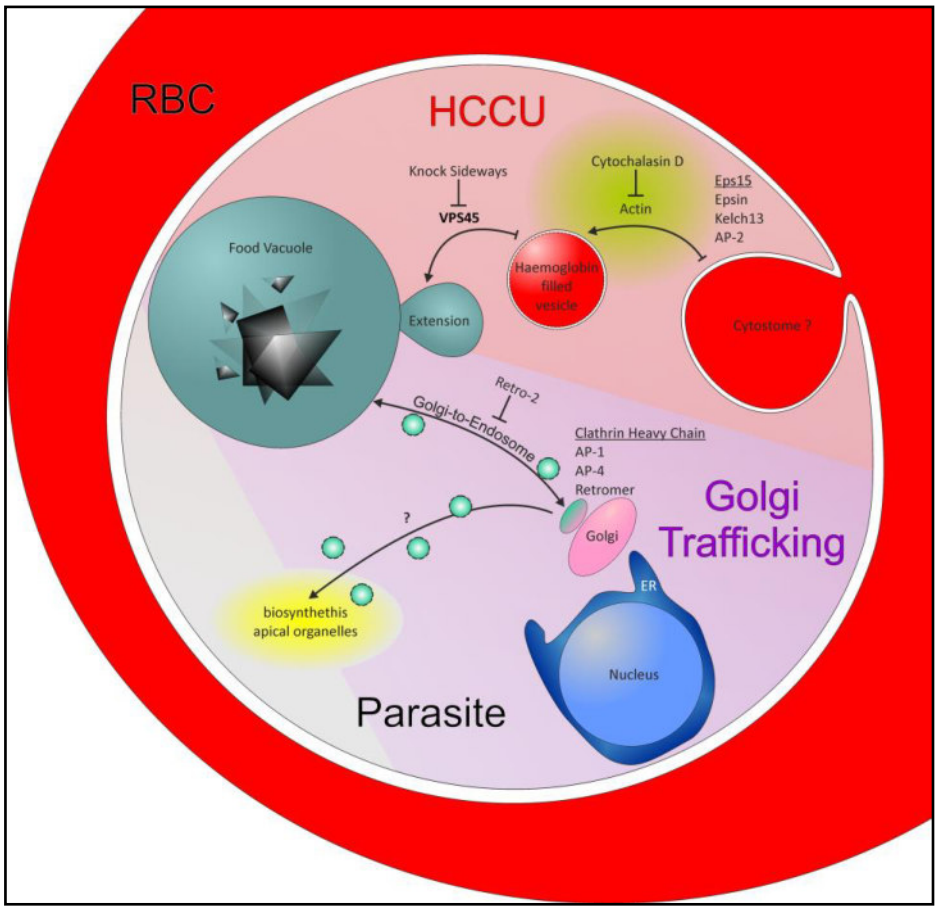

Figure 41: **Working model for the function of Eps15, VPS45 and Clathrin Heavy Chain in endocytosis and trafficking in *Plasmodium falciparum*.** Based on results from this thesis and review of previous work the following working model is proposed: Eps 15, Kelch13 and their potential interacting proteins mediate early steps of HCCU possibly by regulating endocytosis at the Cytostome located at the parasite plasma membrane. Eps15 and Kelch13 are cycling between the plasma membrane and the food vacuole, especially moving to an area adjacent to the extension of the food vacuole. The cycling might represent transport of HCCU vesicular intermediates to the food vacuole in an actin dependent, Cytochalasin D sensitive manner. Delivery of hemoglobin to the food vacuole is dependent on VPS45 since knock sideways of VPS45 leads to accumulation of host cell cytosol filled vesicles and hemoglobin does not reach the food vacuole. In contrast, Clathrin Heavy Chain is involved in a different trafficking pathway at the Golgi compartment, possibly mediating the secretory pathway to the apical organelles as already shown for *Toxoplasma* and Golgi-to-endosome transport of the Retromer machinery. In *Toxoplasma* also intersection of the endocytic and secretory pathways at early endosome like compartments (not depicted in this model) was shown, which might also be the case in *P. falciparum*. Hence, HCCU and Golgi trafficking might not be as mutually exclusive as indicated in this model. AP: adaptor protein; ER: endoplasmic reticulum; HCCU: host cell cytosol uptake; RBC: red blood cell. Turquoise circles depict Clathrin trafficking intermediates. Light green background represents site of Actin-function in HCCU. Black triangles depict Hemozoin-crystal. Grey background: parasite cytosol; Pink and purple shades of the parasite cytosol represent HCCU and Golgi trafficking, respectively.

6. References

Abu Bakar, N., N. Klonis, E. Hanssen, C. Chan, and L. Tilley. 2010. Digestive-vacuole genesis and endocytic processes in the early intraerythrocytic stages of Plasmodium falciparum. *Journal of cell science*. 123:441-450.

Adams, J., R. Kelso, and L. Cooley. 2000. The kelch repeat superfamily of proteins: propellers of cell function. *Trends in cell biology*. 10:17-24.

Adams, T., N.A.A. Ennuson, N.B. Quashie, G. Futagbi, S. Matrevi, O.C.K. Hagan, B. Abuaku, K.A. Koram, and N.O. Duah. 2018. Prevalence of Plasmodium falciparum delayed clearance associated polymorphisms in adaptor protein complex 2 mu subunit (pfap2mu) and ubiquitin specific protease 1 (pfubp1) genes in Ghanaian isolates. *Parasites & vectors*. 11:175.

Agop-Nersesian, C., B. Naissant, F. Ben Rached, M. Rauch, A. Kretzschmar, S. Thiberge, R. Menard, D.J. Ferguson, M. Meissner, and G. Langsley. 2009. Rab11A-controlled assembly of the inner membrane complex is required for completion of apicomplexan cytokinesis. *PLoS pathogens*. 5:e1000270.

Aguilar, R., A. Magallon-Tejada, A.H. Achtman, C. Moraleda, R. Joice, P. Cistero, C.S. Li Wai Suen, A. Nhabomba, E. Macete, I. Mueller, M. Marti, P.L. Alonso, C. Menendez, L. Schofield, and A. Mayor. 2014. Molecular evidence for the localization of Plasmodium falciparum immature gametocytes in bone marrow. *Blood*. 123:959-966.

Aikawa, M. 1966. The fine structure of the erythrocytic stages of three avian malarial parasites, Plasmodium fallax, P. lophurae, and P. cathemerium. *The American journal of tropical medicine and hygiene*. 15:449-471.

Aikawa, M. 1971. Parasitological review. Plasmodium: the fine structure of malarial parasites. *Experimental parasitology*. 30:284-320.

Aikawa, M., R.T. Cook, J.J. Sakoda, and H. Sprinz. 1969. Fine structure of the erythrocytic stages of Plasmodium knowlesi. A comparison between intracellular and free forms. *Zeitschrift fur Zellforschung und mikroskopische Anatomie (Vienna, Austria : 1948)*. 100:271-284.

Aikawa, M., P.K. Hepler, C.G. Huff, and H. Sprinz. 1966a. The feeding mechanism of avian malarial parasites. *The Journal of cell biology*. 28:355-373.

Aikawa, M., C.G. Huff, and H. Spinz. 1966b. Comparative feeding mechanisms of avian and primate malarial parasites. *Military medicine*. 131:Suppl:969-983.

Aikawa, M., C.G. Huff, and H. Sprinz. 1967. Fine structure of the asexual stages of *Plasmodium elongatum*. *The Journal of cell biology*. 34:229-249.

Aikawa, M., and H.B. Jordan. 1968. Fine structure of a reptilian malarial parasite. *The Journal of parasitology*. 54:1023-1033.

Aikawa, M.S., Charles R. 1974. Intracellular Parasititc Protozoa. Academic PRess Inc., New York.

Aley, S.B., J.A. Sherwood, K. Marsh, O. Eidelman, and R.J. Howard. 1986. Identification of isolate-specific proteins on sorbitol-enriched Plasmodium falciparum infected erythrocytes from Gambian patients. *Parasitology*. 92 (Pt 3):511-525.

Alkhalil, A., J.V. Cohn, M.A. Wagner, J.S. Cabrera, T. Rajapandi, and S.A. Desai. 2004. Plasmodium falciparum likely encodes the principal anion channel on infected human erythrocytes. *Blood*. 104:4279-4286.

Aly, A.S., A.M. Vaughan, and S.H. Kappe. 2009. Malaria parasite development in the mosquito and infection of the mammalian host. *Annual review of microbiology*. 63:195-221.

Andenmatten, N., S. Egarter, A.J. Jackson, N. Jullien, J.P. Herman, and M. Meissner. 2013. Conditional genome engineering in Toxoplasma gondii uncovers alternative invasion mechanisms. *Nature methods*. 10:125-127.

Andersen, K.M., K. Hofmann, and R. Hartmann-Petersen. 2005. Ubiquitin-binding proteins: similar, but different. *Essays in biochemistry*. 41:49-67.

Angrisano, F., M.J. Delves, A. Sturm, V. Mollard, G.I. McFadden, R.E. Sinden, and J. Baum. 2012. A GFP-actin reporter line to explore microfilament dynamics across the malaria parasite lifecycle. *Molecular and biochemical parasitology*. 182:93-96.

António M. Mendes, A.S., Ann-Kristin Mueller, Shahid M. Khan, Robert W. Sauerwein, and Miguel Prudêncio. 2017. Whole-Sporozoite Malaria Vaccines. *In* Malaria - Immune Response to Infection and Vaccination. A.R. Maria M. Mota, editor. Springer International Publishing, Cham, Switzerland. 99-138.

Antonny, B., C. Burd, P. De Camilli, E. Chen, O. Daumke, K. Faelber, M. Ford, V.A. Frolov, A. Frost, J.E. Hinshaw, T. Kirchhausen, M.M. Kozlov, M. Lenz, H.H. Low, H. McMahon, C. Merrifield, T.D. Pollard, P.J. Robinson, A. Roux, and S. Schmid. 2016. Membrane fission by dynamin: what we know and what we need to know. *The EMBO journal*. 35:2270-2284.

Ariey, F., B. Witkowski, C. Amaratunga, J. Beghain, A.C. Langlois, N. Khim, S. Kim, V. Duru, C. Bouchier, L. Ma, P. Lim, R. Leang, S. Duong, S. Sreng, S. Suon, C.M. Chuor, D.M. Bout, S. Menard, W.O. Rogers, B. Genton, T. Fandeur, O. Miotto, P. Ringwald, J. Le Bras, A. Berry, J.C. Barale, R.M. Fairhurst, F. Benoit-Vical, O. Mercereau-Puijalon, and D. Menard. 2014. A molecular marker of artemisinin-resistant Plasmodium falciparum malaria. *Nature*. 505:50-55.

Arighi, C.N., L.M. Hartnell, R.C. Aguilar, C.R. Haft, and J.S. Bonifacino. 2004. Role of the mammalian retromer in sorting of the cation-independent mannose 6-phosphate receptor. *The Journal of cell biology*. 165:123-133.

Ashley, E.A., and N.J. White. 2014. The duration of Plasmodium falciparum infections. *Malaria journal*. 13:500.

Atamna, H., and H. Ginsburg. 1993. Origin of reactive oxygen species in erythrocytes infected with Plasmodium falciparum. *Molecular and biochemical parasitology*. 61:231-241.

Ayong, L., G. Pagnotti, A.B. Tobon, and D. Chakrabarti. 2007. Identification of Plasmodium falciparum family of SNAREs. *Molecular and biochemical parasitology*. 152:113-122.

Bailly, E., R. Jambou, J. Savel, and G. Jaureguiberry. 1992. Plasmodium falciparum: differential sensitivity in vitro to E-64 (cysteine protease inhibitor) and Pepstatin A (aspartyl protease inhibitor). *The Journal of protozoology*. 39:593-599.

Balla, T. 2013. Phosphoinositides: tiny lipids with giant impact on cell regulation. *Physiological reviews*. 93:1019-1137.

Bankaitis, V.A., L.M. Johnson, and S.D. Emr. 1986. Isolation of yeast mutants defective in protein targeting to the vacuole. *Proceedings of the National Academy of Sciences of the United States of America*. 83:9075-9079.

Bannister, L.H., J.M. Hopkins, R.E. Fowler, S. Krishna, and G.H. Mitchell. 2000a. A brief illustrated guide to the ultrastructure of Plasmodium falciparum asexual blood stages. *Parasitology today (Personal ed.)*. 16:427-433.

Bannister, L.H., J.M. Hopkins, R.E. Fowler, S. Krishna, and G.H. Mitchell. 2000b. Ultrastructure of rhoptry development in Plasmodium falciparum erythrocytic schizonts. *Parasitology*. 121 (Pt 3):273-287.

Bannister, L.H., J.M. Hopkins, G. Margos, A.R. Dluzewski, and G.H. Mitchell. 2004. Three-dimensional ultrastructure of the ring stage of Plasmodium falciparum: evidence for export pathways. *Microscopy and microanalysis : the official journal of Microscopy Society of America, Microbeam Analysis Society, Microscopical Society of Canada*. 10:551-562.

Banta, L.M., J.S. Robinson, D.J. Klionsky, and S.D. Emr. 1988. Organelle assembly in yeast: characterization of yeast mutants defective in vacuolar biogenesis and protein sorting. *The Journal of cell biology*. 107:1369-1383.

Barois, N., and O. Bakke. 2005. The adaptor protein AP-4 as a component of the clathrin coat machinery: a morphological study. *The Biochemical journal*. 385:503-510.

Barouch, W., K. Prasad, L.E. Greene, and E. Eisenberg. 1994. ATPase activity associated with the uncoating of clathrin baskets by Hsp70. *The Journal of biological chemistry*. 269:28563-28568.

Bartoloni, A., and L. Zammarchi. 2012. Clinical aspects of uncomplicated and severe malaria. *Mediterranean journal of hematology and infectious diseases*. 4:e2012026.

Baum, J., Gilberger, T. W., Frischknecht, F., Meissner, M. 2008. Host-cell invasion by malaria parasites: insights from Plasmodium and Toxoplasma. *Trends in parasitology*. 24:557-563.

Baum, J., D. Richard, J. Healer, M. Rug, Z. Krnajski, T.W. Gilberger, J.L. Green, A.A. Holder, and A.F. Cowman. 2006. A conserved molecular motor drives cell invasion and gliding motility across malaria life cycle stages and other apicomplexan parasites. *The Journal of biological chemistry*. 281:5197-5208.

Baum, J., C.J. Tonkin, A.S. Paul, M. Rug, B.J. Smith, S.B. Gould, D. Richard, T.D. Pollard, and A.F. Cowman. 2008. A malaria parasite formin regulates actin polymerization and localizes to the parasite-erythrocyte moving junction during invasion. *Cell host & microbe*. 3:188-198.

Beaudoin R. L. , S.C.P.A. 1972. The Feeding Process in the Exoerythrocytic Stages of Plasmodium lophurae Based Upon Observations with the Electron Microscope. *In* BASIC RESEARCH IN MALARIA. Vol. 39. E.H. Sadun, editor. The Helminthological Society of Washington, Washington.

Beck, J.R., V. Muralidharan, A. Oksman, and D.E. Goldberg. 2014. PTEX component HSP101 mediates export of diverse malaria effectors into host erythrocytes. *Nature*. 511:592-595.

Bhatt, S., D.J. Weiss, E. Cameron, D. Bisanzio, B. Mappin, U. Dalrymple, K. Battle, C.L. Moyes, A. Henry, P.A. Eckhoff, E.A. Wenger, O. Briet, M.A. Penny, T.A. Smith, A. Bennett, J. Yukich, T.P. Eisele, J.T. Griffin, C.A. Fergus, M. Lynch, F. Lindgren, J.M. Cohen, C.L.J. Murray, D.L. Smith, S.I. Hay, R.E. Cibulskis, and P.W. Gething. 2015. The effect of malaria control on Plasmodium falciparum in Africa between 2000 and 2015. *Nature*. 526:207-211.

Bhattacharjee, S., I. Coppens, A. Mbengue, N. Suresh, M. Ghorbal, Z. Slouka, I. Safeukui, H.Y. Tang, D.W. Speicher, R.V. Stahelin, N. Mohandas, and K. Haldar. 2018. Remodeling of the malaria parasite and host human red cell by vesicle amplification that induces artemisinin resistance. *Blood*. 131:1234-1247.

Bhattacharjee, S., R.V. Stahelin, K.D. Speicher, D.W. Speicher, and K. Haldar. 2012. Endoplasmic reticulum PI(3)P lipid binding targets malaria proteins to the host cell. *Cell*. 148:201-212.

Birnbaum, J. 2017. A novel genetic system for the functional analysis of essential proteins of the human malaria parasite *Plasmodium falciparum*. University Hamburg, Hamburg.

Birnbaum, J., S. Flemming, N. Reichard, A.B. Soares, P. Mesen-Ramirez, E. Jonscher, B. Bergmann, and T. Spielmann. 2017. A genetic system to study Plasmodium falciparum protein function. *Nature methods*. 14:450-456.

Bissig, C., and J. Gruenberg. 2013. Lipid sorting and multivesicular endosome biogenesis. *Cold Spring Harbor perspectives in biology*. 5:a016816.

Bitsikas, V., I.R. Correa, Jr., and B.J. Nichols. 2014. Clathrin-independent pathways do not contribute significantly to endocytic flux. *eLife*. 3:e03970.

Blackburn, W.R., and K. Vinijchaikul. 1970. Experimental mammalian malaria. I. The asexual development of Plasmodium berghei trophozoites in inbred mice. *Laboratory investigation; a journal of technical methods and pathology*. 22:417-431.

Blackman, M.J., and V.B. Carruthers. 2013. Recent insights into apicomplexan parasite egress provide new views to a kill. *Current opinion in microbiology*. 16:459-464.

Boddey, J.A., M.T. O'Neill, S. Lopaticki, T.G. Carvalho, A.N. Hodder, T. Nebl, S. Wawra, P. van West, Z. Ebrahimzadeh, D. Richard, S. Flemming, T. Spielmann, J. Przyborski, J.J. Babon, and A.F. Cowman. 2016. Export of malaria proteins requires co-translational processing of the PEXEL motif independent of phosphatidylinositol-3-phosphate binding. *Nature communications*. 7:10470.

Boersema, P.J., R. Raijmakers, S. Lemeer, S. Mohammed, and A.J. Heck. 2009. Multiplex peptide stable isotope dimethyl labeling for quantitative proteomics. *Nature protocols*. 4:484-494.

Braell, W.A., D.M. Schlossman, S.L. Schmid, and J.E. Rothman. 1984. Dissociation of clathrin coats coupled to the hydrolysis of ATP: role of an uncoating ATPase. *The Journal of cell biology*. 99:734-741.

Bray, P.G., S.A. Ward, and P.M. O'Neill. 2005. Quinolines and artemisinin: chemistry, biology and history. *Current topics in microbiology and immunology*. 295:3-38.

Breinich, M.S., D.J. Ferguson, B.J. Foth, G.G. van Dooren, M. Lebrun, D.V. Quon, B. Striepen, P.J. Bradley, F. Frischknecht, V.B. Carruthers, and M. Meissner. 2009. A dynamin is required for the biogenesis of secretory organelles in Toxoplasma gondii. *Current biology : CB*. 19:277-286.

Brett, T.J., L.M. Traub, and D.H. Fremont. 2002. Accessory protein recruitment motifs in clathrin-mediated endocytosis. *Structure (London, England : 1993)*. 10:797-809.

Bruce, M.C., P. Alano, S. Duthie, and R. Carter. 1990. Commitment of the malaria parasite Plasmodium falciparum to sexual and asexual development. *Parasitology*. 100 Pt 2:191-200.

Bryant, N.J., R.C. Piper, S.R. Gerrard, and T.H. Stevens. 1998. Traffic into the prevacuolar/endosomal compartment of Saccharomyces cerevisiae: a VPS45-dependent intracellular route and a VPS45-independent, endocytic route. *Eur J Cell Biol*. 76:43-52.

Buffet, P.A., I. Safeukui, G. Deplaine, V. Brousse, V. Prendki, M. Thellier, G.D. Turner, and O. Mercereau-Puijalon. 2011. The pathogenesis of Plasmodium falciparum malaria in humans: insights from splenic physiology. *Blood*. 117:381-392.

Burghaus, P.A., and K. Lingelbach. 2001. Luciferase, when fused to an N-terminal signal peptide, is secreted from transfected Plasmodium falciparum and transported to the cytosol of infected erythrocytes. *The Journal of biological chemistry*. 276:26838-26845.

Butterworth, A.S., T.S. Skinner-Adams, D.L. Gardiner, and K.R. Trenholme. 2013. Plasmodium falciparum gametocytes: with a view to a kill. *Parasitology*. 140:1718-1734.

Canning, P., C.D. Cooper, T. Krojer, J.W. Murray, A.C. Pike, A. Chaikuad, T. Keates, C. Thangaratnarajah, V. Hojzan, V. Ayinampudi, B.D. Marsden, O. Gileadi, S. Knapp, F. von Delft, and A.N. Bullock. 2013. Structural basis for Cul3 protein assembly with the BTB-Kelch family of E3 ubiquitin ligases. *The Journal of biological chemistry*. 288:7803-7814.

Capanna, E. 2006. Grassi versus Ross: who solved the riddle of malaria? *International microbiology : the official journal of the Spanish Society for Microbiology*. 9:69-74.

Carlton, J., M. Bujny, B.J. Peter, V.M. Oorschot, A. Rutherford, H. Mellor, J. Klumperman, H.T. McMahon, and P.J. Cullen. 2004. Sorting nexin-1 mediates tubular endosome-to-TGN transport through coincidence sensing of high- curvature membranes and 3-phosphoinositides. *Current biology : CB*. 14:1791-1800.

Carney, D.S., B.A. Davies, and B.F. Horazdovsky. 2006. Vps9 domain-containing proteins: activators of Rab5 GTPases from yeast to neurons. *Trends in cell biology*. 16:27-35.

Carr, C.M., E. Grote, M. Munson, F.M. Hughson, and P.J. Novick. 1999. Sec1p binds to SNARE complexes and concentrates at sites of secretion. *The Journal of cell biology*. 146:333-344.

Carr, C.M., and J. Rizo. 2010. At the junction of SNARE and SM protein function. *Current opinion in cell biology*. 22:488-495.

Carruthers, V.B. 2015. Parasites and their heterophagic appetite for disease. *PLoS pathogens*. 11:e1004803.

Carter, R., and K.N. Mendis. 2002. Evolutionary and historical aspects of the burden of malaria. *Clinical microbiology reviews*. 15:564-594.

Chang, H.H., A.M. Falick, P.M. Carlton, J.W. Sedat, J.L. DeRisi, and M.A. Marletta. 2008. N-terminal processing of proteins exported by malaria parasites. *Molecular and biochemical parasitology*. 160:107-115.

Chen, H., S. Fre, V.I. Slepnev, M.R. Capua, K. Takei, M.H. Butler, P.P. Di Fiore, and P. De Camilli. 1998. Epsin is an EH-domain-binding protein implicated in clathrin-mediated endocytosis. *Nature*. 394:793-797.

Chen, Y.A., and R.H. Scheller. 2001. SNARE-mediated membrane fusion. *Nature reviews. Molecular cell biology*. 2:98-106.

Clayton, E.L., and M.A. Cousin. 2009. Quantitative monitoring of activity-dependent bulk endocytosis of synaptic vesicle membrane by fluorescent dextran imaging. *Journal of neuroscience methods*. 185:76-81.

Clyde, D.F., V.C. McCarthy, R.M. Miller, and R.B. Hornick. 1973. Specificity of protection of man immunized against sporozoite-induced falciparum malaria. *The American journal of the medical sciences*. 266:398-403.

Cocucci, E., F. Aguet, S. Boulant, and T. Kirchhausen. 2012. The first five seconds in the life of a clathrin-coated pit. *Cell*. 150:495-507.

Collins, C.R., S. Das, E.H. Wong, N. Andenmatten, R. Stallmach, F. Hackett, J.P. Herman, S. Muller, M. Meissner, and M.J. Blackman. 2013. Robust inducible Cre recombinase activity in the human malaria parasite Plasmodium falciparum enables efficient gene deletion within a single asexual erythrocytic growth cycle. *Molecular microbiology*. 88:687-701.

Collins, W.E., and G.M. Jeffery. 2005. Plasmodium ovale: parasite and disease. *Clinical microbiology reviews*. 18:570-581.

Commisso, C., S.M. Davidson, R.G. Soydaner-Azeloglu, S.J. Parker, J.J. Kamphorst, S. Hackett, E. Grabocka, M. Nofal, J.A. Drebin, C.B. Thompson, J.D. Rabinowitz, C.M. Metallo, M.G.

Vander Heiden, and D. Bar-Sagi. 2013. Macropinocytosis of protein is an amino acid supply route in Ras-transformed cells. *Nature*. 497:633-637.

Cooke, B.M., N. Mohandas, and R.L. Coppel. 2001. The malaria-infected red blood cell: structural and functional changes. *Advances in parasitology*. 50:1-86.

Coonrod, E.M., and T.H. Stevens. 2010. The yeast vps class E mutants: the beginning of the molecular genetic analysis of multivesicular body biogenesis. *Molecular biology of the cell*. 21:4057-4060.

Cowles, C.R., S.D. Emr, and B.F. Horazdovsky. 1994. Mutations in the VPS45 gene, a SEC1 homologue, result in vacuolar protein sorting defects and accumulation of membrane vesicles. *Journal of cell science*. 107 (Pt 12):3449-3459.

Cowman, A.F., and B.S. Crabb. 2006. Invasion of red blood cells by malaria parasites. *Cell*. 124:755-766.

Cox, F.E. 2010. History of the discovery of the malaria parasites and their vectors. *Parasites & vectors*. 3:5.

Cox, F.E., and K. Vickerman. 1966. Pinocytosis in Plasmodium vinckei. *Annals of tropical medicine and parasitology*. 60:293-296.

Dacks, J.B., and W.F. Doolittle. 2004. Molecular and phylogenetic characterization of syntaxin genes from parasitic protozoa. *Molecular and biochemical parasitology*. 136:123-136.

Daher, W., F. Plattner, M.F. Carlier, and D. Soldati-Favre. 2010. Concerted action of two formins in gliding motility and host cell invasion by Toxoplasma gondii. *PLoS pathogens*. 6:e1001132.

Das, S., L. Lemgruber, C.L. Tay, J. Baum, and M. Meissner. 2017. Multiple essential functions of Plasmodium falciparum actin-1 during malaria blood-stage development. *BMC biology*. 15:70.

Daumke, O., A. Roux, and V. Haucke. 2014. BAR domain scaffolds in dynamin-mediated membrane fission. *Cell*. 156:882-892.

de Carvalho, T.M., E.S. Barrias, and W. de Souza. 2015. Macropinocytosis: a pathway to protozoan infection. *Frontiers in physiology*. 6:106.

de Koning-Ward, T.F., P.R. Gilson, J.A. Boddey, M. Rug, B.J. Smith, A.T. Papenfuss, P.R. Sanders, R.J. Lundie, A.G. Maier, A.F. Cowman, and B.S. Crabb. 2009. A newly discovered protein export machine in malaria parasites. *Nature*. 459:945-949.

De Niz, M., P.C. Burda, G. Kaiser, H.A. Del Portillo, T. Spielmann, F. Frischknecht, and V.T. Heussler. 2017. Progress in imaging methods: insights gained into Plasmodium biology. *Nature reviews. Microbiology*. 15:37-54.

De Niz, M., E. Meibalan, P. Mejia, S. Ma, N.M.B. Brancucci, C. Agop-Nersesian, R. Mandt, P. Ngotho, K.R. Hughes, A.P. Waters, C. Huttenhower, J.R. Mitchell, R. Martinelli, F. Frischknecht, K.B. Seydel, T. Taylor, D. Milner, V.T. Heussler, and M. Marti. 2018. Plasmodium gametocytes display homing and vascular transmigration in the host bone marrow. *Science advances*. 4:eaat3775.

de Souza, W., C. Sant'Anna, and N.L. Cunha-e-Silva. 2009. Electron microscopy and cytochemistry analysis of the endocytic pathway of pathogenic protozoa. *Progress in histochemistry and cytochemistry*. 44:67-124.

Dell'Angelica, E.C., J. Klumperman, W. Stoorvogel, and J.S. Bonifacino. 1998. Association of the AP-3 adaptor complex with clathrin. *Science (New York, N.Y.)*. 280:431-434.

Deponte, M., H.C. Hoppe, M.C. Lee, A.G. Maier, D. Richard, M. Rug, T. Spielmann, and J.M. Przyborski. 2012. Wherever I may roam: protein and membrane trafficking in P. falciparum-infected red blood cells. *Molecular and biochemical parasitology*. 186:95-116.

Desai, S.A. 2012. Ion and nutrient uptake by malaria parasite-infected erythrocytes. *Cellular microbiology*. 14:1003-1009.

Di Paolo, G., and P. De Camilli. 2006. Phosphoinositides in cell regulation and membrane dynamics. *Nature*. 443:651-657.

Dogovski, C., S.C. Xie, G. Burgio, J. Bridgford, S. Mok, J.M. McCaw, K. Chotivanich, S. Kenny, N. Gnadig, J. Straimer, Z. Bozdech, D.A. Fidock, J.A. Simpson, A.M. Dondorp, S. Foote, N. Klonis, and L. Tilley. 2015. Targeting the cell stress response of Plasmodium falciparum to overcome artemisinin resistance. *PLoS biology*. 13:e1002132.

Doherty, G.J., and H.T. McMahon. 2009. Mechanisms of endocytosis. *Annual review of biochemistry*. 78:857-902.

Dou, Z., O.L. McGovern, M. Di Cristina, and V.B. Carruthers. 2014. Toxoplasma gondii ingests and digests host cytosolic proteins. *mBio*. 5:e01188-01114.

Doumbo, O.K., M.A. Thera, A.K. Kone, A. Raza, L.J. Tempest, K.E. Lyke, C.V. Plowe, and J.A. Rowe. 2009. High levels of Plasmodium falciparum rosetting in all clinical forms of severe malaria in African children. *The American journal of tropical medicine and hygiene*. 81:987-993.

Dower, W.J., J.F. Miller, and C.W. Ragsdale. 1988. High efficiency transformation of E. coli by high voltage electroporation. *Nucleic acids research*. 16:6127-6145.

Eaton, S., and F. Martin-Belmonte. 2014. Cargo sorting in the endocytic pathway: a key regulator of cell polarity and tissue dynamics. *Cold Spring Harbor perspectives in biology*. 6:a016899.

Ebrahimzadeh, Z., A. Mukherjee, and D. Richard. 2018. A map of the subcellular distribution of phosphoinositides in the erythrocytic cycle of the malaria parasite Plasmodium falciparum. *International journal for parasitology*. 48:13-25.

Eckhoff, P.A., E.A. Wenger, H.C. Godfray, and A. Burt. 2017. Impact of mosquito gene drive on malaria elimination in a computational model with explicit spatial and temporal dynamics. *Proceedings of the National Academy of Sciences of the United States of America*. 114:E255-e264.

Egan, T.J. 2008. Haemozoin formation. *Molecular and biochemical parasitology*. 157:127-136.

Ehlgen, F., J.S. Pham, T. de Koning-Ward, A.F. Cowman, and S.A. Ralph. 2012. Investigation of the Plasmodium falciparum food vacuole through inducible expression of the chloroquine resistance transporter (PfCRT). *PloS one*. 7:e38781.

Ehrlich, M., W. Boll, A. Van Oijen, R. Hariharan, K. Chandran, M.L. Nibert, and T. Kirchhausen. 2004. Endocytosis by random initiation and stabilization of clathrin-coated pits. *Cell*. 118:591-605.

Elliott, D.A., M.T. McIntosh, H.D. Hosgood, 3rd, S. Chen, G. Zhang, P. Baevova, and K.A. Joiner. 2008. Four distinct pathways of hemoglobin uptake in the malaria parasite Plasmodium falciparum. *Proceedings of the National Academy of Sciences of the United States of America*. 105:2463-2468.

Elsworth, B., K. Matthews, C.Q. Nie, M. Kalanon, S.C. Charnaud, P.R. Sanders, S.A. Chisholm, N.A. Counihan, P.J. Shaw, P. Pino, J.A. Chan, M.F. Azevedo, S.J. Rogerson, J.G. Beeson, B.S. Crabb, P.R. Gilson, and T.F. de Koning-Ward. 2014. PTEX is an essential nexus for protein export in malaria parasites. *Nature*. 511:587-591.

Enayati, A., and J. Hemingway. 2010. Malaria management: past, present, and future. *Annual review of entomology*. 55:569-591.

endmalariacouncil.org. 2018. End Malaria Council.

Escalante, A.A., and F.J. Ayala. 1995. Evolutionary origin of Plasmodium and other Apicomplexa based on rRNA genes. *Proceedings of the National Academy of Sciences of the United States of America*. 92:5793-5797.

Ezougou, C.N., F. Ben-Rached, D.K. Moss, J.W. Lin, S. Black, E. Knuepfer, J.L. Green, S.M. Khan, A. Mukhopadhyay, C.J. Janse, I. Coppens, H. Yera, A.A. Holder, and G. Langsley. 2014. Plasmodium falciparum Rab5B is an N-terminally myristoylated Rab GTPase that is targeted to the parasite's plasma and food vacuole membranes. *PloS one*. 9:e87695.

Fallon, L., C.M. Belanger, A.T. Corera, M. Kontogiannea, E. Regan-Klapisz, F. Moreau, J. Voortman, M. Haber, G. Rouleau, T. Thorarinsdottir, A. Brice, P.M. van Bergen En Henegouwen, and E.A. Fon. 2006. A regulated interaction with the UIM protein Eps15 implicates parkin in EGF receptor trafficking and PI(3)K-Akt signalling. *Nature cell biology*. 8:834-842.

Farfour, E., F. Charlotte, C. Settegrana, M. Miyara, and P. Buffet. 2012. The extravascular compartment of the bone marrow: a niche for Plasmodium falciparum gametocyte maturation? *Malaria journal*. 11:285.

Fasshauer, D., R.B. Sutton, A.T. Brunger, and R. Jahn. 1998. Conserved structural features of the synaptic fusion complex: SNARE proteins reclassified as Q- and R-SNAREs. *Proceedings of the National Academy of Sciences of the United States of America*. 95:15781-15786.

Ferguson, D.J., A. Birch-Andersen, W.M. Hutchison, and J.C. Simm. 1977. The ultrastructure and distribution of micropores in the various developmental forms of Eimeria brunetti. *Acta pathologica et microbiologica Scandinavica. Section B, Microbiology*. 85b:363-373.

Fidock, D.A., T. Nomura, A.K. Talley, R.A. Cooper, S.M. Dzekunov, M.T. Ferdig, L.M. Ursos, A.B. Sidhu, B. Naude, K.W. Deitsch, X.Z. Su, J.C. Wootton, P.D. Roepe, and T.E. Wellems. 2000. Mutations in the P. falciparum digestive vacuole transmembrane protein PfCRT and evidence for their role in chloroquine resistance. *Molecular cell*. 6:861-871.

Fidock, D.A., and T.E. Wellems. 1997. Transformation with human dihydrofolate reductase renders malaria parasites insensitive to WR99210 but does not affect the intrinsic activity of proguanil. *Proceedings of the National Academy of Sciences of the United States of America*. 94:10931-10936.

Field, M.C., and M. Carrington. 2009. The trypanosome flagellar pocket. *Nature reviews. Microbiology*. 7:775-786.

Flemming, S. 2015. Visualization and characterization of endocytic processes in the human Malaria parasite P. falciparum (Welch, 1897). University Hamburg, Hamburg.

Fletcher, A., and B. Maegraith. 1972. The metabolism of the malaria parasite and its host. *Advances in parasitology*. 10:31-48.

Foley, M., and L. Tilley. 1998. Quinoline antimalarials: mechanisms of action and resistance and prospects for new agents. *Pharmacology & therapeutics*. 79:55-87.

Ford, M.G., I.G. Mills, B.J. Peter, Y. Vallis, G.J. Praefcke, P.R. Evans, and H.T. McMahon. 2002. Curvature of clathrin-coated pits driven by epsin. *Nature*. 419:361-366.

Foth, B.J., M.C. Goedecke, and D. Soldati. 2006. New insights into myosin evolution and classification. *Proceedings of the National Academy of Sciences of the United States of America*. 103:3681-3686.

Francia, M.E., and B. Striepen. 2014. Cell division in apicomplexan parasites. *Nature reviews. Microbiology*. 12:125-136.

Frankland, S., A. Adisa, P. Horrocks, T.F. Taraschi, T. Schneider, S.R. Elliott, S.J. Rogerson, E. Knuepfer, A.F. Cowman, C.I. Newbold, and L. Tilley. 2006. Delivery of the malaria virulence protein PfEMP1 to the erythrocyte surface requires cholesterol-rich domains. *Eukaryotic cell*. 5:849-860.

Gaccioli, F., and S. Lager. 2016. Placental Nutrient Transport and Intrauterine Growth Restriction. *Frontiers in physiology*. 7:40.

Gallon, M., and P.J. Cullen. 2015. Retromer and sorting nexins in endosomal sorting. *Biochemical Society transactions*. 43:33-47.

Gantz, V.M., N. Jasinskiene, O. Tatarenkova, A. Fazekas, V.M. Macias, E. Bier, and A.A. James. 2015. Highly efficient Cas9-mediated gene drive for population modification of the malaria vector mosquito Anopheles stephensi. *Proceedings of the National Academy of Sciences of the United States of America*. 112:E6736-6743.

Garcia, P., R. Gupta, S. Shah, A.J. Morris, S.A. Rudge, S. Scarlata, V. Petrova, S. McLaughlin, and M.J. Rebecchi. 1995. The pleckstrin homology domain of phospholipase C-delta 1 binds with high affinity to phosphatidylinositol 4,5-bisphosphate in bilayer membranes. *Biochemistry*. 34:16228-16234.

Garnham, P.C., R.G. Bird, J.R. Baker, and R.S. Bray. 1961. Electron microsope studies of motile stages of malaria parasites. II. The fine structure of the sporozoite of Laverania (Plasmodium) falcipara. *Transactions of the Royal Society of Tropical Medicine and Hygiene*. 55:98-102.

Garoff, H., and W. Ansorge. 1981. Improvements of DNA sequencing gels. *Analytical biochemistry*. 115:450-457.

Gengyo-Ando, K., H. Kuroyanagi, T. Kobayashi, M. Murate, K. Fujimoto, S. Okabe, and S. Mitani. 2007. The SM protein VPS-45 is required for RAB-5-dependent endocytic transport in Caenorhabditis elegans. *EMBO Rep*. 8:152-157.

Genschik, P., I. Sumara, and E. Lechner. 2013. The emerging family of Cullin3-RING ubiquitin ligases (CRL3s): cellular functions and disease implications. *The EMBO journal*. 32:2307-2320.

Gerst, J.E. 2003. SNARE regulators: matchmakers and matchbreakers. *Biochimica et Biophysica Acta (BBA) - Molecular Cell Research*. 1641:99-110.

Gibson, D.G., L. Young, R.Y. Chuang, J.C. Venter, C.A. Hutchison, 3rd, and H.O. Smith. 2009. Enzymatic assembly of DNA molecules up to several hundred kilobases. *Nature methods*. 6:343-345.

Ginsburg, H., and M. Krugliak. 1999. Chloroquine - some open questions on its antimalarial mode of action and resistance. *Drug resistance updates : reviews and commentaries in antimicrobial and anticancer chemotherapy*. 2:180-187.

Gluzman, I.Y., S.E. Francis, A. Oksman, C.E. Smith, K.L. Duffin, and D.E. Goldberg. 1994. Order and specificity of the Plasmodium falciparum hemoglobin degradation pathway. *The Journal of clinical investigation*. 93:1602-1608.

Golani, Y., Y. Kaye, O. Gilhar, M. Ercetin, G. Gillaspy, and A. Levine. 2013. Inositol polyphosphate phosphatidylinositol 5-phosphatase9 (At5ptase9) controls plant salt tolerance by regulating endocytosis. *Molecular plant*. 6:1781-1794.

Goldberg, D.E., and A.F. Slater. 1992. The pathway of hemoglobin degradation in malaria parasites. *Parasitology today (Personal ed.)*. 8:280-283.

Golding, N., R. Burstein, J. Longbottom, A.J. Browne, N. Fullman, A. Osgood-Zimmerman, L. Earl, S. Bhatt, E. Cameron, D.C. Casey, L. Dwyer-Lindgren, T.H. Farag, A.D. Flaxman, M.S. Fraser, P.W. Gething, H.S. Gibson, N. Graetz, L.K. Krause, X.R. Kulikoff, S.S. Lim, B. Mappin, C. Morozoff, R.C. Reiner, Jr., A. Sligar, D.L. Smith, H. Wang, D.J. Weiss, C.J.L. Murray, C.L. Moyes, and S.I. Hay. 2017. Mapping under-5 and neonatal mortality in Africa, 2000-15: a baseline analysis for the Sustainable Development Goals. *Lancet*. 390:2171-2182.

Golgi, C. 1885. Sull'infezione malarica. *Accademiadi medicina Di Torino*.

Goodman, C.D., J.E. Siregar, V. Mollard, J. Vega-Rodriguez, D. Syafruddin, H. Matsuoka, M. Matsuzaki, T. Toyama, A. Sturm, A. Cozijnsen, M. Jacobs-Lorena, K. Kita, S. Marzuki, and G.I. McFadden. 2016. Parasites resistant to the antimalarial atovaquone fail to transmit by mosquitoes. *Science (New York, N.Y.)*. 352:349-353.

Grassi, G.B. 1901. Studi di uno zoologo sulla malaria. R. Accademia dei lincei, Rome.

Greenwood, B.M., D.A. Fidock, D.E. Kyle, S.H. Kappe, P.L. Alonso, F.H. Collins, and P.E. Duffy. 2008. Malaria: progress, perils, and prospects for eradication. *The Journal of clinical investigation*. 118:1266-1276.

Gregson, A., and C.V. Plowe. 2005. Mechanisms of resistance of malaria parasites to antifolates. *Pharmacological reviews*. 57:117-145.

Gruring, C., A. Heiber, F. Kruse, S. Flemming, G. Franci, S.F. Colombo, E. Fasana, H. Schoeler, N. Borgese, H.G. Stunnenberg, J.M. Przyborski, T.W. Gilberger, and T. Spielmann. 2012. Uncovering common principles in protein export of malaria parasites. *Cell host & microbe*. 12:717-729.

Gruring, C., A. Heiber, F. Kruse, J. Ungefehr, T.W. Gilberger, and T. Spielmann. 2011. Development and host cell modifications of Plasmodium falciparum blood stages in four dimensions. *Nature communications*. 2:165.

Gruring, C., and T. Spielmann. 2012. Imaging of live malaria blood stage parasites. *Methods in enzymology*. 506:81-92.

Guo, Z., X. Hou, R.S. Goody, and A. Itzen. 2013. Intermediates in the guanine nucleotide exchange reaction of Rab8 protein catalyzed by guanine nucleotide exchange factors Rabin8 and GRAB. *The Journal of biological chemistry*. 288:32466-32474.

Halachmi, N., and Z. Lev. 1996. The Sec1 family: a novel family of proteins involved in synaptic transmission and general secretion. *J Neurochem*. 66:889-897.

Hallee, S., N.A. Counihan, K. Matthews, T.F. de Koning-Ward, and D. Richard. 2018. The malaria parasite Plasmodium falciparum Sortilin is essential for merozoite formation and apical complex biogenesis. *Cellular microbiology*:e12844.

Hammond, A., R. Galizi, K. Kyrou, A. Simoni, C. Siniscalchi, D. Katsanos, M. Gribble, D. Baker, E. Marois, S. Russell, A. Burt, N. Windbichler, A. Crisanti, and T. Nolan. 2016. A CRISPR-Cas9 gene drive system targeting female reproduction in the malaria mosquito vector Anopheles gambiae. *Nature biotechnology*. 34:78-83.

Han, J., K. Pluhackova, and R.A. Bockmann. 2017. The Multifaceted Role of SNARE Proteins in Membrane Fusion. *Frontiers in physiology*. 8:5.

Hanahan, D. 1983. Studies on transformation of Escherichia coli with plasmids. *Journal of molecular biology*. 166:557-580.

Hanson, P.I., R. Roth, H. Morisaki, R. Jahn, and J.E. Heuser. 1997. Structure and conformational changes in NSF and its membrane receptor complexes visualized by quick-freeze/deep-etch electron microscopy. *Cell*. 90:523-535.

Hanssen, E., C. Knoechel, N. Klonis, N. Abu-Bakar, S. Deed, M. LeGros, C. Larabell, and L. Tilley. 2011. Cryo transmission X-ray imaging of the malaria parasite, P. falciparum. *Journal of structural biology*. 173:161-168.

Haruki, H., J. Nishikawa, and U.K. Laemmli. 2008. The anchor-away technique: rapid, conditional establishment of yeast mutant phenotypes. *Molecular cell*. 31:925-932.

Harvey, K.L., P.R. Gilson, and B.S. Crabb. 2012. A model for the progression of receptor-ligand interactions during erythrocyte invasion by Plasmodium falciparum. *International journal for parasitology*. 42:567-573.

Haucke, V. 2005. Phosphoinositide regulation of clathrin-mediated endocytosis. *Biochemical Society transactions*. 33:1285-1289.

He, K., R. Marsland, III, S. Upadhyayula, E. Song, S. Dang, B.R. Capraro, W. Wang, W. Skillern, R. Gaudin, M. Ma, and T. Kirchhausen. 2017. Dynamics of phosphoinositide conversion in clathrin-mediated endocytic traffic. *Nature*. 552:410-414.

Heiber, A., F. Kruse, C. Pick, C. Gruring, S. Flemming, A. Oberli, H. Schoeler, S. Retzlaff, P. Mesen-Ramirez, J.A. Hiss, M. Kadekoppala, L. Hecht, A.A. Holder, T.W. Gilberger, and T. Spielmann. 2013. Identification of new PNEPs indicates a substantial non-PEXEL exportome and underpins common features in Plasmodium falciparum protein export. *PLoS pathogens*. 9:e1003546.

Heiny, S.R., S. Pautz, M. Recker, and J.M. Przyborski. 2014. Protein Traffic to the Plasmodium falciparum apicoplast: evidence for a sorting branch point at the Golgi. *Traffic (Copenhagen, Denmark)*. 15:1290-1304.

Henriques, G., R.L. Hallett, K.B. Beshir, N.B. Gadalla, R.E. Johnson, R. Burrow, D.A. van Schalkwyk, P. Sawa, S.A. Omar, T.G. Clark, T. Bousema, and C.J. Sutherland. 2014. Directional selection at the pfmdr1, pfcrt, pfubp1, and pfap2mu loci of Plasmodium falciparum in Kenyan children treated with ACT. *The Journal of infectious diseases*. 210:2001-2008.

Henriques, G., A. Martinelli, L. Rodrigues, K. Modrzynska, R. Fawcett, D.R. Houston, S.T. Borges, U. d'Alessandro, H. Tinto, C. Karema, P. Hunt, and P. Cravo. 2013. Artemisinin resistance in rodent malaria--mutation in the AP2 adaptor mu-chain suggests involvement of endocytosis and membrane protein trafficking. *Malaria journal*. 12:118.

Henriques, G., D.A. van Schalkwyk, R. Burrow, D.C. Warhurst, E. Thompson, D.A. Baker, D.A. Fidock, R. Hallett, C. Flueck, and C.J. Sutherland. 2015. The mu-subunit of Plasmodium falciparum clathrin-associated adaptor protein 2 modulates in vitro parasite response to artemisinin and quinine. *Antimicrobial agents and chemotherapy*.

Hirst, J., N.A. Bright, B. Rous, and M.S. Robinson. 1999. Characterization of a fourth adaptor-related protein complex. *Molecular biology of the cell*. 10:2787-2802.

Hirst, J., C. Irving, and G.H. Borner. 2013. Adaptor protein complexes AP-4 and AP-5: new players in endosomal trafficking and progressive spastic paraplegia. *Traffic (Copenhagen, Denmark)*. 14:153-164.

Hollingdale, M.R., and M. Sedegah. 2017. Development of whole sporozoite malaria vaccines. *Expert review of vaccines*. 16:45-54.

Huckaba, T.M., A.C. Gay, L.F. Pantalena, H.C. Yang, and L.A. Pon. 2004. Live cell imaging of the assembly, disassembly, and actin cable-dependent movement of endosomes and actin patches in the budding yeast, Saccharomyces cerevisiae. *The Journal of cell biology*. 167:519-530.

Hulden, L. 2011. The first Finnish malariologist, Johan Haartman, and the discussion about malaria in 18th century Turku, Finland. *Malaria journal*. 10:43.

Hunt, N.H., J. Golenser, T. Chan-Ling, S. Parekh, C. Rae, S. Potter, I.M. Medana, J. Miu, and H.J. Ball. 2006. Immunopathogenesis of cerebral malaria. *International journal for parasitology*. 36:569-582.

Iqbal, M.S., A.A. Siddiqui, A. Alam, M. Goyal, C. Banerjee, S. Sarkar, S. Mazumder, R. De, S. Nag, S.J. Saha, and U. Bandyopadhyay. 2016. Expression, purification and characterization of Plasmodium falciparum vacuolar protein sorting 29. *Protein expression and purification*. 120:7-15.

Iqbal, M.S., A.A. Siddiqui, C. Banerjee, S. Nag, S. Mazumder, R. De, S.J. Saha, S.K. Karri, and U. Bandyopadhyay. 2018. Detection of retromer assembly in Plasmodium falciparum by

immunosensing coupled to Surface Plasmon Resonance. *Biochimica et biophysica acta*. 1866:722-730.

Itoh, T., and T. Takenawa. 2009. Mechanisms of membrane deformation by lipid-binding domains. *Progress in lipid research*. 48:298-305.

Jahn, R.L., Thorsten; Südhof, Thomas C. 2003. Membrane Fusion. *Cell*. 112:519-533.

Jimenez-Ruiz, E., J. Morlon-Guyot, W. Daher, and M. Meissner. 2016. Vacuolar protein sorting mechanisms in apicomplexan parasites. *Molecular and biochemical parasitology*. 209:18-25.

Johnson, D.J., D.A. Fidock, M. Mungthin, V. Lakshmanan, A.B. Sidhu, P.G. Bray, and S.A. Ward. 2004. Evidence for a central role for PfCRT in conferring Plasmodium falciparum resistance to diverse antimalarial agents. *Molecular cell*. 15:867-877.

Jones, M.L., C.L. Tay, and J.C. Rayner. 2012. Getting stuck in: protein palmitoylation in Plasmodium. *Trends in parasitology*. 28:496-503.

Jones, S.A., S.H. Shim, J. He, and X. Zhuang. 2011. Fast, three-dimensional super-resolution imaging of live cells. *Nature methods*. 8:499-508.

Josling, G.A., and M. Llinas. 2015. Sexual development in Plasmodium parasites: knowing when it's time to commit. *Nature reviews. Microbiology*. 13:573-587.

Jovic, M., M. Sharma, J. Rahajeng, and S. Caplan. 2010. The early endosome: a busy sorting station for proteins at the crossroads. *Histology and histopathology*. 25:99-112.

Jullien, N., I. Goddard, S. Selmi-Ruby, J.L. Fina, H. Cremer, and J.P. Herman. 2007. Conditional transgenesis using Dimerizable Cre (DiCre). *PloS one*. 2:e1355.

Kadlecova, Z., S.J. Spielman, D. Loerke, A. Mohanakrishnan, D.K. Reed, and S.L. Schmid. 2017. Regulation of clathrin-mediated endocytosis by hierarchical allosteric activation of AP2. *The Journal of cell biology*. 216:167-179.

Kai, O.K., and D.J. Roberts. 2008. The pathophysiology of malarial anaemia: where have all the red cells gone? *BMC medicine*. 6:24.

Kaksonen, M., and A. Roux. 2018. Mechanisms of clathrin-mediated endocytosis. *Nature reviews. Molecular cell biology*. 19:313-326.

Kampondeni, S.D., M.J. Potchen, N.A. Beare, K.B. Seydel, S.J. Glover, T.E. Taylor, and G.L. Birbeck. 2013. MRI findings in a cohort of brain injured survivors of pediatric cerebral malaria. *The American journal of tropical medicine and hygiene*. 88:542-546.

Kanai, F., H. Liu, S.J. Field, H. Akbary, T. Matsuo, G.E. Brown, L.C. Cantley, and M.B. Yaffe. 2001. The PX domains of p47phox and p40phox bind to lipid products of PI(3)K. *Nature cell biology*. 3:675-678.

Kapitein, L.C., and C.C. Hoogenraad. 2011. Which way to go? Cytoskeletal organization and polarized transport in neurons. *Molecular and cellular neurosciences*. 46:9-20.

Keeling, P.J. 2008. Evolutionary biology: bridge over troublesome plastids. *Nature*. 451:896-897.

Kelly, B.T., S.C. Graham, N. Liska, P.N. Dannhauser, S. Honing, E.J. Ungewickell, and D.J. Owen. 2014. Clathrin adaptors. AP2 controls clathrin polymerization with a membrane-activated switch. *Science (New York, N.Y.)*. 345:459-463.

Killby, V.A., and P.H. Silverman. 1969. Fine structural observations of the erythrocytic stages of Plasmodium chabaudi Landau, 1965. *The Journal of protozoology*. 16:354-370.

Kirchhausen, T. 2009. Imaging endocytic clathrin structures in living cells. *Trends in cell biology*. 19:596-605.

Kitamoto, K., K. Yoshizawa, Y. Ohsumi, and Y. Anraku. 1988. Mutants of Saccharomyces cerevisiae with defective vacuolar function. *Journal of bacteriology*. 170:2687-2691.

Klayman, D.L., A.J. Lin, N. Acton, J.P. Scovill, J.M. Hoch, W.K. Milhous, A.D. Theoharides, and A.S. Dobek. 1984. Isolation of artemisinin (qinghaosu) from Artemisia annua growing in the United States. *Journal of natural products*. 47:715-717.

Klemba, M., W. Beatty, I. Gluzman, and D.E. Goldberg. 2004. Trafficking of plasmepsin II to the food vacuole of the malaria parasite Plasmodium falciparum. *The Journal of cell biology*. 164:47-56.

Klonis, N., D.J. Creek, and L. Tilley. 2013. Iron and heme metabolism in Plasmodium falciparum and the mechanism of action of artemisinins. *Current opinion in microbiology*. 16:722-727.

Klonis, N., M.P. Crespo-Ortiz, I. Bottova, N. Abu-Bakar, S. Kenny, P.J. Rosenthal, and L. Tilley. 2011. Artemisinin activity against Plasmodium falciparum requires hemoglobin uptake and

digestion. *Proceedings of the National Academy of Sciences of the United States of America*. 108:11405-11410.

Knuepfer, E., M. Napiorkowska, C. van Ooij, and A.A. Holder. 2017. Generating conditional gene knockouts in Plasmodium - a toolkit to produce stable DiCre recombinase-expressing parasite lines using CRISPR/Cas9. *Scientific reports*. 7:3881.

Kono, M., S. Herrmann, N.B. Loughran, A. Cabrera, K. Engelberg, C. Lehmann, D. Sinha, B. Prinz, U. Ruch, V. Heussler, T. Spielmann, J. Parkinson, and T.W. Gilberger. 2012. Evolution and architecture of the inner membrane complex in asexual and sexual stages of the malaria parasite. *Molecular biology and evolution*. 29:2113-2132.

Koumandou, V.L., J.B. Dacks, R.M. Coulson, and M.C. Field. 2007. Control systems for membrane fusion in the ancestral eukaryote; evolution of tethering complexes and SM proteins. *BMC evolutionary biology*. 7:29.

Krai, P., S. Dalal, and M. Klemba. 2014. Evidence for a Golgi-to-endosome protein sorting pathway in Plasmodium falciparum. *PloS one*. 9:e89771.

Kremer, K., D. Kamin, E. Rittweger, J. Wilkes, H. Flammer, S. Mahler, J. Heng, C.J. Tonkin, G. Langsley, S.W. Hell, V.B. Carruthers, D.J. Ferguson, and M. Meissner. 2013. An overexpression screen of Toxoplasma gondii Rab-GTPases reveals distinct transport routes to the micronemes. *PLoS pathogens*. 9:e1003213.

Krotoski, W.A., W.E. Collins, R.S. Bray, P.C. Garnham, F.B. Cogswell, R.W. Gwadz, R. Killick-Kendrick, R. Wolf, R. Sinden, L.C. Koontz, and P.S. Stanfill. 1982. Demonstration of hypnozoites in sporozoite-transmitted Plasmodium vivax infection. *The American journal of tropical medicine and hygiene*. 31:1291-1293.

Krugliak, M., J. Zhang, and H. Ginsburg. 2002. Intraerythrocytic Plasmodium falciparum utilizes only a fraction of the amino acids derived from the digestion of host cell cytosol for the biosynthesis of its proteins. *Molecular and biochemical parasitology*. 119:249-256.

Kruse, F. 2014. Charakterisierung einer Phosphatidylinositol-4,5-bisphosphat-angereicherten Struktur der Plasmamembran des humanen Malaria Erregers Plasmodium falciparum (Welch, 1897). Vol. PhD. University Hamburg, Hamburg.

Kural, C., S.K. Tacheva-Grigorova, S. Boulant, E. Cocucci, T. Baust, D. Duarte, and T. Kirchhausen. 2012. Dynamics of intracellular clathrin/AP1- and clathrin/AP3-containing carriers. *Cell reports*. 2:1111-1119.

Kyhse-Andersen, J. 1984. Electroblotting of multiple gels: a simple apparatus without buffer tank for rapid transfer of proteins from polyacrylamide to nitrocellulose. *Journal of biochemical and biophysical methods*. 10:203-209.

Laemmli, U.K. 1970. Cleavage of structural proteins during the assembly of the head of bacteriophage T4. *Nature*. 227:680-685.

Lakadamyali, M., M.J. Rust, and X. Zhuang. 2006. Ligands for clathrin-mediated endocytosis are differentially sorted into distinct populations of early endosomes. *Cell*. 124:997-1009.

Lambros, C., and J.P. Vanderberg. 1979. Synchronization of Plasmodium falciparum erythrocytic stages in culture. *The Journal of parasitology*. 65:418-420.

Langreth, S.G., J.B. Jensen, R.T. Reese, and W. Trager. 1978. Fine structure of human malaria in vitro. *The Journal of protozoology*. 25:443-452.

Laveran, A. 1880. Nature parasitaire des accidents de l'impaludisme : description d'un nouveau parasite trouvé dans le sang des malades atteints de fièvre palustre. J.-B. Baillière, Paris.

Lazarus, M.D., T.G. Schneider, and T.F. Taraschi. 2008. A new model for hemoglobin ingestion and transport by the human malaria parasite Plasmodium falciparum. *Journal of cell science*. 121:1937-1949.

Lee, M.C., P.A. Moura, E.A. Miller, and D.A. Fidock. 2008. Plasmodium falciparum Sec24 marks transitional ER that exports a model cargo via a diacidic motif. *Molecular microbiology*. 68:1535-1546.

Levine, N.D. 1971. Uniform Terminology for the Protozoan Subphylum Apicomplexa. *The Journal of protozoology*. 18:352-355.

Leznicki, P., and Y. Kulathu. 2017. Mechanisms of regulation and diversification of deubiquitylating enzyme function. *Journal of cell science*. 130:1997-2006.

Little, A. 2014. The Caribbean colony that brought down Scotland. BBC News, Darien, Panama.

Liu, J., E.S. Istvan, I.Y. Gluzman, J. Gross, and D.E. Goldberg. 2006. Plasmodium falciparum ensures its amino acid supply with multiple acquisition pathways and redundant proteolytic enzyme systems. *Proceedings of the National Academy of Sciences of the United States of America*. 103:8840-8845.

Loerke, D., M. Mettlen, D. Yarar, K. Jaqaman, H. Jaqaman, G. Danuser, and S.L. Schmid. 2009. Cargo and dynamin regulate clathrin-coated pit maturation. *PLoS biology*. 7:e57.

Lu, R., and D.G. Drubin. 2017. Selection and stabilization of endocytic sites by Ede1, a yeast functional homologue of human Eps15. *Molecular biology of the cell*. 28:567-575.

Lyke, K.E., A.S. Ishizuka, A.A. Berry, S. Chakravarty, A. DeZure, M.E. Enama, E.R. James, P.F. Billingsley, A. Gunasekera, A. Manoj, M. Li, A.J. Ruben, T. Li, A.G. Eappen, R.E. Stafford, N. Kc, T. Murshedkar, F.H. Mendoza, I.J. Gordon, K.L. Zephir, L.A. Holman, S.H. Plummer, C.S. Hendel, L. Novik, P.J. Costner, J.G. Saunders, N.M. Berkowitz, B.J. Flynn, M.C. Nason, L.S. Garver, M.B. Laurens, C.V. Plowe, T.L. Richie, B.S. Graham, M. Roederer, B.K. Sim, J.E. Ledgerwood, S.L. Hoffman, and R.A. Seder. 2017. Attenuated PfSPZ Vaccine induces strain-transcending T cells and durable protection against heterologous controlled human malaria infection. *Proceedings of the National Academy of Sciences of the United States of America*. 114:2711-2716.

MacGurn, J.A., P.C. Hsu, and S.D. Emr. 2012. Ubiquitin and membrane protein turnover: from cradle to grave. *Annual review of biochemistry*. 81:231-259.

Maier, A.G., B.M. Cooke, A.F. Cowman, and L. Tilley. 2009. Malaria parasite proteins that remodel the host erythrocyte. *Nature reviews. Microbiology*. 7:341-354.

Malleret, B., C. Claser, A.S. Ong, R. Suwanarusk, K. Sriprawat, S.W. Howland, B. Russell, F. Nosten, and L. Renia. 2011. A rapid and robust tri-color flow cytometry assay for monitoring malaria parasite development. *Scientific reports*. 1:118.

Marat, A.L., and V. Haucke. 2016. Phosphatidylinositol 3-phosphates-at the interface between cell signalling and membrane traffic. *The EMBO journal*. 35:561-579.

Marti, M., J. Baum, M. Rug, L. Tilley, and A.F. Cowman. 2005. Signal-mediated export of proteins from the malaria parasite to the host erythrocyte. *The Journal of cell biology*. 171:587-592.

Masedunskas, A., and R. Weigert. 2008. Intravital two-photon microscopy for studying the uptake and trafficking of fluorescently conjugated molecules in live rodents. *Traffic (Copenhagen, Denmark)*. 9:1801-1810.

Matuschewski, K. 2006. Getting infectious: formation and maturation of Plasmodium sporozoites in the Anopheles vector. *Cellular microbiology*. 8:1547-1556.

Maude, R.J., F. Barkhof, M.U. Hassan, A. Ghose, A. Hossain, M. Abul Faiz, E. Choudhury, R. Rashid, A. Abu Sayeed, P. Charunwatthana, K. Plewes, H. Kingston, R.R. Maude, K. Silamut, N.P. Day, N.J. White, and A.M. Dondorp. 2014. Magnetic resonance imaging of the brain in adults with severe falciparum malaria. *Malaria journal*. 13:177.

Mayor, S., and R.E. Pagano. 2007. Pathways of clathrin-independent endocytosis. *Nature reviews. Molecular cell biology*. 8:603-612.

Mbengue, A., S. Bhattacharjee, T. Pandharkar, H. Liu, G. Estiu, R.V. Stahelin, S.S. Rizk, D.L. Njimoh, Y. Ryan, K. Chotivanich, C. Nguon, M. Ghorbal, J.J. Lopez-Rubio, M. Pfrender, S. Emrich, N. Mohandas, A.M. Dondorp, O. Wiest, and K. Haldar. 2015. A molecular mechanism of artemisinin resistance in Plasmodium falciparum malaria. *Nature*. 520:683-687.

McFadden, G.I., M.E. Reith, J. Munholland, and N. Lang-Unnasch. 1996. Plastid in human parasites. *Nature*. 381:482.

McGovern, O.L., and V.B. Carruthers. 2016. Toxoplasma Retromer Is Here to Stay. *Trends in parasitology*. 32:758-760.

McGovern, O.L., Y. Rivera-Cuevas, G. Kannan, A.J. Narwold, Jr., and V.B. Carruthers. 2018. Intersection of endocytic and exocytic systems in Toxoplasma gondii. *Traffic (Copenhagen, Denmark)*. 19:336-353.

McGregor, A., T. Doherty, P. Lowe, P. Chiodini, and W. Newsholme. 2015. Hyperreactive Malarial Splenomegaly Syndrome--Can the Diagnostic Criteria Be Improved? *The American journal of tropical medicine and hygiene*. 93:573-576.

McMahon, H.T., and E. Boucrot. 2011. Molecular mechanism and physiological functions of clathrin-mediated endocytosis. *Nature reviews. Molecular cell biology*. 12:517-533.

McMahon, H.T., and J.L. Gallop. 2005. Membrane curvature and mechanisms of dynamic cell membrane remodelling. *Nature*. 438:590-596.

Medana, I.M., and G.D. Turner. 2006. Human cerebral malaria and the blood-brain barrier. *International journal for parasitology*. 36:555-568.

Meinecke, M., E. Boucrot, G. Camdere, W.C. Hon, R. Mittal, and H.T. McMahon. 2013. Cooperative recruitment of dynamin and BIN/amphiphysin/Rvs (BAR) domain-containing proteins leads to GTP-dependent membrane scission. *The Journal of biological chemistry*. 288:6651-6661.

Meissner, M., D. Schluter, and D. Soldati. 2002. Role of Toxoplasma gondii myosin A in powering parasite gliding and host cell invasion. *Science (New York, N.Y.)*. 298:837-840.

Mercer, J., and U.F. Greber. 2013. Virus interactions with endocytic pathways in macrophages and dendritic cells. *Trends in microbiology*. 21:380-388.

Mesen-Ramirez, P., F. Reinsch, A. Blancke Soares, B. Bergmann, A.K. Ullrich, S. Tenzer, and T. Spielmann. 2016. Stable Translocation Intermediates Jam Global Protein Export in Plasmodium falciparum Parasites and Link the PTEX Component EXP2 with Translocation Activity. *PLoS pathogens*. 12:e1005618.

Meshnick, S.R., Y.Z. Yang, V. Lima, F. Kuypers, S. Kamchonwongpaisan, and Y. Yuthavong. 1993. Iron-dependent free radical generation from the antimalarial agent artemisinin (qinghaosu). *Antimicrobial agents and chemotherapy*. 37:1108-1114.

Meszoely, C.A.M.S., R. L. ; Bahr, G. F. . 1972. Morphologic Studies on the Freeze-Etched Avian Malarial Parasite Plasmodium gallinaceum. *In* BASIC RESEARCH IN MALARIA. A.E.H. Sadun, editor. The Helminthological Society of Washington, Washington.

Milani, K.J., T.G. Schneider, and T.F. Taraschi. 2015. Defining the Morphology and Mechanism of the Hemoglobin Transport Pathway in Plasmodium falciparum Infected Erythrocytes. *Eukaryotic cell*.

Miller, L.H., H.C. Ackerman, X.Z. Su, and T.E. Wellems. 2013. Malaria biology and disease pathogenesis: insights for new treatments. *Nature medicine*. 19:156-167.

Miller, L.H., D.I. Baruch, K. Marsh, and O.K. Doumbo. 2002. The pathogenic basis of malaria. *Nature*. 415:673-679.

Miller, L.H., and X. Su. 2011. Artemisinin: discovery from the Chinese herbal garden. *Cell*. 146:855-858.

Milner, D.A., Jr., R.O. Whitten, S. Kamiza, R. Carr, G. Liomba, C. Dzamalala, K.B. Seydel, M.E. Molyneux, and T.E. Taylor. 2014. The systemic pathology of cerebral malaria in African children. *Frontiers in cellular and infection microbiology*. 4:104.

Miranda, K., D.A. Pace, R. Cintron, J.C. Rodrigues, J. Fang, A. Smith, P. Rohloff, E. Coelho, F. de Haas, W. de Souza, I. Coppens, L.D. Sibley, and S.N. Moreno. 2010. Characterization of a novel organelle in Toxoplasma gondii with similar composition and function to the plant vacuole. *Molecular microbiology*. 76:1358-1375.

Mohanty, S., L.A. Benjamin, M. Majhi, P. Panda, S. Kampondeni, P.K. Sahu, A. Mohanty, K.C. Mahanta, R. Pattnaik, R.R. Mohanty, S. Joshi, A. Mohanty, I.W. Turnbull, A.M. Dondorp, T.E. Taylor, and S.C. Wassmer. 2017. Magnetic Resonance Imaging of Cerebral Malaria Patients Reveals Distinct Pathogenetic Processes in Different Parts of the Brain. *mSphere*. 2.

Moon, R.W., J. Hall, F. Rangkuti, Y.S. Ho, N. Almond, G.H. Mitchell, A. Pain, A.A. Holder, and M.J. Blackman. 2013. Adaptation of the genetically tractable malaria pathogen Plasmodium knowlesi to continuous culture in human erythrocytes. *Proceedings of the National Academy of Sciences of the United States of America*. 110:531-536.

Mordmuller, B., G. Surat, H. Lagler, S. Chakravarty, A.S. Ishizuka, A. Lalremruata, M. Gmeiner, J.J. Campo, M. Esen, A.J. Ruben, J. Held, C.L. Calle, J.B. Mengue, T. Gebru, J. Ibanez, M. Sulyok, E.R. James, P.F. Billingsley, K.C. Natasha, A. Manoj, T. Murshedkar, A. Gunasekera, A.G. Eappen, T. Li, R.E. Stafford, M. Li, P.L. Felgner, R.A. Seder, T.L. Richie, B.K. Sim, S.L. Hoffman, and P.G. Kremsner. 2017. Sterile protection against human malaria by chemoattenuated PfSPZ vaccine. *Nature*. 542:445-449.

Morrison, H.A.D., Heather; Rusten, Tor Erik; Brech,, W.W.P. Andreas; Fisher, Barret D. ; Celniker, Susan E.; Stenmark, Harald , and D. and Bilder. 2008. Regulation of Early Endosomal Entry by the Drosophila Tumor Suppressors Rabenosyn and Vps45. *Molecular biology of the cell*. 19:9.

Mueller, C., A. Graindorge, and D. Soldati-Favre. 2017. Functions of myosin motors tailored for parasitism. *Current opinion in microbiology*. 40:113-122.

Murphy, S.C., S. Fernandez-Pol, P.H. Chung, S.N. Prasanna Murthy, S.B. Milne, M. Salomao, H.A. Brown, J.W. Lomasney, N. Mohandas, and K. Haldar. 2007. Cytoplasmic remodeling of erythrocyte raft lipids during infection by the human malaria parasite Plasmodium falciparum. *Blood*. 110:2132-2139.

Musacchio, A., C.J. Smith, A.M. Roseman, S.C. Harrison, T. Kirchhausen, and B.M. Pearse. 1999. Functional organization of clathrin in coats: combining electron cryomicroscopy and X-ray crystallography. *Molecular cell*. 3:761-770.

Nevin, W.D., and J.B. Dacks. 2009. Repeated secondary loss of adaptin complex genes in the Apicomplexa. *Parasitology international*. 58:86-94.

Nielsen, E., S. Christoforidis, S. Uttenweiler-Joseph, M. Miaczynska, F. Dewitte, M. Wilm, B. Hoflack, and M. Zerial. 2000. Rabenosyn-5, a novel Rab5 effector, is complexed with hVPS45 and recruited to endosomes through a FYVE finger domain. *The Journal of cell biology*. 151:601-612.

Nonnenmacher, M.E., J.C. Cintrat, D. Gillet, and T. Weber. 2015. Syntaxin 5-dependent retrograde transport to the trans-Golgi network is required for adeno-associated virus transduction. *Journal of virology*. 89:1673-1687.

Nussenzweig, R., J. Vanderberg, and H. Most. 1969. Protective immunity produced by the injection of x-irradiated sporozoites of Plasmodium berghei. IV. Dose response, specificity and humoral immunity. *Military medicine*. 134:1176-1182.

Nussenzweig, R.S., J. Vanderberg, H. Most, and C. Orton. 1967. Protective immunity produced by the injection of x-irradiated sporozoites of plasmodium berghei. *Nature*. 216:160-162.

Nzila, A. 2006. Inhibitors of de novo folate enzymes in Plasmodium falciparum. *Drug discovery today*. 11:939-944.

O'Neill, P.M., V.E. Barton, and S.A. Ward. 2010. The molecular mechanism of action of artemisinin--the debate continues. *Molecules (Basel, Switzerland)*. 15:1705-1721.

Oakley, M.S., N. Gerald, T.F. McCutchan, L. Aravind, and S. Kumar. 2011. Clinical and molecular aspects of malaria fever. *Trends in parasitology*. 27:442-449.

Okamoto, N., T.P. Spurck, C.D. Goodman, and G.I. McFadden. 2009. Apicoplast and mitochondrion in gametocytogenesis of Plasmodium falciparum. *Eukaryotic cell*. 8:128-132.

Olliaro, P., W.R. Taylor, and J. Rigal. 2001. Controlling malaria: challenges and solutions. *Tropical medicine & international health : TM & IH*. 6:922-927.

Olotu, A., G. Fegan, J. Wambua, G. Nyangweso, K.O. Awuondo, A. Leach, M. Lievens, D. Leboulleux, P. Njuguna, N. Peshu, K. Marsh, and P. Bejon. 2013. Four-year efficacy of RTS,S/AS01E and its interaction with malaria exposure. *The New England journal of medicine*. 368:1111-1120.

Olotu, A., G. Fegan, J. Wambua, G. Nyangweso, A. Leach, M. Lievens, D.C. Kaslow, P. Njuguna, K. Marsh, and P. Bejon. 2016. Seven-Year Efficacy of RTS,S/AS01 Malaria Vaccine among Young African Children. *The New England journal of medicine*. 374:2519-2529.

Opitz, C., and D. Soldati. 2002. 'The glideosome': a dynamic complex powering gliding motion and host cell invasion by Toxoplasma gondii. *Molecular microbiology*. 45:597-604.

Pagola, S., P.W. Stephens, D.S. Bohle, A.D. Kosar, and S.K. Madsen. 2000. The structure of malaria pigment beta-haematin. *Nature*. 404:307-310.

Pan, X., N. Zaarur, M. Singh, P. Morin, and K.V. Kandror. 2017. Sortilin and retromer mediate retrograde transport of Glut4 in 3T3-L1 adipocytes. *Molecular biology of the cell*. 28:1667-1675.

Pandey, A.V., V.K. Babbarwal, J.N. Okoyeh, R.M. Joshi, S.K. Puri, R.L. Singh, and V.S. Chauhan. 2003. Hemozoin formation in malaria: a two-step process involving histidine-rich proteins and lipids. *Biochemical and biophysical research communications*. 308:736-743.

Parish, L.A., and J.C. Rayner. 2009. Plasmodium falciparum secretory pathway: characterization of PfStx1, a plasma membrane Qa-SNARE. *Molecular and biochemical parasitology*. 164:153-156.

Park, S.Y., and X. Guo. 2014. Adaptor protein complexes and intracellular transport. *Bioscience reports*. 34.

Payne, D. 1987. Spread of chloroquine resistance in Plasmodium falciparum. *Parasitology today (Personal ed.)*. 3:241-246.

Pennisi, E. 2015. Gene drive turns mosquitoes into malaria fighters. *Science (New York, N.Y.)*. 350:1014.

Perez-Victoria, F.J., C. Schindler, J.G. Magadan, G.A. Mardones, C. Delevoye, M. Romao, G. Raposo, and J.S. Bonifacino. 2010. Ang2/fat-free is a conserved subunit of the Golgi-associated retrograde protein complex. *Molecular biology of the cell*. 21:3386-3395.

Periz, J., J. Whitelaw, C. Harding, S. Gras, M.I. Del Rosario Minina, F. Latorre-Barragan, L. Lemgruber, M.A. Reimer, R. Insall, A. Heaslip, and M. Meissner. 2017. Toxoplasma gondii F-actin forms an extensive filamentous network required for material exchange and parasite maturation. *eLife*. 6.

Phillips, M.A., J.N. Burrows, C. Manyando, R.H. van Huijsduijnen, W.C. Van Voorhis, and T.N.C. Wells. 2017. Malaria. *Nature reviews. Disease primers*. 3:17050.

Pieperhoff, M.S., M. Schmitt, D.J. Ferguson, and M. Meissner. 2013. The role of clathrin in post-Golgi trafficking in Toxoplasma gondii. *PloS one*. 8:e77620.

Piper, R.C., E.A. Whitters, and T.H. Stevens. 1994. Yeast Vps45p is a Sec1p-like protein required for the consumption of vacuole-targeted, post-Golgi transport vesicles. *Eur J Cell Biol*. 65:305-318.

Pluess, B., F.C. Tanser, C. Lengeler, and B.L. Sharp. 2010. Indoor residual spraying for preventing malaria. *The Cochrane database of systematic reviews*:Cd006657.

Posor, Y., M. Eichhorn-Grunig, and V. Haucke. 2015. Phosphoinositides in endocytosis. *Biochimica et biophysica acta*. 1851:794-804.

Potchen, M.J., S.D. Kampondeni, K.B. Seydel, G.L. Birbeck, C.A. Hammond, W.G. Bradley, J.K. DeMarco, S.J. Glover, J.O. Ugorji, M.T. Latourette, J.E. Siebert, M.E. Molyneux, and T.E. Taylor. 2012. Acute brain MRI findings in 120 Malawian children with cerebral malaria: new insights into an ancient disease. *AJNR. American journal of neuroradiology*. 33:1740-1746.

Pulcini, S., H.M. Staines, A.H. Lee, S.H. Shafik, G. Bouyer, C.M. Moore, D.A. Daley, M.J. Hoke, L.M. Altenhofen, H.J. Painter, J. Mu, D.J. Ferguson, M. Llinas, R.E. Martin, D.A. Fidock, R.A. Cooper, and S. Krishna. 2015. Mutations in the Plasmodium falciparum chloroquine resistance transporter, PfCRT, enlarge the parasite's food vacuole and alter drug sensitivities. *Scientific reports*. 5:14552.

Quevillon, E., T. Spielmann, K. Brahimi, D. Chattopadhyay, E. Yeramian, and G. Langsley. 2003. The Plasmodium falciparum family of Rab GTPases. *Gene*. 306:13-25.

Rached, F.B., C. Ndjembo-Ezougou, S. Chandran, H. Talabani, H. Yera, V. Dandavate, P. Bourdoncle, M. Meissner, U. Tatu, and G. Langsley. 2012. Construction of a Plasmodium falciparum Rab-interactome identifies CK1 and PKA as Rab-effector kinases in malaria parasites. *Biology of the cell*. 104:34-47.

Raymond, C.K., I. Howald-Stevenson, C.A. Vater, and T.H. Stevens. 1992. Morphological classification of the yeast vacuolar protein sorting mutants: evidence for a prevacuolar compartment in class E vps mutants. *Molecular biology of the cell*. 3:1389-1402.

Reichard, N. 2015. A screen to characterize unknown proteins in the human malaria parasite *Plasmodium falciparum.* University of Lübeck, Lübeck.

Reyes-Lopez, M., C. Pina-Vazquez, and J. Serrano-Luna. 2015. Transferrin: Endocytosis and Cell Signaling in Parasitic Protozoa. *BioMed research international*. 2015:641392.

Richie, T.L., P.F. Billingsley, B.K. Sim, E.R. James, S. Chakravarty, J.E. Epstein, K.E. Lyke, B. Mordmuller, P. Alonso, P.E. Duffy, O.K. Doumbo, R.W. Sauerwein, M. Tanner, S. Abdulla, P.G. Kremsner, R.A. Seder, and S.L. Hoffman. 2015. Progress with Plasmodium falciparum sporozoite (PfSPZ)-based malaria vaccines. *Vaccine*. 33:7452-7461.

Rieckmann, K.H., R.L. Beaudoin, J.S. Cassells, and K.W. Sell. 1979. Use of attenuated sporozoites in the immunization of human volunteers against falciparum malaria. *Bulletin of the World Health Organization*. 57 Suppl 1:261-265.

Rink, J., E. Ghigo, Y. Kalaidzidis, and M. Zerial. 2005. Rab conversion as a mechanism of progression from early to late endosomes. *Cell*. 122:735-749.

Robinson, J.S., D.J. Klionsky, L.M. Banta, and S.D. Emr. 1988. Protein sorting in Saccharomyces cerevisiae: isolation of mutants defective in the delivery and processing of multiple vacuolar hydrolases. *Molecular and cellular biology*. 8:4936-4948.

Robinson, M.S. 2004. Adaptable adaptors for coated vesicles. *Trends in cell biology*. 14:167-174.
Robinson, M.S., D.A. Sahlender, and S.D. Foster. 2010. Rapid inactivation of proteins by rapamycin-induced rerouting to mitochondria. *Developmental cell*. 18:324-331.
Romisch, K. 2012. Diversion at the ER: How Plasmodium falciparum exports proteins into host erythrocytes. *F1000Research*. 1:12.
Ross, R. 1889. The role of the mosquito in the evolution of the malaria parasite. *Lancet*.
Roth, T.F., and K.R. Porter. 1964. Yolk protein uptake in the oocyte of the mosquito *Aedes aegypti*. *The Journal of cell biology*. 20:313-332.
Rothman, J.E., and G. Warren. 1994. Implications of the SNARE hypothesis for intracellular membrane topology and dynamics. *Current biology : CB*. 4:220-233.
Rothman, J.H., and T.H. Stevens. 1986. Protein sorting in yeast: mutants defective in vacuole biogenesis mislocalize vacuolar proteins into the late secretory pathway. *Cell*. 47:1041-1051.
Roux, K.J., D.I. Kim, M. Raida, and B. Burke. 2012. A promiscuous biotin ligase fusion protein identifies proximal and interacting proteins in mammalian cells. *The Journal of cell biology*. 196:801-810.
RTS, S.C.T.P. 2015. Efficacy and safety of RTS,S/AS01 malaria vaccine with or without a booster dose in infants and children in Africa: final results of a phase 3, individually randomised, controlled trial. *Lancet*. 386:31-45.
Rudzinska, M.A. 1969. The fine structure of malaria parasites. *International review of cytology*. 25:161-199.
Rudzinska, M.A., and W. Trager. 1958. [The mechanism of feeding of Plasmodium malariae; electron-microscopic studies]. *Wiadomosci parazytologiczne*. 4:617-618; English transl 618-619.
Rudzinska, M.A., and W. Trager. 1959. Phagotrophy and two new structures in the malaria parasite Plasmodium berghei. *The Journal of biophysical and biochemical cytology*. 6:103-112.
Rudzinska, M.A., W. Trager, and R.S. Bray. 1965. Pinocytotic uptake and the digestion of hemoglobin in malaria parasites. *The Journal of protozoology*. 12:563-576.
Russo, I., S. Babbitt, V. Muralidharan, T. Butler, A. Oksman, and D.E. Goldberg. 2010. Plasmepsin V licenses Plasmodium proteins for export into the host erythrocyte. *Nature*. 463:632-636.
Sabitzki, R. 2017. haracterization of the cavity and associated structures of the human malaria parasite *P. falciparum*. University Bremen, Bremen.
Sachs, J., and P. Malaney. 2002. The economic and social burden of malaria. *Nature*. 415:680-685.
Sadasivaiah, S., Y. Tozan, and J.G. Breman. 2007. Dichlorodiphenyltrichloroethane (DDT) for indoor residual spraying in Africa: how can it be used for malaria control? *The American journal of tropical medicine and hygiene*. 77:249-263.
Sakura, T., F. Sindikubwabo, L.K. Oesterlin, H. Bousquet, C. Slomianny, M.A. Hakimi, G. Langsley, and S. Tomavo. 2016. A Critical Role for Toxoplasma gondii Vacuolar Protein Sorting VPS9 in Secretory Organelle Biogenesis and Host Infection. *Scientific reports*. 6:38842.
Sangare, L.O., T.D. Alayi, B. Westermann, A. Hovasse, F. Sindikubwabo, I. Callebaut, E. Werkmeister, F. Lafont, C. Slomianny, M.A. Hakimi, A. Van Dorsselaer, C. Schaeffer-Reiss, and S. Tomavo. 2016. Unconventional endosome-like compartment and retromer complex in Toxoplasma gondii govern parasite integrity and host infection. *Nature communications*. 7:11191.
Scalzi, H.A., and G.F. Bahr. 1968. An electron microscopic examination of erythrocytic stages of two rodent malarial parasites, Plasmodium chabaudi and Plasmodium vinckei. *Journal of ultrastructure research*. 24:116-133.
Scheidel, N., J. Kennedy, and O.E. Blacque. 2018. Endosome maturation factors Rabenosyn-5/VPS45 and caveolin-1 regulate ciliary membrane and polycystin-2 homeostasis. *The EMBO journal*. 37.
Schindler, C., Y. Chen, J. Pu, X. Guo, and J.S. Bonifacino. 2015. EARP is a multisubunit tethering complex involved in endocytic recycling. *Nature cell biology*. 17:639-650.
Schmid, E.M., and H.T. McMahon. 2007. Integrating molecular and network biology to decode endocytosis. *Nature*. 448:883-888.
Schmitz, S., M. Grainger, S. Howell, L.J. Calder, M. Gaeb, J.C. Pinder, A.A. Holder, and C. Veigel. 2005. Malaria parasite actin filaments are very short. *Journal of molecular biology*. 349:113-125.

Schmoranzer, J., M. Goulian, D. Axelrod, and S.M. Simon. 2000. Imaging constitutive exocytosis with total internal reflection fluorescence microscopy. *The Journal of cell biology*. 149:23-32.

Schofield, L., M.C. Hewitt, K. Evans, M.A. Siomos, and P.H. Seeberger. 2002. Synthetic GPI as a candidate anti-toxic vaccine in a model of malaria. *Nature*. 418:785-789.

Scholtyseck, E., and H. Mehlhorn. 1970. Ultrastructural study of characteristic organelles (paired organelles, micronemes, micropores) of sporozoa and related organisms. *Zeitschrift fur Parasitenkunde (Berlin, Germany)*. 34:97-127.

Schottenfeld-Roames, J., J.B. Rosa, and A.S. Ghabrial. 2014. Seamless tube shape is constrained by endocytosis-dependent regulation of active Moesin. *Current biology : CB*. 24:1756-1764.

Schuler, H., and K. Matuschewski. 2006. Plasmodium motility: actin not actin' like actin. *Trends in parasitology*. 22:146-147.

Scorza, J.V. 1971. Electron microscope study of the blood stages of Plasmodium tropiduri, a lizard malaria parasite. *Parasitology*. 63:1-20.

Seaman, M.N., J.M. McCaffery, and S.D. Emr. 1998. A membrane coat complex essential for endosome-to-Golgi retrograde transport in yeast. *The Journal of cell biology*. 142:665-681.

Sergent, E. 1910. Sur l'immunite dans le paludisme des oiseaux. Conservation in vitro des sporozoites de Plasmodium relictum. Immunite relative obtenue par inoculation de ces sporozoites. *C R Acad Sci*. 151:407–409.

Shanks, S.G., L.N. Carpp, M.S. Struthers, R.K. McCann, and N.J. Bryant. 2012. The Sec1/Munc18 protein Vps45 regulates cellular levels of its SNARE binding partners Tlg2 and Snc2 in Saccharomyces cerevisiae. *PloS one*. 7:e49628.

Shaw, M.K., and L.G. Tilney. 1999. Induction of an acrosomal process in Toxoplasma gondii: visualization of actin filaments in a protozoan parasite. *Proceedings of the National Academy of Sciences of the United States of America*. 96:9095-9099.

Sherman, I.W. 1998. Malaria: Parasite Biology, Pathogenesis, and Protection. ASM Press, Washington.

Shortt, H.E., P.C. Garnham, and et al. 1948. The pre-erythrocytic stage of human malaria, Plasmodium vivax. *British medical journal*. 1:547.

Sijwali, P.S., and P.J. Rosenthal. 2004. Gene disruption confirms a critical role for the cysteine protease falcipain-2 in hemoglobin hydrolysis by Plasmodium falciparum. *Proceedings of the National Academy of Sciences of the United States of America*. 101:4384-4389.

Sinden, R.E. 1974. Excystment by sporozoites of malaria parasites. *Nature*. 252:314.

Sinden, R.E. 2009. Malaria, sexual development and transmission: retrospect and prospect. *Parasitology*. 136:1427-1434.

Sinden, R.E. 2015. The cell biology of malaria infection of mosquito: advances and opportunities. *Cellular microbiology*. 17:451-466.

Singh, B., and C. Daneshvar. 2013. Human infections and detection of Plasmodium knowlesi. *Clinical microbiology reviews*. 26:165-184.

Sinka, M.E., M.J. Bangs, S. Manguin, M. Coetzee, C.M. Mbogo, J. Hemingway, A.P. Patil, W.H. Temperley, P.W. Gething, C.W. Kabaria, R.M. Okara, T. Van Boeckel, H.C. Godfray, R.E. Harbach, and S.I. Hay. 2010. The dominant Anopheles vectors of human malaria in Africa, Europe and the Middle East: occurrence data, distribution maps and bionomic precis. *Parasites & vectors*. 3:117.

Sinka, M.E., M.J. Bangs, S. Manguin, Y. Rubio-Palis, T. Chareonviriyaphap, M. Coetzee, C.M. Mbogo, J. Hemingway, A.P. Patil, W.H. Temperley, P.W. Gething, C.W. Kabaria, T.R. Burkot, R.E. Harbach, and S.I. Hay. 2012. A global map of dominant malaria vectors. *Parasites & vectors*. 5:69.

Slomianny, C. 1990. Three-dimensional reconstruction of the feeding process of the malaria parasite. *Blood cells*. 16:369-378.

Slomianny, C., G. Prensier, and P. Charet. 1985. Ingestion of erythrocytic stroma by Plasmodium chabaudi trophozoites: ultrastructural study by serial sectioning and 3-dimensional reconstruction. *Parasitology*. 90 (Pt 3):579-588.

Sloves, P.J., S. Delhaye, T. Mouveaux, E. Werkmeister, C. Slomianny, A. Hovasse, T. Dilezitoko Alayi, I. Callebaut, R.Y. Gaji, C. Schaeffer-Reiss, A. Van Dorsselear, V.B. Carruthers, and S. Tomavo. 2012. Toxoplasma sortilin-like receptor regulates protein transport and is essential for apical secretory organelle biogenesis and host infection. *Cell host & microbe*. 11:515-527.

Smith, C.J., N. Grigorieff, and B.M. Pearse. 1998. Clathrin coats at 21 A resolution: a cellular assembly designed to recycle multiple membrane receptors. *The EMBO journal*. 17:4943-4953.

Smythe, W.A., K.A. Joiner, and H.C. Hoppe. 2008. Actin is required for endocytic trafficking in the malaria parasite Plasmodium falciparum. *Cellular microbiology*. 10:452-464.

Sollner, T., M.K. Bennett, S.W. Whiteheart, R.H. Scheller, and J.E. Rothman. 1993. A protein assembly-disassembly pathway in vitro that may correspond to sequential steps of synaptic vesicle docking, activation, and fusion. *Cell*. 75:409-418.

Spielmann, T., and T.W. Gilberger. 2010. Protein export in malaria parasites: do multiple export motifs add up to multiple export pathways? *Trends in parasitology*. 26:6-10.

Spitz, S. 1946. The pathology of acute falciparum malaria. *Military surgeon*. 99:555-572.

Spork, S., J.A. Hiss, K. Mandel, M. Sommer, T.W. Kooij, T. Chu, G. Schneider, U.G. Maier, and J.M. Przyborski. 2009. An unusual ERAD-like complex is targeted to the apicoplast of Plasmodium falciparum. *Eukaryotic cell*. 8:1134-1145.

Staines, H.M., A. Alkhalil, R.J. Allen, H.R. De Jonge, E. Derbyshire, S. Egee, H. Ginsburg, D.A. Hill, S.M. Huber, K. Kirk, F. Lang, G. Lisk, E. Oteng, A.D. Pillai, K. Rayavara, S. Rouhani, K.J. Saliba, C. Shen, T. Solomon, S.L. Thomas, P. Verloo, and S.A. Desai. 2007. Electrophysiological studies of malaria parasite-infected erythrocytes: current status. *International journal for parasitology*. 37:475-482.

Stanway, R.R., T. Witt, B. Zobiak, M. Aepfelbacher, and V.T. Heussler. 2009. GFP-targeting allows visualization of the apicoplast throughout the life cycle of live malaria parasites. *Biology of the cell*. 101:415-430, 415 p following 430.

Stechmann, B., S.K. Bai, E. Gobbo, R. Lopez, G. Merer, S. Pinchard, L. Panigai, D. Tenza, G. Raposo, B. Beaumelle, D. Sauvaire, D. Gillet, L. Johannes, and J. Barbier. 2010. Inhibition of retrograde transport protects mice from lethal ricin challenge. *Cell*. 141:231-242.

Stenmark, H. 2009. Rab GTPases as coordinators of vesicle traffic. *Nature reviews. Molecular cell biology*. 10:513-525.

Stenmark, H., and V.M. Olkkonen. 2001. The Rab GTPase family. *Genome biology*. 2:Reviews3007.

Sterling, C.R.A., M; Nussenzweig, R. S. 1972. Morphological Divergence in a Mammalian Malarial Parasite: The Fine Structure of Plasmodium brasilianum. *In* BASIC RESEARCH IN MALARIA. Vol. 39. A.E.H. Sadun, editor. The Helminthological Society of Washington, Washington.

Stimpson, H.E., C.P. Toret, A.T. Cheng, B.S. Pauly, and D.G. Drubin. 2009. Early-arriving Syp1p and Ede1p function in endocytic site placement and formation in budding yeast. *Molecular biology of the cell*. 20:4640-4651.

Stogios, P.J., G.S. Downs, J.J. Jauhal, S.K. Nandra, and G.G. Prive. 2005. Sequence and structural analysis of BTB domain proteins. *Genome biology*. 6:R82.

Straimer, J., N.F. Gnadig, B. Witkowski, C. Amaratunga, V. Duru, A.P. Ramadani, M. Dacheux, N. Khim, L. Zhang, S. Lam, P.D. Gregory, F.D. Urnov, O. Mercereau-Puijalon, F. Benoit-Vical, R.M. Fairhurst, D. Menard, and D.A. Fidock. 2015. Drug resistance. K13-propeller mutations confer artemisinin resistance in Plasmodium falciparum clinical isolates. *Science (New York, N.Y.)*. 347:428-431.

Struck, N.S., S. de Souza Dias, C. Langer, M. Marti, J.A. Pearce, A.F. Cowman, and T.W. Gilberger. 2005. Re-defining the Golgi complex in Plasmodium falciparum using the novel Golgi marker PfGRASP. *Journal of cell science*. 118:5603-5613.

Struck, N.S., S. Herrmann, I. Schmuck-Barkmann, S. de Souza Dias, S. Haase, A.L. Cabrera, M. Treeck, C. Bruns, C. Langer, A.F. Cowman, M. Marti, T. Spielmann, and T.W. Gilberger. 2008. Spatial dissection of the cis- and trans-Golgi compartments in the malaria parasite Plasmodium falciparum. *Molecular microbiology*. 67:1320-1330.

Sullivan, D.J., Jr., I.Y. Gluzman, and D.E. Goldberg. 1996. Plasmodium hemozoin formation mediated by histidine-rich proteins. *Science (New York, N.Y.)*. 271:219-222.

Sun, Y., A.C. Martin, and D.G. Drubin. 2006. Endocytic internalization in budding yeast requires coordinated actin nucleation and myosin motor activity. *Developmental cell*. 11:33-46.

Sutherland, C.J., P. Lansdell, M. Sanders, J. Muwanguzi, D.A. van Schalkwyk, H. Kaur, D. Nolder, J. Tucker, H.M. Bennett, T.D. Otto, M. Berriman, T.A. Patel, R. Lynn, E. Gkrania-Klotsas, and P.L. Chiodini. 2017. pfk13-Independent Treatment Failure in Four Imported Cases of

Plasmodium falciparum Malaria Treated with Artemether-Lumefantrine in the United Kingdom. *Antimicrobial agents and chemotherapy*. 61.

Sutton, R.B., D. Fasshauer, R. Jahn, and A.T. Brunger. 1998. Crystal structure of a SNARE complex involved in synaptic exocytosis at 2.4 A resolution. *Nature*. 395:347-353.

Taketo, A. 1988. DNA transfection of Escherichia coli by electroporation. *Biochimica et biophysica acta*. 949:318-324.

Tardieux, I., and J. Baum. 2016. Reassessing the mechanics of parasite motility and host-cell invasion. *The Journal of cell biology*. 214:507-515.

Tawk, L., G. Chicanne, J.F. Dubremetz, V. Richard, B. Payrastre, H.J. Vial, C. Roy, and K. Wengelnik. 2010. Phosphatidylinositol 3-phosphate, an essential lipid in Plasmodium, localizes to the food vacuole membrane and the apicoplast. *Eukaryotic cell*. 9:1519-1530.

Taylor, M.J., D. Perrais, and C.J. Merrifield. 2011. A high precision survey of the molecular dynamics of mammalian clathrin-mediated endocytosis. *PLoS biology*. 9:e1000604.

Teasdale, R.D., and B.M. Collins. 2012. Insights into the PX (phox-homology) domain and SNX (sorting nexin) protein families: structures, functions and roles in disease. *The Biochemical journal*. 441:39-59.

Thakur, V., M. Asad, S. Jain, M.E. Hossain, A. Gupta, I. Kaur, S. Rathore, S. Ali, N.J. Khan, and A. Mohmmed. 2015. Eps15 homology domain containing protein of Plasmodium falciparum (PfEHD) associates with endocytosis and vesicular trafficking towards neutral lipid storage site. *Biochimica et biophysica acta*. 1853:2856-2869.

Thomas, J.A., M.S.Y. Tan, C. Bisson, A. Borg, T.R. Umrekar, F. Hackett, V.L. Hale, G. Vizcay-Barrena, R.A. Fleck, A.P. Snijders, H.R. Saibil, and M.J. Blackman. 2018. A protease cascade regulates release of the human malaria parasite Plasmodium falciparum from host red blood cells. *Nature microbiology*. 3:447-455.

Tilley, L., J. Straimer, N.F. Gnadig, S.A. Ralph, and D.A. Fidock. 2016. Artemisinin Action and Resistance in Plasmodium falciparum. *Trends in parasitology*. 32:682-696.

Tomavo, S., C. Slomianny, M. Meissner, and V.B. Carruthers. 2013. Protein trafficking through the endosomal system prepares intracellular parasites for a home invasion. *PLoS pathogens*. 9:e1003629.

Toonen, R.F., and M. Verhage. 2003. Vesicle trafficking: pleasure and pain from SM genes. *Trends in cell biology*. 13:177-186.

Towbin, H., T. Staehelin, and J. Gordon. 1979. Electrophoretic transfer of proteins from polyacrylamide gels to nitrocellulose sheets: procedure and some applications. *Proceedings of the National Academy of Sciences of the United States of America*. 76:4350-4354.

Trager, W., and J.B. Jensen. 1976. Human malaria parasites in continuous culture. *Science (New York, N.Y.)*. 193:673-675.

Turusov, V., V. Rakitsky, and L. Tomatis. 2002. Dichlorodiphenyltrichloroethane (DDT): ubiquity, persistence, and risks. *Environmental health perspectives*. 110:125-128.

Ubl, J. 2005. Olympus cell R: imaging station for life science. *Altex*. 22:175-183.

Ueda-Nakamura, T., M. Attias, and W. de Souza. 2001. Megasome biogenesis in Leishmania amazonensis: a morphometric and cytochemical study. *Parasitology research*. 87:89-97.

Ullrich, O., S. Reinsch, S. Urbe, M. Zerial, and R.G. Parton. 1996. Rab11 regulates recycling through the pericentriolar recycling endosome. *The Journal of cell biology*. 135:913-924.

Umlas, J., and J.N. Fallon. 1971. New thick-film technique for malaria diagnosis. Use of saponin stromatolytic solution for lysis. *The American journal of tropical medicine and hygiene*. 20:527-529.

Ungar, D., and F.M. Hughson. 2003. SNARE protein structure and function. *Annual review of cell and developmental biology*. 19:493-517.

Ungewickell, A., M.E. Ward, E. Ungewickell, and P.W. Majerus. 2004. The inositol polyphosphate 5-phosphatase Ocrl associates with endosomes that are partially coated with clathrin. *Proceedings of the National Academy of Sciences of the United States of America*. 101:13501-13506.

Ungewickell, E. 1985. The 70-kd mammalian heat shock proteins are structurally and functionally related to the uncoating protein that releases clathrin triskelia from coated vesicles. *The EMBO journal*. 4:3385-3391.

Vaid, A., R. Ranjan, W.A. Smythe, H.C. Hoppe, and P. Sharma. 2010. PfPI3K, a phosphatidylinositol-3 kinase from Plasmodium falciparum, is exported to the host erythrocyte and is involved in hemoglobin trafficking. *Blood*. 115:2500-2507.

Vaidya, A.B., and M.W. Mather. 2009. Mitochondrial evolution and functions in malaria parasites. *Annual review of microbiology*. 63:249-267.

van Bergen En Henegouwen, P.M. 2009. Eps15: a multifunctional adaptor protein regulating intracellular trafficking. *Cell communication and signaling : CCS*. 7:24.

van Delft, S., R. Govers, G.J. Strous, A.J. Verkleij, and P.M. van Bergen en Henegouwen. 1997a. Epidermal growth factor induces ubiquitination of Eps15. *The Journal of biological chemistry*. 272:14013-14016.

van Delft, S., C. Schumacher, W. Hage, A.J. Verkleij, and P.M. van Bergen en Henegouwen. 1997b. Association and colocalization of Eps15 with adaptor protein-2 and clathrin. *The Journal of cell biology*. 136:811-821.

van Dooren, G.G., M. Marti, C.J. Tonkin, L.M. Stimmler, A.F. Cowman, and G.I. McFadden. 2005. Development of the endoplasmic reticulum, mitochondrion and apicoplast during the asexual life cycle of Plasmodium falciparum. *Molecular microbiology*. 57:405-419.

Vekemans, J. 2017. Immune Responses to the RTS,S/AS01 Malaria Vaccine Candidate: Lessons from Human Immunology, Parasitologic and Clinical Evaluations. *In* Malaria Immune Response to Infection and Vaccination. A.R. Maria M. Mota, editor. Springer International Publishing, Cham, Switzerland. 139-156.

Venugopal, K., E. Werkmeister, N. Barois, J.M. Saliou, A. Poncet, L. Huot, F. Sindikubwabo, M.A. Hakimi, G. Langsley, F. Lafont, and S. Marion. 2017. Dual role of the Toxoplasma gondii clathrin adaptor AP1 in the sorting of rhoptry and microneme proteins and in parasite division. *PLoS pathogens*. 13:e1006331.

Verges, M., F. Luton, C. Gruber, F. Tiemann, L.G. Reinders, L. Huang, A.L. Burlingame, C.R. Haft, and K.E. Mostov. 2004. The mammalian retromer regulates transcytosis of the polymeric immunoglobulin receptor. *Nature cell biology*. 6:763-769.

Vonderheit, A., and A. Helenius. 2005. Rab7 associates with early endosomes to mediate sorting and transport of Semliki forest virus to late endosomes. *PLoS biology*. 3:e233.

Wall, R.J., M. Roques, N.J. Katris, L. Koreny, R.R. Stanway, D. Brady, R.F. Waller, and R. Tewari. 2016. SAS6-like protein in Plasmodium indicates that conoid-associated apical complex proteins persist in invasive stages within the mosquito vector. *Scientific reports*. 6:28604.

Walliker, D., I.A. Quakyi, T.E. Wellems, T.F. McCutchan, A. Szarfman, W.T. London, L.M. Corcoran, T.R. Burkot, and R. Carter. 1987. Genetic analysis of the human malaria parasite Plasmodium falciparum. *Science (New York, N.Y.)*. 236:1661-1666.

Walters, J.H., and G.I. Mc. 1960. The mechanism of malarial hepatomegaly and its relationship to hepatic fibrosis. *Transactions of the Royal Society of Tropical Medicine and Hygiene*. 54:135-145.

Wandinger-Ness, A., and M. Zerial. 2014. Rab proteins and the compartmentalization of the endosomal system. *Cold Spring Harbor perspectives in biology*. 6:a022616.

Wang, L., A. Johnson, M. Hanna, and A. Audhya. 2016. Eps15 membrane-binding and -bending activity acts redundantly with Fcho1 during clathrin-mediated endocytosis. *Molecular biology of the cell*. 27:2675-2687.

Wassmer, S.C., T.E. Taylor, P.K. Rathod, S.K. Mishra, S. Mohanty, M. Arevalo-Herrera, M.T. Duraisingh, and J.D. Smith. 2015. Investigating the Pathogenesis of Severe Malaria: A Multidisciplinary and Cross-Geographical Approach. *The American journal of tropical medicine and hygiene*. 93:42-56.

Weinberg, J.S., and D.G. Drubin. 2014. Regulation of clathrin-mediated endocytosis by dynamic ubiquitination and deubiquitination. *Current biology : CB*. 24:951-959.

Weisman, L.S., S.D. Emr, and W.T. Wickner. 1990. Mutants of Saccharomyces cerevisiae that block intervacuole vesicular traffic and vacuole division and segregation. *Proceedings of the National Academy of Sciences of the United States of America*. 87:1076-1080.

Weiss, G.E., B.S. Crabb, and P.R. Gilson. 2016. Overlaying Molecular and Temporal Aspects of Malaria Parasite Invasion. *Trends in parasitology*. 32:284-295.

Welch, C.M., H. Elliott, G. Danuser, and K.M. Hahn. 2011. Imaging the coordination of multiple signalling activities in living cells. *Nature reviews. Molecular cell biology*. 12:749-756.

Wellems, T.E., and C.V. Plowe. 2001. Chloroquine-resistant malaria. *The Journal of infectious diseases*. 184:770-776.

Wendt, C., R. Rachid, W. de Souza, and K. Miranda. 2016. Electron tomography characterization of hemoglobin uptake in Plasmodium chabaudi reveals a stage-dependent mechanism for food vacuole morphogenesis. *Journal of structural biology*. 194:171-179.

Wetzel, D.M., S. Hakansson, K. Hu, D. Roos, and L.D. Sibley. 2003. Actin filament polymerization regulates gliding motility by apicomplexan parasites. *Molecular biology of the cell*. 14:396-406.

White, N.J. 2011. Determinants of relapse periodicity in Plasmodium vivax malaria. *Malaria journal*. 10:297.

White, N.J., S. Pukrittayakamee, T.T. Hien, M.A. Faiz, O.A. Mokuolu, and A.M. Dondorp. 2014. Malaria. *Lancet*. 383:723-735.

WHO. 2017. World Malaria Report. World Health Organization, Geneva.

Wieffer, M., T. Maritzen, and V. Haucke. 2009. SnapShot: endocytic trafficking. *Cell*. 137:382.e381-383.

Wissing, F., C.P. Sanchez, P. Rohrbach, S. Ricken, and M. Lanzer. 2002. Illumination of the malaria parasite Plasmodium falciparum alters intracellular pH. Implications for live cell imaging. *The Journal of biological chemistry*. 277:37747-37755.

Wu, X., M.J. Bradley, Y. Cai, D. Kummel, E.M. De La Cruz, F.A. Barr, and K.M. Reinisch. 2011. Insights regarding guanine nucleotide exchange from the structure of a DENN-domain protein complexed with its Rab GTPase substrate. *Proceedings of the National Academy of Sciences of the United States of America*. 108:18672-18677.

Yayon, A., R. Timberg, S. Friedman, and H. Ginsburg. 1984. Effects of chloroquine on the feeding mechanism of the intraerythrocytic human malarial parasite Plasmodium falciparum. *The Journal of protozoology*. 31:367-372.

Yeh, E., and J.L. DeRisi. 2011. Chemical rescue of malaria parasites lacking an apicoplast defines organelle function in blood-stage Plasmodium falciparum. *PLoS biology*. 9:e1001138.

Yoshimura, S., A. Gerondopoulos, A. Linford, D.J. Rigden, and F.A. Barr. 2010. Family-wide characterization of the DENN domain Rab GDP-GTP exchange factors. *The Journal of cell biology*. 191:367-381.

Yuan, W.C., Y.R. Lee, S.Y. Lin, L.Y. Chang, Y.P. Tan, C.C. Hung, J.C. Kuo, C.H. Liu, M.Y. Lin, M. Xu, Z.J. Chen, and R.H. Chen. 2014. K33-Linked Polyubiquitination of Coronin 7 by Cul3-KLHL20 Ubiquitin E3 Ligase Regulates Protein Trafficking. *Molecular cell*. 54:586-600.

Zerial, M., and H. McBride. 2001. Rab proteins as membrane organizers. *Nature reviews. Molecular cell biology*. 2:107-117.

Zhou, H.C., Y.H. Gao, X. Zhong, and H. Wang. 2009. Dynamin like protein 1 participated in the hemoglobin uptake pathway of Plasmodium falciparum. *Chinese medical journal*. 122:1686-1691.

Zhuang, M., M.F. Calabrese, J. Liu, M.B. Waddell, A. Nourse, M. Hammel, D.J. Miller, H. Walden, D.M. Duda, S.N. Seyedin, T. Hoggard, J.W. Harper, K.P. White, and B.A. Schulman. 2009. Structures of SPOP-substrate complexes: insights into molecular architectures of BTB-Cul3 ubiquitin ligases. *Molecular cell*. 36:39-50.

Ziemann, H. 1889. Ueber Malaria- und andere Blutparastien - nebst Anhang - eine wirksame Methode der Chromatin- und Blutfärbung. Verlag von Gustav Fischer, Jena.

Zouhar, J., E. Rojo, and D.C. Bassham. 2009. AtVPS45 is a positive regulator of the SYP41/SYP61/VTI12 SNARE complex involved in trafficking of vacuolar cargo. *Plant Physiol*. 149:1668-1678.

7. List of publications

Birnbaum, J., Flemming S., Reichard N., Blancke-Soares, A., Mesen-Ramirez, P., **Jonscher, E.**, Bergmann, B., and Spielmann, T. 2017. A genetic system to study Plasmodium falciparum protein function. *Nature methods*. 14:450-456.

Jonscher, E., Erdbeer, A., Gunther, M. and Kurth M. 2015. Two COWP-like cysteine rich proteins from Eimeria nieschulzi (coccidia, apicomplexa) are expressed during sporulation and involved in the sporocyst wall formation. *Parasites & vectors*. 8:395.

Khosh-Naucke, M., Becker, J., Mesen-Ramirez, P., Kiani, P., Birnbaum, J., Frohlke, U., **Jonscher, E.**, Schluter, H., and Spielmann, T. 2017. Identification of novel parasitophorous vacuole proteins in P. falciparum parasites using BioID. *International journal of medical microbiology : IJMM*.

Parts of this thesis are submitted for publication and the manuscript is currently in editorial revision:

Jonscher, E., Flemming, S., Schmitt, M., Birnbaum, J., Bergmann, B., Höhn, K., Spielmann, T. 2018. PfVPS45 is required for host cell cytosol uptake in malaria blood stage parasites.

Darstellung zum Eigenanteil

Gemäß Geschäftsordnung des Fach-Promotionsausschuss Biologie zur Promotionsordnung der Fakultät für Mathematik, Informatik und Naturwissenschaft vom 1. Dezember 2010;
Zu § 7 Dissertation Absatz 2

an dem nicht veröffentlichten Artikel

Jonscher, E., Flemming, S., Schmitt, M., Birnbaum, J., Bergmann, B., Höhn, K., Spielmann, T. 2018. PfVPS45 is required for host cell cytosol uptake in malaria blood stage parasites.

Ernst Jonscher, Sven Flemming, Marius Schmitt, Nick Reichard, Jakob Birnbaum, Bärbel Bergmann und Tobias Spielman haben die Experimente durchgeführt:

Sven Flemming und Nick Reichard haben den die VPS45-2xFKBP-GFP Integrations-Zelllinie erstellt und zuerst den VPS45 KS Phenotyp beschrieben. Sven Flemming und Tobias Spielmann haben ein Replikat der Experimentes mit beladenen Erythrozyten durchgeführt. Jakob Birnbaum hat den „*Bloated Food Vacuole Assay"* mit entwickelt. Marius Schmitt hat geholfen, den „*Bloated Food Vacuole Assay*" durchzuführen. Bärbel Bergmann hat ein Replikat des „*FACS growth assays*" durchgeführt. Ernst Jonscher hat die Transfektion der Zelllinie mit den diversen Plasmiden für Mislokalisations-Experimente, Fluoreszenzmikroskopie, Elektronenmikroskopie, Video-Mikroskopie, Durchführung der Assays und alle nicht bereits oben erwähnten Experimente durchgeführt. Alle weiteren Arbeiten, an denen Dritte Personen beteiligt waren, die jedoch nicht in dem Manuskript Eingang gefunden haben, sind in dem Methoden- und Ergebnis-Teilen genannt.

Ernst Jonscher, Sven Flemming, Jakob Birnbaum und Tobias Spielmann haben die Experimente entworfen.

Katharina Höhn hat die elektronenmikroskopischen Experimente betreut.

Tobias Spielmann konzipierte die Publikation und das Projekt und hat die Publikation mit Beteiligung von allen Autoren verfasst. Ernst Jonscher und Tobias Spielmann haben die Figuren erstellt.

Danksagung

An erster Stelle möchte ich Dr. Tobias Spielmann dafür danken, dass er mir die Möglichkeit gegeben hat, meine Doktorarbeit in seiner Arbeitsgruppe zu schreiben. Die regelmäßigen Besprechungen und deine stete Verfügbarkeit waren von unschätzbarem Wert, um das Projekt in die richtigen Richtungen zu lenken. Du hattest dabei stets ein offenes Ohr für neue Ideen und ermöglichtest mir den Freiraum, diese umzusetzen. Deine umfangreiches Wissen in dem Umgang mit den Parasiten und den Methoden hast du stets bereitwillig geteilt und akute Fragen und Probleme umgehend geholfen zu lösen. Danke für diese kreative und produktive Atmosphäre, in der ich lernen und mich weiter entwickeln konnte.

Ich möchte mich bei meinen Betreuern und Co-Betreuern Herrn Prof. Tim-Wolf Gilberger, Frau Dr. Iris Bruchaus und Herrn Prof. Egbert Tannich für die zusätzlichen Anregungen, Ideen und die motivierenden Worte in unseren Gesprächen bedanken.

Darüber hinaus gilt mein Dank auch dem GRK 1459 für die Finanzierung und insbesondere Herrn Prof. Thomas Braulke und Frau Dr. Dorthe Labonté für das Management des Programms, in dem der Input für uns Doktoranden stets im Mittelpunkt stand. Die zahlreichen hochgradigen Gastsprecher haben für viele neue wissenschaftliche Ideen und persönlichen Input gesorgt.

Ich bedanke mich auch bei allen ehemaligen und aktuellen Mitarbeitern der AG Spielmann und der AG Gilberger für das kollegiale und schöne Miteinander. Auch die schönen Erlebnisse außerhalb des Labors werden mir in guter Erinnerung bleiben.

Für die Hilfe während Ihres Praktikums im Rahmen des DAAD RISE Germany Programms danke ich Sarah Smith und Lea Sanchez-Milde für ihren Beitrag zu meiner Laborarbeit.

Schließlich bedanke ich mich bei meinen Eltern, meiner Familie und meinen Freunden für die Unterstützung und tolle Zeit. Besonderem Dank gilt meiner Frau Mackenzie, die mich in all den Jahren begleitet, mich stets unterstützt, den Rücken frei gehalten und immer an mich geglaubt hat. Ohne dich wäre ich nicht so weit gekommen. Danke!

Appendix

A-1

Flow cytometry growth curves for PfClathrin Heavy Chain of independent experiments

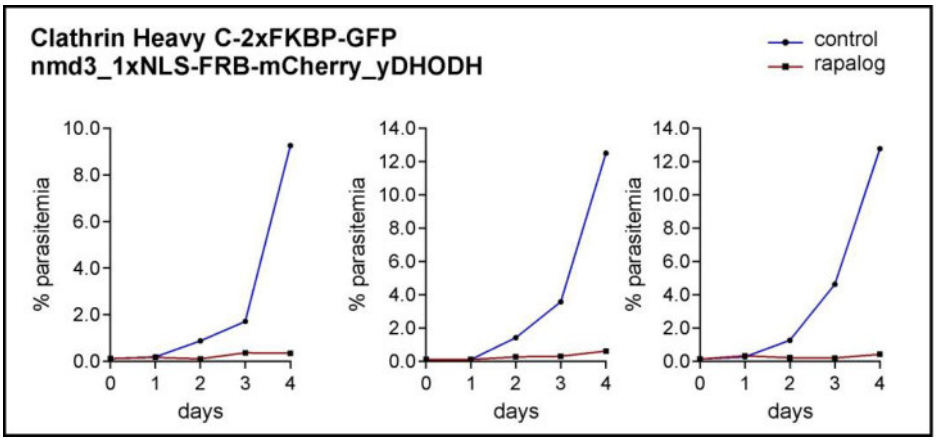

A-2

Flow cytometry growth curves for PfEps15 of independent experiments

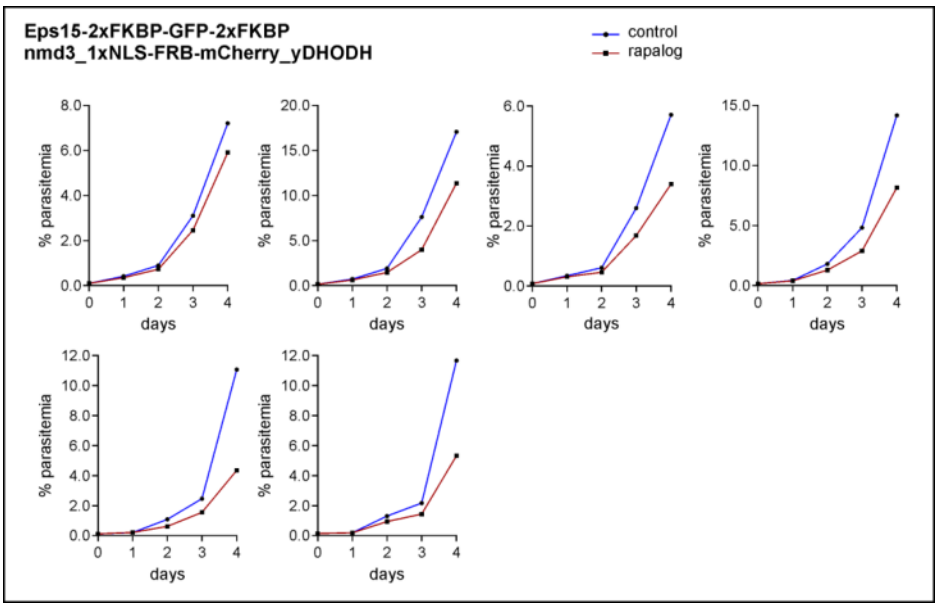

A-3

Diagnostic PCRs of SLI-TGD experiments attempted for PfClathrin Heavy Chain and PfEps15

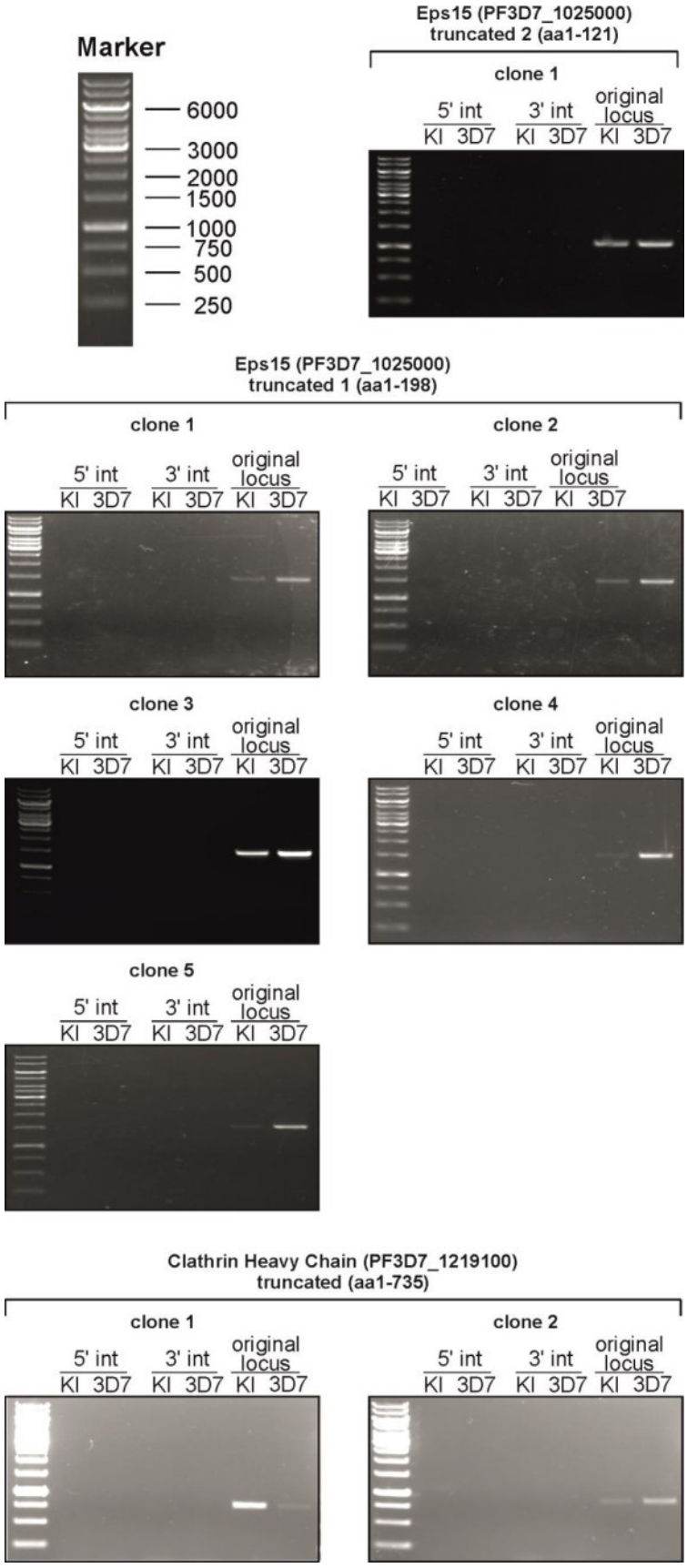

B

Results of DiQ-BioID for PfClathrin Heavy Chain.

Analysis and Table done by Wieteke Hoeijmakers (Radboud Institute, Nijmegen, Netherlands). Legend is shown in A-6

Quantitative Bio-ID of Clathrin HC interactome (proteins enriched in Clathrin HC rapalog-treated over control Bio-ID, ranked on average log2 normalized ratio, high -> low)

Majority protein IDs	PlasmoDB33_ProteinProduct	GeneDB Updated Product Name	Gene Name or Symbol	log2 Ratio H/L normalized CHC+BirA*-NL exp1	log2 Ratio L/H normalized CHC+BirA*-NL exp2	log2 Ratio H/L normalized CHC+BirA*-CL exp1	log2 Ratio L/H normalized CHC+BirA*-CL exp2	average log2 Ratio normalized Clathrin HC	CHC+BirA*-NL exp1 Significance B (two-sided)	CHC+BirA*-NL exp2 Significance B (two-sided)	CHC+BirA*-CL exp1 Significance B (two-sided)	CHC+BirA*-CL exp2 Significance B (two-sided)	Clathrin HC # significantly enriched FDR<1%	Number of proteins	Peptides	Unique peptides	Peptides CHC+BirA*-NL exp1	Peptides CHC+BirA*-NL exp2	Peptides CHC+BirA*-CL exp1	Peptides CHC+BirA*-CL exp2	Unique peptides CHC+BirA*-NL exp1	Unique peptides CHC+BirA*-NL exp2	Unique peptides CHC+BirA*-CL exp1	Unique peptides CHC+BirA*-CL exp2
PF3D7_1435500	conserved Plasmodium protein, unknown function	clathrin light chain, putative	null	4,922246	5,038551	4,963104	5,463899	5,09695	2,92931E-24	4,49626E-40	7,63645E-22	1,92817E-49	4	1	18	18	11	15	12	16	11	15	12	16
PF3D7_1219100	clathrin heavy chain, putative	null	null	4,61953	4,699372	4,544362	4,961732	4,706249	1,49859E-21	3,88296E-35	1,24452E-18	3,44147E-41	4	3	119	118	98	109	99	102	97	109	98	101
PF3D7_0408100	conserved Plasmodium protein, unknown function	null	null	4,267161	4,290617	4,222496	4,219498	4,249943	1,30658E-18	1,23587E-29	2,39906E-16	2,05824E-30	4	1	25	25	20	21	19	19	20	21	19	19
PF3D7_1459600	conserved Plasmodium protein, unknown function	null	null	3,454702	4,032589	3,582074	3,971951	3,760329	1,06107E-12	2,06465E-26	2,8333E-12	3,40088E-27	4	1	41	41	31	35	25	35	31	35	25	35
PF3D7_1455500	AP-1 complex subunit gamma, putative	null	null	3,967169	4,064893	3,259031	3,507583	3,699669	2,75029E-16	8,35567E-27	1,85197E-10	1,15274E-21	4	1	28	28	18	21	17	16	18	21	17	16
PF3D7_1118100	AP-1 complex subunit sigma, putative	null	null	3,555939	3,48321	3,385707	3,611738	3,5091485	2,26689E-13	4,40157E-14	5,8139E-11	7,56485E-23	4	1	3	3	2	1	2	1	2	1	2	1
PF3D7_0202600	conserved Plasmodium protein, unknown function	nucleic acid binding protein, p	null	3,452727	3,437229	3,098251	3,237047	3,3063135	1,09303E-12	1,02729E-19	1,29321E-09	9,53433E-19	4	1	46	46	30	36	26	34	30	36	26	34
PF3D7_1432800	HP12 protein homolog, putative	null	null	3,329985	3,661164	2,689344	3,371131	3,262906	6,69493E-12	4,10891E-22	1,20462E-07	3,64119E-20	4	1	30	30	25	25	18	22	25	25	18	22
PF3D7_0915400	ATP-dependent 6-phosphofructokinase	null	PFK9	3,099076	3,015666	3,275156	3,371115	3,1917533	1,70564E-10	1,35216E-15	1,51637E-10	3,13822E-20	4	1	101	101	79	87	80	86	79	87	80	86
PF3D7_1408700	conserved Plasmodium protein, unknown function	null	null	3,163628	2,892821	3,39053	2,982905	3,107471	7,0566E-11	1,71608E-14	3,53144E-11	3,28414E-16	4	1	177	177	137	114	141	110	137	114	141	110
PF3D7_0904100	AP-4 complex subunit epsilon, putative	null	null	3,532068	3,275228	2,802297	2,773097	3,0956725	3,27476E-13	4,52553E-18	3,65011E-08	2,90115E-14	4	1	35	35	23	27	17	26	23	27	17	26
PF3D7_1247500	serine/threonine protein kinase, putative	null	null	3,241688	3,448666	2,619859	2,964207	3,068605	2,37103E-11	7,81174E-20	3,0413E-07	3,08008E-12	4	1	22	22	16	10	6	11	16	10	6	11
PF3D7_1227300	conserved Plasmodium protein, unknown function	null	null	3,276154	NaN	2,8855	NaN	3,055827	2,94595E-12	1	1,11241E-46	1	2	1	12	12	10	1	4	1	10	1	4	1
PF3D7_1307700	conserved Plasmodium protein, unknown function	null	null	2,830235	3,121549	3,107504	2,933022	2,9980775	5,5793E-09	1,3958E-16	1,15921E-09	9,80113E-16	4	1	44	44	40	38	37	35	40	38	37	35
PF3D7_0929700	conserved Plasmodium protein, unknown function	null	null	2,836045	2,816647	2,560617	NaN	2,7377697	1,57932E-09	1,17284E-07	6,40658E-05	1	3	1	6	6	6	2	4	1	6	2	4	1
PF3D7_1421000	conserved Plasmodium protein, unknown function	DIX domain-containing protein	null	2,811985	2,525829	2,678725	2,56371	2,6450623	6,99263E-09	1,86876E-11	1,34463E-07	1,8676E-12	4	1	8	8	6	5	5	6	6	5	5	6
PF3D7_0406700	conserved Plasmodium protein, unknown function	null	null	2,756148	2,975624	2,120153	2,69778	2,6374263	1,38326E-08	3,12984E-15	2,5157E-05	1,34435E-13	4	1	27	27	23	16	12	17	23	16	12	17
PF3D7_0526200	ADP-ribosylation factor GTPase-activating protein, putative	null	ARF-GAP	2,851859	3,056971	2,098217	2,541534	2,6371453	4,26196E-09	5,6256E-16	3,02219E-05	2,85132E-12	4	1	20	20	16	19	15	18	16	19	15	18
PF3D7_0730200	AP-4 complex subunit beta, putative	null	null	1,362498	3,768194	NaN	NaN	2,565346	0,004044899	2,87685E-12	1	1	2	1	4	4	4	2	0	1	4	2	0	1
PF3D7_0724000	Rab GTPase activator and protein kinase, putative	null	null	2,553975	2,530989	2,673715	2,421515	2,5450485	1,46669E-07	2,73261E-08	1,77711E-07	8,96492E-09	4	1	19	19	17	12	8	11	17	12	8	11
PF3D7_0528100	AP-1 complex subunit beta, putative	null	null	2,955443	2,268747	2,841611	2,017592	2,5208483	1,14157E-09	5,45725E-07	3,12607E-08	1,31397E-06	4	9	19	19	14	11	10	10	14	11	10	10
PF3D7_1205400	kelch domain-containing protein, putative	null	null	2,833781	2,234058	2,74771	1,960328	2,4439693	1,62756E-09	7,93446E-07	8,35965E-08	2,49679E-06	4	1	16	16	7	11	5	9	7	11	5	9
PF3D7_0411800	conserved Plasmodium protein, unknown function	null	null	2,405557	1,984674	2,716859	2,428178	2,383817	7,4489E-07	1,00734E-05	1,1474E-07	8,20125E-09	4	1	22	22	14	10	12	13	14	10	12	13
PF3D7_1411300	conserved Plasmodium protein, unknown function	null	null	2,09788	2,40767	2,127402	2,37692	2,252468	1,61786E-05	1,46811E-10	2,36687E-05	5,92227E-11	4	1	12	12	10	10	8	8	10	10	8	8
PF3D7_0503500	protein kinase, putative	null	null	2,100843	2,110729	1,937947	2,043586	2,0482763	1,57354E-05	2,88092E-06	0,000118236	9,76604E-07	4	1	17	17	12	9	11	5	12	9	11	5
PF3D7_0815800	vacuolar protein sorting-associated protein 9, putative	null	VPS9	2,10608	2,320991	1,716991	2,04115	2,046303	1,498E-05	6,27976E-10	0,00056301	1,60561E-08	4	1	47	47	30	42	25	34	30	42	25	34
PF3D7_0419500	conserved Plasmodium membrane protein, unknown function	null	null	2,066193	2,268956	1,81619	1,929446	2,0201963	1,16319E-05	5,4449E-07	0,000291438	0,000235938	4	1	7	7	6	6	3	2	6	6	3	2
PF3D7_1210100	syntaxin, Qa-SNARE family	null	SYN2	1,333767	3,726768	0,853517	NaN	1,9713506	0,004908181	4,8392E-12	0,125215773	1	2	1	5	5	5	2	3	1	5	2	3	1
PF3D7_0704400	phosphoinositide-binding protein, putative	null	null	1,906467	2,088776	1,958137	1,879595	1,9582438	9,02061E-05	2,4139E-08	9,37812E-05	1,80024E-07	4	1	27	27	20	26	18	22	20	26	18	22
PF3D7_0305200	conserved Plasmodium protein, unknown function	null	null	1,979842	2,280825	1,427123	1,795308	1,8707745	4,75184E-05	1,2109E-09	0,003741938	5,91433E-07	4	1	57	57	32	50	30	41	32	50	30	41
PF3D7_1401200	Plasmodium exported protein, unknown function	null	null	-0,381047	4,754889	0,044884	2,363948	1,6931684	0,471859292	6,37055E-36	0,748212502	8,90859E-11	2	1	2	2	2	1	2	2	2	1	2	2
PF3D7_0914900	BSD-domain protein, putative	null	null	1,623305	1,568623	1,572405	1,311112	1,5188613	0,000594337	2,37131E-05	0,010143362	0,001181983	3	1	17	17	9	12	4	9	9	12	4	9
PF3D7_0419800	60S ribosomal protein L7ae/L30e, putative	null	null	4,378373	0,3728601	2,268853	1,056029	1,4910143	9,18671E-21	0,295645927	7,94803E-06	0,15337881	2	1	2	2	2	2	2	2	2	2	2	2
PF3D7_0705500	inositol-phosphate phosphatase, putative	null	null	1,591775	1,6092	1,3003	1,406751	1,4770065	0,001099612	1,47605E-05	0,007845959	7,57844E-05	4	1	50	50	38	38	29	34	38	38	29	34
PF3D7_1019600	conserved Plasmodium protein, unknown function	null	null	1,555963	1,146116	1,582508	NaN	1,4281957	0,001002914	0,019394301	0,009724164	1	2	1	17	17	16	3	3	1	16	3	3	1
PF3D7_0804900	GTPase-activating protein, putative	null	null	1,436428	1,576562	1,193519	1,249822	1,3640828	0,002419331	2,16308E-05	0,01381234	0,000402133	3	1	11	11	7	8	5	10	7	8	5	10
PF3D7_0416900	conserved Plasmodium protein, unknown function	null	null	1,68818	0,842801	0,691713	1,861082	1,275944	0,001466796	0,042528724	0,193706365	5,91114E-08	2	1	21	21	2	8	5	6	2	8	5	6
PF3D7_1247400	peptidyl-prolyl cis-trans isomerase FKBP35	null	FKBP35	1,296487	0,9159629	1,252779	1,582642	1,2619677	0,006275735	0,011423543	0,010094671	9,57231E-06	2	1	16	16	9	11	8	13	9	11	8	13
PF3D7_1451800	sortilin	null	null	1,773068	1,160653	1,059355	0,9825056	1,2438954	0,000273462	0,001546648	0,027686181	0,004720682	3	1	18	18	16	15	13	15	16	15	13	15
PF3D7_0708400	heat shock protein 90	null	HSP90	0,6882251	0,249565	1,751378	2,085037	1,1935513	0,163856097	0,42574137	0,000441335	8,07105E-09	2	11	58	52	40	42	40	46	35	37	35	41
PF3D7_1434800	mitochondrial acidic protein MAM33, putative	null	null	NaN	1,361305	0,556699	1,537173	1,1517257	1	0,001856158	0,2692416	0,002738525	2	1	2	2	1	2	1	2	1	2	1	2
PF3D7_0830400	conserved Plasmodium protein, unknown function	CRA domain-containing protein	null	-0,767732	1,65145	1,125453	2,19674	1,0514777	0,170199194	0,000200068	0,019531531	1,58894E-07	2	1	6	6	2	2	3	2	2	2	3	2
PF3D7_0220000	liver stage antigen 3	null	LSA3	-2,687521	1,692688	NaN	3,527458	0,8442083	4,8604E-07	0,00094547	1	1,09732E-10	2	1	5	5	2	5	2	3	2	5	2	3

Results of DiQ-BioID for PfEps15 .

Analysis and Table done by Wieteke Hoeijmakers (Radboud Institute, Nijmegen, Netherlands). Legend is shown in A-6

Quantitative Bio-ID of Eps15 interactome (proteins enriched in Eps15 rapalog-treated over control Bio-ID, ranked on average log2 normalized ratio, high -> low)

Majority protein IDs	PlasmoDB33_ProteinProduct	GeneDB Updated Product Name	Gene Name or Symbol	log2 Ratio H/L normalized EPS15+BirA*-NL exp1	log2 Ratio L/H normalized EPS15+BirA*-NL exp2	log2 Ratio H/L normalized EPS15+BirA*-NL exp3	log2 Ratio L/H normalized EPS15+BirA*-NL exp4	average log2 Ratio normalized Eps15	EPS15+BirA*-NL exp1 Significance B (two-sided)	EPS15+BirA*-NL exp2 Significance B (two-sided)	EPS15+BirA*-NL exp3 Significance B (two-sided)	EPS15+BirA*-NL exp4 Significance B (two-sided)	Eps15 # significantly enriched FDR< 1%	Number of proteins	Peptides	Unique peptides	Peptides EPS15+BirA*-NL exp1	Peptides EPS15+BirA*-NL exp2	Peptides EPS15+BirA*-NL exp3	Peptides EPS15+BirA*-NL exp4	Unique peptides EPS15+BirA*-NL exp1	Unique peptides EPS15+BirA*-NL exp2	Unique peptides EPS15+BirA*-NL exp3	Unique peptides EPS15+BirA*-NL exp4
PF3D7_1025000	formin 2, putative	* Eps15	null	3,101869	4,331336	4,400811	4,190813	4,0062073	5,03667E-72	9,42E-33	2,65748E-62	2,21783E-27	4	1	43	43	23	33	24	25	23	33	24	25
PF3D7_0708400	heat shock protein 90	null	HSP90	1,298541	4,267371	3,469365	4,011937	3,2618035	5,47696E-14	7,767E-32	2,16587E-39	3,07438E-25	4	11	58	52	44	50	48	53	38	45	42	48
PF3D7_1246300	conserved Plasmodium protein, unknown	null	null	2,575603	3,515447	3,310282	3,630001	3,2578333	3,08978E-50	4,444E-22	1,3047E-26	5,69051E-21	4	1	28	28	14	18	11	20	14	18	11	20
PF3D7_1247400	peptidyl-prolyl cis-trans isomerase FKBP35	null	FKBP35	2,390007	3,749853	3,181071	3,536905	3,214459	1,65352E-43	6,399E-25	2,17884E-33	5,39806E-20	4	1	16	16	8	14	12	15	8	14	12	15
PF3D7_0914400	conserved Plasmodium protein, unknown	null	null	2,36028	3,415022	3,113667	3,010309	2,9748195	5,98318E-19	6,454E-21	1,05011E-23	6,23069E-15	4	1	15	15	7	9	5	11	7	9	5	11
PF3D7_0813000	conserved Plasmodium protein, unknown	null	null	3,185343	2,681955	1,910464	2,659905	2,6094168	7,55009E-76	1,939E-13	9,39536E-10	5,32946E-12	4	1	15	15	10	10	5	9	10	10	5	9
PF3D7_1343700	kelch protein K13	null	K13	1,935271	2,537675	2,317536	2,176838	2,24183	3,99751E-29	3,564E-12	1,76356E-18	1,58515E-08	4	1	55	55	23	28	14	20	23	28	14	20
PF3D7_1138700	conserved Plasmodium protein, unknown	null	null	2,175908	2,656444	1,849439	2,110106	2,1979743	2,30226E-36	3,282E-13	3,20636E-09	4,24903E-08	4	1	48	48	21	24	6	18	21	24	6	18
PF3D7_0609700	conserved Plasmodium protein, unknown	null	null	2,010207	2,532574	2,433681	1,766505	2,1857418	2,73432E-31	3,939E-12	5,16304E-15	4,32699E-06	4	1	51	51	17	29	11	27	17	29	11	27
PF3D7_0104300	ubiquitin carboxyl-terminal hydrolase 1,	null	UBP1	2,075704	2,08614	2,053633	1,673969	1,9723615	3,0082E-33	1,174E-08	4,53376E-11	1,32072E-05	4	1	88	88	47	41	16	35	47	41	16	35
PF3D7_0700800	Pfmc-2TM Maurer's cleft two	null	MC-2TM	NaN	NaN	2,357102	1,518288	1,937695	1	1	1,8383E-07	0,000137794	2	2	3	1	1	1	3	1	1	1	1	1
PF3D7_1438400	metacaspase-like protein	null	MCA2	1,721023	2,413192	1,659468	1,671485	1,866292	2,21479E-23	2,43E-06	0,000232334	2,64782E-05	4	1	52	52	21	13	5	9	21	13	5	9
PF3D7_1227700	conserved Plasmodium protein, unknown	null	null	1,812827	1,836501	1,49503	1,800325	1,7361708	9,22943E-26	5,376E-07	1,53286E-08	2,83884E-06	4	3	61	61	30	34	24	33	30	34	24	33
PF3D7_0933600	mitochondrial-processing peptidase subunit beta, putative	null	MAS1	NaN	1,1633	2,372395	1,270243	1,6019793	1	0,0877635	1,53247E-07	0,004807936	2	1	5	5	0	3	2	2	0	3	2	2
PF3D7_0915400	ATP-dependent 6-phosphofructokinase	null	PFK9	1,721854	1,282684	1,70217	1,22085	1,4818895	2,11021E-23	0,0005029	1,17926E-10	0,001425869	4	1	101	101	73	82	82	76	73	82	82	76
PF3D7_0606000	conserved Plasmodium protein, unknown	null	null	1,077175	1,644803	1,114833	1,477141	1,328488	4,37518E-10	7,406E-06	2,45826E-05	0,000118314	4	1	74	74	31	28	28	30	31	28	28	30
PF3D7_1442400	conserved Plasmodium protein, unknown	null	null	1,098824	1,381085	1,140713	1,048024	1,1671615	1,95037E-10	0,0080233	0,000302489	0,006066824	4	1	73	73	31	18	14	26	31	18	14	26
PF3D7_1410600	eukaryotic translation initiation factor 2 subunit gamma, putative	null	eIF2gamma	-0,17842	1,657263	1,323946	1,822095	1,1562209	0,523173927	6,297E-06	2,55665E-05	2,15592E-06	3	1	14	14	4	10	6	9	4	10	6	9
PF3D7_0314700	zinc finger protein, putative	null	null	0,2625534	1,534119	1,091666	1,51342	1,1004396	0,126098238	2,976E-05	3,6135E-05	8,04512E-05	3	1	25	25	12	19	16	9	12	19	16	9
PF3D7_1024800	conserved Plasmodium protein, unknown	exported p	null	1,988739	0,563028	0,9026525	0,7695264	1,0559865	4,13268E-06	0,3096019	0,004538758	0,006480004	2	1	11	11	4	5	7	5	4	5	7	5
PF3D7_0708100	DNA-directed RNA polymerases I, II, and III subunit RPABC5, putative	null	RPB10	-0,459695	0,9558718	1,046421	2,099185	0,9104457	0,003317538	0,01004	7,50686E-05	4,97944E-08	2	1	5	5	5	5	4	5	5	5	4	5
PF3D7_0813200	CS domain protein, putative	null	null	-0,889049	1,308787	1,597126	1,558079	0,8929858	0,077046189	0,0121903	0,000394249	0,000629793	2	1	9	9	3	8	3	8	3	8	3	8
PF3D7_1142100	conserved Plasmodium protein, unknown	null	null	0,6863437	1,032035	0,7382058	0,977128	0,8584281	6,88763E-05	0,0053479	0,005224385	0,010421773	3	1	129	129	91	78	69	77	91	78	69	77
PF3D7_1336800	nuclear movement protein, putative	null	NUDC	0,2867629	1,208794	0,7046949	1,213303	0,8533887	0,094987386	0,001058	0,007675824	0,001524794	3	1	15	15	10	13	11	11	10	13	11	11
PF3D7_1345800	conserved Plasmodium protein, unknown	null	null	0,2775088	1,248588	0,7637516	1,115935	0,8513459	0,27892009	0,0007123	0,017040807	0,005311177	2	1	19	19	10	14	12	12	10	14	12	12
PF3D7_1457300	conserved Plasmodium protein, unknown	null	null	0,0824301	1,097703	0,8469546	1,060638	0,7719314	0,725379988	0,0030063	0,007890421	0,005492369	3	1	18	18	4	12	8	12	4	12	8	12
PF3D7_1134700	DNA-directed RNA polymerase I subunit	null	RPA2	-0,31642	0,9975207	1,197425	0,9831329	0,7154146	0,243807195	0,0071506	0,000145983	0,009966743	3	1	29	29	7	20	11	19	7	20	11	19
PF3D7_1105600	translocon component PTEX88	null	PTEX88	0,445303	0,3481699	0,830093	0,3395151	0,4657703	0,009699116	0,3723419	0,009272933	0,508389589	2	1	23	23	14	15	11	12	14	15	11	12

Legend for Results of DiQ-BioID in A-4 and A-5

Legend done by Wieteke Hoeijmakers (Radboud Institute, Nijmegen, Netherlands).

LEGEND

Subtables:

Table SxA: Quantitative Bio-ID of Kelch13 interactome (proteins enriched in Kelch13 rapalog-treated over control Bio-ID, ranked on average log2 normalized ratio, high -> low)

Table SxB: Quantitative Bio-ID of Eps15 interactome (proteins enriched in Eps15 rapalog-treated over control Bio-ID, ranked on average log2 normalized ratio, high -> low)

Table SxC: Quantitative Bio-ID of Clathrin HC interactome (proteins enriched in Clathrin HC rapalog-treated over control Bio-ID, ranked on average log2 normalized ratio, high -> low)

Table SxD: Quantitative Bio-ID of all 3 datasets combined (ranked on PlasmoDB gene_ID, low->high)

Collumn name	**Explanation**
Majority protein IDs	gene-ID of protein(s) that match to at least half of the peptides belonging to a protein group, e.g. the most likely candidate(s) identified
PlasmoDB33_ProteinProduct	PlasmoDB protein product description of the associated gene-ID. In case of multiple Majority protein hits, product descriptions are separated by ';'
GeneDB Updated Product Name	Updated protein product description not yet present in the latest annotation, 'null' if no geneDB updated protein product is given. Eps15 is highlighted with an *
Gene Name or Symbol	PlasmoDB gene name or symbol
Previous ID(s)	Previous/alternative gene-IDs associated with the annotation
log2 Ratio normalized	log2-transformed normalized H/L (forward, exp 1 and 3) or L/H (reverse, exp 2 and 4)-ratios that reflect the level of enrichement/depletion
average log2 Ratio normalized	average log2-transformed normalized ratios of the four replicate experiments per bait
Significance B (two-sided)	FDR value resulting from the 2-sides intensity-based Benjamini-Hochberg procedure
significantly enriched FDR<1%	+' if significantly enriched with an FDR<1%
# significantly enriched FDR<1%	the number of times a protein is found to be significantly enriched with an FDR<1% out of the 4 replicate experiments
Number of proteins	number of protein IDs in this protein group
Peptides	number of peptides identified for this protein group. Either the sum of all peptides identified in all experiments combined, or the number of peptides detected per experiment is given
Unique peptides	number of unique peptides identified for this protein group. Either the sum of all unique peptides identified in all experiments combined, or the number of unique peptides detected per experiment is given. Unique peptides are those peptides that match to this protein group only and not to other proteins/protein-groups.
Sequence coverage [%]	% of the protein covered by the identified peptides. Either the total sequence coverage in all experiments combined, or the sequence coverage per experiment is given
Unique sequence coverage [%]	% of the protein covered by the identified unique peptides. Either the total sequence coverage in all experiments combined, or the sequence coverage per experiment is given
Mol. weight [kDa]	Molecular weight of the (leading) majority protein hit
Sequence length	Sequence length of the (leading) majority protein hit
Q-value	adjusted p-value found using an optimized FDR approach that reflects the chance that this identification is wrong (the lower the better)
log10 Intensity	log10-transformed summed intensity of all detected peptides belonging to this protein group given for all experiments combined (log10 intensity), per experiment for all labels combined, or per experiment per label
iBAQ	iBAQ score. Either total iBAQ is given for all data combined or iBAQs are given per experiment and per label
Protein IDs of proteins in ProteinGroup	gene-ID of all proteins that match one or more peptides in the protein group

Colour code

used as bait in BioID
selected for validation
Significant with FDR<1% in 3 out of 4 reactions of any bait (very stringent filtering) (Table SxA, SxB & SxC only)
Significant with FDR<1% in 2 out of 4 reactions of any bait ONLY (less stringent filtering) (Table SxA, SxB & SxC only)

A-7

Flow cytometry growth curves for PfVPS45 of independent experiments

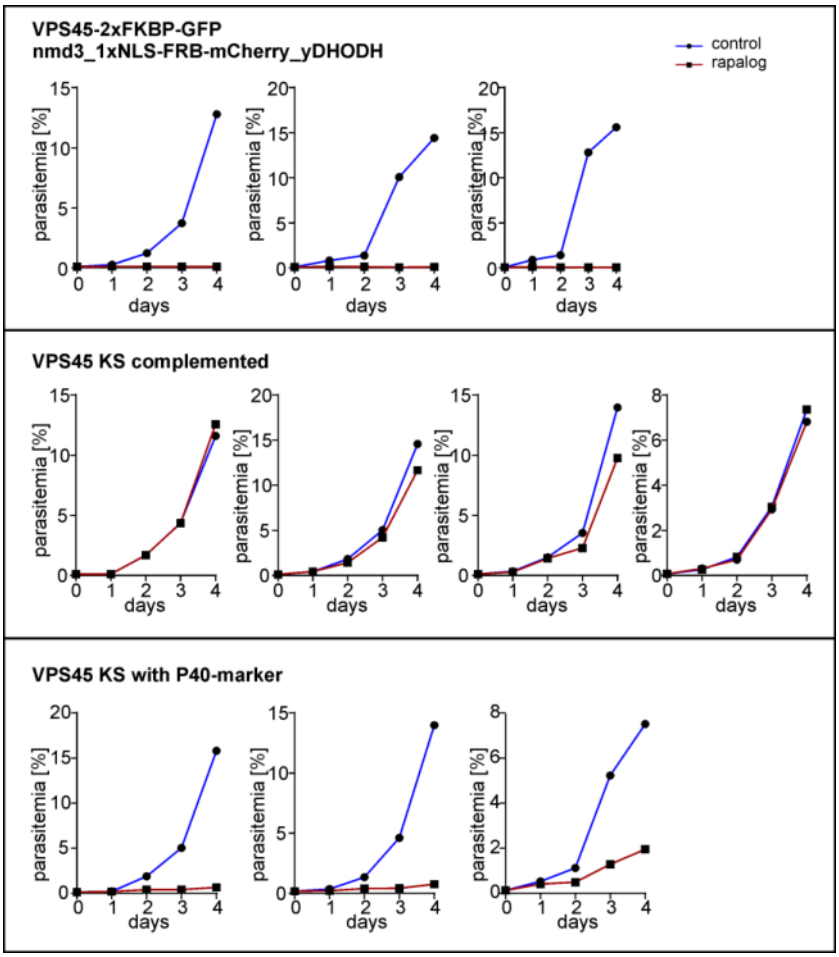

A-8

Vesicle accumulation assay for PfVPS45 (three independent experiments)

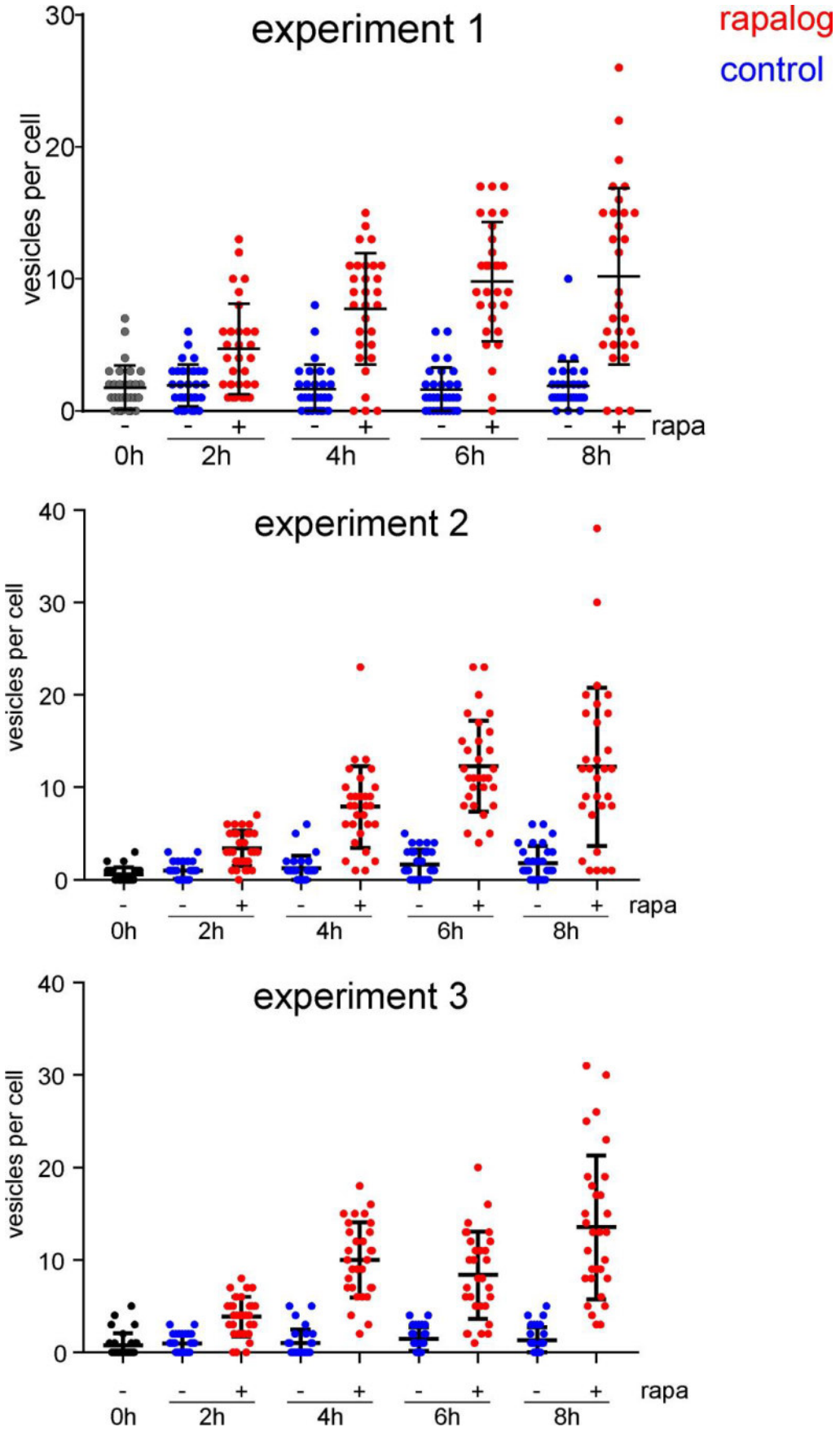

A-9

Replicates of the bloated food vacuole assay for PfVPS45 (three independent experiments)

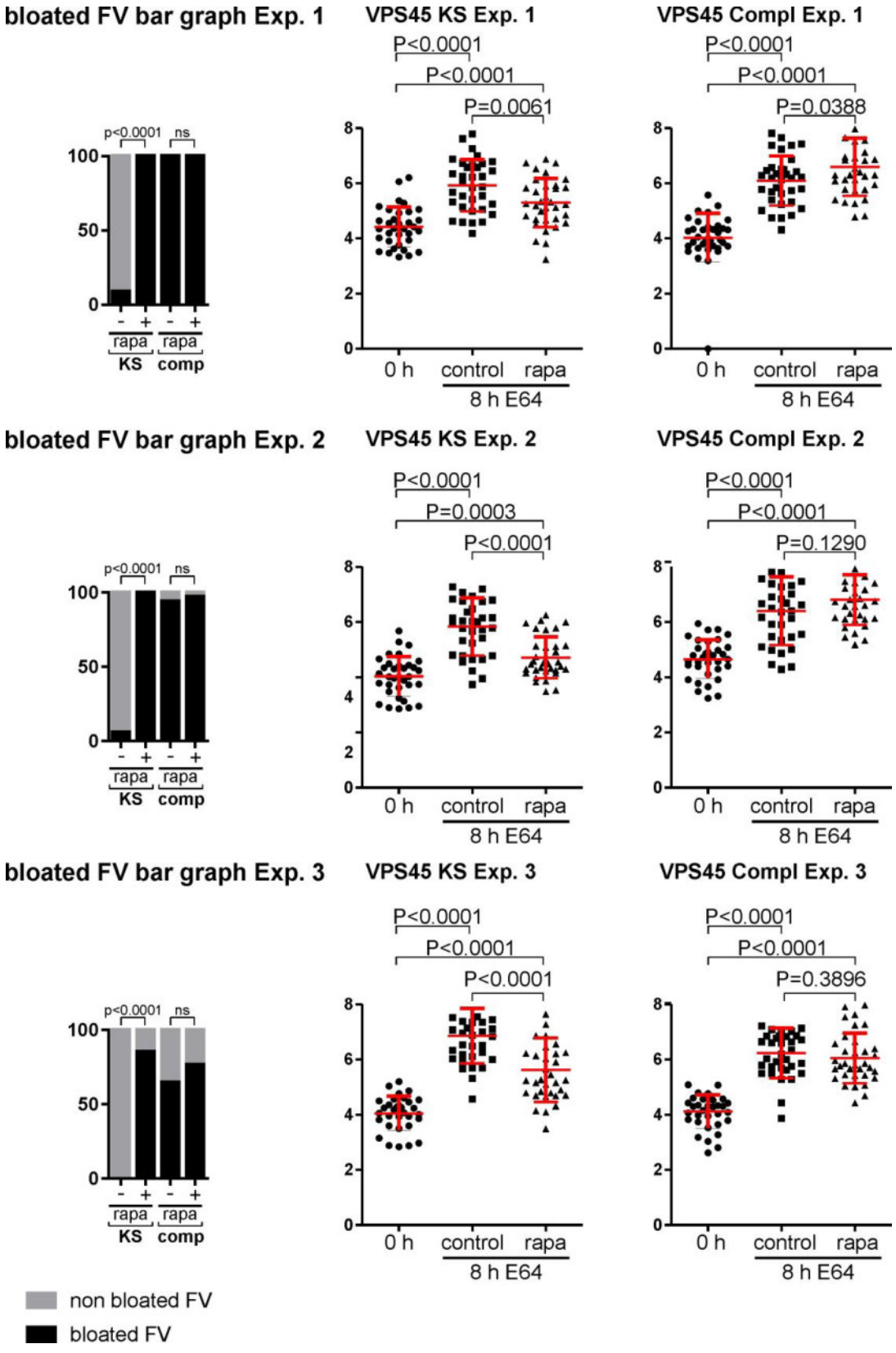

A-10

Hemozoin accumulation assay for PfVPS45 (three independent experiments)

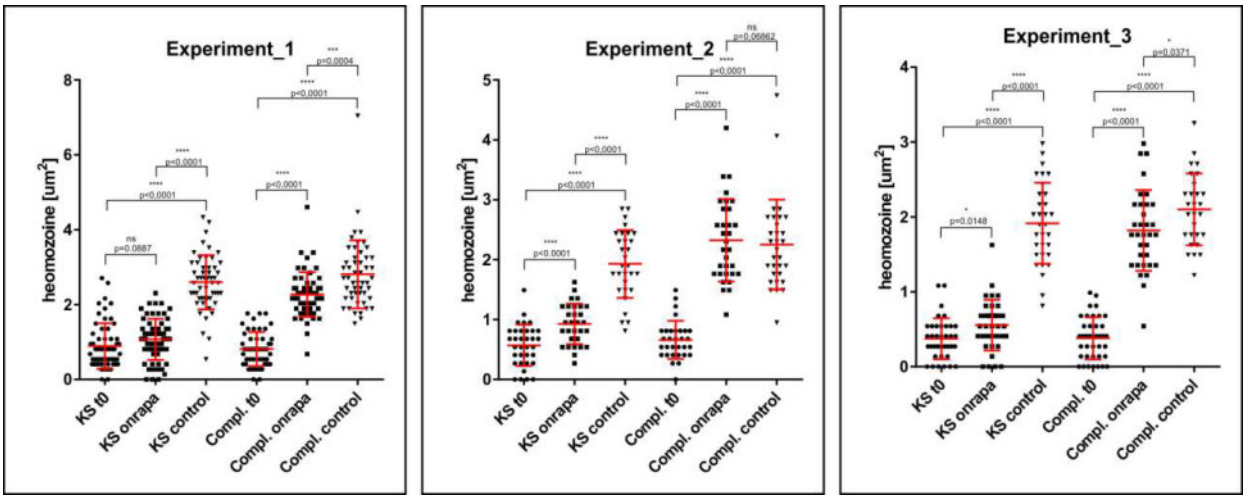

A-11

Coomassie stained PAA-Gels of replicates of the quantitative western blot assay for hemoglobin uptake for PfVPS45 (three independent experiments)